

Inaugural - Dissertation

zur Erlangung der Doktorwürde

der

Naturwissenschaftlich-Mathematischen Gesamtfakultät

der Ruprecht-Karls-Universität

Heidelberg

vorgelegt von

Diplom-Chemiker Thomas Heinlein

aus Nürnberg

Tag der mündlichen Prüfung: 17.12.2004

**Entwicklung von Methoden zur Struktur- und Funktionsaufklärung
in Lebenden und Fixierten Zellen auf Einzelmolekülniveau mittels
Koinzidenzanalyse und Spektral-Aufgelöster
Fluoreszenzlebensdauer-mikroskopie [SFLIM]**

**(Development of Methods for Structure and Function Determination
in Living and Fixated Cells on the Single-Molecule Level Based on
Coincidence Analysis and Spectrally-Resolved Fluorescence
Lifetime Imaging Microscopy [SFLIM])**

Gutachter: Prof. Dr. Jürgen Wolfrum
Prof. Dr. Joachim Spatz

Zusammenfassung

Die fortschreitende Entwicklung im Bereich der Molekularbiologie und Biochemie hat in den letzten Jahren zu bahnbrechenden Ergebnissen, wie zum Beispiel der Entschlüsselung des menschlichen Genoms, geführt. Die Konsequenz der immer detaillierteren Kenntnis von biologischen Strukturen und Mechanismen ist, dass immer kleinere und seltener auftretende Einheiten, die mit herkömmlichen Methoden oftmals nicht mehr aufgeklärt werden können, Gegenstand der Forschung sind. Angetrieben durch die ersten Nachweise einzelner Fluorophore durch Mörner und Orrit Anfang der 90er Jahre, wurden photostabile Farbstoffe, effiziente Kopplungsmechanismen und hochsensible optische Elemente entwickelt, die es ermöglichen, einzelne Biomoleküle selektiv zu markieren, sie aufzuspüren und zu charakterisieren.

Prinzipiell gibt es zwei Fragestellungen bei der Strukturaufklärung von biologischen Systemen: Wo sind die Einzelkomponenten lokalisiert bzw. welche Abstände haben sie zueinander und aus welchen oder wie vielen Einheiten bestehen sie? Um diese Fragen zu beantworten, ist die Einzelmolekülspektroskopie ein hervorragendes Hilfsmittel.

Die Lokalisation von farbstoffmarkierten Biomolekülen ist heutzutage vergleichsweise einfach, solange der Abstand der einzelnen Fluorophore größer als die optische Auflösungsgrenze von ungefähr 200 nm, gegeben durch das Rayleigh Kriterium, ist. Für Distanzen von 1 bis 10 nm kann der FRET-Effekt (Fluoreszenz Resonanz Energie Transfer) ausgenutzt werden, der auf einer abstandsabhängigen Dipol-Dipol-Wechselwirkung zwischen den Molekülen beruht. Im Zwischenbereich von 10 bis 200 nm, der sogenannten Auflösungslücke, gibt es nur wenige Methoden zur Distanzbestimmung. Diese sind zumeist technisch anspruchsvoll, auf zwei Dimensionen beschränkt oder erfordern die Photozerstörung mindestens eines der Fluorophore. Da aber viele biologisch relevante Moleküle, zum Beispiel biomolekulare Maschinen, genau in dieser Größenordnung liegen, ist es von höchster Wichtigkeit, eine einfache dreidimensionale Methode zur Hand zu haben, die diese Lücke schließt.

Dazu wurde in unserer Arbeitsgruppe ein Algorithmus, basierend auf bildgebender kofokaler Mikroskopie, entwickelt, der es ermöglicht, zwei kolokalisierte (überlappende

Punktabbildungsfunktionen) Farbstoffe über ihre Fluoreszenzlebensdauern und spektrale Charakteristika zu trennen. Die Genauigkeit und Anwendbarkeit der Methode sollte im ersten Teil dieser Arbeit mittels eines Eichmoleküls getestet werden. Dazu wurden verschieden lange DNA Moleküle (44, 70, 148 und 200 Basenpaare), deren doppelsträngiges Gerüst als sehr rigide bekannt ist, endständig mit den Farbstoffen Bodipy 630 und Cy 5.5 markiert. Bei Voruntersuchungen stellte sich heraus, dass alle Farbstoffe, besonders Carbocyanine wie Cy 5.5, zu einem gewissen Anteil auf trockenen Oberflächen irreversibel in einen nicht fluoreszenten Zustand übergehen, während dieses Verhalten in Lösung nicht auftritt. Aus diesem Grunde wurden die Messungen in einer wässrigen Agarosematrix durchgeführt, die eine zellähnliche, jedoch homogene Einschlussverbindung, darstellt. Im Vergleich von zweidimensional aufgenommenen Messdaten mit „Worm-like Chain“-Modellrechnungen zeigte sich, dass die ermittelten Werte innerhalb des stark intensitätsabhängigen Fehlers von etwa 5 bis 15 nm gut mit dem Modell übereinstimmen. Deutliche Abweichungen konnten zumeist durch photophysikalische Effekte, wie „Blinking“, einem reversiblen Übergang in den Triplet-Zustand oder durch Bleichen der Fluorophore, erklärt werden. Weiterhin wurden erste dreidimensionale Messungen in Zellen durchgeführt, die die Eignung der Methode auch in biologischer Umgebung bestätigen.

Neben der Lokalisation von Biomolekülen rückt die quantitative Aufklärung komplexer zellulärer Einheiten immer weiter in den Vordergrund. Oftmals handelt es sich nicht mehr ausschließlich um die Bestimmung verschiedener Untereinheiten, die mit Hilfe unterschiedlicher Farbstoffe gegeneinander diskriminiert werden können, sondern um identische Moleküle, die sich in einem Zellkompartiment ansammeln oder dort gebildet werden. Zum Beispiel findet das Ablesen und die Weitergabe der genetischen Information, die Transkription, durch Polymerasen in sogenannten Transkriptionsfabriken statt. Eine typische HeLa-Zelle enthält im Nukleus etwa 8.000 solcher 40 bis 80 nm großer Zentren, in denen sich durchschnittlich etwa 8 Polymerase II Enzyme befinden. Der Grund für diese Akkumulation, ebenso wie die exakte Anzahl der Polymerasen, konnte mangels geeigneter Techniken bislang nicht aufgeklärt werden. Für das Verständnis der Zellfunktion ist es aber von großer Bedeutung, diese grundlegenden Einheiten zu untersuchen.

Der erste Schritt in diese Richtung, die Zählung der Polymerase II Moleküle in Transkriptionsfabriken, sollte im zweiten Teil dieser Arbeit durchgeführt werden.

Um mehrere kolokalisierte Moleküle quantifizieren zu können, gibt es die Möglichkeit, Photon-Antibunching Messungen durchzuführen. Antibunching ist ein quantenmechanischer Effekt, der darauf beruht, dass ein Molekül aus seinem angeregten Zustand, im Durchschnitt die Fluoreszenzlebensdauer, nur ein Photon emittieren kann. Werden innerhalb dieser Zeit jedoch mehrere Photonen gezählt, muss es sich um mehrere Moleküle handeln. Durch Analyse von Interphotonenzeiten können so Rückschlüsse auf die Anzahl der gleichzeitig im Laserfokus vorhandenen Emitter gezogen werden. Um die maximal mögliche Information aus jedem Fluorophor zu erhalten, werden die Farbstoffe in einer mikroskopischen Abbildung lokalisiert, nachfolgend einzeln im Laserfokus positioniert und die Fluoreszenz bis zur Photozerstörung aufgenommen. Besonders die Carbopyronin-Derivate Atto 620 und Atto 647 stellten sich aufgrund ihrer hohen Photostabilität und Emissionsrate für die Experimente als geeignet heraus. Um die Eignung der Methode in zellulärem Umfeld zu prüfen, wurde ein Farbstoff markiertes Oligonukleotid, bestehend aus 40 Thyminen, in lebende und fixierte Zellen eingebracht. Es wurde gezeigt, dass dieses selektiv und teilweise mehrfach an die bis zu 200 Basenpaar langen Polyadenosinenden der mRNA hybridisiert und dass das Fluoreszenzsignal der Farbstoffe mit einer Wahrscheinlichkeit von über 97 % von Zellautofluoreszenz unterschieden werden kann. Über Koinzidenzanalyse konnte die Anzahl der Emitter für einzelne Bildpunkte in Zellen bis zu einer Zahl von vier eindeutig bestimmt werden.

Um die Dichte der Transkriptionszentren bei der Bildaufnahme zu erniedrigen und eine Molekülzählung für die 3.000 Transkriptionsfabriken pro Zellkern zu ermöglichen, mussten sogenannte „Cryosections“, Zellschnitte mit einer Dicke von 100 nm, eingesetzt werden. Die einfachste Möglichkeit Polymerase II Moleküle zu markieren, erfolgt über spezifische farbstoffmarkierte Antikörper, die sich jeweils nur einfach an die Polymerasen binden. Eine wesentliche Voraussetzung für den Erfolg des Experiments ist eine stöchiometrische Kopplung der Farbstoffe an die Antikörper, *d.h.* es dürfen weder mehrfach- noch unmarkierte Einheiten vorhanden sein. Hierzu wurde eine neue Methode entwickelt, die es erlaubt, eins zu eins markierte Proteine und Quantendots mittels einer affinen Gruppe am Farbstoff herzustellen. Die Einbringung derart markierter Antikörper in Cryosections wurde in einer Kooperation mit Ana Pombo in London durchgeführt. Es konnte gezeigt werden, dass die Antikörper selektiv an ihr Ziel binden und erste wegbetretende Experimente konnten an diesen Proben bereits durchgeführt werden.

Summary

The proceeding evolution in molecular biology and biochemistry led to groundbreaking results in the recent years, for example to the mapping of the human genome. The consequence of the rising knowledge of biological structures and mechanism is that gradually smaller and infrequent units, which are often not resolvable by common methods anymore, are subject to investigation. Driven by the first verifications of single fluorophores in the early nineties by Orrit and Mörner, photostabile dyes, efficient labeling procedures and highly sensitive optical elements were developed, which enable to selectively tag, detect and characterize single biomolecules.

In principle there are two question in the structural exploration of biological systems: Where are the single components localized, or what distances do they have in respect to each other, and from which or how many units are they composed? To solve these questions single-molecule spectroscopy is an excellent tool.

The localization of dye-labeled biomolecules is nowadays comparatively easy, as long as the distance between the single fluorophores is larger than the optical diffraction limit of about 200 nm given by the Rayleigh criterion. For distances between 1 and 10 nm the FRET-effect (Fluorescence Resonance Energy Transfer) can be exploited, which bases on a distance dependent dipol-dipol interaction between molecules. In the intermediate range of 10 to 200 nm, the so-called resolution gap, only few methods for distance determinations are available. Commonly these are technically demanding, limited to two dimensions or require the photodestruction of at least one of the fluorophores. Since many biological relevant molecules, for example biomolecular machines, are exactly in this order of magnitude, it is of major importance to have a simple three-dimensional method at hand, which closes the gap.

For this purpose an algorithm based on confocal imaging microscopy has been developed in our group, which facilitates the separation of two colocalized (overlapping point-spread-functions) dyes by their fluorescence lifetimes and spectral characteristics. The accuracy and applicability of the method ought to be tested in the first part of this work using a biological calibration compound. Therefore DNA molecules of different lengths (44, 70, 148 and 200 basepairs), whose double-

stranded backbone is known to be very rigid, were terminally labeled with the dyes Bodipy 630 and Cy 5.5. In early experiments it was found that all dyes, especially carbocyanines like Cy 5.5, pass into a non-fluorescent state on dry surfaces, whereas in solution this behavior is not apparent. For this reason the measurements were performed in an aqueous agarose matrix, a cell-like but homogenous inclusion reagent. Comparison of the acquired two-dimensional data with “worm-like chain” model calculations showed that the determined values were in good agreement with the model within the strong intensity dependent error of about 5 to 15 nm. Significant deviations could mostly be explained by photo-physical effects like blinking, a reversible transition into the triplet state, or by bleaching of the fluorophores. Furthermore, first three-dimensional measurements in cells were accomplished, which affirmed the suitability of the method also in biological environment.

Beside the localization of biomolecules more and more quantitative investigations of complex cellular units come to the fore. Often the matter is not exclusively anymore the determination of various subunits, which can be discriminated against each other by different dyes, but rather the detection of identical molecules, which assemble or are generated within a cell compartment. For example the read-out and transduction of the genetic information by polymerases, the transcription, takes place in so-called transcription factories. A typical HeLa-cell contains about 8.000 of such 40 to 80 nm sized centers in the nucleus each containing on average 8 polymerase II enzymes. The reason for this accumulation, as well as the exact number of polymerases, could not be determined so far due to a lack of suitable techniques. However, for the comprehension of the cell function it is of great importance to study these basic units. The first step in this direction, the counting of polymerase II molecules in transcription sites, ought to be conducted in the second part of this work.

To be able to quantify several colocalized molecules, antibunching measurements can be used. Antibunching is a quantum mechanical cause basing on the fact, that a molecule can only emit one photon from its excited state, whose duration is in average the fluorescence lifetime. If more photons are counted, the signal must arise from several fluorophores. By analysis of interphoton times conclusions about the number of simultaneously present emitters in the laser focus can be drawn. To gain the maximal possible information from each fluorophore, the dyes are located in a microscopic image, subsequently singly positioned in the laser focus and the fluorescence is collected until photodestruction. Especially the carbopyronine

derivatives Atto 620 and Atto 647 turned out to be best suitable for the experiments because of their high photostability and emission rate. To investigate the applicability of the method in cellular environment, a dye labeled oligonucleotide consisting of 40 thymines was incorporated into living and fixated cells. It was shown that it selectively and partly multiply hybridizes to the up to 200 basepair long polyadenosine ends of the mRNA and that the fluorescence signal of the dyes can be discriminated against cell autofluorescence with a probability of more than 97 %. By coincidence analysis the number of emitters in single image spots could be clearly determined for up to four molecules.

To reduce the density of the transcription centers for imaging and to enable molecule counting for the 3.000 transcription factories per nucleus, so-called "cryosections", cell slices with a thickness of 100 nm, were introduced. The simplest method to label polymerase II molecules uses specific dye labeled antibodies, which singly bind to the polymerases. A fundamental requirement for the success of the experiment is a stoichiometric labeling of the antibodies with the dyes, *i.e.* no multiply- or unlabeled compounds are allowed to be present. Therefore a new method was developed, which allows preparing one to one labeled proteins and quantum dots by the introduction of an affine group at the dye. The incorporation of suchlike labeled antibodies into cryosections was done in collaboration with Ana Pombo in London. It could be shown that the antibodies selectively bind to their targets and first experiments with these probes towards the success of the experiment could be initiated.

| | | |
|----------|---|------------|
| 1 | INTRODUCTION | 1 |
| 2 | THEORY | 7 |
| | 2.1 Fluorescence Spectroscopy | 7 |
| | 2.2 Cell Biology | 17 |
| 3 | MATERIALS AND METHODS | 25 |
| | 3.1 Setup for Spectrally Resolved Lifetime Imaging Microscopy (SFLIM) | 25 |
| | 3.2 Extensions and Variations of the SFLIM-Setup | 33 |
| | 3.3 Software | 37 |
| | 3.4 Determination of the Number of Independent Emitters by Polarization Modulation and Antibunching Measurements | 39 |
| | 3.5 Time and Spectrally Resolved Precision-Distance Microscopy on Single-Molecule Level | 43 |
| | 3.6 Conjugation of Biomolecules with Fluorescence Dyes | 46 |
| | 3.7 Synthesis of Mono-Labeled Antibodies | 48 |
| | 3.8 Cell Culturing and Cell Preparation | 49 |
| | 3.9 Standard Laboratory Equipment..... | 52 |
| | 3.10 Preparation of Coated Glass Surfaces | 53 |
| 4 | RESULTS AND DISCUSSION | 54 |
| | 4.1 Characterization and Selection of Fluorescent Dyes | 54 |
| | 4.2 Precision Distance Measurements between Fluorophores Separated by Double-Stranded DNA..... | 64 |
| | 4.3 Antibunching Measurements inside the Cell Nucleus of Fixated and Living Cells | 80 |
| | 4.4 Stoichiometric 1:1-Labeling of Biomolecules with Fluorescent Markers by the Usage of Affine Groups..... | 99 |
| | 4.5 Detection and Quantification of Polymerase II Molecules in Transcription Factories | 107 |
| 5 | CONCLUSION AND OUTLOOK | 118 |
| | 5.1 Three-Dimensional Precision Distance Measurements | 118 |
| | 5.2 Quantitative Revelation of Biomolecular Machines..... | 121 |
| | 5.3 Orientational Studies of Interacting Fluorophores by Polarization Modulation | 122 |

| | | |
|----------|---|---|
| 5.4 | Preparation and Application of DNA-Spaced Quantum Dots..... | 125 |
| 6 | APPENDIX | 130 |
| 6.1 | Index of Abbreviations | 130 |
| 6.2 | Fluorescence Dyes Structures | 132 |
| 7 | REFERENCES | 133 |
| 8 | PUBLICATION LIST | FEHLER! TEXTMARKE NICHT DEFINIERT. |

1 Introduction

The rising significance of biosciences in the recent years is not only reflected in the formation of a great number of work groups and projects in this field, but also in the establishment of study courses like biotechnology, and the foundation of start-up companies in the life sciences sector.

The basis for the expansion is found in the rapid increase of biochemical knowledge throughout the last decade. Beside their scientific challenges, especially nanobiosciences gained reputation as an important economy factor, as advances in the fabrication of new drugs and medicaments can more and more only be accomplished by investigations on the molecular level.

Upon this huge research area, a very fascinating and important subject is the exploitation of nature's machinery at length scales below the dimensions of a cell. Already astonishing insights into cellular components were gained. Among these are biological molecular motors, whose deployment can be used to guide the design of nanoscale machines [Peterman 2004]. The potential utilization of single molecules as functional devices has been heralded as the dawn of a new era in biology and medicine. It is not surprising, therefore, that the efforts of numerous multidisciplinary teams have been focused in attempts to study these systems [Wang 1999; Ishii 2001].

To go one step further, the vision behind the investigation of cell compartments is to be able to virtually travel through a living cell and meanwhile collect information about its structure and dynamics. The first step towards such a three-dimensional online imaging technique is the exact position determination of single subunits. These could be localized by a Cellular Positioning System (CPS) in analogy to the Global Positioning System (GPS). With GPS a position is exactly determined using three or more fix reference points. If all references send isochronal signals, the point of interest receives them with a delay proportional to the distance to the emitters (triangulation). For the investigation of cells, the method needs to be reversed: the signal is emitted by a fluorophore attached to the molecule of interest, and its exact position is determined by a single-molecule technique.

The position of a single emitter within a cell is nowadays relatively easy to determine by spectroscopic methods. As emitters, mostly fluorescent labels, like dyes, quantum dots, or autofluorescent proteins are used [Weiss 1999; Bruchez 1998; Chalfie 1998]. Since fluorophores are much smaller than the wavelength of light they emit, they can be regarded as a point source. The response of the optical system to this point source, the point-spread-function (PSF), is a spot of light, whose center can be localized with an accuracy of a few nanometers. This localization precision has been used to follow the motion of individual motor proteins, the diffusional trajectories of labeled lipid molecules in membranes, and the diffusion of molecules in gels, in solutions, and even in living cells [Sase 1995; Schmidt 1995; Dickson 1996; Schütz 1997; Xu 1997; Schütz 2000].

Alongside the localization of single molecules, the resolution of distances between several subunits is of substantial interest. However, there are limitations on the length scales over which optical studies can be used to measure distances. In conventional far-field microscopy the spatial resolution is limited to about 200 nm given by the Rayleigh criterion [Strutt 1874], which can only be circumvented by technically demanding two-dimensional methods, which furthermore require the photo-destruction of at least one fluorophore [Hirschfeld 1979; Gordon 2004; Qu 2004].

For considerably smaller distances, fluorescence resonance energy transfer (FRET) can be utilized. FRET occurs over distances between approximately 1 and 10 nm, depending on the Förster radius of the interacting dye molecules [Förster 1946; Stryer 1967]. However, FRET only gives the relative distance between two probes, whereas their absolute positions remain unknown.

Consequently, there is a resolution gap between 10 and 200 nm in optical microscopy, on which length scale exactly the desired molecular machines are found [Badjic 2004].

In the first part of this work a method capable of measuring distances between 10 and 200 nm in cellular environment shall be introduced. To prove the versatility of this method, a molecular ruler with an exactly defined length is needed. Furthermore, this reference molecule needs to be rigid, chemically modifiable for the attachment of fluorophores, and soluble in the aqueous cellular environment. Oligonucleotides and DNA molecules fulfill this condition best, and advantageously their properties and behavior are well known [Bustamante 1994; Smith 1992; Smith 1996]. Thus, the method of choice to confirm distances in the range of the resolution gap is to

terminally attach two different fluorophores separable by their emission characteristics and fluorescence lifetimes to a double-stranded DNA, immobilize them, and determine the distance by imaging microscopy.

For the analysis of such a system a mathematical algorithm has been developed in our group [Müller 2003]. It is designed for analysis of multi-parameter data, and allows splitting the point-spread-functions of overlaying diffraction-limited spots into two separated images and determining their distance. Model calculations predict the error of an assignment to be only in the range of a few nanometers.

With this algorithm it should be possible to close the resolution gap, which would constitute a major step towards a cellular three-dimensional map.

Beside the exact localization, also the quantification of subunits in molecular machines or cell compartment plays an important role in the investigation of biological processes. Since different molecules in such complexes can be labeled with distinguishable fluorophores, the main problem arises from structurally equal units. In cell biology it is, for example, important to be able to count the number occupied antigen binding sites on an antibody, or determine the number of nascent RNA transcripts in the cell nucleus [Löscher 1998; Cook 1999]. The accomplishment of quantitative studies with fluorescent dyes is difficult, because the collected fluorescence signal of a sample does not correspond to the sum of the single intensities, but rather only to a fraction due to energy transfer between the fluorophores [Harms 2001]. On single-molecule level, the fluorescence emission is additionally affected by intensity fluctuations induced by different environmental conditions and photo-physical effects, such as quenching (figure 1.1) or triplet blinking [Heinlein 2003; Schmidt 1995].

Basically two methods are available to reliably quantify colocalized fluorophores on the single-molecule level: polarization modulation of the excitation light and antibunching experiments. The fluorescence intensity of a single emitter directly depends on the direction of its absorption dipole moment. By modulation of the linearly polarized excitation light, the fluorescence intensity of an immobilized molecule follows this modulation. In the case of several emitters, which rarely exhibit the same dipole moment orientation, the measured fluorescence intensity remains basically unchanged. Thus, a differentiation between one and more emitters can be accomplished [Güttler 1993; Ha 1996; Hofkens 2003].

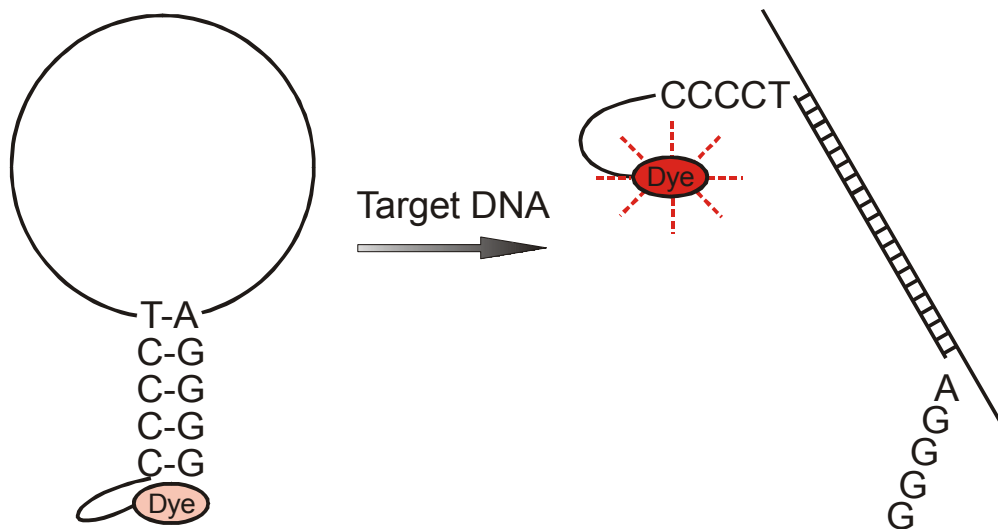


Figure 1.1: Schematic presentation of the functionality of a “smart probe”. In the closed loop form the fluorophore is quenched by guanosine nucleobases in the stem of the hairpin. Upon hybridization with target DNA dye and quenchers are separated and the fluorescence intensity is raised.

If the number of fluorophores to be determined in a colocalized spot exceeds one, the only viable approach is by photon antibunching [Zou 1990; Ambrose 1997; Michler 2000; Basche 1992]. Antibunching bases on the quantum mechanical effect that a single molecule cannot emit several photons simultaneously due to its non-zero excited state lifetime. Consequently, two consecutive photons are separated by that time in average, and the frequent appearance of lower interphoton times definitely proves the existence of more than one emitter. It has been shown on dry surfaces, that analysis of the relative interphoton arrival times facilitates a save determination for up to four emitters [Weston 2002].

A very important question in molecular biology nowadays is the revelation of the gene transcription process *in-vivo*. Transcription is known to take place in discrete sites in the cell nucleus, the so-called transcription factories. In these centers the genetic information, stored in form of DNA, is read-out and copied into messenger RNA (mRNA), which is transported into the cytoplasm for translation into proteins. It has been shown that in a single cell nucleus about 2.000 such transcription factories each with a diameter of 40 to 80 nm are located (figure 1.2) [Iborra 1996; Pombo 1999]. By measuring the amount of nascent RNA transcripts produced by a single cell, the number of active polymerase II (RNAP II) molecules has been determined to be on average between 4 and 20 in each transcription site [Cook 1999]. The reason for the accumulation in factories has not been solved yet,

as well as what the exact number of polymerase II molecules in a factory exactly is, or even if this number is always constant or not. By solving this question information about the transcription process is acquired, which is essential for the comprehension of the cell utilities, and thus for the design of *in-vivo* transcription experiments.

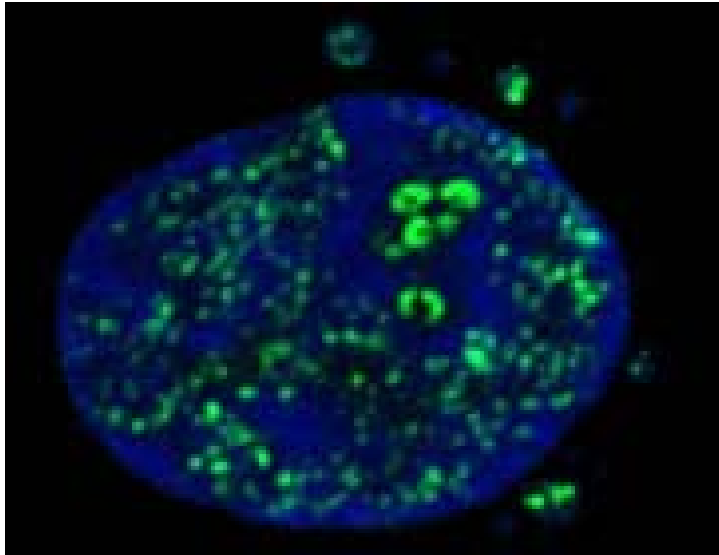


Figure 1.2: Transcription factories (green) in the nucleus of a HeLa cell. Labeling is accomplished by incorporation of Br-dUTP into nascent RNA and subsequent secondary staining with FITC-marked antibodies against bromine. The nucleus (blue) is counterstained with TOTO-3 for better visualization.

(Courtesy of Ana Pombo, MRC London)

In the second part of this work efforts towards the enlightenment of the transcription factory consistency shall be introduced. To determine the number of polymerase II molecules per transcription site, antibunching measurements with antibodies against RNAP II point out a promising pathway. In the sample preparation it has to be assured, that the antibodies are exactly stoichiometric single-labeled. This is not trivial, as both, free antibody, which blocks binding sites without being recognized, and free fluorophores, which raise the detection signal, interfere with quantitative measurements. Furthermore, it has to be confirmed, that the dye signal can be safely discriminated against the cell autofluorescence, and that the antibodies bind to the polymerase in a constant ratio. The high number of about 2.000 transcription sites per cell nucleus inhibits direct measurements by optical methods. To reduce the density, cryosections, 100 nm thick cell slices, can be used [Tokuysau 1973, 1976, 1986].

Being able to achieve a quantification of polymerases in transcription sites, or at least enable counting experiments in cellular environment on the single-molecule level, would open new perspectives for the investigation of living organisms, their structures and dynamics.

To be able to conduct this work, both localizing and quantifying, a setup is needed, which combines high-resolution optical spectroscopy with multi-parameter data acquisition. A suitable technique is Spectrally-resolved Fluorescence Lifetime Imaging Microscopy (SFLIM) [Tinnefeld 2002]. It is based on an inverted confocal microscope, and enables the simultaneous measurement of intensity, fluorescence lifetime, and spectral information of individual emitters. By combining pulsed excitation with highly sensitive Single-Photon Avalanche Diodes (SPADs) as detectors, and a PC-plug-in card for Time-Correlated Single-Photon Counting (TCSPC), the above parameters can be determined with high time and spatial resolution [Becker 1999].

Summarizing, confocal multi-parameter spectroscopy holds the capability for the resolution of structure and dynamics of molecular machines, especially in the range of the resolution gap between 10 and 200 nm. To prove its versatility, the length of a molecular DNA ruler is compared with theoretical predictions. Furthermore, in combination with antibunching experiments, this technique promises an exact and easy quantification of nanoscale complexes in a cell. By investigation of transcription factories in the cell nucleus, the exact number of polymerase II molecules in a single transcription site shall be determined.

A successful outcome of these experiments would be a major step towards the understanding of molecular machines and would make the dream of a three-dimensional cellular map become a little more real.

2 Theory

2.1 Fluorescence Spectroscopy

An important problem in physics before the adoption of the quantum theory has been the differentiation between particles and wave phenomena. At a first glance, both concepts have very little in common: Nobody would treat a flying object as a wave packet or the propagation of sound as a particle stream, but when particles and wave-lengths get smaller, things aren't so clear. In the 17th century, Newton used both theories to cover the different aspects of light, explaining its periodicity and interference as wave, as well as its linear propagation as particle phenomenon. Later, the wave-theory of light has been generally accepted, as scientists like Young and Fresnel could explain most particulate behavior within the realm of the wave-formalism. On the particle front, Boltzmann developed his gas-theory based on atomistic concepts and experiments with cathode rays. He showed that electric charges always come in multiples of the elementary charge e which is about $1.6 \cdot 10^{-19}$ Coulomb. In 1924, de Broglie assumed that, in analogy to photons, every particle of energy E and momentum \vec{p} can in fact be treated as a wave, whose frequency ω and wave-vector \vec{k} are given by:

$$\omega = \frac{E}{\hbar} \quad \text{and} \quad \vec{k} = \frac{\vec{p}}{\hbar} \quad 2.1$$

This relation was verified in 1927 in diffraction experiments with electrons by Davison and Germer [Davison 1927]. The inverse effect, particle behavior of photons, has been demonstrated in 1933 by Compton in electron-photon dispersion experiments. These considerations are referred as the Wave-Particle Dualism. It states that a light wave consists of two components, a magnetic and a electronic field vector, which are perpendicular to each other and to the propagation direction of the light (figure 2.1).

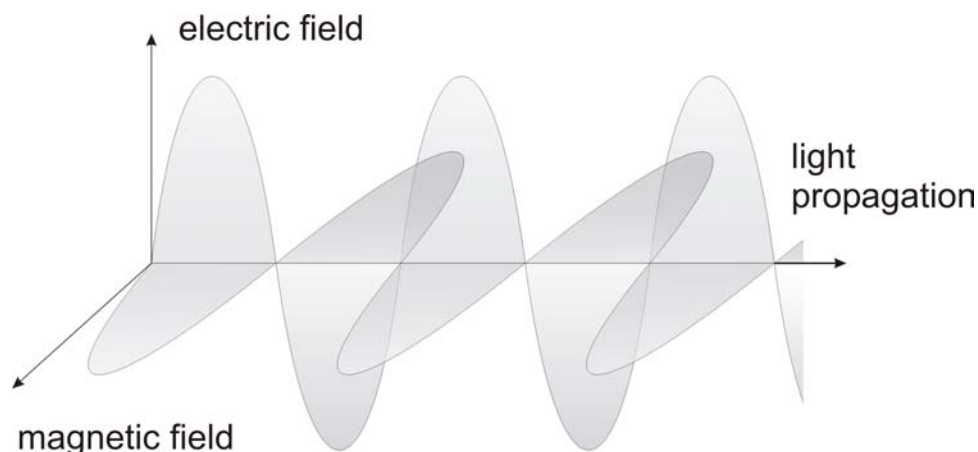


Figure 2.1: Schematic representation of light as a transverse electromagnetic wave. The two components oscillate perpendicular to each other and to the propagation direction of the light wave.

Light Absorption and Emission of Fluorescence Dyes

When a light wave and matter (e.g. a molecule) are energetically in resonance with each other, Bohr's frequency condition is valid:

$$h\nu = \Delta E = E' - E'' \quad 2.2$$

Energy can be transmitted from a light wave onto a molecule, whereby the molecule is promoted into an energetically higher state. Depending on the wavelength of the light wave, rotations ($>20 \mu\text{m}$), vibrations ($20 \mu\text{m}$ to $1 \mu\text{m}$) and electronic states ($<1 \mu\text{m}$) are excited. It has to be mentioned, that all energy levels are *quantized*, that means only discrete energies are absorbed, which can be determined by quantum mechanical calculations or absorption experiments.

Transitions can only take place, when the direction of the electric vector is oriented parallel to the electronic transition moment of the molecule. Furthermore, the transition has to be quantum-mechanically "allowed", i.e. the transition moment has to be nonzero.

Because the electronic dipole moment operator and the wave functions of ground and excited states are dependent on the electron and core coordinates, vibrations and rotations accompany transitions between electronic levels, for example in light absorption by fluorescence dyes. This leads to a huge quantity of energetically close transitions, which are broadened to absorption bands by solvent molecules or surface interactions in ensemble measurements. Absorption $A(\lambda)$ can be described and

quantified by the Lambert-Beer Law (equation 2.3), where λ is the wavelength of the incident light, $\varepsilon(\lambda)$ the molar absorption coefficient, c_i the molar concentration and d the length of the light path through the sample.

$$A(\lambda) = \log_{10} \frac{I_0}{I(\lambda)} = \varepsilon(\lambda)c_i d \quad 2.3$$

Transitions with their molecular electronic states and relative energies can be presented best in a Jablonski diagram (figure 2.2). Singlet ground electronic state, S_0 , as well as singlet first, S_1 , and higher electronic excited states, S_N , are shown. At each energy level, fluorophores can exist in a number of vibrational energy levels, represented by the multiple lines of the electronic states. The spacing between these energy levels is about 1500 cm^{-1} , which exceeds the energy necessary to populate excited vibrational states by thermal energy at room temperature. Transitions between states are depicted by lines that traverse between ground and excited states. Electronic transitions are almost instantaneous in nature, often occurring in time frames ranging from nano to sub-pico seconds, which are far too short to observe a significant lateral displacement of nuclei during fluorescence and phosphorescence events (Franck-Condon Principle).

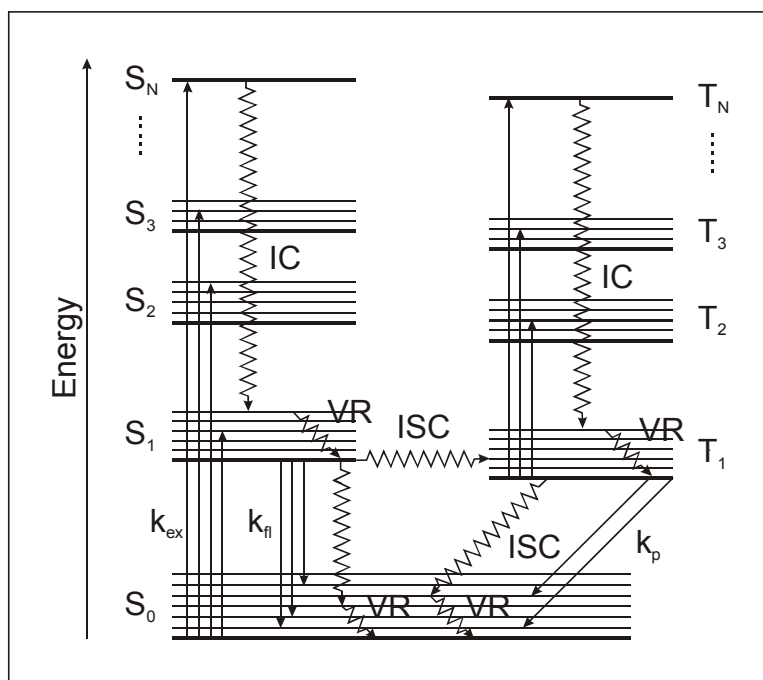


Figure 2.2: Jablonski diagram showing the molecular electronic states (horizontal lines) with their relative energies. Excitation and relaxation processes are depicted by arrows. Radiative transitions are specified with straight arrows, while radiationless transitions are shown as wavy arrows.

When a fluorophore absorbs energy in the form of light, the molecule is usually excited to a higher vibrational energy level in an excited state before rapidly relaxing to a lower energy level. This event, depicted VR, is termed *vibrational relaxation* and

occurs on picosecond time scale. If a molecule is excited into higher electronic excited states ($S_N, T_N; N>1$), the relaxation to the corresponding first excited state takes place by *internal conversion, IC*. In case of the first singlet state the decay to the ground state is called fluorescence. Fluorescence lifetimes are typically four orders of magnitude slower than *vibrational relaxation*, giving the molecules sufficient time to achieve a thermally equilibrated lowest-energy excited state prior to fluorescence emission. Phosphorescence is similar to fluorescence, except the electron undergoes a spin conversion into a formally forbidden triplet state, T , instead of the lowest singlet excited state, a process known as *intersystem crossing, ISC*. Emission from the triplet state usually occurs with lower energy relative to fluorescence, hence emitted photons have longer wavelengths. With delayed fluorescence, the electron first decays into the triplet state, and then is excited into the lowest singlet excited state before returning to the ground state.

It is interesting to note that the emission spectrum of a fluorophore is typically a mirror image of the S_0 to S_1 absorption spectrum. This is due to the fact that electronic excitation does usually not alter the molecular geometry significantly and the spacing of excited state vibrational levels is similar to that of the ground state. The result is that fluorescence emission spectra often display similar, but reversed vibrational structures to those observed in the absorption spectra.

The above-mentioned processes, which lead to fluorescence or more general, to the emission of light, do not convert all absorbed energy into light, but do also produce heat, which is mainly dissipated in impacts with other molecules, for example the solvent. If the irradiated energy cannot be released quick enough by the molecule, photobleaching is likely to happen (figure 2.3).

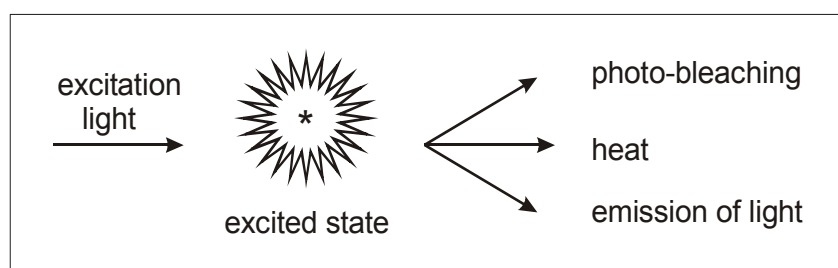


Figure 2.3: After excitation a molecule can take three different pathways for relaxation: photobleaching, heat development or emission of a photon.

Photobleaching denotes a fluorophore, which permanently loses its ability to fluoresce due to photon-induced chemical damage and covalent modification of its structure. Upon transition from an excited singlet state to the excited triplet state, fluorophores may interact with other molecules to produce irreversible covalent

changes. The triplet state is relatively long-lived with respect to the singlet state, thus allowing excited molecules a much longer timeframe for chemical reactions with components in the environment. The average number of excitation and emission cycles that occur for a particular fluorophore before photobleaching is dependent on its molecular structure and local environment. Some fluorophores bleach quickly after emitting only a few photons, while others are more robust and undergo thousands or millions of cycles before decomposition.

Fluorescence Lifetimes and Time Correlated Single-Photon Counting

The transition of a molecule from the first electronic excited state, S_1 , back to its ground state, S_0 , by fluorescence emission takes place on the nanosecond (10^{-9} s) timescale. The average time over an ensemble of transition cycles leads to the fluorescence lifetime τ . In this work, the fluorescence lifetime of single molecules is determined by Time-Correlated Single-Photon Counting (TCSPC) [Connor 1984], whose operation mode is explained in the following.

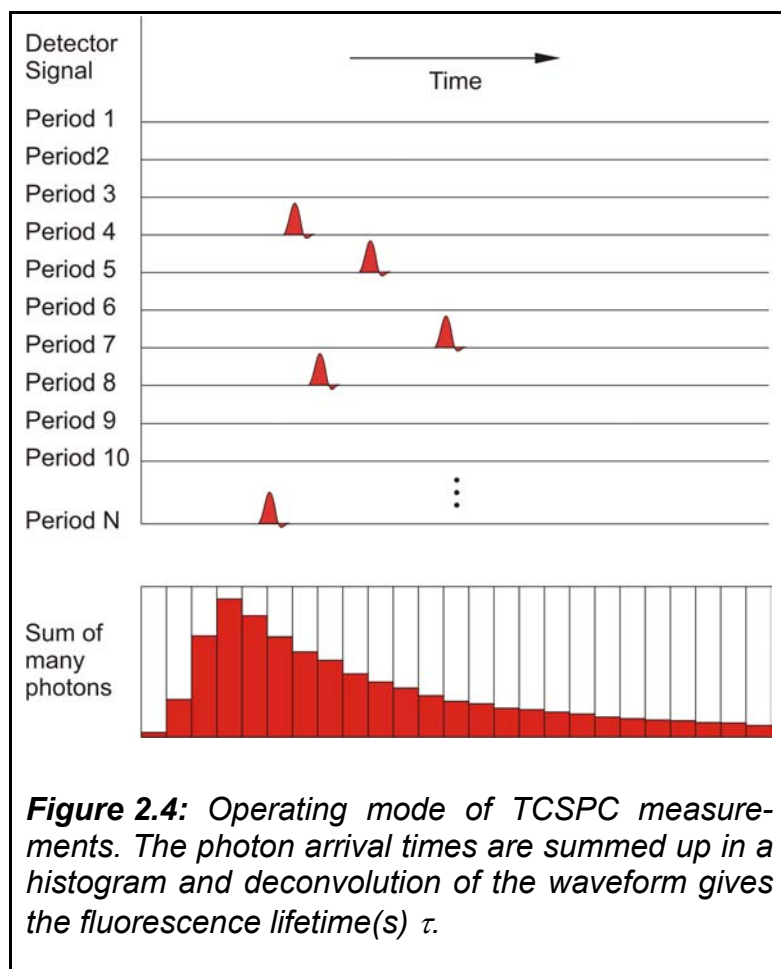


Figure 2.4: Operating mode of TCSPC measurements. The photon arrival times are summed up in a histogram and deconvolution of the waveform gives the fluorescence lifetime(s) τ .

TCSPC is based on the detection of single photons, the measurement of the detection times of the individual photons with respect to the exciting laser pulse, and the reconstruction of the waveform from the individual time measurements. The TCSPC technique uses the effect that for high repetition rates the light emission intensity is so low, that the probability to detect one photon per signal period is far below one. Thus, the detection of several photons in one pulse can be

neglected and the principle shown in figure 2.4 is used. The detector signal represents individual photons in the time domain, which arrive in the form of a series of randomly distributed pulses. Most signal periods are without photons, the others mostly contain one photon pulse, while periods with more than one photon are very rare. When a photon is detected, the time of the corresponding detector pulse is measured and the event is collected in a memory by adding a count to a channel proportional to the detection time. After many photons, the histogram of the detection times, *i.e.* the waveform of the optical pulse, builds up. This method is very exact, because the accuracy of the time measurement is not limited by the width of the detector pulse. Thus, the time resolution is much better than the same detector used with an oscilloscope or any other analog signal acquisition device. All detected photons contribute to the result of the measurement, as there is no counting loss due to *gating*. Depending on the desired accuracy, the excitation power must not be higher than 0.01 to 0.1 photon counts per signal period, otherwise the so-called pile-up effect may occur.

The acquired histogram can be analyzed by several methods, of which least-square fitting and maximum likelihood estimation (MLE) are the most prominent. In several publications these two methods are discussed with the result that for fluorescence lifetime determinations of single molecules, the MLE tends to be more reliable, and its algorithm was exclusively used in this work [Tellingh. 1993, Soper 1994, Maus 2001]. The MLE is based on the following relation:

$$1 + \left(e^{-T/\tau} - 1 \right)^{-1} - m \left(e^{-mT/\tau} - 1 \right)^{-1} = N^{-1} \sum_{i=1}^m i N_i \quad 2.4$$

T is the width of each channel, m the number of utilized time channels (bins), N the number of photon counts considered, and N_i the number of photon counts in time channel i . Equation 2.4 was numerically solved with respect to the fluorescence lifetime τ using the Newton algorithm.

It should be mentioned, that the equation holds only for mono-exponential decays disregarding the convolution with the laser pulse. Free dyes often show mono-exponential fluorescence kinetics. Multi-exponential decays, for example, occur with linked dyes, dyes in viscose solvents, or in photo-induced electron transfer reactions [Becker 1999, Sauer 1999].

In this work mostly fluorescent dyes linked to biomolecules are used, which should show multi-exponential decays. For the analysis of single molecule lifetimes, mostly too few photon counts for a multi-exponential lifetime fitting are acquired. In first approximation, it is tolerable to assign a single “average” lifetime, if the fraction of the main lifetime component is close to one, or if the single lifetimes of a multi-exponential decay do not differ significantly from each other. In this work, fluorescence lifetimes were used to separate background from real signal, and to distinguish fluorescence dyes from each other. With two different dyes, the fluorescence emission is spectrally split onto two detectors by a beamsplitter, which allows estimating the fluorescence lifetimes separately as two quasi mono-exponential decays.

Basics of Single Molecule Spectroscopy

“Recent advances in single-molecule detection and single-molecule spectroscopy at room temperature by laser-induced fluorescence offer new tools for the study of individual macromolecules under physiological conditions” states the first sentence of a Science review published about five years ago [Weiss 1999]. Already at this time the biological context played an important role in this originally pure physical discipline, though first successful experiments with single fluorophores were accomplished not until the early 90’s [Shera 1990; Moerner 1989]. Nowadays almost every research project in single-molecule spectroscopy is somehow engaged into biology or biochemistry. This leads to the question what special properties are available by investigating single molecules instead of an ensemble.

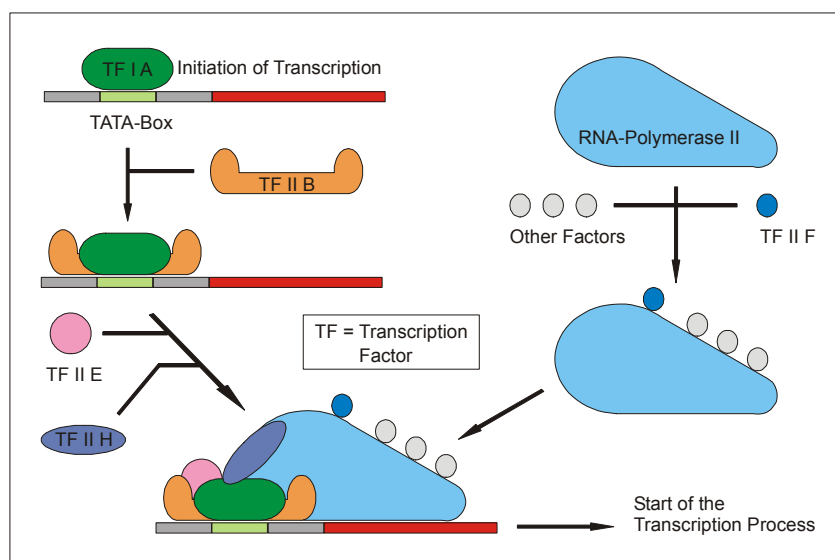


Figure 2.5: Aggregation of cofactors around a polymerase II enzyme in gene transcription.

First, it is possible to study progression or sequential dynamics. In a series of single reaction steps, like in the aggregation of cofactors around an enzyme (figure 2.5), the single events can not be resolved in details, because not all steps run parallel, but rather follow kinetic rate laws. On the single-molecule level, the individual members of a population can be identified and sorted, which allows the quantitative comparison of subpopulations [Tinnefeld 2002; Neuweiler 2002].

Another advantage of single-molecule spectroscopy arises from the fact, that single molecules exist in particular conformational states depending on their local environment. Monitoring of population averages only leaves the essential dynamic and mechanistic features of biological molecules undetected. At low temperatures conformational changes are slower and the motions become accessible to investigation. Under these conditions optical spectra can be obtained without the presence of inhomogeneous broadening, allowing to research populations exhibiting energetically close transition steps (figure 2.6) [Göhde 1997; Vácha 1999].

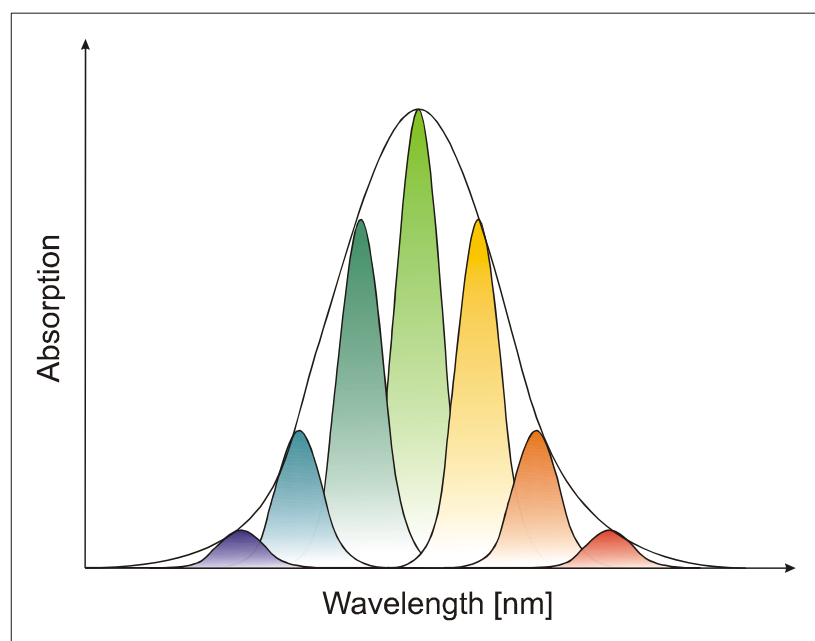


Figure 2.6: Absorption spectra of different molecules with energetically close transition steps at room (black) and the single resolved spectra at low temperatures (colored).

Finally, in combination with other experiments, single-molecule methods allow the determination of mechanical or electrical properties in biomolecules. By atomic force microscopy for example, the binding energy and conductivity of organic macromolecules can be analyzed [Hernando 2004; Kim 2004].

To be able to successfully accomplish single-molecule experiments within an acceptable error, it has to be assured that the maximal possible information is deduced from each fluorophore. A typical dye molecule, for example a rhodamine in

ethanol, emits about $1.7 \cdot 10^6$ photons until photo-destruction [Soper 1991]. With ultra-sensitive instrumentation an overall detection efficiency of about 5 % can be reached [Nie 1997]. Consequently, 10^4 to 10^5 photons are observed from a typical single fluorophore [Ambrose 1997], sufficient not only for single-molecule detection, but also for spectroscopic identification and real-time monitoring over an extended time period.

Beside the photo-stability of a fluorophore the background intensity plays a crucial role in single-molecule spectroscopy. The background mostly arises from three different sources: (a) Raman scattering, (b) Rayleigh scattering, and (c) fluorescence from impurities. Most of the background interference can be removed by the use of ultra-pure solvents and appropriate optical filters, which block the Rayleigh scattering. However, the key to single-molecule sensitive measurements is the minimization of the background by a reduction of the detection volume, because the signal from a single fluorophore is independent of the probe volume, whereas the background rises proportional with size. For illustration, a focused laser beam illuminates a volume of about one femtoliter (10^{-15} l), which in the case of water contains approximately 10^{10} solvent molecules. Thus, a fluorescent impurity of as few as 0.0001 % would already mean that 1.000 interfering molecules are present in this little detection volume.

The reduction of the excitation volume can be achieved by laser excitation in (A) near-field, (B) evanescent, and (C) confocal configurations, as displayed in figure 2.7 [Dunn 1999; Axelrod 1992; Schmidt 1996].

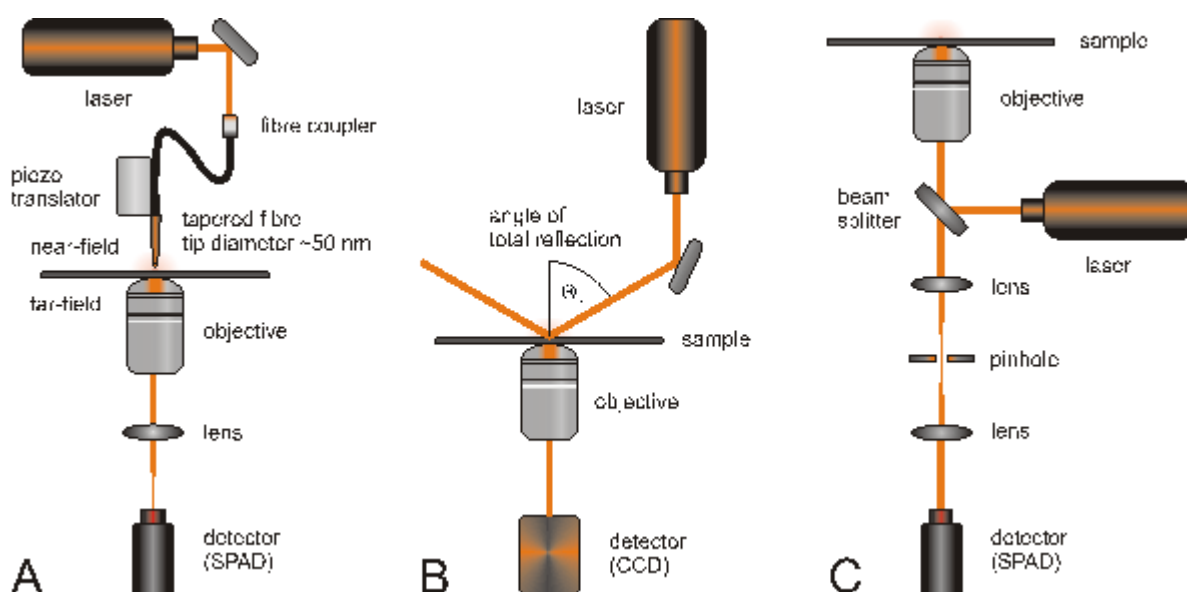


Figure 2.7: Comparison of the three most frequently used setups for single-molecule detection: (A) near field, (B) evanescent, and (C) confocal excitation.

As most optical single-molecule techniques nowadays base on at least one of these methods, they are discussed in the following:

Near-field Scanning Optical Microscopy (NSOM) has been developed primarily to break the optical diffraction limit, which restricts the spatial resolution of conventional optical measurements to approximately half of the light wavelength ($\lambda/2$). In NSOM a spatial resolution in the order of 50 to 100 nm is achieved by positioning the sample within a few nanometers distance to the optical aperture, so that photons emitted by the light source do not have enough distance to experience diffraction [Nie 1997]. In most NSOM setups the molecules are excited through an optical fiber with an outlet diameter of around 50 nm, and the fluorescence is collected through an objective in the far-field, but also near-field detection can be applied (figure 2.7 A). It has been shown that NSOM is suitable for surface imaging, the determination of dynamics and dipole orientations of single-molecules, and for simultaneous atomic force measurements [Garcia 1998; Betzig 1993; Trautman 1994; Hernando 2004]. The advantages on the near-field side consist in a higher spatial resolution and the ability to correlate spectroscopic with topographic information. However, NSOM suffers from several limitations, such as limited excitation power density and sample perturbation by the aluminium coated fiber probe [Ambrose 1994; Xie 1994].

Evanescent wave excitation is commonly achieved by total internal reflection at the glass to liquid or glass to air interface. At this interface the optical electromagnetic field does not abruptly drop to zero, but rather drops exponentially into the liquid or air phase. The decaying optical field can excite molecules in a thin layer of up to about 150 nm to this interface. Although the field of view is wide, the illuminated volume is extremely thin providing a small overall excitation volume (figure 2.7 B). This technique is particularly suitable for imaging single molecules at electromagnetic boundaries and has allowed the observation of fluorescently labeled myosin and kinesin molecules, as well as individual ATP turnover reactions [Vale 1996; Funatsu 1995].

In confocal microscopy a laser beam is brought to a near diffraction-limited focus inside a sample using a high numerical aperture objective [Pawley 1995]. The fluorescence is collected through the same objective and the emission light is separated from excitation light by a dichroic beamsplitter (figure 2.7 C). A pinhole (50 to 100 μm in diameter) is placed at the image plane in the detection path to reject signal from defocused regions. In this arrangement a small detection volume of

around one femtoliter is realized, which is suitable for the detection of single molecules [Eggeling 2001; Deniz 2001]. Meanwhile this technique finds broad application, for example in the detection of tumor antibodies and pathogenic DNA in solution [Neuweiler 2002; Knemeyer 2000], and in the study of biomolecular systems by imaging and tracking of single fluorophores and quantum dots [Weiss 2001; Xu 1997; Michalet 2001].

The development of high precision piezo-translators and the availability of sufficiently fast computer processors in the recent years made possible the simultaneous acquisition of a variety of independent fluorescence parameters, *e.g.* intensity, spectral characteristics, fluorescence lifetime, and position. In this work mainly a confocal setup based on Spectrally-resolved Fluorescence Lifetime Imaging Microscopy (SFLIM) [Tinnefeld 2002] is used, which allows multi-parameter data collection, and additionally, with one some minor changes, the quantification of fluorophores by polarization modulation and antibunching experiments [Güttler 1993; Weston 2002].

Recapitulating, single-molecule techniques not only proved their outstanding applicability for the investigation of dynamics and structures of molecular assemblies, but also showed their complementarity to other perceptive methods like AFM. This makes single-molecule detection an excellent tool for highly sensitive biological *in vitro* and *in vivo* experiments.

2.2 Cell Biology

DNA, RNA and Proteins

Life depends on the storage, conversion and duplication of the genetic information. This information is stored in the genes, which consist of a linear sequence of four different deoxyribonucleic acids, commonly abbreviated DNA. The DNA function was discovered in the 1940s and its structural determination by Watson and Crick [Watson 1953], who received the Nobel Prize for this discovery in 1962, initiated a new era in cell biology.

DNA consists of two helically wound strands, which contain the information the cell requires to synthesize proteins and to replicate itself. There are basically four building blocks, the nucleotide bases, which make up DNA: adenine (A), guanine (G),

thymine (T) and cytosine (C). Each base primarily binds to its complementary base, A to T, and G to C. Natural DNA molecules are incredibly long: the human genome for example contains 3 billion nucleobases. DNA is divided into bits and is tightly wound into chromosomes; humans have 23 chromosome pairs. These chromosomes are further broken down into about 70.000 genes, which all have different functions.

Double-stranded DNA (dsDNA) is a very stiff molecule [Hogen 1987]. However, dsDNA in solution is not exactly straight, it is rather bent and curves locally as a result of thermal fluctuations. Such fluctuations shorten the end-to-end distance of the molecule. This purely entropic elasticity can be investigated by applying a variety of forces, for example hydrodynamic drag [Perkins 1995], magnetic beads [Smith 1992], glass needles [Cluzel 1996] or optical traps [Smith 1996; Wang 1997].

Two models are commonly used to describe the behavior of dsDNA. In the freely jointed chain (FJC) model, the molecule is made up of rigid, orientationally independent segments, whose length is a measure of the chain stiffness. The alignment of segments by tension is described by the Boltzmann distribution. In the inextensible worm-like chain (WLC) model, the molecule is treated as a flexible rod of length L that curves smoothly as a result of thermal fluctuations:

$$\frac{FP}{k_B T} = \frac{1}{4} \left(1 - \frac{x}{L} \right)^{-2} + \frac{x}{L} - \frac{1}{4} \quad 2.5$$

The rod's local direction decorrelates at the distance s along the curve, according to $e^{-s/P}$, where the decay length P is the persistence length of the chain [Austin 1997; Bustamante 1994]. The stiffer the chain, the longer the persistence length is. For dsDNA in physiological salt, the persistence length reaches about 50 nm. Forces F in the order $k_B T/P = 0.1$ pN, where k_B is the Boltzmann constant and T the temperature, are required to align polymer segments with these dimensions.

The importance of DNA in biology is very big. Its sequence is comparable to a language that instructs the cell to manufacture particular proteins. An intermediate

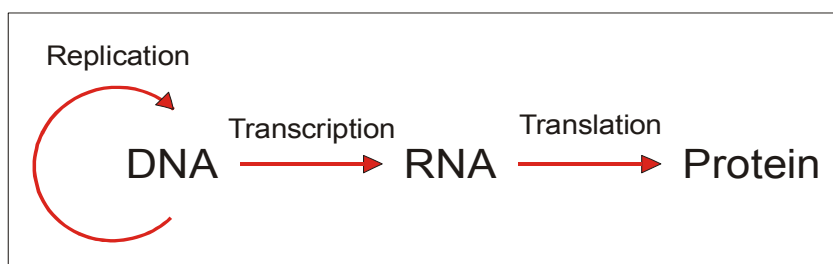


Figure 2.8: *The Central Dogma of Life. DNA is transcribed into RNA, which induces proteins synthesis by translation.*

language, RNA, encoded in the sequence of ribonucleic acid, translates a message of a gene into the amino acid sequence of a protein. Proteins exclusively accomplish structural and functional tasks in a cell. The pathway from DNA to RNA to proteins, which is not invertible (with the exception of retroviruses), is called the Central Dogma of Life (figure 2.8).

RNA is similar to DNA; they both are nucleic acids of nitrogen-containing bases joined by a sugar-phosphate backbone. However, structural and functional differences distinguish RNA from DNA. Structurally, RNA is single-stranded, whereas DNA is double stranded. DNA has thymine, where as RNA has uracil. RNA nucleotides include the sugar ribose, rather than the deoxyribose that is part of DNA. Functionally, DNA maintains the protein-encoding information, whereas RNA uses the information to enable the cell to synthesize the particular protein. An overview over the similarities and differences between DNA and RNA is given in table 2.1:

| RNA | DNA |
|-----------------------------------|--|
| Single-stranded | Double-stranded |
| Uracil as a base | Thymine as a base |
| Ribose as sugar | Deoxyribose as the sugar |
| Uses protein-encoding information | Maintains protein-encoding information |

Table 2.1: Comparison of the differences and similarities of deoxyribonucleic (DNA) and ribonucleic acid (RNA).

Transcription and Translation

On the biological side of this work, experiments for the localization of polymerases in the cell nucleus were done. Therefore a deeper view into the principles of transcription and translation shall be given.

Transcription is the process of creating RNA, the transcript, from a template DNA in the cell nucleus [Kimura 2002]. In the synthesis of proteins three different types of RNA participate with different tasks: messenger RNA (mRNA) transports the genetic information forward from DNA and is used as a template for protein synthesis, ribosomal RNA, rRNA, is a major constituent of the cellular particles called ribosomes, on which protein synthesis actually takes place, and transfer RNA, tRNA, is incorporated in particular amino acid subunits, which recognize specific base groups of the mRNA. Messenger RNA transmits information of a gene to cellular

structures that build proteins. Each three mRNA bases in a row form a codon that specifies a particular amino acid. Ribosomal RNA and proteins form ribosomes, which physically support the other participants in protein synthesis and help to catalyze bond formations between amino acids. In eukaryotes, RNA is often altered before it becomes active (figure 2.9):

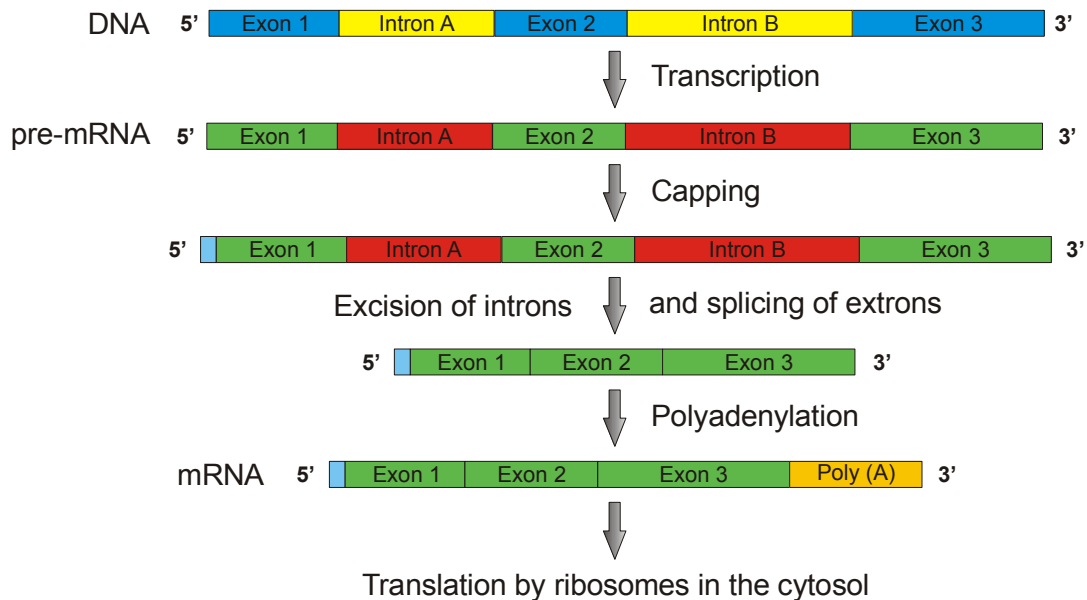


Figure 2.9: Biochemical pathway from DNA to mRNA on the example of an eukaryotic cell. By transcription, capping, splicing and adenylation, a mRNA strand is synthesized, which is then transported into the cytosol for translation.

First the messenger RNA gains a cap of modified guanine, which is attached to the 5' end of the pre-mRNA as soon as it is produced by RNA polymerase II (RNAP II). The cap protects the RNA from being degraded by enzymes that digest RNA from the 5' end. Then the introns are removed step-by-step and the remaining exons are reattached by ribozymes. This process is called splicing. When transcription is complete, the transcript is cut at a site and a poly(A) tail consisting of more than 50 adenine nucleobases is attached to the exposed 3' end. This completes the mRNA molecule, which is then exported into the cytosol.

As translation begins, mRNA, tRNA with bound amino acids, ribosomes, energy molecules and protein factors, assemble. The mRNA leader sequence binds to rRNA in a small subunit of a ribosome and the first codon attracts a tRNA bearing methionine. Next, as the chain elongates, the large ribosomal subunit attaches and the appropriate anticodon parts of tRNA molecules form peptide bonds, a polypeptide grows (figure 2.10). At a stop codon, protein synthesis ceases. As translation

proceeds, protein folding begins with the help of shape giving enzymes and chaperone proteins.

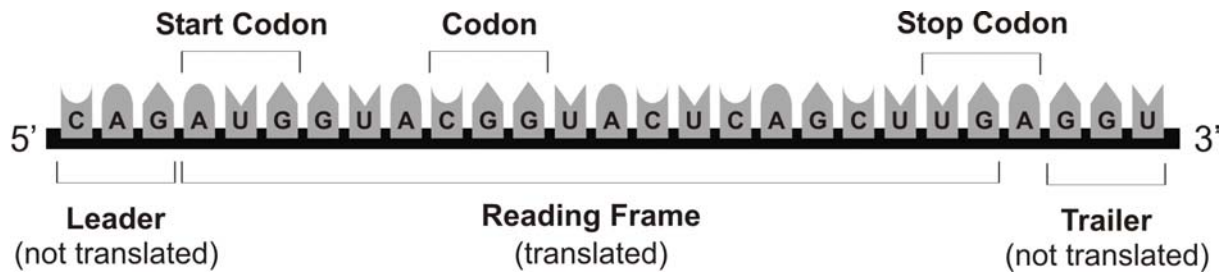


Figure 2.10: Translation of mRNA and its recognition system. Start and stop codons mark the area where the information to be translated is situated. Three nucleobases of the readout correspond to one amino acid.

Generally, the amount of a certain protein produced depends directly on how much RNA transcript is created. If a cell needs more of a protein, it synthesizes more RNA, which is exported to the cytoplasm and translated. If the cell wants to stop gene expression, it stops RNA transcription and the protein synthesis turns off, because RNA molecules are rapidly degraded by nucleases inside the cell.

Polymerases and Transcription Factories

As mentioned above, transcription takes place in the cell nucleus by RNA polymerases (RNAPs). In eukaryotes, three different species of these huge multi-subunit protein complexes with a molecular mass of several hundred kilo-Daltons (kDa) are found: RNA polymerase I transcribes the rRNA genes for the precursor of the 28S, 18S, and 5.8S molecules and is the busiest of the RNA polymerases. RNAP II synthesizes mRNA from protein-encoding genes, while RNA polymerase III produces the 5S rRNA and all the tRNA genes [Lee 2000].

Polymerases are generally not spread throughout the nucleoplasm, but rather are concentrated in 10.000 discrete sites with diameters of 40 to 80 nm each [Fay 1997; Iborra 1998; Jackson 1998; Pombo 1999, Wansink 1996]. Because each site contains on average 125 polymerase I or on average 8 polymerase II enzymes plus associated transcripts, such sites have been named transcription factories.

Although the function and exact composition of the polymerase II factories is not understood completely, much is known about polymerase I. For example, fibrillar centers store polymerase I for transcription. The process is initiated as rDNA slides

through polymerases on the centers surface, and nascent rRNA is extruded into the so-called dense fibrillar component. After termination, the rRNA moves to the granular component for maturation (capping, splicing, adenylation) [Hozák 1994]. While most RNAP I is present in fibrillar centers (pol I transcription factories), the distribution of active polymerase II molecules is less clear and complicated by the fact that only about 25% of the polymerases seem to be active [Iborra 1996, Jackson 1998].

Antibodies

Antibodies are immune system related units called immunoglobulins (Igs). An antibody monomer consists of four polypeptides, two heavy chains and two light chains, which are joined by disulfide bridges to form an Y-shaped molecule (figure 2.11):

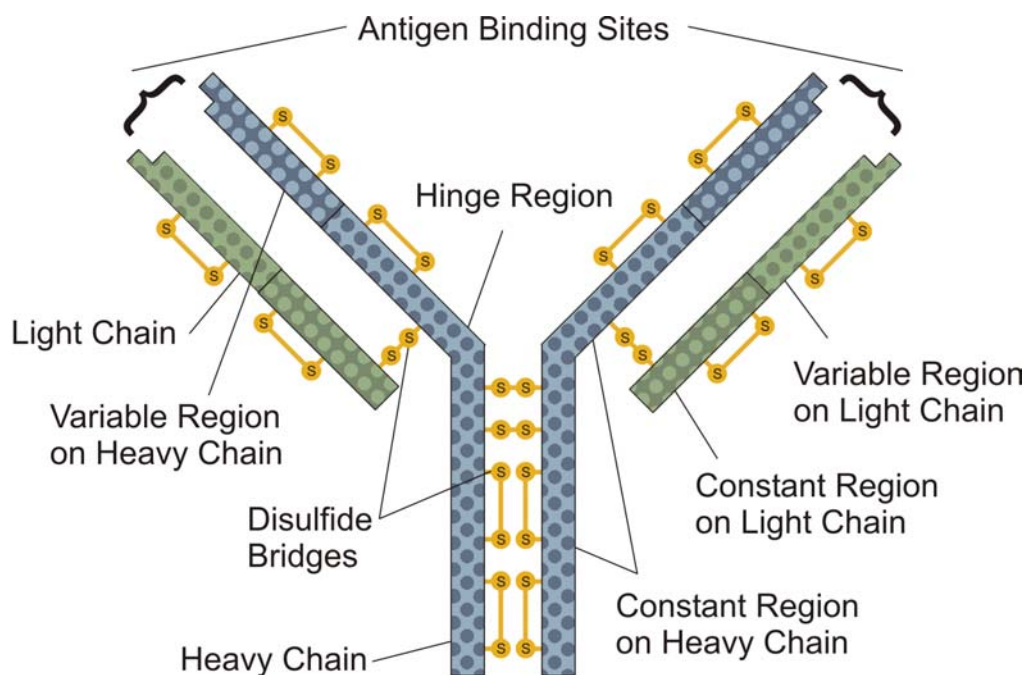


Figure 2.11: Structure of a monomer antibody subunit. Heavy and light chains are connected by disulfide bonds, which give the antibody its characteristic Y-shape.

The amino acid sequence in the tips of the Y varies greatly among different antibodies. This variable region, composed of about 120 amino acids, gives the antibody its specificity for antigen binding. The variable region includes the ends of the light and heavy chains. If the antibody is treated with a protease, this region can

be cleaved producing the so-called *Fab* fragments, which are active for antigen binding. The constant region determines the mechanism used to destroy antigen. The variable region is further divided into hypervariable, *HV*, and framework, *FR*, regions. Hypervariable regions have a high ratio of different amino acids in a given position relative to the most common amino acid in that position. Within light and heavy chains, three such regions exist – *HV* 1, 2 and 3. Four *FR* regions, which have more conserved amino acid sequences, separate the *HV* parts. The *HV* regions directly contact a portion of the antigen's surface. For this reason, *HV* regions are also sometimes referred to as complementarity determining regions, or *CDRs*. The *FR* regions form a beta-sheet structure, which serves as a scaffold to hold the *HV* regions in position to contact antigen.

Antibodies are divided into five major classes, IgA, IgD, IgE, IgG, and IgM, but the three most abundant are the classes A, G, and M.

IgA antibodies are exported into glands found in the alimentary, respiratory, urinary, and genital tracts. They help to protect against infections. The IgA molecule has a dimeric structure made up of two Y-shaped molecules linked together at the ends of the constant heavy chains by a *J* (joining) chain, a polypeptide with a molecular mass of ~17 kDa. Altogether there are about 10^{10} cells that release IgA antibody.

The monomeric IgD antibody is found in trace amounts in the blood serum and serves as a surface receptor for B-type lymphocytes.

Immunoglobulines E are rare. They are responsible for allergic reactions and are synthesized by B-cells that lie below the respiratory and intestinal surfaces. Stimulated by the presence of an antigen, IgE triggers the release of histamine in response. On the other side the same IgE response is also responsible for hay fever, asthma, and eczema.

IgG antibodies are the major ones found in plasma and body fluids and the ones that activates complement proteins. They consist of the basic Y-shaped structure and easily disperse into tissues. For instance, small amounts are normally found in the cerebrospinal fluid surrounding the brain. IgG is particularly effective against certain bacteria, viruses, and toxins.

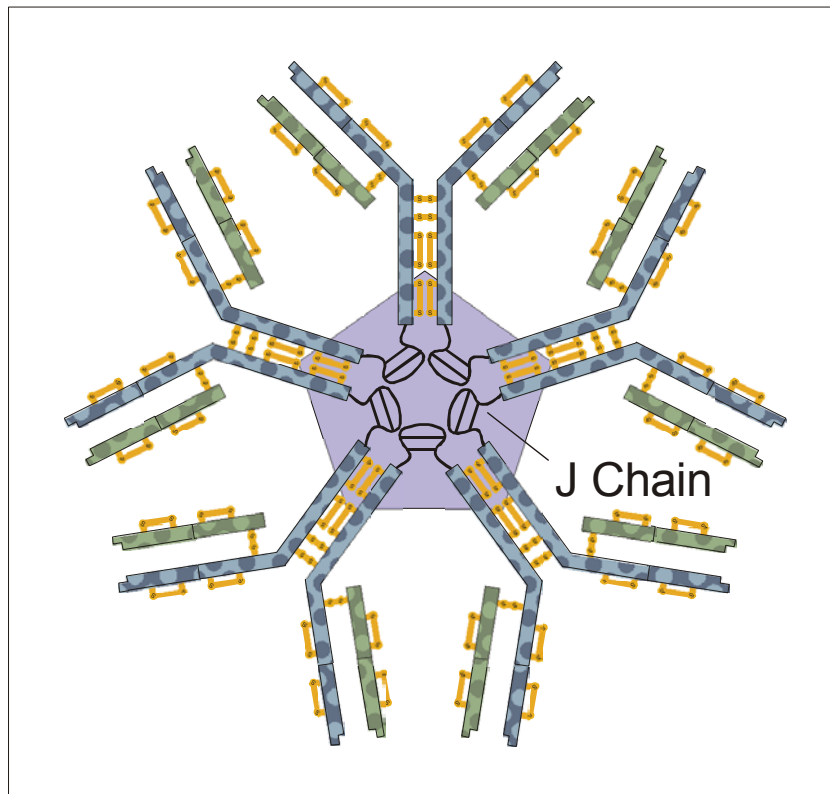


Figure 2.12: Schematic structure of an IgM antibody. The five monomer units are linked with J chains, polypeptides with a molecular mass of ~17 kDa each.

IgM is the largest type of antibody (figure 2.12). It is found in blood plasma in the form of five J chain linked monomers [Fazel 1997]. This induces that with five times more binding sites for antigen, the IgM molecule is far more powerful than an IgG or IgA. In an immune response first IgM appears, often one day or two before IgG, but is then stepwise replaced by IgG antibodies. It is also the first to appear in the fetal development, and it is the most ancestral type of antibody, which has been found in primitive fishes.

3 Materials and Methods

In this chapter the instruments and fundamental procedures used in this work are introduced. First the single-molecule setup and several software programs are explained, followed by the illustration of various labeling strategies for biomolecules, including cell culturing and cell fixation. Finally selected laboratory equipment, chemicals and standard procedures are presented.

3.1 Setup for Spectrally Resolved Lifetime Imaging Microscopy (SFLIM)

Almost all experiments in this work have been designed for measurements on the single-molecule level. Thus, the setup for Spectrally Resolved Lifetime Imaging Microscopy (SFLIM), used with several variations depending on the problem, takes a major place in this and the consecutive chapter. A schematic diagram of the basic version of the setup is given in figure 3.1.

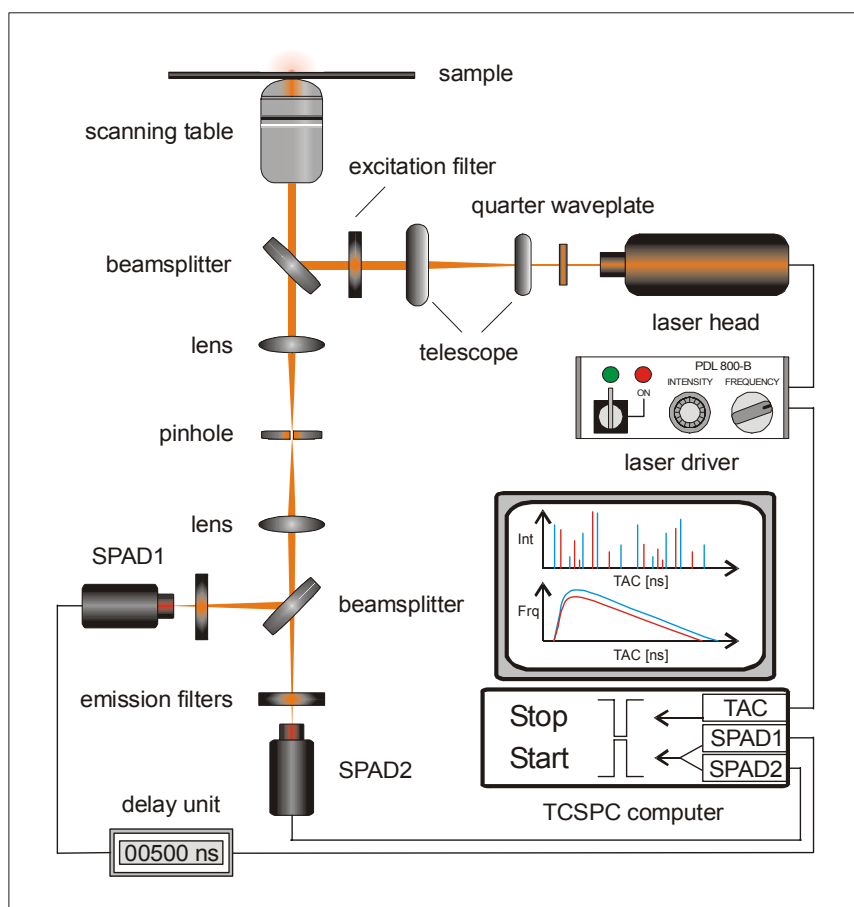


Figure 3.1: Scheme of the main components of the SFLIM setup. A laser diode emitting at 635 nm is focused through an objective onto the sample. The fluorescence signal is collected by the same objective and focused through a pinhole onto two spectrally separated detectors.

First an overview of the setup is given, before the single components with additional features are discussed.

A fiber coupled, pulsed 635 nm laser diode (LDH-P-635, Picoquant GmbH, Berlin) and two spectrally separated detectors are employed in a sample scanning confocal microscope. The collimated laser beam is sent through a band-pass filter and directed into the side port of an inverted microscope (Axiovert 100TV, Carl Zeiss AG, Jena). Within the microscope, the beam is reflected by a dichroic mirror and focused to a tight spot by an oil-immersion objective (100 x, NA 1.4, Nikon Corp., Japan, or alternately Olympus GmbH, Hamburg). The emitted fluorescence is collected by the same objective and passed through a pinhole to suppress signal from scattered light. A beamsplitter (685DCLP, Chroma Technology Corp., USA) spectrally splits the beam and focuses it through emission filters onto the active areas of two avalanche photo diodes, APDs. The sample x, y and z positions are controlled using a closed-loop piezostage with a parallel PC interface for imaging the sample and positioning individual fluorescing spots in the focused excitation beam. Signals are fed into the router of a TCSPC PC interface card and the laser SYNC signal is connected to the boards SYNC input. In this arrangement, both of the APD signals can operate as the start signal of the time-to-amplitude converter, TAC, and the laser SYNC operates as the stop signal. Time-resolved data are acquired using the FIFO mode, in which the microscopic and macroscopic arrival time, as well as the detection channel are registered for each fluorescence photon detected.

The Excitation Source

As excitation source a fiber coupled, pulsed 635 nm laser diode with a repetition rate tunable in steps between 10 and 80 MHz (PDL800B, Picoquant GmbH, Berlin) is used. For SFLIM experiments 40 MHz is applied, because at 80 MHz the excitation intensity tends to oscillate. The pulse width of the laser beam is less than 90 ps FWHM (full width half maximum), but depends on the excitation energy, which is continuously adjustable up to 1 mW. The exact emission wavelength of the diode is limited by the temperature and the applied power (figure 3.2).

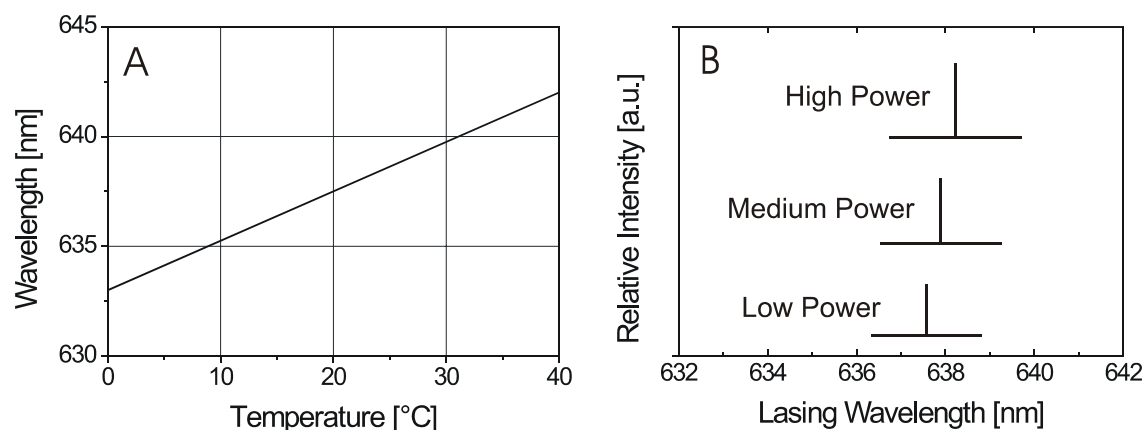


Figure 3.2: Typical temperature (A) and power dependence (B) of a laser diode emitting at 635 nm. With increasing power and rising temperature the emission wavelength is shifted towards longer wavelengths.

Because of the varying emission wavelength of the laser light, an excitation filter has to be implemented into the optical path. A complete list of all filters used is given in chapter 3.2. Alongside the filtering, the polarization vector of the light is oriented by a revoluble $\frac{1}{4}$ -waveplate for linear and circular excitation light, respectively. The circular shape of the laser beam profile is widened by two achromatic telescope lenses until the bottom outlet lens of the objective is outshone completely, which leads to a homogenous illuminated light field in the objective.

The Detector

As detectors avalanche photodiodes (APDs) model AQR-14, from Perkin Elmer (Perkin Elmer Optoelectronics, Canada) are deployed. These semiconductor photon counters are highly sensitive in the wavelength region from 500 to 850 nm. In figure 3.3 the sensitivity is plotted versus the wavelength.

Especially in the emission region of red absorbing fluorescence dyes, which emit between 620 and 750 nm, the APD exhibits its optimal detection efficiency of up to 70 %, which is considerably higher than the yield of photomultipliers [Louis 1988]. The active areas of the avalanche photodiodes hold a diameter of 180 μm , a dark-count rate of 80 to 100 Hz, and a maximum count rate of a few thousand kHz.

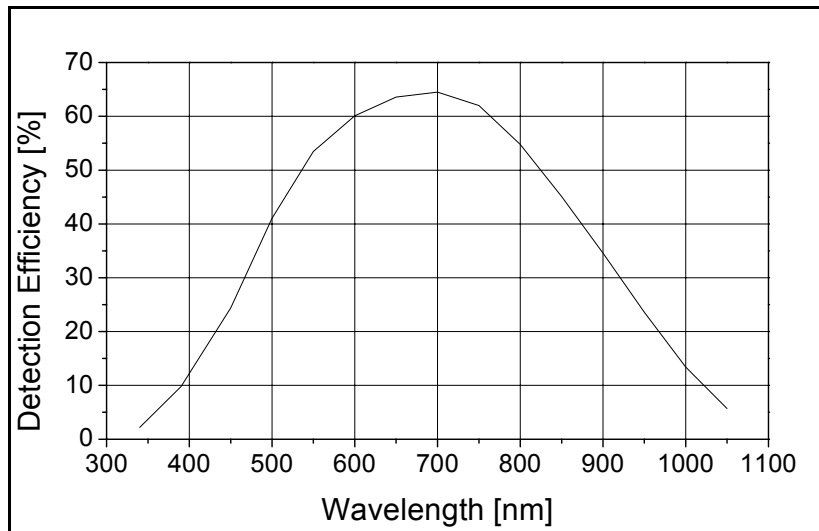


Figure 3.3: Photon detection efficiency of an APD of the AQR-14 series at different wavelengths. The efficiency reaches its maximum just below 700 nm, in the region where the red absorbing dyes used in this work emit.

The Scanning Stage

For imaging experiments the scanning stage NPS-XYZ-100A/15 with the NPS3330 controller from Queensgate Corp. (Torquay, UK) has been used. This piezo-controlled table is mobile in the lateral (X, Y) dimensions in steps down to 0.5 nm and in 0.15 nm in the axial (Z) with errors of about 0.02 %. The maximal lateral range is $\pm 55 \mu\text{m}$ and $\pm 8 \mu\text{m}$ axial. The table works with resonance frequencies up to 350 Hz, depending on the sample weight, which might be as much as 500 g. The controller can be operated in two modes, a closed loop mode, where the position of the piezo table is guided by a feedback mechanism, which immediately compensates for any mispositioning, and an open loop mode, where no control or correction of the table position is implemented. In this work, predominantly the open loop mode has been applied using the software introduced later in this chapter.

The Computer Interface Card for TCSPC

The PC-plug in card SPC 630 from Becker & Hickl GmbH (Berlin) for Time-Correlated Single-Photon Counting, TCSPC, is the main part of the data acquisition. For the basic principles of TCSPC please refer to chapter 2.1. The operation mode of the card is presented in figure 3.4 and discussed in the following. Further information about TCSPC hard- and software can be found in the literature [Becker 1999].

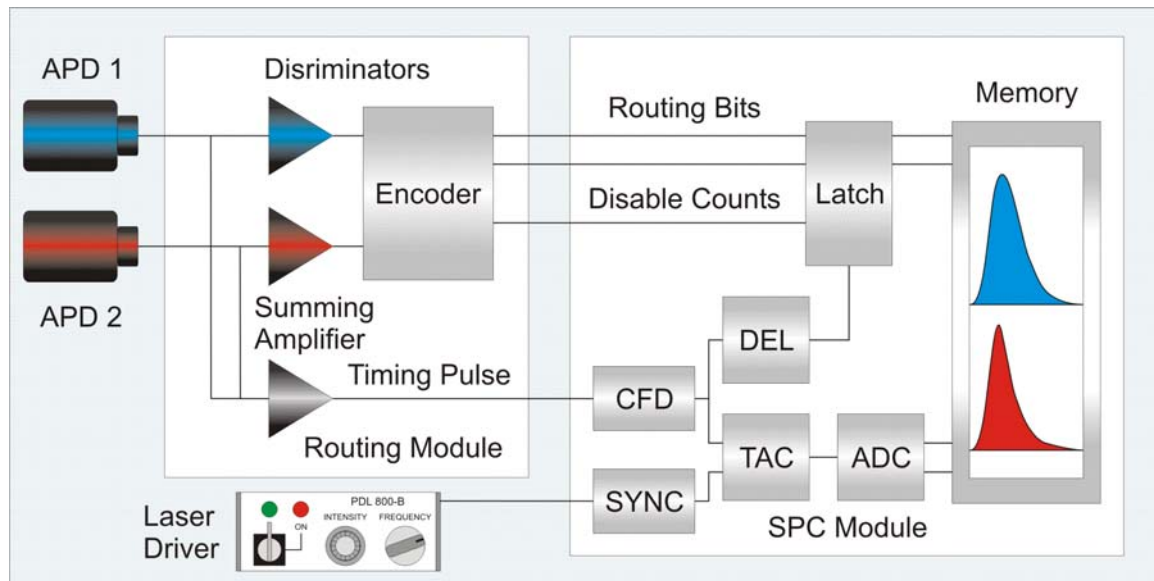


Figure 3.4: Schematic representation of the TCSPC data processing in a two detector setup.

The single-photon pulses from the detectors are fed into a router where they are coded for the constant fraction discriminator, CFD. Due to the stochastic gain mechanism of the detector, these pulses have a considerable amplitude jitter and are also broad (~20 ns) compared to the required time resolution (down to 3 ps). The CFD has to deliver an output pulse that correlates as exactly as possible with the real temporal position of the detector pulse. This is achieved by triggering on the zero cross point of the sum of the input pulse and the delayed and inverted input pulse, as depicted in figure 3.5.

Since the temporal position of the crossover point is independent of the pulse amplitude, this timing method minimizes the time jitter of the CFD due to the amplitude jitter of the detector pulses. Additionally, the CFD uses a window discriminator rejecting input pulses outside a selected amplitude window. This enables the reduction of interfering noise from the environment, for example from delay units, preamplifiers or - more common - from *after-pulses*, that are frequently emitted from APDs.

The signal from the laser pulser, SYNC, corresponds in time to the single light pulses and is used to assign measured photons an arrival time relative to a laser pulse. The SYNC signal is received by the SYNC handler on the SPC module that, as the CFD, has fraction trigger characteristics to reduce the influence of amplitude fluctuations. Controlled by the software, the internal SYNC frequency can be divided by a factor of 2, 4, 8, or 16. In this case several signal periods are displayed in the result.

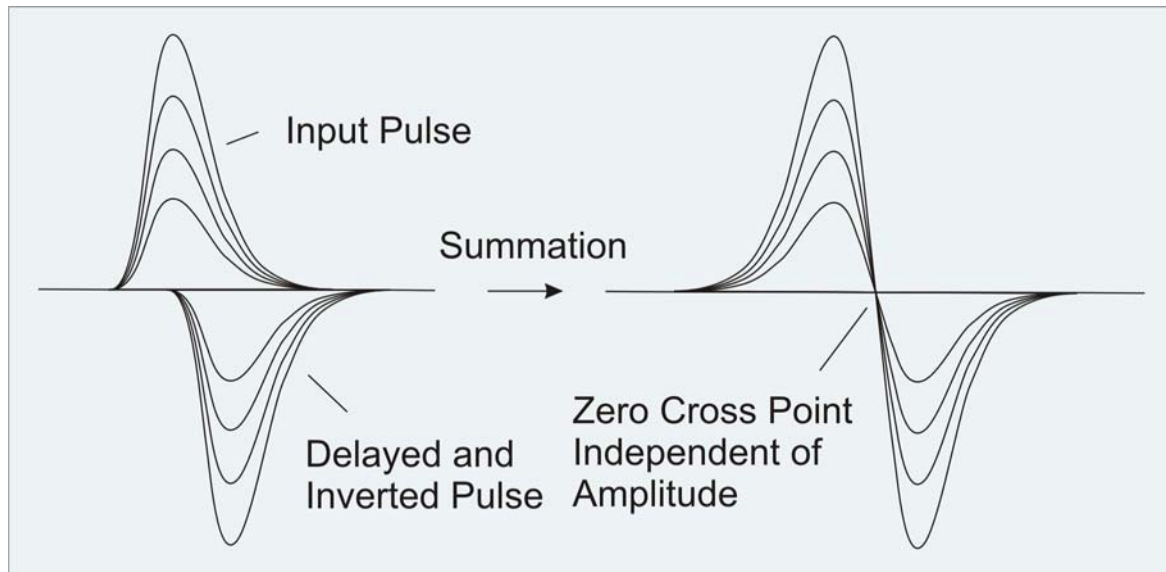


Figure 3.5: TCSPC pulse processing for signal acquisition in the time domain. The input pulse is delayed and inverted (left), followed by an overlay of original and modified pulse (right). The crossing point with the abscissa correlates to the measured time.

The time-to-amplitude converter, TAC, determines the temporal position of a detected photon within the SYNC pulse sequence. When a pulse at the start input starts the TAC, it generates a linear ramp voltage until a stop pulse activates the stop trigger. Thus, the TAC generates an output voltage depending linearly on the temporal position of the photon. The time is determined from the photon to the next SYNC pulse. Intuitively one would measure from the SYNC pulse to the photon, but this “inverse start-stop” method is the key to process high photon count rates at high pulse repetition rates. It reduces the speed requirements, because the working cycle of the TAC, consisting of start, stop and reset, has to be performed only with the photon detection rate instead of the considerably higher pulse repetition rate. The TAC output voltage is fed to the programmable gain amplifier, PGA. The PGA is used to stretch a selectable part of the TAC characteristic over the complete time measurement window. To increase the effective count rate at high PGA gains, the output voltage of the PGA is checked by the window discriminator, which rejects the processing of events outside the time window of interest.

The analog-digital converter, ADC, converts the amplified TAC signal into the address of the memory. It resolves the TAC signals into 4096 time channels (12 bit), which results in a maximum time resolution of 3 ps per bin. Also lower values are possible, for example 2048 (8 bit) and 1024 (4 bit), but these were not used for this work.

Simultaneous multi-channel operation with several detectors is accomplished by combining the photon pulses from all detectors into one common timing pulse and providing a routing signal, which assigns photons from the individual detectors into different memory blocks, the routing bits. These bits are stored for each photon together with the ADC data and the Macro Time. Additional control over the measurement is given by the CNT signal. CNT is a “Count Enable” signal, *i.e.* a photon is stored only if CNT is 1 in the moment of its detection. The CNT signal is used to suppress photons for which no valid routing information is provided or to confine the recording to externally controlled time intervals. All external control signals are read by the latch register. The signals are latched at an adjustable delay time after the start pulse. Adjusting this delay assures that every photon is processed with the corresponding state of the control signals.

The general used TCSPC settings are listed in table 3.1. It has to be mentioned that no exact values can be given, as every alteration of the setup influences the parameters. If, for example, a cable one meter longer replaces a cable for the delivery of the SYNC or the detector signal, the signal in the TAC window is shifted by about 4 ns.

| SYNC | | CFD | | TAC | | Data format | |
|------------|----------|--------------|----------|--------------|-------|--------------|--------|
| freq. div. | 1 | lower limit | -78.4 mV | lower limit | 9.8 % | ADC resol. | 12 bit |
| threshold | -19.6 mV | higher limit | 80.0 mV | higher limit | 80 % | detectors | 2 |
| zero cross | 0 mV | zero cross | 4.54 mV | range | 50 ns | dither range | 0 |
| holdoff | 4 ns | holdoff | 5 ns | gain | 2 | count incr. | 1 |
| | | | | offset | 0 % | latch delay | 1 ns |

Table 3.1: Parameter settings of the SPC 630 board for all single-molecule measurements done within this work.

FIFO Mode

The SPC 630 board offers the possibility for FIFO (First In First Out) data acquisition. In this mode information about the individual photons is collected and stored. This includes the photon arrival time with respect to the corresponding laser pulse (microscopic time) and the absolute arrival time after the start of the measurement (macroscopic time). Additionally, the detector number on which the photon was counted is saved. The principle of the FIFO mode is schematically shown in figure 3.6:

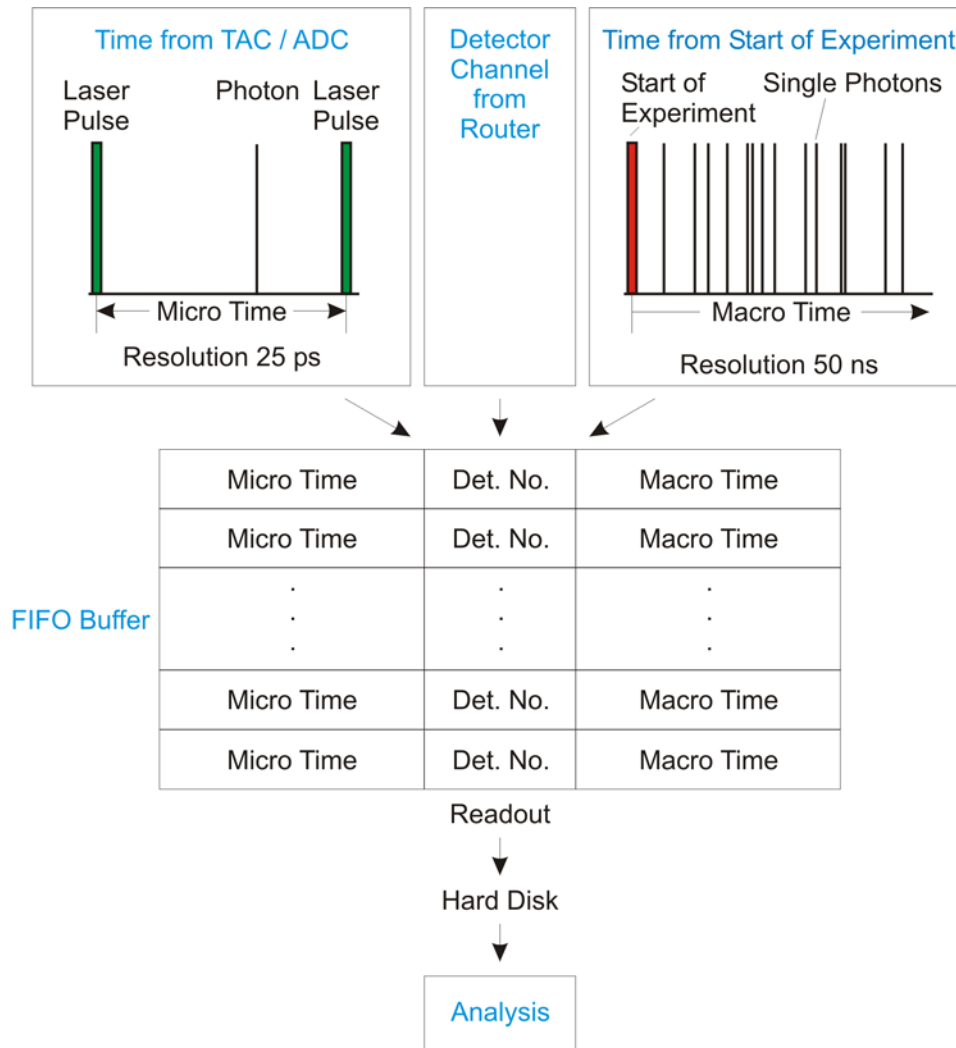


Figure 3.6: Scheme of the data acquisition in the FIFO mode. For every detected photon the macroscopic time, the microscopic time, and the detector number is recorded.

Both times, the time of the current photon within the excitation pulse sequence and the time since the start of the measurement (the microscopic and macroscopic time), are fed to the input of the FIFO memory. At the output, the software continuously reads out the FIFO memory. A FIFO memory can be seen as a data shift register, which accepts data at its input while providing them in the same order at the output. The FIFO mode (in the literature also denoted as TTTR- or bifl-mode [Tinnefeld 2000; Eggeling 2001]) offers unique possibilities for data analysis, as the data acquisition is independent of the time resolution. After data acquisition, the photons can be sorted and handled freely with criterions such as count rate or fluorescence lifetime.

3.2 Extensions and Variations of the SFLIM-Setup

Starting from the “standard” SFLIM-setup introduced in chapter 3.1, several features were additionally integrated to enable a broad variety of experiments without dismantling previously installed components.

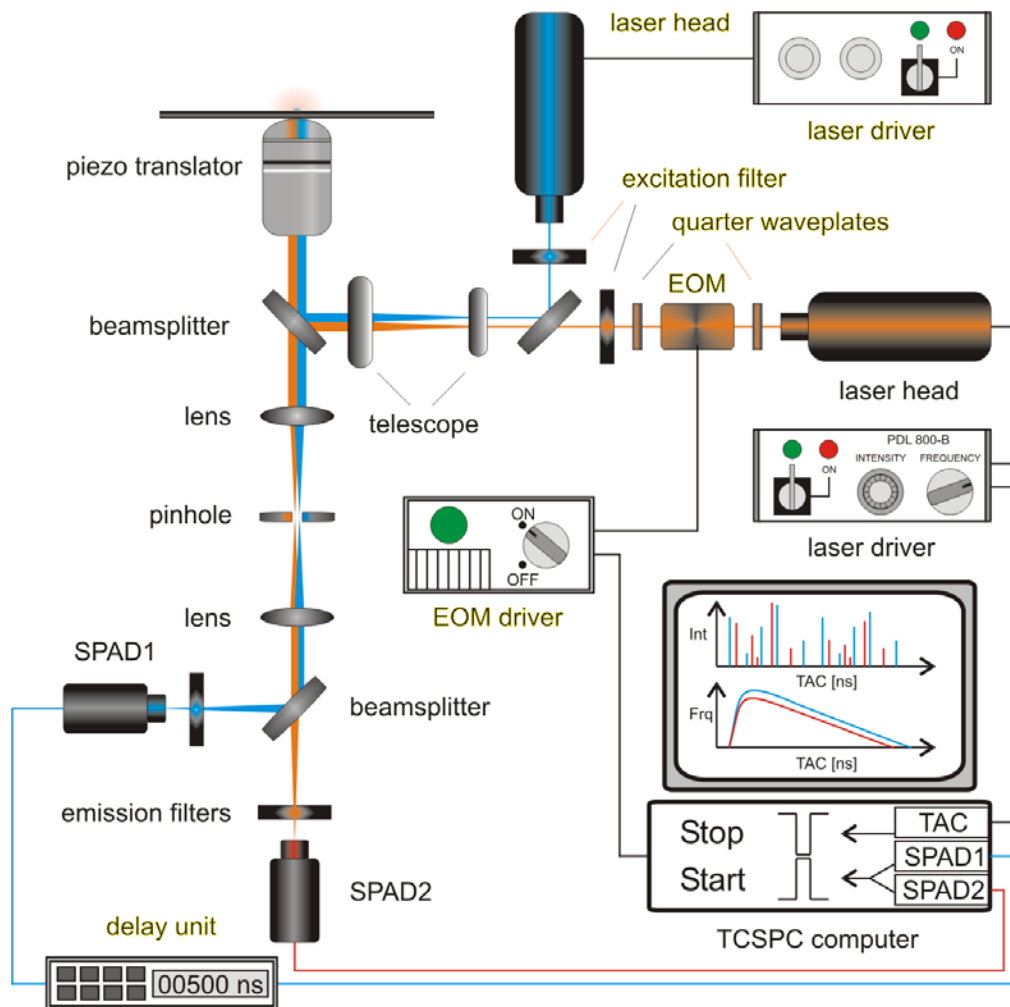


Figure 3.7: Schematic representation of the extended SFLIM setup. Denominations of additional features are highlighted in yellow. An argon-ion laser for two color excitation, a delay line for antibunching measurements, and an electro optic modulator, EOM, for polarization modulation have been installed. The broad band mercury lamp and the CCD camera for imaging are not mapped.

Polarization Modulation

Starting from the 635 nm excitation source, the first modification in the optical path is the electro optic modulator, EOM, model LM0202 (Linos AG, Göttingen; HV-generator: Trek 601C from BFI Optilas, Puchheim) with its corresponding quarter

waveplates. The first waveplate aligns the polarization vector of the linearly polarized laser beam to an incidence angle of 45° with respect to the direction of the electric field applied in the EOM. This provides two equal parallel and perpendicular components with respect to the electrode structure. Their relative phase $\Phi(x)$ is given in equation 3.1:

$$\Phi(x) = \frac{2\pi}{\lambda} \int_{y=0}^l \Delta n(\theta(x, y)) dy \quad 3.1$$

λ represents the wavelength in vacuum and l is the thickness of the electro optic material.

Changes in the applied voltage, and thus the electric field strength, result in a shift in the relative phase between the two light components. By placing a second quarter waveplate at the output of the EOM, the light intensity can be varied as a function of the relative phase according to the following relation:

$$T = \frac{1}{2}a^2 + \frac{1}{2}b^2 + ab \sin(\Phi) \quad 3.2$$

Here T is the transmittance, Φ the relative phase, and a^2 and b^2 are the single transmittances for the orthogonal components of the light [Shames 1998].

Polarization modulation is a feasible tool for the investigation of single- and multichromophoric systems [Güttler 1993, Ha 1996]. Chromophores are only excited when their absorption dipole is parallel to the electronic vector of the exciting light. Consequently, only a subset of chromophores adsorbed on surfaces or immobilized in polymers is excited by a linearly polarized laser beam. This enables a discrimination between image spots arising from single and multiple emitters (chapter 3.4).

For the investigation of multichromophoric systems, for example in antibunching experiments, linearly polarized light is not suitable, because in order to state about the fluorescence of a molecular aggregate, all chromophores should be excited equally. Thus, measurements without polarization modulation are carried out with circularly polarized light obtainable by turning the quarter waveplate after the EOM by 45° in the plane perpendicular to the laser beam.

Antibunching Setup

For antibunching experiments with consecutive coincidence analysis, the nanosecond delay generator (Stanford Research) was implemented [Weston 2001]. It delays the short wavelength detector channel by 500 ns to ensure that the dead time of the SPC-card (~200 ns) does not prevent the detection of simultaneously emitted photons. As a delay is a possible source of electronic distortions, which interferes with lifetime determinations, the short wavelength channel was delayed. The delay was necessary, because the SPC-card cannot detect consecutive photons below its dead-time simultaneously. Hence, photons that belong to the same laser pulse arrive with a time delay of 500 ns plus the offset caused by unequal cable lengths used to deliver the electronic pulses to the TCSPC board.

Two-Color Excitation

To be able to measure a wider field of fluorescent dyes, an argon-ion laser with an emission wavelength of 488 nm is built in. It is coupled into the excitation path of the red laser diode by a spectrally separating beamsplitter. This setup allows not only to switch between the lasers, but also enables simultaneous two-color excitation, for example for colocalization or FRET-studies. Here, the emitted fluorescence light is spectrally split onto the detectors by a corresponding spectral beamsplitter (table 3.2). That way the fluorescence light is collected without noticeable crosstalk of the emitting dyes into the unwanted perpendicular detection channel.

Broad-Band Excitation

The laser beams enter the microscope via the side port and are reflected by a dichroic mirror into the objective. Alternatively, a mercury lamp can be applied from the back port, which is suitable to homogeneously illuminate larger areas of fluorescence labeled sample, especially counterstained cells. To detect the fluorescence light, a Picostar CCD-camera (LaVision, Göttingen) is mounted onto a second outlet next to the ocular. A moveable unit, on which different beamsplitters and filters are affixed, enables to switch between the different excitation sources keeping the illuminated sample area constant. This system is used to find and image counterstained cells and cryosections, and allows positioning them for SFLIM-

scanning experiments. Also ensemble FRET-studies in cells have been accomplished with this setup.

Filters and Beamsplitters

Different spectroscopic methods and excitation sources require different optical filters and beamsplitters. Depending on the problem, the following filter sets have been used:

| Filter | SFLIM setup | Antibunching experiments | Two color excitation | Broad band excit. (DAPI) |
|-------------------------------------|-------------|----------------------------|-----------------------|--------------------------|
| Excitation filter(s) | 630DF10 | 630DF10 | 630DF10, 488NB3 | D360DF40 |
| Excitation beamsplitter | 645DLRP | 645DLRP | 51008bs | 400DCLP |
| Emission beamsplitter | 685DCLP | non-polarizing cubic 50/50 | 585DCXR | - |
| Emission filter(s) short wavelength | HQ667/30m | HQ679/60m 660DCLP | D540/50m HQ560/80m | - |
| Emission filter(s) long wavelength | HQ710/50m | HQ679/60m 660DCLP | S695/55m | D480/60m CCD-camera |

Table 3.2: Index of filter sets used in this work. All units except 488NP3 (Omega Optics Corp., USA) were purchased from Chroma Technology Corp. (USA).

The selection of appropriate filter sets is a crucial issue for single- and multi-dye experiments. Especially the discrimination of different dyes on single-molecule level, for example in FRET- or colocalization experiments, where the fluorescence emission of one dye species should preferably fall only onto one detector and the signal of the other dye(s) onto the other detector(s), the demands towards the filters and beamsplitters are tremendous.

Excitation filters should transmit only those wavelengths of the illumination light that efficiently excite a specific dye or dye pair. Beside filters, which are diaphanous in a certain spectral region, also bandpass filters (mostly longpass) can be used, which transmit light up to or from a certain wavelength on. A suitable emission filter should attenuate the scattered excitation light and efficiently transmit any fluorescence emitted from the specimen. In some cases (table 3.2), the use of two emission filters in front of a detector becomes necessary to suppress scattered light or, in multi-dye experiments, signal from other different dye molecules, even though it reduces the

photon detection efficiency. A dichroic beamsplitter is a coated glass slide set at a 45-degree angle to the optical path of the microscope. The coating has the unique ability to reflect photons up to a certain wavelength, but it transmits longer wavelengths. Usually in a confocal microscope with two detectors, one beamsplitter separates the excitation light from the emitted fluorescence in the excitation path, and a second dichroic spectrally divides the emitted fluorescence light. For antibunching measurements, where the fluorescence signal should be equally split onto two detectors, a 50/50 non-polarizing beamsplitter is used. It is important to note, that a beamsplitter is extremely sensitive to changes of its angle in the optical path. A few degrees deviation lead to a shift of up to 20 nm, while the shape of the transmission curve remains unchanged. By measuring the transmission curves for each detector, it becomes obvious, that no linear correlation between fractional intensities (F_2 -values) and emission wavelength exists [Tinnefeld 2002]. The F_2 -value is defined as the number of photon counts collected by the long-wavelength detector divided by the sum of both detectors:

$$F_2 = \frac{I_{long}}{I_{short} + I_{long}} \quad 3.3$$

Furthermore it should be mentioned, that identical fluorophores do not always give similar F_2 -values when immobilized on a surface. This is because practically all optical elements, like filters and beamsplitters, have polarizing effects and change the (already polarized) emission light of the fluorophores on its way to the detector depending on the orientation of the absorption and emission dipole of the dye. Thus, an emission beamsplitter separates photons not only by their spectral properties, but also by the orientation of the molecules dipole moment.

3.3 Software

Throughout this work many computer programs have been used for the acquisition and analysis of data. Amongst them are the commercially available Origin 6.0G (Microcal Corp.) and DIAdem Academic 8.0 (National Instruments, both for analysis and graphical transformation of data), CorelDRAW 9.0 and 11.0 (Corel Corp., sketches, drawings and image processing), Office 2000 (Microsoft Corp., documentation and presentation), Davis (LaVision, CCD-camera control, image

acquisition and analysis) as well as LabView 6.1 (National Instruments, graphic-based platform for the development of data acquisition and analysis programs based on the programming language G).

Burst-Scout

Alongside these programs various home-built or free available versions played an important part. For the analysis of single-molecule solution measurements Burst-Scout version 1.11B (Atto-Tec GmbH, Siegen) has been used. The program allows assigning a group of photons to a single fluorescence labeled molecule, called a burst in the time-domain. These bursts are separated with the help of several parameters, *i.e.* the recognition threshold, the separation threshold and the separation limit. The F_2 -values and fluorescence lifetimes of single molecules in solution are determined by this analysis program.

Cyclize

The theoretical end-to-end distributions of double-stranded DNA (dsDNA) are calculated with Cyclize_v0.4. This program is based on the worm-like-chain assumptions and uses the Monte Carlo model to simulate DNA chains of several lengths.

Labview Based Programs

For data acquisition and analysis several programs based on Labview 6.1 have been developed in our group. Especially K. D. Weston, D.-P. Herten and C. M. Roth wrote programs on FIFO (First-In First-Out) mode basis. The advantage of FIFO mode is, that data can be analyzed after the measurement without any prior assumptions and limitations. Three pieces of information are stored for every collected photon: the absolute arrival time in 50 ns resolution (macroscopic time), the arrival time relative to the corresponding laser pulse (microscopic time) and the detection channel.

In this work we use two different acquisition and analysis programs, one for image scanning and one for the collection of time trajectories of single molecules on surfaces or in cells.

An image scan is recorded as follows: The object is placed down right of the laser focus. The piezo-table scans one line in x-direction and resets afterwards to the starting point of this line. Then the table moves one step in y-direction and repeats the x-direction move within this offset. This procedure is continued until the whole size of the scan is done (usually 20x20 μm). For three-dimensional objects a third axis can be accessed. Please note, that the table does not fulfill a constant movement, it rather moves along the axis in a predefined raster, given by the parameters pixel resolution and integration time. The collected photons of the detection channels are summarized pixelwise and are transferred into an online RGB- or false color image. Afterwards, the analysis software does not only allow to create intensity, fluorescence lifetime or F_2 -images, it also holds the possibility to pick groups of pixels, e.g. spots, by a variety of selectable criteria and deduces information from the separate detection channels.

The program for the acquisition of time traces places one molecule in the laser beam and collects its fluorescence signal until photodestruction. Thereby the maximal possible information is recorded from a single molecule. The procedure is based on an x-scan mode, where the highest intensity pixel above a threshold is determined. After every line the piezo-table moves back to that maximum point and remains until the fluorophore is photobleached. Afterwards the next line is scanned with an offset of 2 μm in y-direction to approach molecules without the risk of photodestruction due to prior excitation.

The collected data is plotted in an intensity vs. time diagram and with the analysis software the fluorescence lifetime, F_2 -values and antibunching information can be extracted from any part of the trajectories.

3.4 Determination of the Number of Independent Emitters by Polarization Modulation and Antibunching Measurements

In recent years it was discussed that multi-parameter studies are required to gain a complete overview over the spectroscopic states and the local environment of fluorescent molecules [Weiss 2001]. Most of these, like fluorescence intensity and lifetime, emission wavelength, orientation vector, and polarization anisotropy are relatively easily accessible [Lakowicz 1983, Schaffer 1999, Weston 2001].

With the investigation of the local environment of a molecule the question arises, how to prove single molecules [Betzig 1993], or more general, how to quantify the number of fluorophores located in the detection volume. The first issue can be attended by polarization modulation experiments due to the fact that single molecules have a fixed transition dipole [Güttler 1993, Ha 1996].

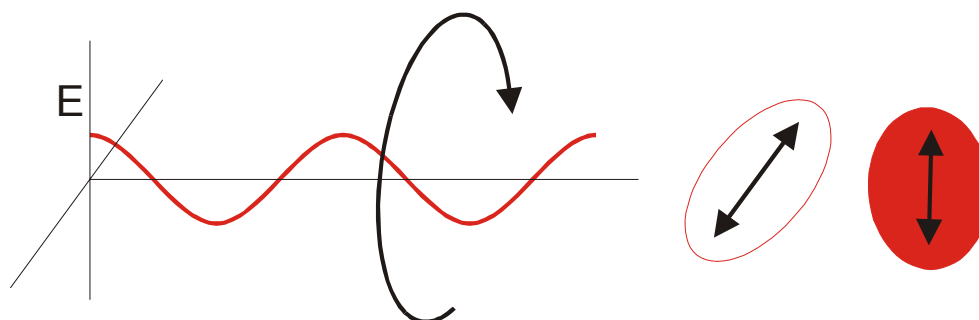


Figure 3.8: Excitation of a fluorophore with linearly polarized light. By modulation of the polarization angle of the incident light, the fluorescence intensity follows the modulation due to the fix transition dipole of the molecule.

By the modulation of linearly polarized excitation light, the fluorescence intensity follows the modulation and drops to the background level, when the polarization angle of the exciting light and the transition dipole moment of the molecule are perpendicular to each other (figure 3.8). Multichromophoric systems do not noticeable follow the modulation, since the molecules rarely have the same absorption dipole in respect to each other and thus can be safely distinguished from single emitters. If the EOM voltage is modulated with time by application of a sawtooth pattern, the polarization vector of the excitation light is rotated similarly. By choosing the pattern repetition rate significantly (2 to 10 times) shorter than the integration time of a scanned pixel (resolution 50 nm), an immobilized molecule exhibits stripes in an image scan and can be distinguished from several colocalized molecules (figure 3.9):

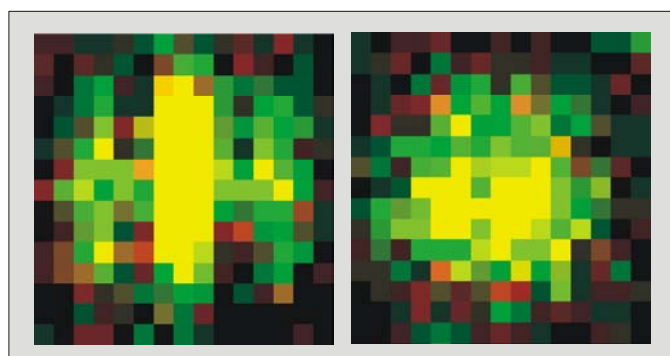


Figure 3.9: Polarization modulation experiment with a single (left) and two colocalized (right) Atto 620 dye molecules using a sawtooth pattern with a full modulation every 5 pixels. Image settings: integration time 3 ms per pixel, resolution 50 nm per pixel, 100 μm pinhole, excitation power 0.4 kW/cm^2 .

For the quantification of more than one emitter, the only viable pathway leads across antibunching measurements [Dagenais 1983, Zou 1990]. Antibunching can be seen as the opposite of bunching, which means that photons arrive in bunches, visible in single-molecule time-traces, which show blinking due to intersystem crossing. Antibunching arises from the fact, that a single emitter cannot emit two consecutive photons in time intervals shorter than the excited-state lifetime. In other words, a single molecule cannot emit two photons simultaneously, when excited with a sufficiently short laser pulse. After photon emission it must be re-excited and wait, on average, one fluorescence lifetime before another photon can be emitted. Thus, this process occurs on the nanosecond timescale (bunching is in the range of ms to μ s), and exhibits sub-Poissonian statistics.

In 2002 Weston *et. al.* introduced a versatile method based on antibunching for measuring the number of independent emitters alongside with the fluorescence intensity, lifetime, and emission wavelength of single molecules and multichromophoric systems [Weston 2002, Tinnefeld 2002]. They applied a single PC plugin card for TCSPC onto the classical Hanbury-Brown and Twiss setup [Hanbury 1956] with the difference, that both of the APD signals can operate as the start signal of the TAC and the laser SYNC operates as the stop signal, whereas in classical antibunching experiments, one of the detectors gives the start signal and the other the stop signal. Time-resolved data are acquired using the FIFO mode in which the microscopic and macroscopic arrival time, and the detection channel is registered for each photon detected (setup see chapter 3.2). In both methods, one of the detectors has to be delayed to circumvent the dead-time of the signal-processing module, here the TCSPC card.

For the determination of the number of independent emitters the interphoton distances, *i.e.* the time lags between two consecutive photons, are arranged in a histogram. For pulsed laser excitation, the distribution is largely dominated by the laser repetition rate, as interphoton times are always a multiple of the times between the laser pulses (neglecting the randomly arriving background counts). In figure 3.10, typical distributions for a single (A) and an ensemble (B) of molecules using a time delay of 500 ns are given:

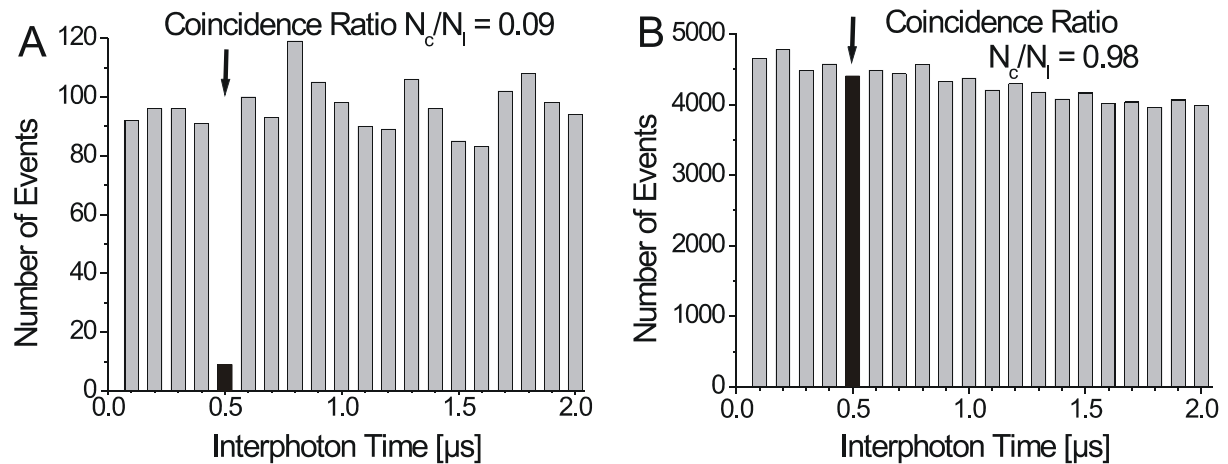


Figure 3.10: Typical distributions of the interphoton distances for a single (A) and an ensemble (B) of emitters. With a repetition rate of 10 MHz, the histogram bins are in units of 100 ns, corresponding to a multiple of the time between the laser pulses. The positions of the central peaks, indicated by arrows, correspond to the delay of 0.5 μs .

The position of the indicated peaks at 0.5 μs corresponds to the APD delay time and is called central or zero peak, N_c . Its counts equal the number of photon pairs generated during the same laser pulse, only shifted by a small offset due to the unequal lengths of the cables used to deliver the electronic pulses to the TCSPC board. The ratio of the number of interphoton time distances contributing to the central peak to the average number of counts in the lateral peaks, \bar{N}_l , is dependent on the number of chromophores in the considered detection volume. The expected ratios N_c/\bar{N}_l for one to ten emitters are shown in figure 3.10 (A). In real measurements background signal contributes to the interphoton statistics, too, and causes a shift of the N_c/\bar{N}_l ratio. Expected correction factor for different signal to background (S/B) ratios are plotted in figure 3.11 (B).

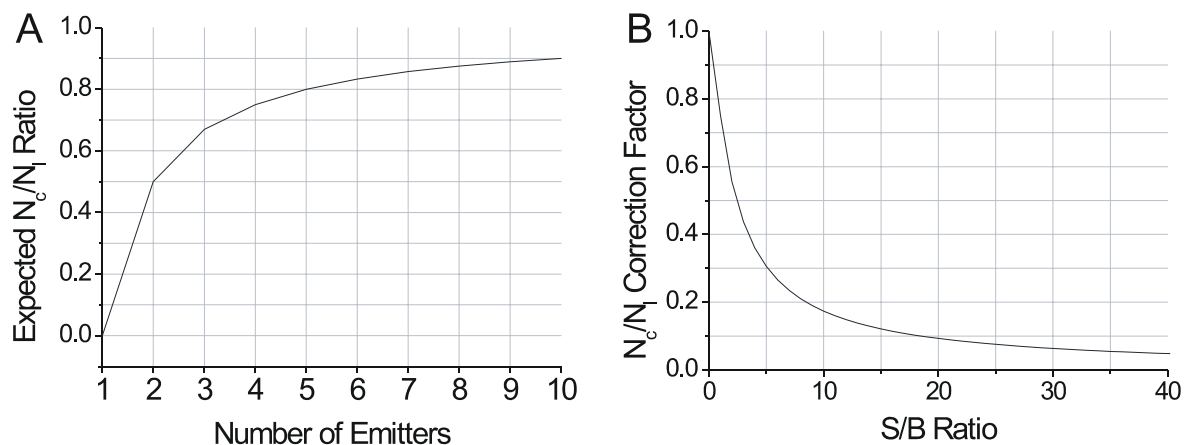


Figure 3.11: Expected coincidence ratios for 1 to 10 emitters neglecting background (A) and the correction factors for different signal to background ratios (B).

3.5 Time and Spectrally Resolved Precision-Distance Microscopy on Single-Molecule Level

In this chapter an introduction to the theory of time and spectrally resolved precision distance measurements shall be given, whose comprehension is required in chapter 4.2. The abstract mainly summarizes the thesis of C. Müller [Müller 2003], who introduced and applied the algorithm for all distance determinations presented in this work.

The goal of the algorithm is to describe a system of two single colocalized (overlapping PSFs) fluorophores distinguishable by the parameters F_2 -value and fluorescence lifetime. The experimental data is collected with a setup as described in chapter 3.1 with two detectors, a TCSPC card, and a scanning piezo-stage.

In confocal imaging microscopy samples are measured in raster-like scan steps, so-called pixels, which in this work usually have got a size of 50x50 nm. These pixels are fully described by the parameters fluorescence intensity (I), fractional intensity (F_2 -value), and a decay ($d(T_i)$). This decay, the time average, reflects the mean arrival time of the photons after the excitation pulse. By measuring the single dyes, the characteristic interrelations between the above parameters are obtained, and a distribution can be assigned for a given I , F_2 , and $d(T_i)$, which yields the fractions of dye 1 and dye 2 with their probabilities in the considered pixel. By that way an image containing both dyes can be split into two separate pictures including the errors. From the images the centers of gravity are determined separately for each fluorophore, and the distance can be easily obtained.

In more detail, after conduction of a sample scan, the fluorophores in an image are represented by bright, mostly round spots. Technically, a spot is a round shaped ensemble of pixels, whose intensity is higher than the background level. In the results presented in chapter 4.2, a background correction has been incorporated, but for this summary an ideal measurement without noise and background photons is assumed. The image spots are analyzed pixel by pixel for their intensity, F_2 -value, and time average. To be able to distinguish and separate two colocalized fluorophores, calibration measurements with only one kind of fluorophore on the surface at a time, need to be conducted. The acquired spot pixels for both dyes are first analyzed for their F_2 -values in dependency on the fluorescence intensity (figure 3.12):

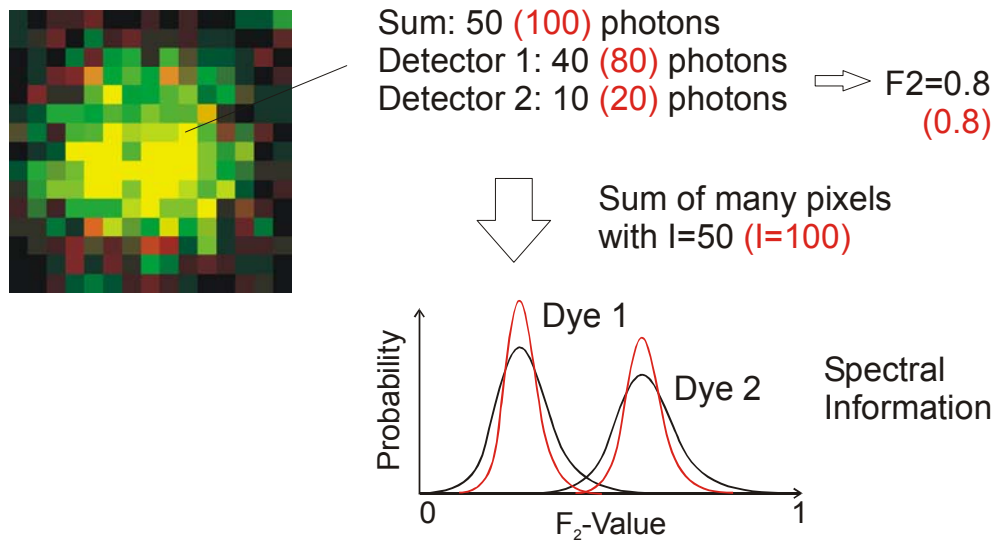


Figure 3.12: Pixelwise analysis of image spots consisting of two fluorophores by the classification of F_2 -values for different intensities. This enables, for a given pixel with an intensity and an F_2 -value, to assign fractions of photons to the dyes within a certain probability and error.

In figure 3.12 the F_2 -value distributions of for two different fluorophores are depicted. An important point is that even though the positions of the F_2 -values of each dye stay constant for different intensities, their broadness strongly varies with the number of photons in a pixel. This broadness directly relates to the error of an assignment, as the error and the broadness of the distributions are both dependent on the photon statistics [Ober 2004]. For a pixel intensity of 100 photons yielding an F_2 -value of 0.8, for example, meaning that 80 photons are counted on the long and only 20 on the short wavelength detector, the error and the distribution are much smaller than in the case of a pixel with 50 photons, where the F_2 -value is also determined to be 0.8 (40:10 counts). By analysis of a sufficiently high number of pixels, sets of probability linear combinations for different intensities are achieved, which exactly describe the F_2 -value of a fluorescent dye.

Similar to this procedure, the photon arrival times after the excitation pulse are analyzed (figure 3.13).

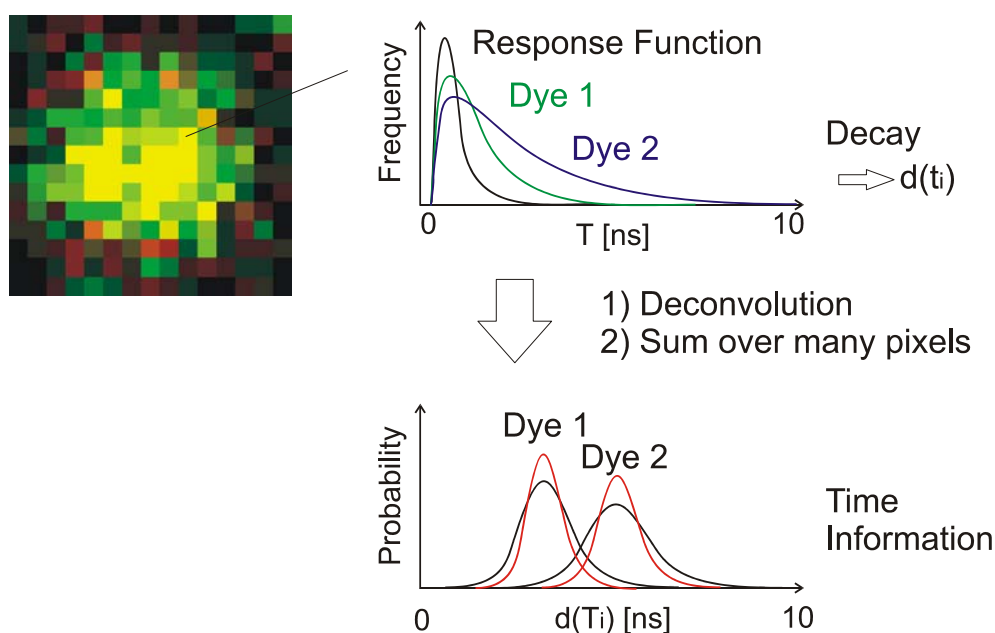


Figure 3.13: Pixelwise analysis of image spots consisting of two fluorophores by the classification of time averages $d(T_i)$ for different emission intensities. This enables, for a given pixel with an intensity and an F_2 -value, to assign fractions of photons to the dyes within a certain probability and error.

Figure 3.13 bases on histograms of photon arrival times with respect to the laser pulse. By fitting these experimentally determined histogram times for each single pixel to curves, the decays in the upper graph are obtained. They hold information about the fluorescence lifetime of a fluorophore, which can be investigated by deconvolution of the function with the excitation pulse and subsequent exponential fitting. Instead of the fit, the time average $d(T_i)$ is deduced from the pattern, which holds the advantage that all photon counts are taken into account, and not the subset the photons in the fitted part of the decay. Thus, a lower error is obtained. By investigation of many pixels, sets of time averages for different intensities are achieved, which - similar to the procedure with the F_2 -values - leads to differently broad probability distributions.

By combination of the two parameters fractional intensity and time average, an exacter assignment can be made in comparison to the single factors only. For a given number of photons within a pixel, a probability for the ratio of photons arisen from each fluorophores can be given. Thus, a false color image containing the information of both detector channels, can be separated into two images each representing the information of a single kind of fluorophore (figure 3.14):

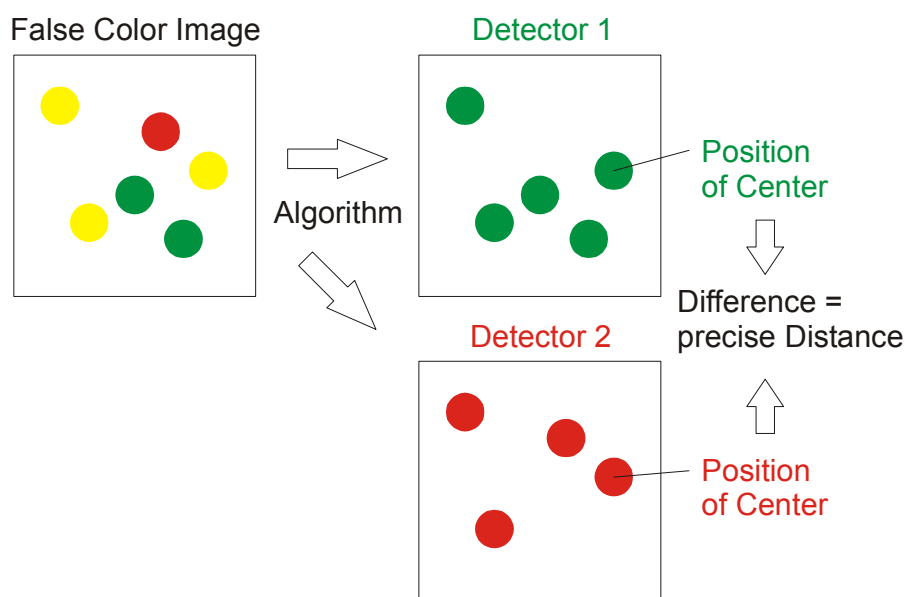


Figure 3.14: Dispartment of a false color image containing two different kinds of fluorophores. By appliance of a combination of the F_2 -value and the time average algorithm, the recorded image can be separated by the fluorescent dyes. From these a center of mass analysis gives the coordinates and thus the distance between the colocalized dyes.

The determination of the image spot centers is accomplished by a center of mass algorithm, which allows giving distances between the separated dyes. The resulting error directly depends on the probability with which the photon ratios are assigned.

3.6 Conjugation of Biomolecules with Fluorescence Dyes

Oligonucleotides and DNA

Oligonucleotides were custom synthesized by IBA GmbH (Göttingen) and used as delivered. Fluorescence dyes were purchased as NHS-esters from Amersham Pharmacia, Braunschweig (Cy-dyes), MoBiTec GmbH, Göttingen (Bodipy 630/650, Rhodamin Green), and Atto Tec GmbH, Siegen (Atto-Dyes), or were kindly provided as carboxylic acids by K. H. Drexhage, Universität-Gesamthochschule Siegen (JA-dyes, JF 9 and MR 121).

The following protocol was used for conjugation of oligonucleotides to dyes: One equivalent of activated fluorescence dye is dissolved in anhydrous DMF in a concentration of 2 mg/ml and a 5-fold excess of oligonucleotide in 0.05 M carbonate buffer (pH 9.0) is added. After 2 h stirring the product is purified by HPLC using a

linear solvent gradient of 0-75 % acetonitrile in 0.1 M aqueous triethylammonium acetate.

For colocalization and antibunching experiments double-stranded oligonucleotides and DNAs were prepared. Lengths below 100 basepairs were synthesized by hybridization of single-stranded oligonucleotides using a temperature gradient of 95 °C to room temperature in one hour. Longer DNAs were made by PCR using a Taq-polymerase from Roche AG (Grenzach) and the standard protocol provided. The PCR primers consisted of fluorescent dye labeled 12-mers. The sequences of all deployed chains are displayed in table 3.3:

| Name | Sequence (5' to 3') |
|---------------------|--|
| DNA 200 | GGTGCTGCTATCGATGGTTTCATTGGTGACGTTTCCGGCCTTGC TAATGGTAATGGTGCTACTGGTGATTTTGCTGGCTCTAATTCCCA AATGGCTCAAGTCGGTGAGCGTGATAATTCACCTTTAATGAATAAT TTCCGTCAATATTTACCTTCCCTCCCTCAATCGGTTGAATGTCGC CCTTTTGTCTTTAGCGCTGG |
| DNA 148 | ATGGTGCTACTGGTGATTTTGCTGGCTCTAATTCCCAAATGGCTC AAGTCGGTGAGCGTGATAATTCACCTTTAATGAATAATTTCCGTCA ATATTTACCTTCCCTCCCTCAATCGGTTGAATGTCGCCCTTTTGTC TTTAGCGCTGG |
| DNA 70 | ACATTCTCTGAAGTATCTTTTCTTATTGTTATTTTTATATTATCTAAT TGTTATGCGTCAACTCACTACT |
| DNA 44 | CCGAGAATAGGGATCCGAATTCAATATTGGTACCTACGGGCTTT |
| DNA 10 | CCGAGAATAGGGATCCGAATTCAATATTGGTACCT ^x ACGGGCTTT |
| polyA ₄₀ | AA |
| polyT ₄₀ | TT |

Table 3.3: Sequences of the deployed DNA and oligonucleotide molecules. Of the double-stranded chains only one sequence is listed, the others consist of the complementary strands. Fluorescent dye labels were introduced at the 5' and/ or the 3' termini. In the case of DNA 10 an internal dye label on a thymine was built in, symbolized by T^x.

Proteins

Thermo Electron GmbH (Ulm) delivered all peptides in 95 % purity.

Conjugations of proteins with fluorophores were carried out as follows: one equivalent of activated fluorescence dye is dissolved in anhydrous DMF in a concentration of 4 mg/ml, a 5-fold excess of peptide in 0.05 M carbonate buffer (pH 8.5) is added and the solution is stirred for 2 h. If the protein contains sulfohydate groups, the pH-value is lowered (PBS, pH = 7.4) to avoid conjugation of

the activated ester to thiol groups. The conjugate is purified by HPLC using a linear solvent gradient of 0-80 % acetonitrile in 0.4 M aqueous triethylammonium acetate. The consistency is checked by MALDI mass spectrometry.

Antibodies

In this work mainly IgG antibodies were used because of their stability and frequency in nature in comparison to other antibody classes. Beside pre-labeled polyclonal IgG-dye conjugates from MoBiTec GmbH (Göttingen), several antibodies were ordered. Especially polyclonal mouse-anti-goat IgG (205-3102) from Biomol GmbH (Hamburg) and monoclonal mouse-anti-human IgG (BK61023) from Progen Biotechnik GmbH (Heidelberg) have to be mentioned, because they were used for the development of the mono-labeling strategy for antibodies (chapter 3.7). They were ordered free of stabilizing reagents (BSA) and amino-containing buffers (TRIS) to avoid interception with amino reactive coupling compounds.

For the preparation of statistically labeled antibodies, the following procedure has been followed: an excess of activated fluorescence dye is dissolved in anhydrous DMF in a concentration of 4 mg/ml and added to the antibody (5-10 mg/ml) in 0.05 M carbonate buffer (pH 8.5). After 2 h of gentle stirring at 4 °C the product is purified by chromatography using a Sephadex G25 packed NAP-column (Amersham Pharmacia, Braunschweig). The labeling degree is distinguished by absorption spectroscopy using the ratio between absorption maximum of protein (280 nm) and dye corrected by their theoretical extinction coefficients in water ($\epsilon(\text{IgG}) = 203.000 \text{ l/mol}\cdot\text{cm}$).

3.7 Synthesis of Mono-Labeled Antibodies

The synthesis of mono-labeled antibodies requires several reaction steps, which are listed in the following. All reactions and work-up steps were done at 4 °C under sterile conditions to avoid degradation and contamination.

Synthesis of the Dye-Peptide Conjugate

Analogue as described in chapter 3.6. The peptide (sequence: GHHHHHC) has to be handled oxygen free in the first two steps (degassed solvents, inert gas) to avoid auto oxidation of the SH-group.

Attachment of the Crosslinker to the Antibody

The SMCC crosslinker is dissolved in anhydrous DMF in a concentration of 0.5 mg/ml and a 20-fold excess is added to the IgG antibody in PBS (pH 7.4), concentration 5-10 mg/ml. The solution is stirred for 30 min, the activated antibody is reduced in volume to a final concentration of 5-10 mg/ml, and changed to PBS (pH 7.4) by centrifugal filtering using Microcon filter units with a nominal molecular weight limit of 50.000 Da (Millipore GmbH, Schwalbach).

Linkage of the Peptide Conjugate to the Antibody

To reconstitute oxidized sulfohydrates of the cysteine group in the dye marked peptide, TCEP (0.5 mg/ml in DMF) is added in 5-fold excess to the peptide and the solution is stirred for 15 min. The solution is mixed with activated antibody in 5-fold excess, is stirred for one hour and bound to immobilized Ni-NTA agarose beads (Qiagen AG, Hilden). After several washing steps with high salt carbonate buffer (0.5 M, pH 8.5, 300 mM NaCl, 15 mM imidazole) to avoid unspecific absorption, the product is recovered under native conditions (carbonate buffer 0.5 M, pH 8.5, 300 mM NaCl, 250 mM imidazole), and is further purified by affinity chromatography with immobilized protein A (Perbio GmbH, Bonn) using the standard protocol from Pierce Biotechnology (www.piercenet.com).

3.8 Cell Culturing and Cell Preparation

For this work several tumor cell lines have been used (table 3.4). Depending on the problem, the absolute size of the cells, the relative size between nucleus and cell, the robustness at room temperature and the occurrence of particular RNA sequences decided, which cell line best suited for the single experiment.

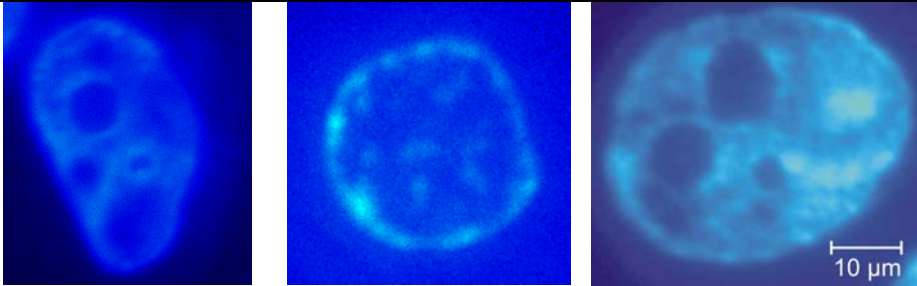
| Name: | 3T3 | JURKAT | HeLa |
|---------------------|--|---------------------|---------------------|
| Origin: | mouse | human | human |
| Reference | Green 1974 | Kaplan 1976 | Gey 1952 |
| Cell type: | embryonic fibroblast | cervical carconima | T-cell lymphoma |
| Average cell size* | 15-30 μm | 10-25 μm | 20-40 μm |
| Size nucleus / cell | 0.7 | 0.9 | 0.7 |
| Robustness | good | average | average |
| Picture** |  | | |

Table 3.4: Selected characteristics of the deployed cell lines; *on surface, in suspension 30-40 % less; **fixated and counterstained with DAPI, excitation source Hg-lamp, detector CCD-camera, 100 x NA 1.4 oil objective.

The cell lines were kept in a medium consisting of 500 ml Dulbecco's MEM, 12.5 ml HEPES buffer (1 M), 8 ml glutamine, 5 ml penicilline-streptomycin and 50 ml fetal bovine serum and grown under physiologic conditions (10 % CO₂ at 37 °C).

Cell Fixation

For cell fixation, cells are grown on cover slips in small petri dishes. The medium is drained and the cells are washed with warm (37 °C) PBS for 5 minutes twice. The cells are fixated by placing them for 20 minutes in warm formalin solution (3.7 % in PBS). The solution is removed and the cells are immersed for 20 minutes in warm PBS containing 0.1 % Triton X-100 und 1 % BSA. Rinsing with PBS twice finishes the fixation process and leaves the cells ready for labeling

Labeling of Fixated Cells

Fixated cells should be washed with warm PBS twice, if they were stored after fixation. The cells are prepared with warm SSC- (0.3 M NaCl, 0.3 sodium citrate in PBS) and TNT-buffer for 5 minutes twice, followed by PBS rinsing. The incubation is

carried out with 50 μ l labeling solution at 37 °C for 2 h in the dark, followed by rinsing steps with SSC-buffer (two times 15 minutes) and PBS to reduce unspecific signal. To prepare the cells for microscopic measurements, a cover glass is cleaned with anhydrous alcohol and dried with nitrogen. 100 μ l mounting medium (1:1 PBS : glycerol and 1 % DABCO) is applied onto the middle of the cover glass and the carrier with the cells is put on top vice versa. Inclusion of bubbles should be avoided, surplus solvent is removed and the sample is sealed with nail polish.

Cryosectioning of Cells

Successful immunocytochemistry is only possible when antibodies or other affinity markers are able to bind to their target ligands. For extracellular antigens this is not a problem, but for molecules inside cells the affinity markers must gain access. The best way is to cut cells into small slices. Water within the material is usually replaced with a medium that can be hardened, either by freezing or by polymerization. The cryosection technique [Griffiths 1986, 1993, Singer 1986, Tokuyasu 1973, 1976, 1986] is nowadays one of the most important techniques for subcellular immunocytochemistry.

The following protocol for the preparation of cryosections has been applied within a corporation with the group of Ana Pombo from the MRC London:

Cells are fixated by immersion in buffered aldehyde solution. The material is cut into small pieces, infused with a sucrose solution, which acts as a cryoprotectant, and is then placed onto small specimen pins. The pins are frozen by immersion in liquid nitrogen, quickly transferred to a cooled cryochamber fitted on an ultramicrotome and sectioned. The sections are obtained using a diamond knife on which they are collected, too. The sections are retrieved from the knife by picking them up on a small drop of sucrose and transferred onto carbon-coated specimen grids. The grids are floated on buffered saline with the section-side in the liquid. The sections on the grids are immunolabeled and incubated. Finally the sections are dried in the presence of a thin plastic film to avoid surface tension damage.

3.9 Standard Laboratory Equipment

Chemicals

Laboratory chemicals and solvents are purchased from Sigma-Aldrich GmbH and Fluka GmbH (Ebersdorf) unless otherwise stated.

Absorption, Fluorescence and Time-resolved Ensemble Spectroscopy

UV-vis absorption spectra are taken on a Cary 500 Scan spectrometer from Varian (Darmstadt). The samples are measured in Suprasil silica cuvettes from Hellma (Müllheim) in concentrations below 10^{-6} M to maintain linearity of absorption with concentration.

Steady state fluorescence spectra are measured on a Cary Eclipse fluorescence spectrometer from Varian equipped with a multi cell holder and a cryostat for temperatures between 0 and 80 °C.

Ensemble fluorescence lifetimes are determined at the emission maximum of the dye using a 5000MC spectrometer from IBH (Glasgow, Scotland). As excitation source serves a pulsed laser diode with an emission maximum at 635 nm (repetition rate 1 MHz, FWHM 200 ps). To exclude polarization effects, the fluorescence is observed under magic angle conditions (54.7 °). Histograms of 10^4 photon counts in the maximum channel (4096 channels) are taken in the Time Correlated Single-Photon Counting mode, TCSPC. Fluorescence lifetimes are deduced by a multi exponential deconvolution routine (Data Station 2000) provided with the spectrometer.

High Performance Liquid Chromatography (HPLC)

For purification and control of oligonucleotide and peptide reactions an HPLC from Agilent (Waldbronn) series 1100 is used. It consists of the degasser G1322A, the binary pump G1312A, the diode array detector G1315A and the fluorescence detector G1321A. Separation is achieved by a reverse-phase column, length 250 mm with an inner diameter of 4 mm from Knauer (Berlin), which is packed with ODS-Hypersil size 5 μ m.

3.10 Preparation of Coated Glass Surfaces

Commercially available glass cover slips usually need to be cleaned for single-molecule measurements. This is especially important for excitation wavelengths below 600 nm, where many biomolecules show autofluorescent signal. There are two reasonable ways for purification:

Variant 1: Treatment of the cover glass with 0.5 % hydrofluoric acid for 30 seconds followed by several washing steps with desalinated water. HF etches and thereby flattens the surface and removes contaminants.

Variant 2: Exposure of the surface to plasma for five minutes. Plasma chemically cracks and dislodges organic contaminants by activation of chemical reactions with radicals and ultraviolet energy. Further rinsing is not necessary.

Both variants induce that treated glass is afterwards passivated for the deposition of biomolecules or fluorescence dyes, and further surface coating (activation) is required. Several coating reagents, hydrophobic and hydrophilic, charged and non-charged, can be applied depending on the desired characteristics. For this work, coatings with amino-propyl silane (APS), polystyrene (PS) and 2-morpholinoethanesulfonic acid (MES) are used: The cover glass is dispensed in the coating solution for 5 minutes, rinsed with water twice and dried in a nitrogen stream.

To apply the sample onto the coated surface, two alternative methods were used:

Method 1: Spin-coating: The cover slip is fixed onto a quickly rotating platform and several drops of sample ($\sim 10^{-8}$ M) are deposited on it. By rotational motion the solution gets thinly distributed on the surface. With further spinning the solvent evaporates and leaves a dry and homogenous surface.

Method 2: About 100 μ l of sample ($\sim 10^{-10}$ M) is put onto the coated surface for a few minutes, followed by two rinsing steps with desalinated water.

4 Results and Discussion

This chapter is divided into three major parts: first the characterization and selection of fluorescent dyes including studies for their photostability and emission rate, second precision distance measurements on the nanometer scale between two colocalized fluorescent dyes spatially separated by DNA, and third quantification of polymerase II molecules localized in transcription sites inside the cell nucleus.

4.1 Characterization and Selection of Fluorescent Dyes

Single-molecule spectroscopy has experienced an intense development in the past 15 years since the first prove of single fluorophores [Shera 1990; Moerner 1989]. Until today, single emitters were verified in different environments, like in solution [Deniz 2001; Funatsu 1995], in solid [Basche 1992], on surfaces [Güttler 1996; Heilemann 2002], in capillaries [Becker 1999], in cell membranes [Sako 2000, Schutz 2000], and in fixated and living cells [Giuliano 1995; Harms 2001].

The different environmental and measurement conditions require that suitable fluorophores have to be separately determined for every experiment. In cellular environment, for example, the fluorescence signal is commonly superposed by cell autofluorescence and the images are distorted by fluctuations in the refractive indices.

Before the characteristics of fluorophores can be discussed and proper dyes can be selected, the setup components and available fluorophores have to be introduced first, as they are giving the general framework of the measurements.

For excitation, a laser diode emitting at 635 nm has been chosen, because it offers significant advantages in comparison to other, generally shorter wavelength excitation sources. These diodes are relatively cheap, rugged, energy efficient, and can be used in place of more expensive and shorter-lived gas lasers. An even more relevant advantage of 635 nm excitation light is the reduction in background, which significantly improves the sensitivity achievable. There are three dominant sources of background: (i) elastic scattering, *i.e.* Rayleigh scattering, (ii) inelastic scattering, *i.e.* Raman scattering, and (iii) fluorescence from impurities. Both, Rayleigh and Raman scattering, are dramatically reduced by deploying spectrally longer excitation light, because of their reciprocal $1/\lambda^4$ dependence on the wavelength. Likewise, the

number of fluorescent impurities is significantly reduced with longer excitation and detection wavelengths [Aubin 1979, Affleck 1996]. Furthermore, an excitation wavelength in the red spectral region allows measuring in cellular, or more general, in biological material that is known to exhibit strong autofluorescence at wavelengths below 550 nm. Recent reports demonstrated, that with red absorbing fluorescent dyes, even in human sera individual antigen and antibody molecules could be detected [Sauer 1997, Neuweiler 2002].

These advantages have prompted efforts to develop new fluorescent dyes, which absorb and emit above 620 nm, but still exhibit a sufficiently high fluorescence quantum yield [Patonay 1991, Sauer 1995, William 1995]. Among these are oxazine [Sauer 1995, Lieberwirth 1998], indocarbocyanine [Mujumdar 1993, Flanagan 1997], bora-diazaindacene [Sauer 1998, Haugland 2004], rhodamine [Sauer 1995, Arden 1997], and carbopyronine dyes [Kemnitzer 2001]. The underlying structures of these dye classes are depicted in figure 4.1:

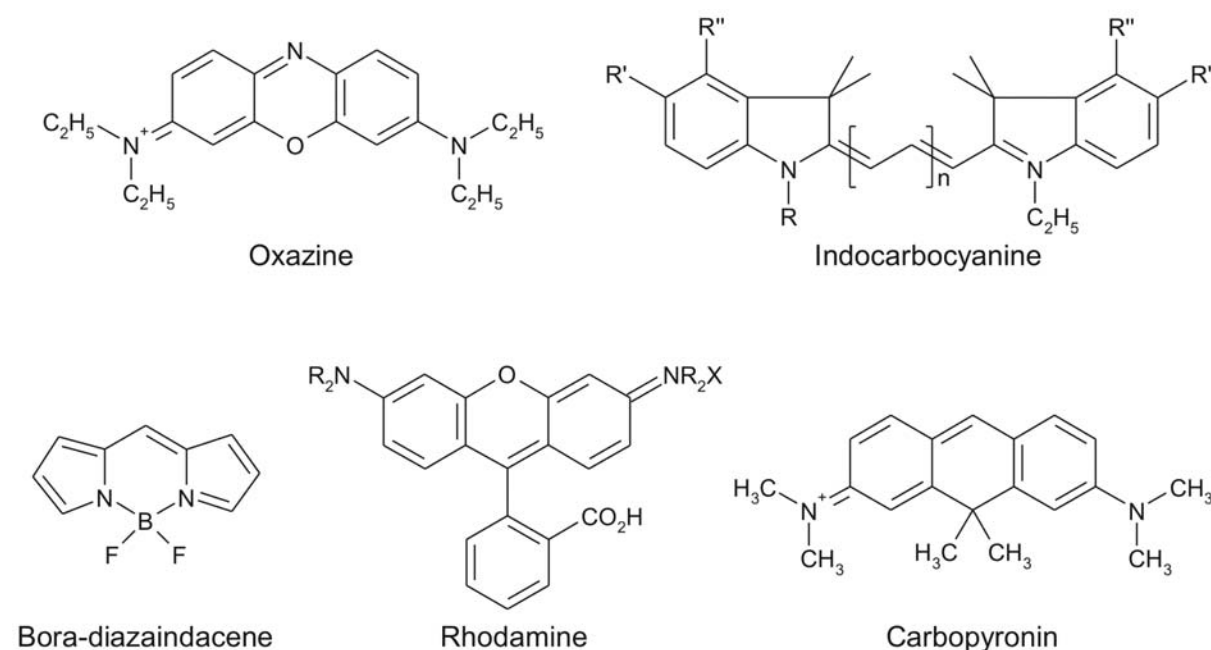


Figure 4.1: Chemical structures of common fluorescent dye classes used in single-molecule spectroscopy, namely oxazines, indocarbocyanines, bora-diazaindacenes, rhodamines and carbopyronines.

Several fluorescent dyes from these classes have been characterized for their properties as listed in table 4.1. The similarities in structure within a dye class induce, that certain spectral parameters are often comparable in their values, for example the extinction coefficient or the fluorescence lifetime. Thus, by just knowing the structure

of a fluorophore, predictions about its behavior can be made, which facilitates a preselection.

| Fluorophore | Basic Structure | Absorption Wavelength [nm] | Emission Wavelength [nm] | Fluoresc. Lifetime [ns] | Extinction Coefficient [l/(M·cm)] |
|---------------|---------------------|----------------------------|--------------------------|-------------------------|-----------------------------------|
| Bodipy 630 | bora-diazaindacence | 629 | 646 | 3.89 | 97 000 |
| Atto 620 | carbopyronine | 619 | 643 | 2.90 | 120 000 |
| Atto 635 | carbopyronine | 635 | 659 | 1.90 | 120 000 |
| Atto 647 | carbopyronine | 645 | 669 | 2.30 | 120 000 |
| Cy 5 | carbocyanine | 647 | 663 | 0.91 | 250 000 |
| Cy 5.5 | carbocyanine | 675 | 692 | 0.83 | 250 000 |
| Dy 640 | carbocyanine | 645 | 671 | ~ 0.9 | 190 000 |
| JA 243 | oxazine | 683 | 700 | 1.89 | 120 000 |
| MR 121 | oxazine | 662 | 676 | 1.83 | 100 000 |
| JF 9 | rhodamine | 630 | 652 | 3.86 | 100 000 |
| Rhodamine 700 | rhodamine | 647 | 670 | ~ 2.5 | 90 000 |

Table 4.1: Spectral characteristics of selected fluorescent dyes measured in water. Absorption and emission spectra are taken at dye concentrations below 10^{-7} M. For the determination of fluorescence lifetimes by TCSPC, 5000 photon counts were collected in the maximum time bin using 2056 detection channels and a monoexponential deconvolution algorithm.

The major criteria for the applicability of a fluorescent dye in a certain experiment are its chemical and photophysical properties. These are given by the spectral characteristics, *i.e.* absorption and emission wavelength and blinking, the fluorescence lifetime, the extinction coefficient, the fluorescence quantum yield, the photostability and the molecular brightness [Buschmann 2003].

Fluorescence Lifetime and F_2 -Value

Two important measures of a fluorophore are its fluorescence lifetime and emission characteristic. These two points are mentioned under the same caption as they are commonly acquired together by Spectrally-resolved Fluorescence Lifetime Imaging Microscopy (SFLIM) [Tinnefeld 2002], the primary used method throughout this work. Since the determination of fluorescence lifetimes has been introduced in chapter 2.1, it is not further discussed here.

The emission characteristic can be expressed as the so-called F_2 -value when two spectrally separated detectors are employed. The F_2 -value is defined as the

number of photon counts collected by the long-wavelength detector divided by the sum of both detectors:

$$F_2 = \frac{I_{long}}{I_{short} + I_{long}} \quad 4.1$$

To classify fluorophores by these two attributes, a selection of the dyes in table 4.1, are immobilized on APS-coated surfaces and imaged. The result of the spot analysis of more than 500 single fluorophores containing over 500 photon counts each is plotted in figure 4.2:

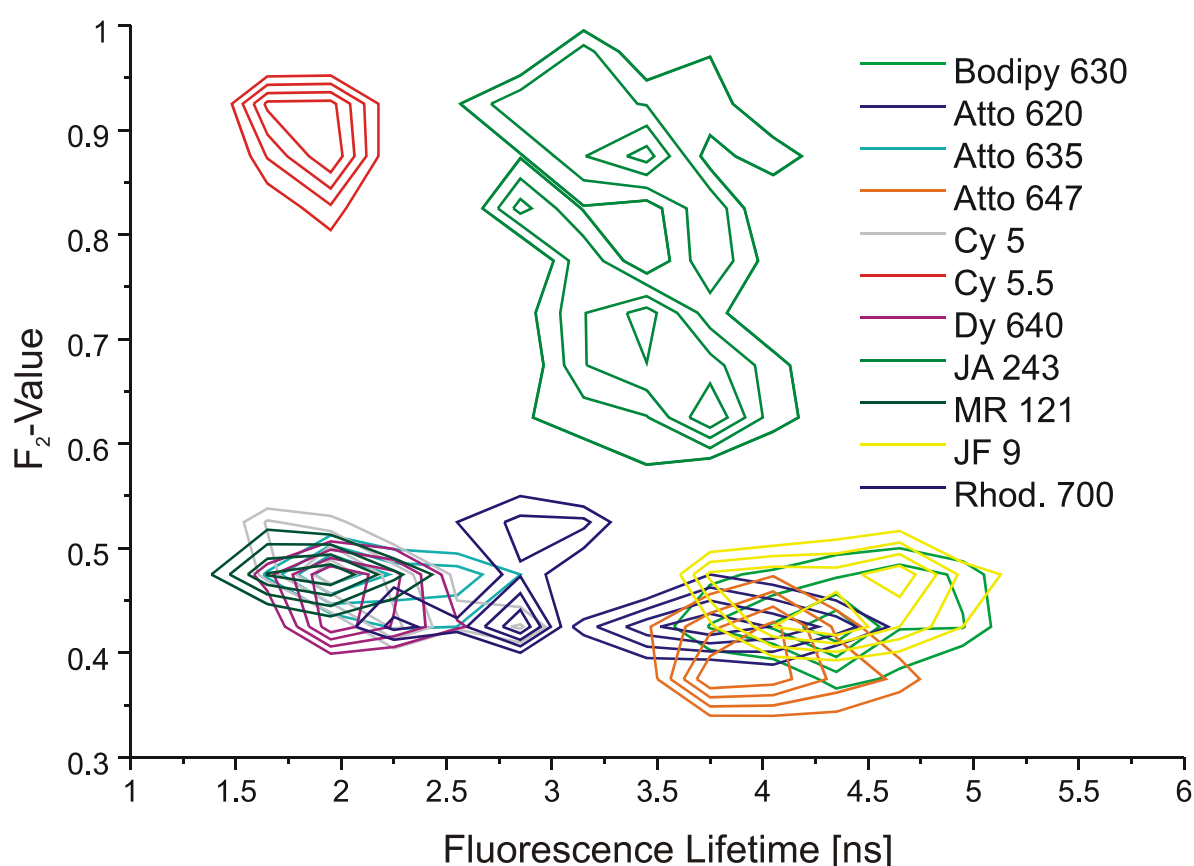


Figure 4.2: F_2 -value vs. fluorescence lifetime contour plot of surface immobilized fluorescent dyes from different chemical classes. More than 500 molecules contributed to every normalized graph. The data are collected on APS surfaces using an integration time of 3 ms per pixel, a resolution of 50 nm per pixel, and an excitation power of 400 W/cm² at the sample.

These initial experiments have been done on dry surfaces as under these conditions molecules can be easily immobilized and do not need to be fixed to the surface as necessary in aqueous environment. Furthermore the number of detected photon

counts is generally higher on dry surfaces than in solution, which noticeably reduces the deviation margin and thus the error.

In figure 4.2 four main populations are found: two with an F_2 -value above 0.6 only populated with one dye each and two with F_2 -values between 0.4 and 0.5 containing several dyes with lifetimes around 2.5 and 4 ns, respectively. This means the properties of the selected fluorophores do not differ as strongly as would be expected by comparison with the parameters in table 4.1, but are rather similar within the single populations. This might partly be due to the non-linear relation between F_2 -value and emission wavelength, as the F_2 -value is extremely sensitive to maximum emission wavelength in the region of the used 685 nm beamsplitter, but is almost not affected by changes more than 15 nm away.

Photostability and Molecular Brightness

Other important points affecting the characteristics of a fluorophore are its photostability and molecular brightness. Photostability plays an important role not only for single-molecule detection by laser-induced fluorescence [Brand 1997, Widengren 1996], and in dye laser chemistry [Antonov 1983], but in practically all applications of fluorescence spectroscopy, where a high signal rate is crucial. The key property influencing photostability is the photobleaching rate [Eggeling 1999], which is a dynamic, mostly irreversible process in which fluorescent molecules are subject to a photo-induced chemical destruction upon absorption of light, thus losing their ability to fluoresce. Hence, the statistical accuracy of the detection is limited, because for every absorption process there is a certain fixed probability Φ_b of the molecule to be bleached. The probability P to survive n absorption cycles and become bleached in the $(n+1)^{\text{th}}$ cycle is given by:

$$P(\text{survival of } n \text{ absorptions}) = (1 - \Phi_b)^n \Phi_b \quad 4.1$$

Despite the central importance of good fluorophores, information on the photophysical parameters is sparse, and little is known about how to design efficient dyes. One reason is, that some of the relevant parameters that influence the photostability are unknown, or have not been investigated in detail. The quantum yield of triplet formation, the triplet lifetime, and absorption properties of excited electronic states are examples for that category. Experimental techniques, which give

information on populated short-lived species, are transient absorption [Carmichael 1986, Jasny 1994] and fluorescence correlation spectroscopy [Szollosi 1998, Selvin 2000, Haugland 2004]. Again the problem of using these parameters is, that they are often sensitive to their environment, and therefore prevent comparing the results of different investigations.

However, when selecting a dye for a certain experiment, simplifications can be made. First, it is not necessary to measure absolute values. It is sufficient to deduce relative parameters for the fluorescent dyes on the setup and under the environmental conditions of the subsequent experiment. Second, the multifaceted photostability can be reduced to two simple determinable values: the overall photon counts until photodestruction and the photon rate per time unit.

It is intuitively easy to agree that the quality of a single-molecule experiment directly depends on the number of emitted photons. That means only if the dye releases sufficient photons - assuming they can be detected - before it undergoes irreversible photodestruction, good statistics and small errors in the parameter determinations can be achieved.

The second point, the photon rate per time unit, is a synonym for molecular brightness. Molecular brightness was initially used as a measure for the average number of photons a fluorophore emits when diffusing through the laser focus in FCS experiments [Köppel 1974]. For immobilized fluorophores this parameter is commonly substituted by the molecular brightness per time unit [Chen 1999].

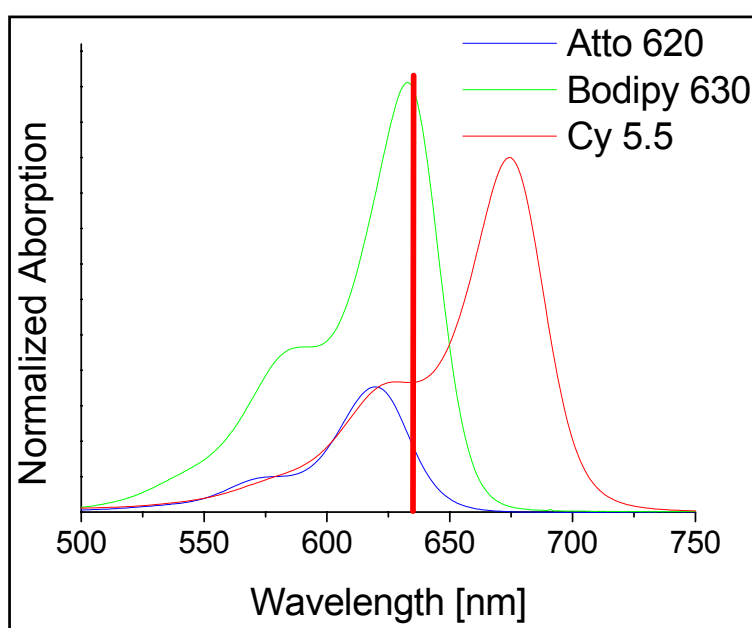


Figure 4.3: Absorption spectra of selected fluorescent dyes normalized to identical concentrations and the corresponding laser excitation wavelength (red line). The cross-over point of the line with the spectra is a direct measure for the excitation efficiency.

It is important to notice that the molecular brightness is strongly dependent on the excitation wavelength. The farther the absorption maximum of the fluorophore deviates from the laser excitation wavelength, the lower the brightness is (figure 4.3). Also the quantum yield influences the brightness as it represents the ratio of emitted to absorbed photons per molecule. In general these two measures give an indication how well a fluorescent dye is suitable for the certain measurement, but as other less conspicuous parameters influence the molecular brightness, too, a reliable value is only given by the experimental determination of its value.

The relevance of the molecular brightness per time unit for immobilized molecules arises from the influence of the background signal. With a constant background level the quality of the data depends solely on the collected fluorescence intensity of the dye. In other words, the higher the signal per fluorophore is in comparison to the background (signal-to-background ratio, S/B), the better the statistics are. Therefore dyes need to be found, which emit their photons in a sufficiently short time interval.

The determination of molecular brightness can be accomplished by single-molecule experiments, but as a limit the collected absolute values depend on the experimental setup, as components like filters and dichroics cut out certain wavelength regions, and distort comparing different measurements.

To be still able to deduce significant values for photostability and molecular brightness per time unit, all measurements have to be done on the setup and under the conditions of the subsequent application. Therefore, single fluorescent dyes are immobilized on APS-coated surfaces, imaged and located in the laser focus until photodestruction (chapter 3.1). The fluorescence signal is recorded separately for every fluorophore, and analyzed for its fluorescence lifetime and emission characteristic.

For imaging, circularly polarized excitation light with a low excitation power of 0.6 kW/cm^2 at the sample is chosen to excite all fluorophores on the surface and to avoid photodestruction of the fluorescent dyes prior to selection. Afterwards, all homogeneous image spots are selected ("picked") and individually approached to gain a representative average over all molecules independent of their local environment and thus of their intensity in the scan image. For this part of the experiment a higher laser power of 1.9 kW/cm^2 is chosen to collect a high number of photons in a short time interval. At higher excitation energies the fluorophores show saturation effects, visible in sooner photobleaching with less overall photon counts.

About 500 time trajectories of every fluorescent dye species (see selection above) are analyzed for their overall photon counts per molecule and count rate per second. Both parameters are summed up in separate logarithmic plotted histograms (figure 4.4 A, B) and fitted linearly.

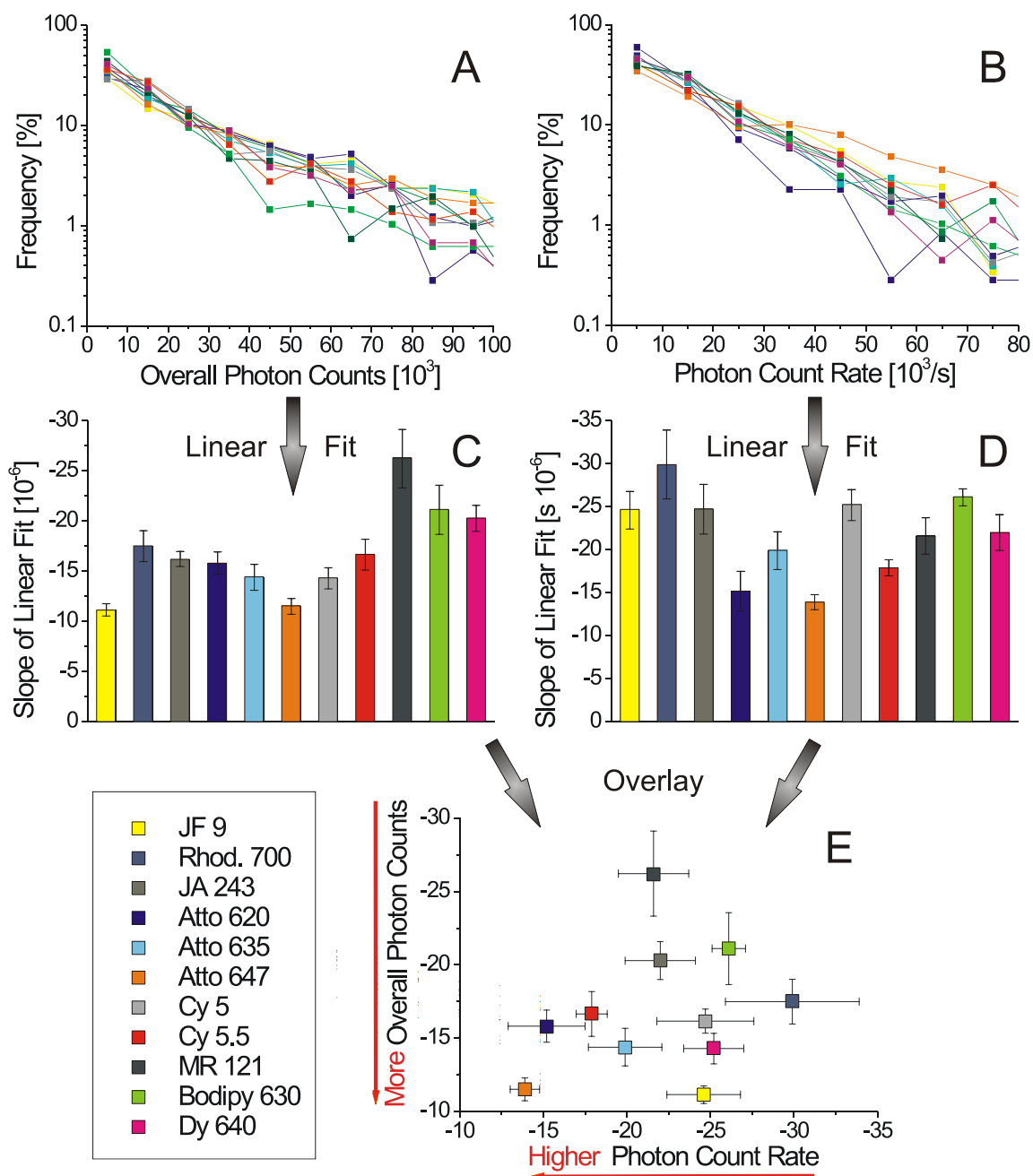


Figure 4.4: Analysis of time trajectories of different fluorescent dyes. More than 500 immobilized fluorophores from each species are evaluated upon their photostability (A) and molecular brightness (B) per molecule. The logarithmic plotted distributions are linearly fitted, and the resulting slope histograms including errors (C, D) are plotted against each other (E). A for single-molecule measurements suitable dye - having a high number of photon counts and a high photon rate - appears close to the origin of diagram E.

The obtained slopes with their errors are shown in C and D, respectively. By plotting the photon number versus the photon rate (E), conclusions about the suitability of a fluorophore for antibunching measurements can be made. The closer a dye is to the origin of diagram E, the more photostable it is and the more photon counts it emits per time interval.

By far the best dye is Atto 647, followed by the other Atto Tec labels and Amersham's Cy 5.5. These fluorescent dyes can undergo lots of excitation cycles and are relatively inert to photobleaching. The worst fluorophores are Rhodamin 700, Bodipy 630 and MR 121, at least under the chosen conditions. JF 9 has got an excellent overall photon number and could be used in experiments with low background, but unfortunately it has got no functional group for labeling.

Blinking

Blinking is a reversible transition into a triplet state, which causes a halt in the photon emission. This photo-physical effect occurs on the millisecond or shorter timescale and strongly reduces the average count rate per fluorophore.

MR 121 and JA 243, for example, show extensive blinking as depicted in figure 4.5. Here a fluorophore showing blinking is plotted against a continuous emitting specimen:

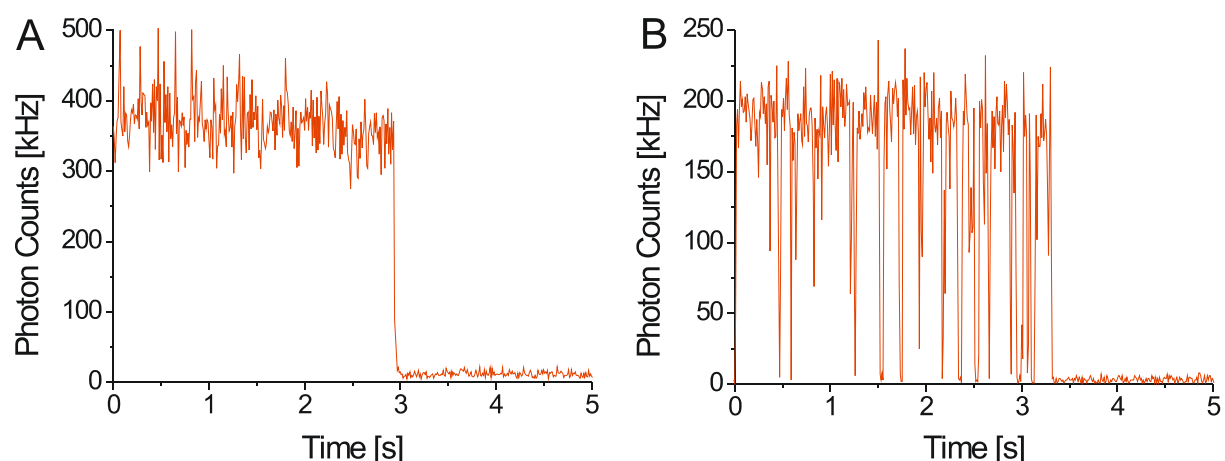


Figure 4.5: Time trajectories of Atto 647 (A) showing continuous photon emission, and MR 121 (B), those trace exhibits numerous dark states on millisecond timescale. The traces are collected from molecules immobilized on an APS-surface with an excitation power of 1.9 kW/cm^2 , and a repetition rate of 10 MHz.

There are some reagents available, which depopulate the triplet state quickly and reduce blinking, but their applicability is limited to measurements in aqueous

environment and furthermore their use is often accompanied by an increased background signal. Examples for such triplet-quenchers are 2-mercaptoethyl-amine (MEA), cyclooctatetraene (COT), or 1,4-diazabicyclooctane (DABCO).

Strong intensity fluctuations due to blinking have an effect on the photon count rate and the overall photon-counts, but their influence is already included in the results presented in figure 4.4 and thus it does not need to be discussed in further detail. For imaging things are more delicate. Here, the position of a fluorophore is mainly given by its Point-Spread-Function (PSF), a two-dimensional Gaussian shaped homogenous image spot. If the integration time per pixel during data acquisition is shorter than the off-times, the PSF looks patchy due to pixels, which contain no, or only few fluorescence counts. Thus, the center of the spots is virtually shifted, and position or distance determinations are subject to a significant rise of the error.

For this reason fluorophores that exhibit strong blinking should be avoided or at least a triplet quenching reagent should be added.

Summary

Throughout this work basically two different approaches on the single-molecule level are undertaken, for which suitable fluorophores need to be determined. The first are colocalization experiments whose goal is the separation and distance measurement between two colocalized fluorophores by their different spectral and lifetime characteristics. The second is the resolution of the number of identical colocalized fluorophores by antibunching measurements.

For the resolution of the exact positions of colocalized fluorophores mainly the independent parameters fluorescence lifetime and F_2 -value are interesting [Heilemann 2002; Tinnefeld 2002]. Thus dyes with orthogonal attributes need to be found.

In the fluorescence lifetime vs. F_2 -value diagram in figure 4.2 mainly four populations are found of which the orthogonal arranged ones represent a suitable choice. Thus a combination of Cy 5.5 (upper left corner) with a dye from the lower right, or JA 243 (upper right) with one dye of the lower left corner are possible. The drawback of JA 243 is its extremely broad distribution, which favors Cy 5.5 in the long wavelength emission sector. Different complementary fluorophores to Cy 5.5 are Bodipy 630, Atto 620, Atto 635, and Atto 647. The two latter are perfectly suited for colocalization with Cy 5.5, but unluckily at the time of the experiments, these dyes were too

unstable under the alkaline conditions needed for labeling and could not be utilized. Recently, Atto Tec GmbH released a stabilized derivative of Atto 647, which should be perfectly suited for the experiment. The remaining dyes Bodipy 630 and Atto 620 exhibit similar spectral characteristics and both of them are used for the colocalization experiments described later in this chapter.

The quality of antibunching experiments on the single-molecule level mainly depends on good statistics [Weston 2002] and thus directly on the number of considered photon counts and on the molecular brightness per time unit. Consequently, antibunching experiments require fluorophores with high photon rates and good overall photon numbers.

In figure 4.4 E the best fluorophores can be directly taken from the graph. The closer a dye is to the origin of the graph, the better suitable it is. Consequently the Atto fluorophores are ideal for antibunching experiments, even though that Atto 647 and Atto 635 tend to be unstable under the basic coupling conditions. Therefore Atto 620 is mainly used throughout this work.

4.2 Precision Distance Measurements between Fluorophores Separated by Double-Stranded DNA

In the recent years the expansion of single-molecule spectroscopy into new areas like biology or medicine induced a rising demand for new detection [Tinnefeld 2000, Herten 2003] and test methods [Giesendorf 1998, Neuweiler 2002]. Especially image acquisition on single-molecule level led to a new understanding of the physical parameters underlying biological processes [Weiss 1999]. In this area an important issue is the determination of precise locations in space and time in an attempt to decode the cell machinery and circuitry [Fritz 2000, Stolz 2000]. Indeed, many cell functions are performed by highly organized structures, for example cellular machines that are self-assembled from a large number of interacting molecules and translocated from one cell compartment to another. To unravel the organization and dynamics of these molecular machines in cells, tools are needed that provide three-dimensional microscopic information about individual molecules interacting with each other.

Conventional far-field microscopy, limited by the Rayleigh criterion [Strutt 1874], allows to measure down to 200 nm in the x- and y-axes, and down to 500 nm in the z-axis [Pawley 1995]. On the other hand, Fluorescence Resonance Energy Transfer

(FRET) can be used to measure distances on the lower nanometer scale [Selvin 2000]. Due to its strong distance dependence ($\sim 1/R^6$) [Förster 1946], only distances of less than 10 nm can be monitored well. Thus, there is a resolution gap between 10 and 200 nm in optical spectroscopy.

In the recent decade several advances have been made to bridge this band. These include wide-field image restoration by computational deconvolution [Carrington 1995], wide-field single-molecule localization and tracking [Dickson 1996, van Oijen 1999, Dyba 2002], 4PI microscopy [Hell 1995]; and point-spread-function engineering by Stimulated Transmission Emission Depletion (STED) [Klar 1999, Klar 2000]. Although these methods have proved themselves to work successfully, each of them holds particular limitations. For example, deconvolution algorithms do not have unique solutions, require subsequent signal processing, and have a limited ability to correct aberrations. Near-field Optical Scanning Microscopy (NSOM) is limited to surfaces, which in a wider view include also cell membranes [Enderle 1997], and it is very difficult to implement for hydrated samples. 4PI microscopy requires accurate alignment of two objectives, signal postprocessing, and put constraints on the sample size. PSF engineering by STED requires ultrafast oscillators and amplifier systems and is not easily expandable to multicolor probes. More generally, aside from NSOM, all these approaches are restricted by basic limitations of far-field optics, like spherical and chromatic aberrations that can never be fully corrected for all wavelengths.

To circumvent these limitations, two competing systems have been developed. On one hand, recently introduced low-noise high-quantum yield Charge-Coupled Device (CCD) cameras enabled the position determination of single molecules at room temperature with a precision of 1.5 nm [Yildiz 2003] by using Total Internal Reflection (TIR) microscopy and a CCD. The collection of the fluorescence signal of two colocalized fluorescent dyes until photobleaching of one of them and subsequent localization of the position of the remaining fluorophore leads to a separation resolution down to 5 nm [Gordon 2004, Qu 2004]. Despite the excellent results of this method, the main limitation lies in its applicability to only two dimensions. When measuring in cellular environment, often three variables need to be resolved.

On the other hand, a multicolor emission system using only one excitation wavelength has been developed on the basis of a confocal microscope [Lacoste 2000]. Here, single fluorescent beads and semiconductor quantum dots are

immobilized on a surface and detected with a sample-scanning confocal microscope similar to figure 3.1, which allows to image each fluorescent emitter free of chromatic aberrations. Scanning the sample with a piezo-scanner in nanometer scale steps, and fitting the resulting PSF images to a two-dimensional Gaussian function can localize their centers with a precision of about ten nanometers. This resolution is limited by shot noise, photophysical behavior of the fluorescence signal (triplet states, blinking, photobleaching), as well as to electronic and mechanical noise of the piezo-scanning device.

Based on this ultrahigh-resolution multicolor colocalization, an improved method has been developed in our group. By implementation of multi-parameter data acquisition, whereby focusing on the parameters F_2 -value and fluorescence lifetime, the error of identifying a fluorophore can be reduced significantly [Tinnefeld 2000, Heilemann 2002, Tinnefeld 2002]. Thus, an algorithm has been developed to predict the error of a system consisting of two colocalized fluorescent emitters separated by a given distance [Müller 2003] (for a summary see chapter 3.4). To check the accuracy of the algorithm, two different fluorescent dyes spaced by double-stranded DNA (dsDNA) of various lengths are synthesized. The distances of the fluorophores are compared with theoretical values. DNA was used as spacer as it tends to be very stiff when hybridized to its complementary chain, thus presuming reproducible results (chapter 2.2). Furthermore, it is of great importance to use biomolecules in the experiments, as subsequent applications are carried out mainly in cells or at least in biological material, and the spacer should not differ too much from the measurement environment in its solubility and behavior.

Characterization of Fluorescent Dye Labeled DNA on Surfaces and in Solution

Before precision distance measurements are initiated, a characterization of the fluorescent dye labeled oligonucleotides and DNA molecules is necessary. Especially the differences in the behavior of the fluorophores alone in comparison to their properties when attached to a biomolecule is of substantial interest. Since the fluorophores were measured on dry surfaces, also the oligonucleotides are characterized under these conditions.

In chapter 4.1 Cy 5.5 and Bodipy 630 are shown to be well suited for colocalization experiments. Therefore these two dyes are attached to the termini of the DNA strands as described in chapter 3.5.

Two commercially available 44-mer oligonucleotides (DNA 44) are selected for the first experiment. A separation of 44 basepairs between the fluorophores, corresponding to a distance of about 15 nm, shall prevent the appearance of Fluorescence Resonance Energy Transfer (FRET). FRET commonly occurs at fluorophore distances below 10 nm and causes a change in the fluorophore brightness' and emission wavelengths, which complicates distance measurements. Both sequences are labeled at the 5'-ends with the fluorophores Bodipy 630 and Cy 5.5, respectively, hybridized to each other, and immobilized on an APS-coated glass coverslip. As reference, both single-stranded sequences are hybridized to their unlabeled complementary strands, and all three samples are measured on the setup described in chapter 3.1.

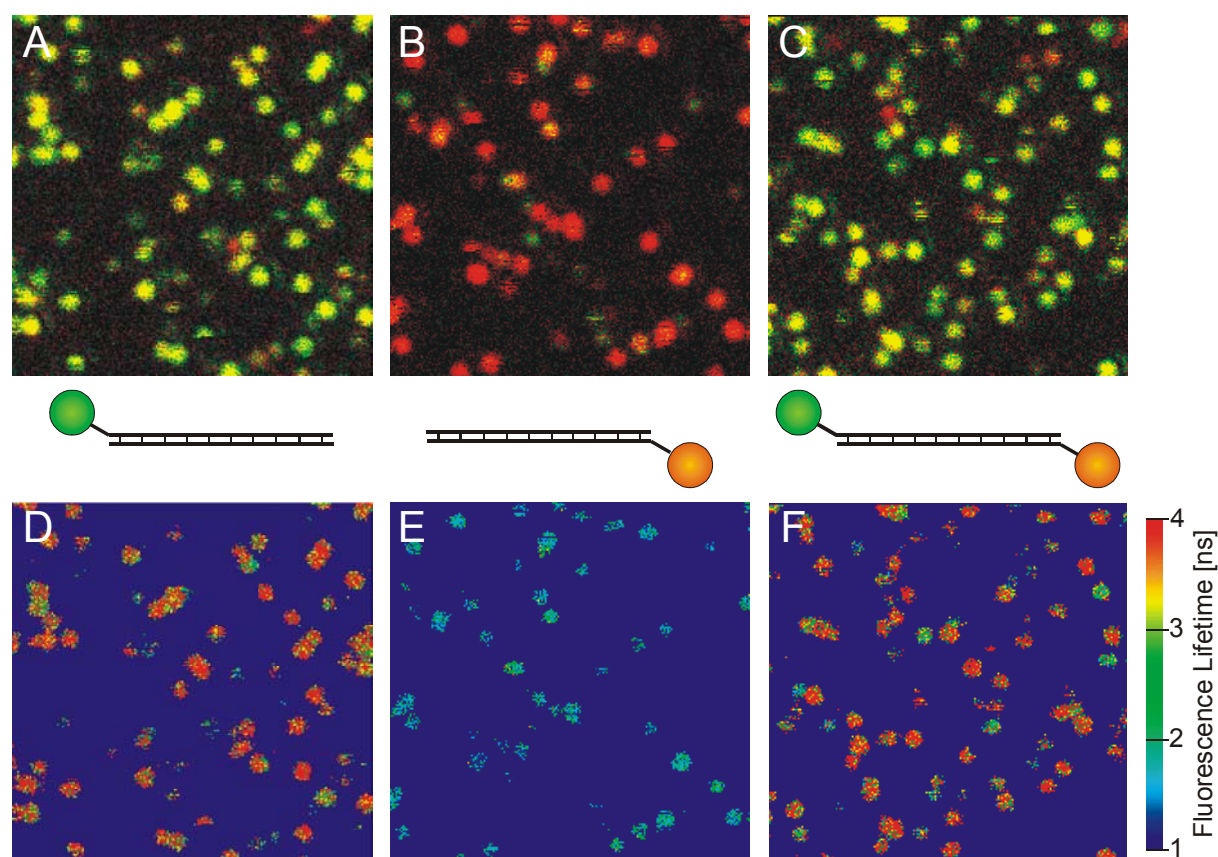


Figure 4.6: False color intensity (A-C) and corresponding fluorescence lifetime (D-F) images of three different Bodipy 630 (green spots) and Cy 5.5 (red spots) 44-mer oligonucleotides immobilized on APS-surfaces. In the intensity pictures the colors are a synonym for the F_2 -value. The codes are green for the short and red for the long wavelength channel. Lifetime images are also color-coded; the values are determined using a monoexponential MLE algorithm. Scan size $10 \times 10 \mu\text{m}$, excitation power 0.4 kW/cm^2 , repetition rate 40 MHz, pinhole $100 \mu\text{m}$, resolution 50 nm/pixel , integration time 3 ms/pixel , threshold 20 counts.

The samples containing a single fluorescent dye (figure 4.6 A, B and D, E) show similar behavior as the corresponding free fluorophores on surface (data not shown). Ensemble measurements suggest, that the absorption maximum in oligonucleotide conjugates is bathochrome shifted less than three nanometers in comparison to free dyes. This effect is about similar for single strands as well as for double strands, and relatively independent of the DNA length. Probably only the few closest nucleobases cause a significant spectral shift, but for longer sequences as used here, these are negligible. In the presented surface experiment, this effect is additionally superposed by property variations of the dyes due to interactions with the surface. Thus, the small differences are not observable and are neglected in the following.

The double strand containing both dyes (figure 4.6 C and F) surprisingly shows almost the same image characteristics as Bodipy 630 alone. Even the fluorescence lifetime is not significantly altered by the presence of Cy 5.5. To better visualize this effect, the properties of single spots are compared with this result in figure 4.7:

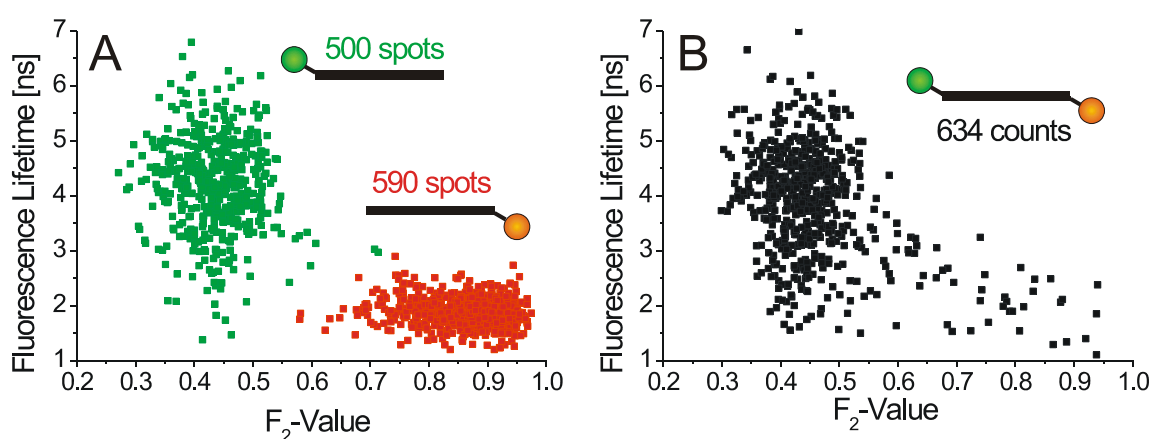


Figure 4.7: F_2 -value vs. fluorescence lifetime plots of mono- (A) and double-labeled (B) 44-mer oligonucleotides. The statistics are derived from more than 500 single image spots collected under the conditions listed in figure 4.6.

The spot analysis used for the above figure and in all the following statistics is based on an automated selection algorithm. The algorithm recognizes a spot due to different criteria, of which the most important is the size. The size of a spot is defined as a group of neighbored pixels with a fluorescence intensity above a certain threshold limit; in figure 4.6 for example 20 photon counts. By applying a circular mask of a definite size around the pixels (for our setup generally with a diameter of 300 nm corresponding to 6 pixels), and summing all the photons in this area, the fluorescence lifetimes and F_2 -values can be determined. More criteria, for example

the roundness or homogeneity, as well as a minimum or maximum intensity per spot, can be additionally taken into account. If any of these parameters is altered, an extra note is given in the text.

Comparison of figure 4.7 A and B clearly shows, that the Cy 5.5 population is virtually inexistent in the images representing both dyes. The double labeled construct is expected to give average values of the single fluorophores, thus being localized at a fluorescence lifetime of 2 to 3 ns and an F_2 -value between 0.5 and 0.8. In image B no such accumulation is visible.

Before further discussion about the populations, some facts about the lifetime analysis used have to be introduced. For the analysis of the fluorescence decays of colocalized molecules it is essential to set proper limits for the fit. A typical histogram of single colocalized Cy 5.5 and Bodipy 630 molecules is shown in figure 4.8:

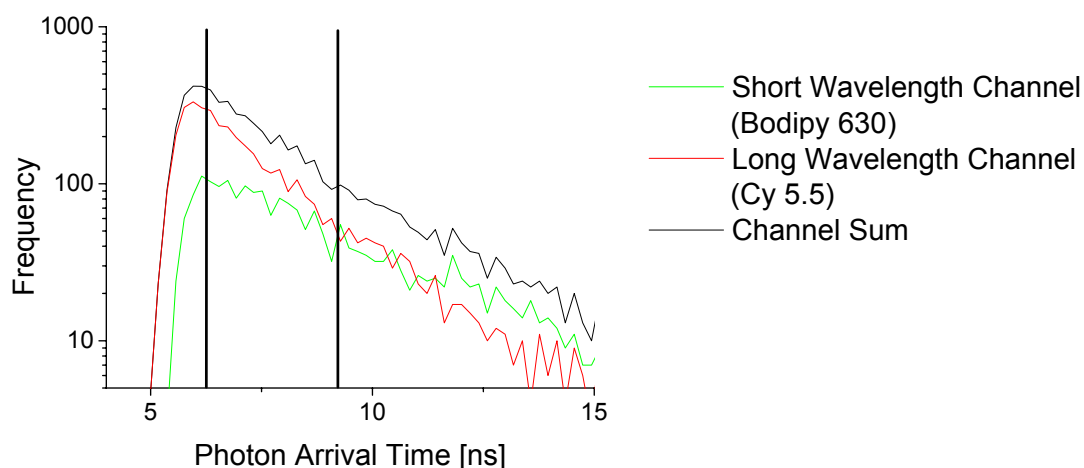


Figure 4.8: Histogram of the photon arrival times for colocalized Cy 5.5 and Bodipy 630 fluorophores, as well as the sum of both channels. The roughly linear decay between the vertical lines is fitted by a maximum likelihood estimator (MLE). The short wavelength graph (green) equals a fluorescent lifetime of 4.31 ns, whereas the spectrally longer curve is determined to 2.02 ns.

In an ideal measurement the fluorophores are perfectly separated by their emission wavelengths, and both detection channels can be fitted over the whole time window (disregarding the excitation pulse function) by a monoexponential algorithm, for example a maximum likelihood estimator (MLE). If two different kinds of fluorophores are excited with the same laser, it is inevitable that the emission distributions of both dyes overlap to a certain extent. This induces a crosstalk signal from one fluorescent dye into the detection channel of the other. The degree of the influence, which thereby furthermore induces a change in the fluorescence lifetime as well, is given by

the F_2 -value. Especially Bodipy 630 with its F_2 -value around 0.4 has got a strong effect on the measured lifetime of the Cy5.5 dye in the long wavelength channel. The crosstalk influence can be reduced in the analysis by setting a small time window for the fit, even though the number of considered photon counts is lowered, which is equivalent to a higher error.

However, for the spot analysis used in this chapter, the sum of both channels, which obviously follows a biexponential decay law, is fitted monoexponentially, thus giving roughly the average value of both separate fitted decays. For investigations and classifications, a small change of the limits of the fit leads to a significant change in the determined fluorescence lifetime, and thus the fitting window is always kept constant.

To investigate the vanished Cy 5.5 population, a similar experiment is repeated using other surfaces, for example using polystyrene (PS) and morpholinoethanesulfonic acid (MES) coatings, and plasma cleaned glass. Also the pH-values of the preparation reagents are modified, but within small deviations, the results remain unchanged.

Another reason for the disappearance of the carbocyanine dye is the dissociation of the two strands in combination with significantly different absorption properties to the surface (figure 4.9 A). Such behavior is typical for unequally charged fluorophores. Comparing the charges of the dyes, Bodipy 630 is found to be neutral in its bound form, and Cy 5.5 carries a charge of minus three.

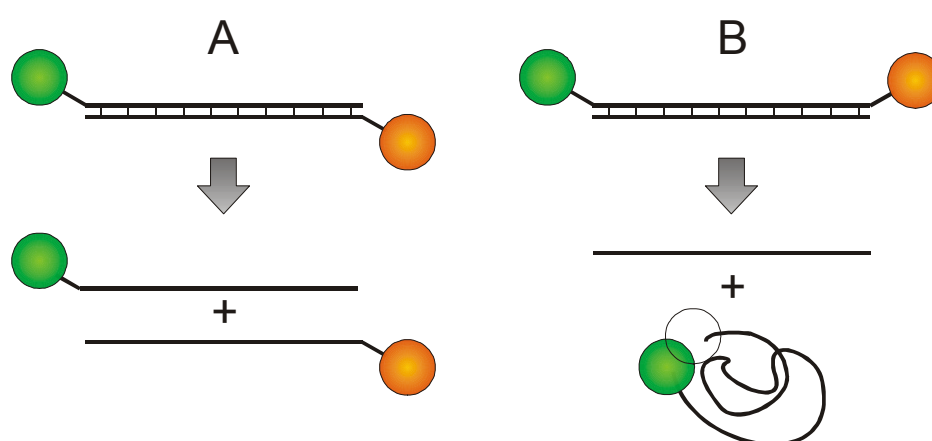


Figure 4.9: Possible reasons for the disappearance of the Cy 5.5 signal upon surface immobilization. Dissociation or mishybridization of the double strand, followed by different absorption properties of the fluorophores (A). Dissociation of the double strand with subsequent agglutination of the fluorescent dyes, thus leading to a quenched state.

For investigation of the surface attachment properties of the fluorophores, Cy 5.5 and Bodipy 630 are attached to the 5' and 3' termini of the same strand, and hybridized to the unlabeled complementary chain to have a rigid spacer between the dyes. Under these conditions, the statistics remain unchanged. A possible reason could be dissociation and subsequent agglutination of the labeled strands, which could lead to energy transfer and thus quenching between the fluorescent dyes (figure 4.9 B).

The evidence that both fluorophores are properly hybridized and do not interact with each other, is given by single-molecule measurements in solution. The result of the analysis of more than 10.000 photon bursts is shown in figure 4.10:

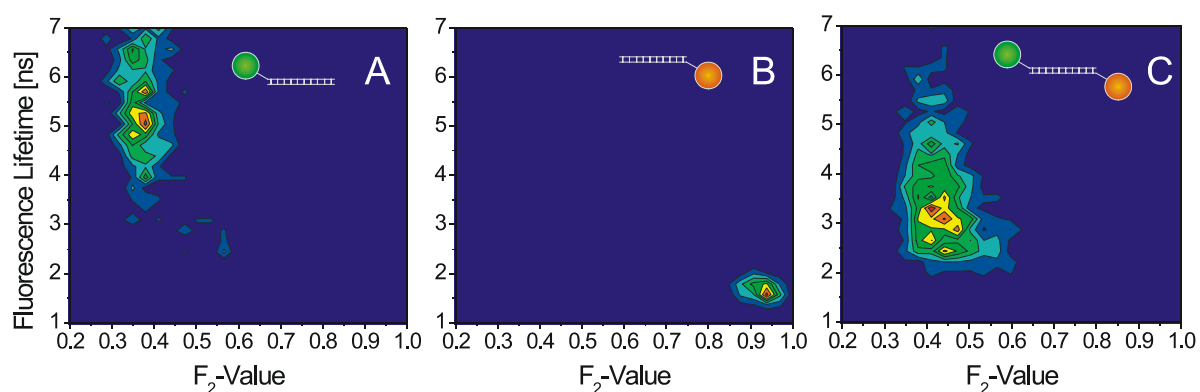


Figure 4.10: Single-molecule measurements of Bodipy 630 (A), Cy 5.5 (B), and double labeled (C) 44-mer oligonucleotides in solution. The data is deduced from burst analysis of more than 10^4 photon bursts each. Excitation power 25 kW/cm^2 , repetition rate 40 MHz, pinhole $100 \mu\text{m}$.

In the plot it becomes obvious, that in solution most molecules carry both fluorophores, since there is a new population between the ones of the single dyes. That means the disappearance of the Cy 5.5 signal is an effect, which appears mainly on dry surfaces, perhaps by oxidation of the fluorophore with aerial oxygen, or by interaction of the chromophoric system of Cy 5.5 with the surface.

To further investigate this behavior, several oligonucleotides labeled on the 5' and 3' termini with identical fluorophores are prepared, hybridized to their complementary strands, deposited on a surface, and checked for the number of emitters by antibunching measurements. The fluorescent dyes Atto 620, Atto 647, and Bodipy 630 are tested, and with any of these fluorophores more than 95 % of the scanned spots consist of one emitting fluorophore only. This implies that this effect is not only eminent for a Cy 5.5 or all carbocyanines, but occurs within several dye classes. Since with Cy 5.5 almost all molecules stop emitting in comparison to

Bodipy 630 (figure 4.7 B), and Bodipy 630 itself is also not quantitatively emitting on dry surfaces, the probability to find colocalized molecules is close to zero in this dye combination. This furthermore indicates, that the fluorophores are unequally sensitive to the surface conditions, but a direct stability or emission rating cannot be given, as the major part of all fluorophores is not in a fluorescent state. Anyway, having such strong influence, the effect itself has to be eliminated or at least reduced.

The consequence of the non-emitting dyes is, that quantifying measurements are not meaningful when dry surfaces are used, as the counting of fluorescent markers requires the simultaneous emission of all fluorophores during photon collection.

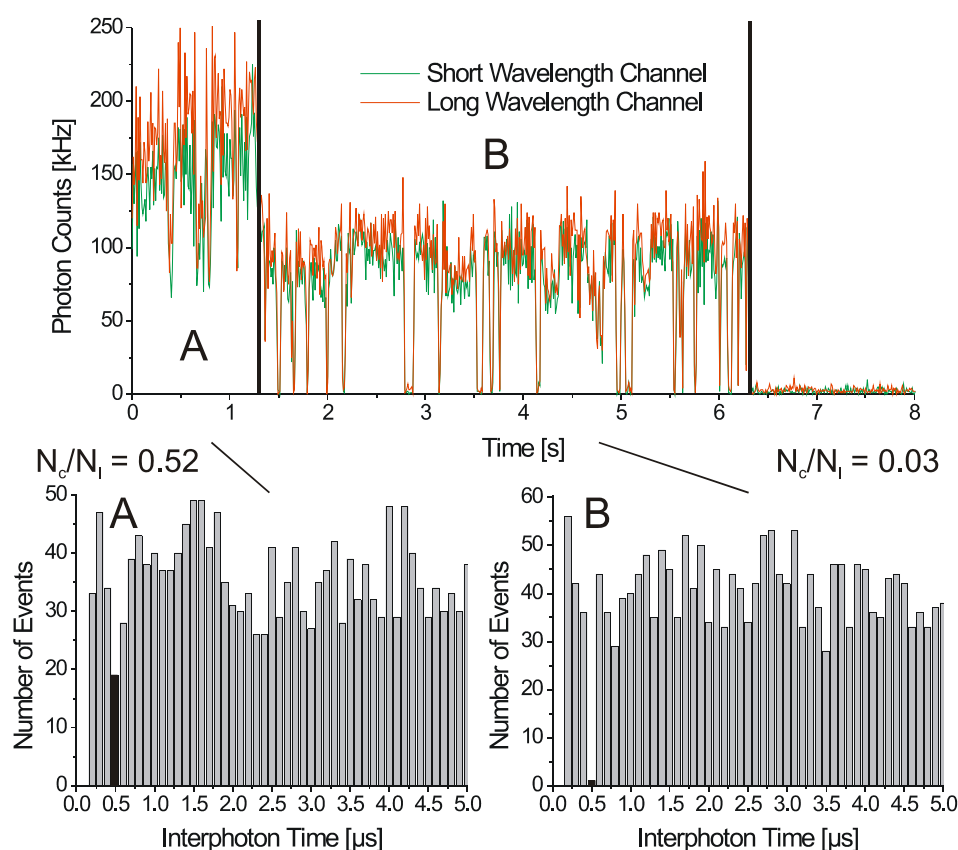


Figure 4.11: Time trace and coincidence histograms of a typical immobilized oligonucleotide terminally labeled with two Atto 647 fluorophores and one biotin. The time trajectory shows an abrupt drop in the emission intensity at 1.3 and 6.3 s each due to photobleaching of a fluorophore. The corresponding coincidence histograms A and B represent the calculated interphoton times in the horizontally split time intervals and by comparison with graph 3.11 give the number of emitters. The immobilization was accomplished using a streptavidin coated surface and PBS buffer as solvent. Excitation power 1.9 kW/cm^2 , repetition rate 10 MHz.

To estimate if this effect is also apparent in aqueous environment, like in cells, which are the dominant measurement environment throughout this work, a double strand

terminally carrying two identical fluorophores and one biotin, is immobilized on a streptavidin coated surface [Piestert 2003]. In an image scan the positions of the fluorophores on the surface are determined, and time trajectories of the single spots are collected. The result is that most of the spots show the behavior presented in figure 4.11.

In the graph a typical time trajectory of a double-stranded oligonucleotide terminally labeled with two Atto 647 dyes is shown. It shows two bleaching steps, one at 1.3 s and a second at about 6.3 s, which are both accompanied by an abrupt drop in the fluorescence intensity. As the two bleaching steps already indicated, the N_c/N_i -ratios of 0.52 and 0.03, respectively, additionally prove the presence of initially two emitters. This kind of intensity trajectory shows the typical behavior of a two-emitter system, which is almost never visible on dry surfaces with similar probes. To investigate the quantity of molecules not emitting in aqueous environment, a statistic from more than 300 spots of three different dyes using their time trajectories and coincidence histograms is composed:

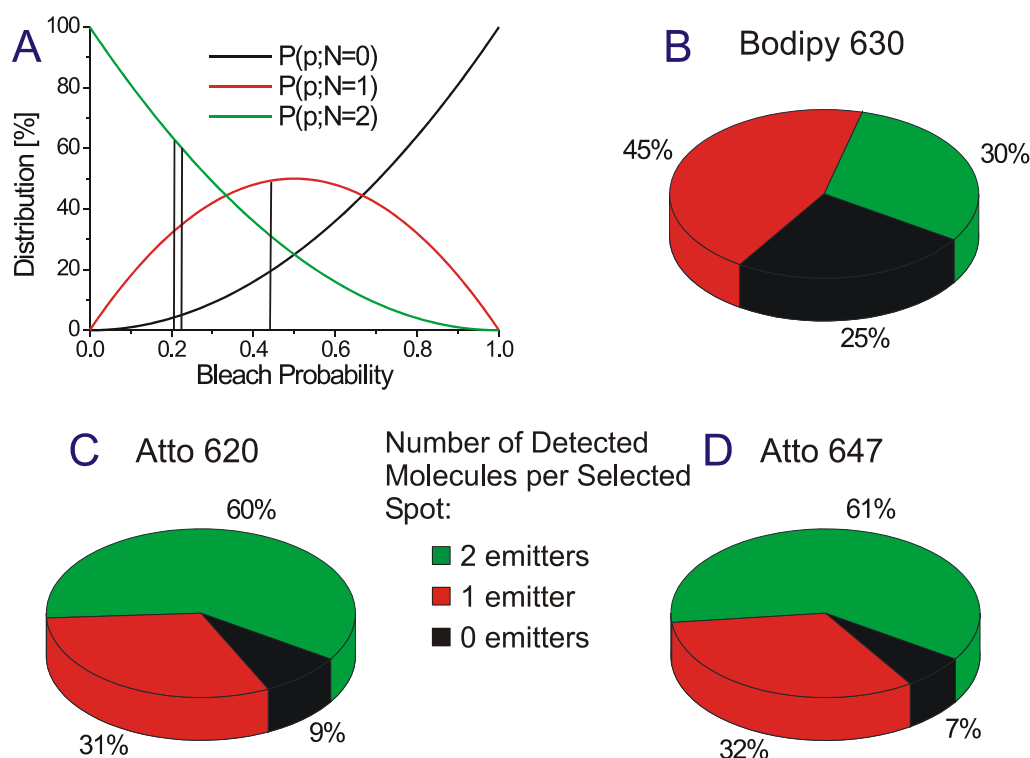


Figure 4.12: Theoretical (A) and experimental (B, C, D) predictions of the number of emitters in a single fluorescent spot. As sample immobilized oligonucleotides terminally labeled with two identical fluorophores, i.e. Bodipy (B), Atto 620 (C), and Atto 647 (D), are used under the conditions listed in figure 4.11. The ratios are taken from coincidence histograms of about 300 spots each. Graph A gives a theoretical prediction of the expected distribution depending on the photostability of the emitter. The vertical lines represent the positions of the three dyes measured.

In graph A the number of emitters of a sample containing two independent fluorophores is predicted assuming that no other factors than the photostability, or in other words the probability p that a fluorophore remains emitting after the scan, influences the number of non-emitting fluorophores (equation 4.2):

$$P(p;N = 0) = (p)^2 \quad P(p;N = 1) = p(1-p) \quad P(p;N = 2) = (1-p)^2 \quad 4.2$$

Especially the occurrence of a vanishing population as on dry surfaces is excluded. By comparing the distributions of the experimental graphs (B, C, D) with the theoretical prediction, a good agreement of the values is found. Only for Bodipy 630 the number for zero emitters in the experiment is found to be higher than expected. This may be due to misinterpretations of the time trajectories, as most of the traces only give very low photon intensities, which reduces the significance of the coincidence statistic. Furthermore, the dye emission is close to the background intensity, which even more decreases the significance. Another possibility for the shifted distribution is the spot selection. With low intensities, the localization of the spot centers becomes difficult, and the result is an increasing number of “mispicked” spots, whose can easily reach a divergence 5 %, or 12 spots, as found in the experiment.

This means that in aqueous environment the effect of non-fluorescing dyes is not apparent and quantifying antibunching measurements can be performed without worrying about the real number of labels in the laser focus. On the other hand it has to be mentioned, that for the two Atto-dyes the number of double labels is determined to be 60 %, but from the sample preparation it is known that their number is 100 %. Thus, even for photostabile fluorophores the effect of photobleaching of a single emitter prior to the antibunching measurement is as high as 20 to 25 % using the settings mentioned above. Therefore, all quantifying results should be corrected with that probability, or for altered conditions this value has to be determined newly.

Biotinylated surfaces represent an excellent basis for measurements with immobilized molecules under aqueous conditions. The disadvantage to their appliance is that they are often not reproducible in preparation and problems, such as low surface density or pollution with autofluorescent particles, are apparent. Hopefully, further investigations will eliminate these problems and make streptavidin coated surfaces an excellent tool for studies in quasi-aqueous environment.

To escape these problems, agarose has been tested as medium for precision distance measurements. Agarose is known to consist of micelles, which enable the incorporation of bigger molecules. Even though the used DNA molecules and oligonucleotides are too short to be immobilized quantitatively, agarose holds a good basis for the experiments, as it simulates an environment similar to cells.

The double Bodipy 630 and Cy 5.5 labeled 44-mer oligonucleotides are dissolved in warm liquid agarose and after three hours the solidified solution is measured. It has to be waited such a long time, as the oligonucleotides are too small to get properly immobilized in the agarose micelles, and first have to be brought to halt on the glass coverslip surface. The resulting spot analysis is presented in figure 4.13:

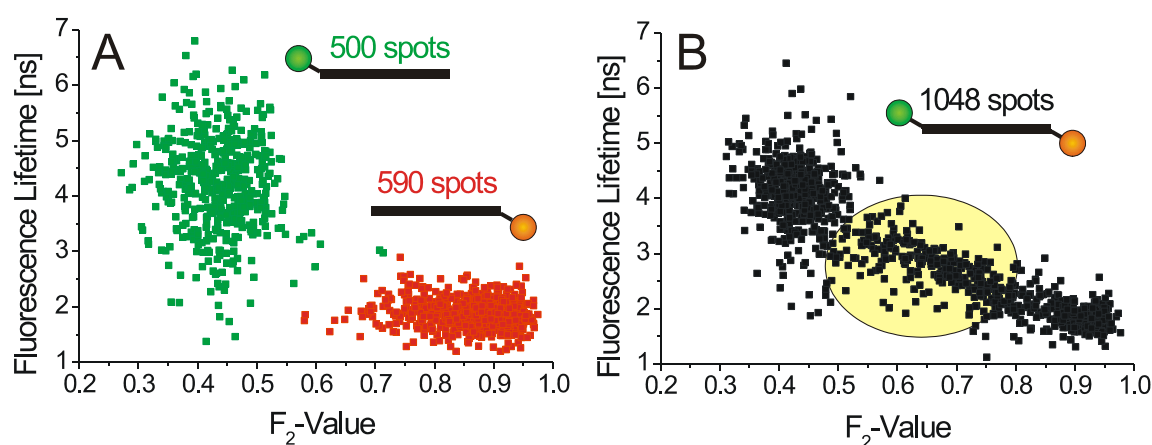


Figure 4.13: Lifetime vs. F_2 -value plots of single-labeled ds44-mer oligonucleotides (A) measured on dry APS-surfaces, and for comparison the statistics of the double labeled analogue in agarose (B). The graph B shows a significant population of colocalized spots, represented by the yellow circle, in a position, where no single labeled DNA molecules in graph A give a signal.

In difference to the behavior of the fluorophores on dry surfaces, in agarose the Cy 5.5 fluorophores remain emitting, even though not all molecules show this effect. It is again difficult to deduce a certain percentage of fluorescing Cy 5.5 molecules, because agarose is not a perfect medium for this kind of experiment, too. After the immobilization time not all molecules are properly immobilized, which leads to horizontal stripes in the scan images due to slowly diffusing molecules. With increasing time, more fluorophores appear, but only in rare island-like regions smaller than 1 mm², colocalized molecules can be found. This makes it very difficult to ascertain if a scan image is in such an island with its complete size or if it is partly outside in a “dry” area, where predominantly the single Bodipy 630 population is

found. As second restriction the Cy 5.5 signal in the islands disappears again after two hours at the latest, probably because at this point the surface has dried and the aqueous conditions are no longer given.

It is significant, that the distributions in figure 4.10 are far narrower than on surface (figure 4.13), which is easy to agree with, as a molecule in solution is surrounded by homogenous distributed solvent molecules, whereas on surface interactions are directed and vary with the environment and the arrangement of the fluorophores. Surface immobilized molecules in aqueous environment show an average between both extremes, as - depending on the linker lengths between fluorophore and biomolecule - the fluorophores can partly rotate similar as in solution and are partly fixed in their position on the surface or at the biomolecule. This implies that in aqueous environment a separation of colocalized fluorophores is easier and within a smaller error than on surfaces. As cell samples also belong to this mixed category, excellent preconditions are given.

Precision Distance Measurements with Fluorophore Labeled DNA

With the perceptions from the above chapter and the basics introduced in chapter 3.4 precision distance measurements are started.

For the distance experiments between the desired 10 and 200 nm, DNA strands of four different lengths are used. At distances longer than 100 nm increasingly broad distributions are expected, as DNA starts to bend [Munteanu 1998]. Thus, units with 44, 70, 148 and 200 basepairs (bp) are synthesized; the two short by hybridization of complementary single-stranded oligonucleotides, and the two long by polymerase chain reaction (PCR) with dye labeled primers. As the average DNA length in helix form is about 3.4 nm per 10 bp, the following lengths of ideal DNA strands are expected:

| DNA length [basepairs] | DNA length [nm] | Synthesis Method |
|------------------------|-----------------|------------------|
| 44 | 15.0 | hybridization |
| 70 | 23.8 | hybridization |
| 148 | 50.3 | PCR |
| 200 | 68.0 | PCR |

Table 4.2: Length of selected DNA double strands in basepairs and nanometers with their synthesis methods.

This approximation is suitable to quickly estimate the length of a DNA, but at a closer look the exact length is dependent on its nucleobase sequence. The sequence of a DNA determines the flexibility and intramolecular interactions, which are necessary to fulfill the task of the DNA in the cell. Lots of models have been developed, which are able to predict distance distribution of given DNA sequences, for example the Freely Jointed Chain (FJC) [Flory 1969] model, which assumes that chemical bonds are free to rotate and possess a uniform distribution of bond angles, and the Worm-Like Chain (WLC) model, where the bond angles are fixed at $180-\theta$, but are free to rotate, giving rise to a uniform distribution of dihedral angles [Bustamante 1994]. In this work the program Cyclize is used, which bases on the WLC model. The calculated persistence lengths of the DNA strands used in this work are given in figure 4.14:

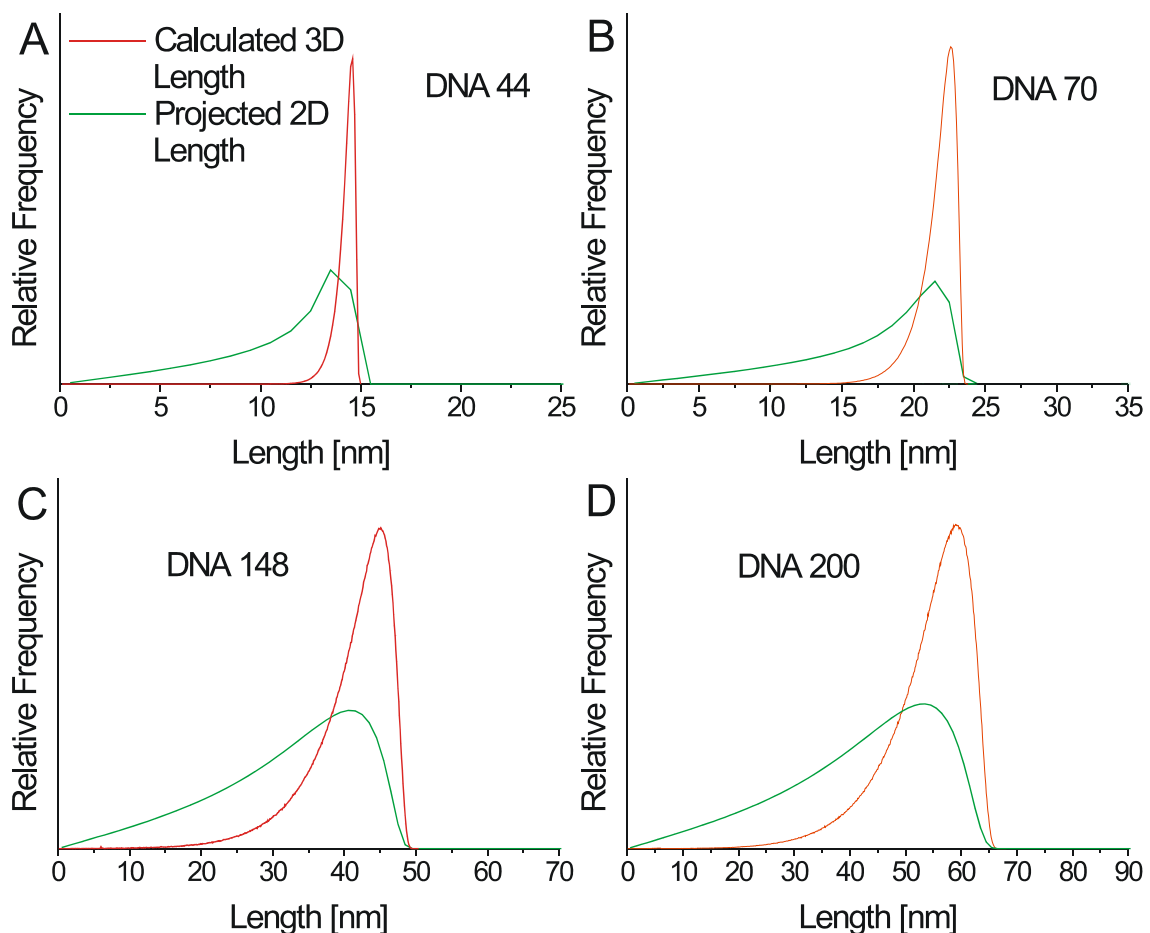


Figure 4.14: Persistence lengths of different DNA double strands calculated with the WLC model based program Cyclize (red graphs). The green lines are the 2D-projections assuming random distribution of the strands.

Figure 4.14 shows the three-dimensional distributions of the DNA assuming no interaction with the glass surface or the agarose. Due to the far better optical

resolution of the confocal setup in the lateral positions than in the Z-axis [Pawley 1995], the measurements are done only primarily in the XY- plane. Therefore the 3D-distributions have to be converted into 2D-projections, which are pictured as green lines in figure 4.14. Theoretically a three dimensional measurement can also be done, but the limits are mainly due to fluorophore stability, which needs to be considerable higher compared to two dimensions. For a deeper insight refer to chapter 5.

With about 20 to 60 colocalized spots of each DNA length, corresponding to about 10 scan images per DNA, the distance algorithm was started. The results in comparison with the 2D-projections are presented in figure 4.15:

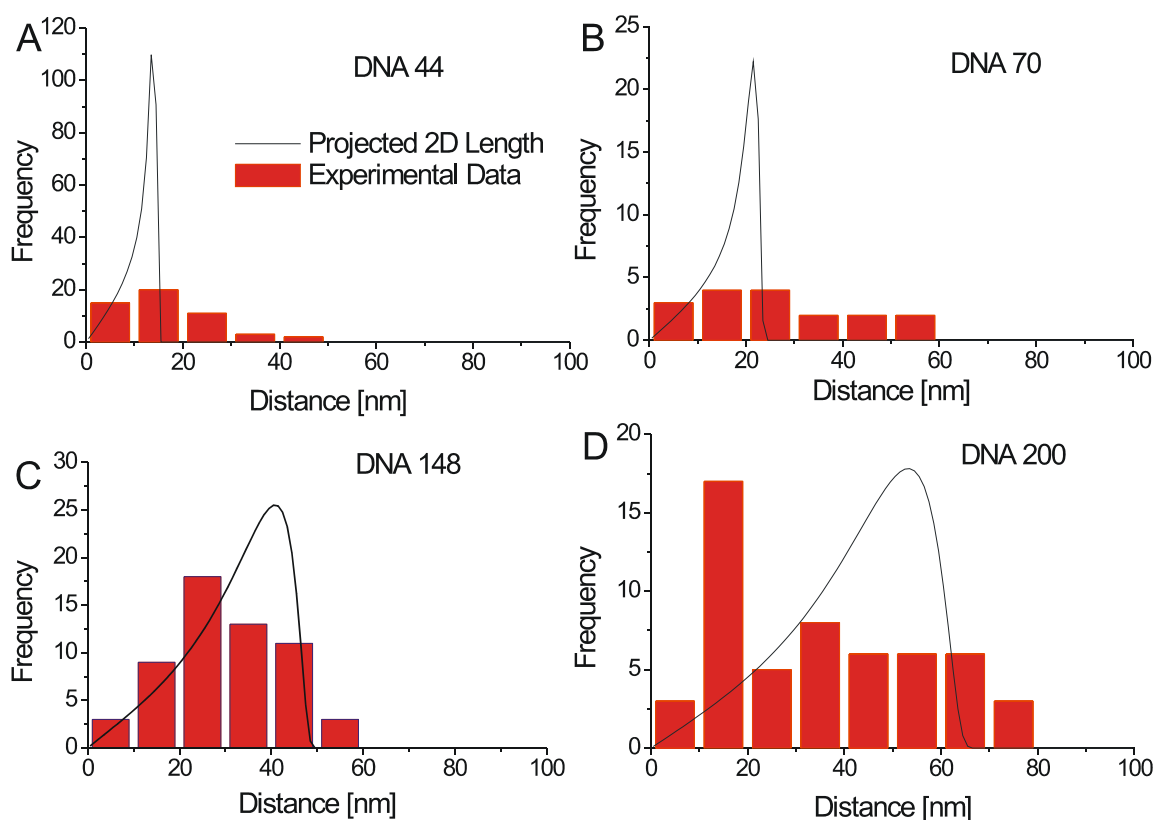


Figure 4.15: Experimental data of four different colocalized DNAs (red) in comparison with the projected 2D-distributions.

The errors for the assignments are between 7 and 15 nm, and are strongly depending on the spot intensity (chapter 3.4). For the longer strands (DNA 148 and DNA 200) all experimental lengths are in the range within the error, whereas the shorter chains show deviations towards longer distances. These could arise from the greater instability of the shorter nucleotides, which might melt and slowly drift apart

during sample preparation. The longer DNA 200 strand is also not perfectly consistent with theory, as a strong accumulation appears around 15 nm, but almost no shorter values are found. A reason could be a dissociation of the double strand, followed by a collapse of the monomers in a way that the fluorophores accumulate. Since lengths shorter than 10 nm are underlying FRET symptoms, which favor the emission of Cy 5.5 and reduce the Bodipy 630 intensity, such spots would not be selected for analysis and thus do not appear in the histograms. The consequence is that almost no distances below than 15 are measured. Only above the FRET regime these spots become visible and give a rise in the distribution. It can only be speculated why the other DNA strands do not show this behavior, but maybe the long sequence monomers interact not only as the 200-mer, but also hybridize in a way that leaves the dyes only a short distance apart from each other. When planning the sequences this possibility has been checked using a computer model, but probably the fluorophores play a decisive role within the interaction.

Another difficulty is, that the two detection channels cannot be assumed to be 100% orthogonal, as this would only be possible using a continuously running feedback mechanism for the adjustment of the detectors. Thus, a varying shift in the acquired distances is always apparent. Its extent can be for example determined by imaging a single fluorophore under similar conditions and split its emission signal equally on both detectors. Subsequent analysis between the channel-separated point spread functions should ideally yield the same shapes and positions. Any deviance equals the misalignment of the detectors. A correction or meaningful determination requires continuous monitoring of the image acquisition, which is yet unsustainable with the analysis time of the collected data. Thus, this error source has to be neglected, and to rule out systematic inaccuracy as far as possible, data originating from different measurements with a separately aligned setup are summed, and subsequently analyzed.

Recapitulating, it has been proved that the experimental and theoretical data are in good agreement with each other, even though that small shifts of the population maxima are found. The system developed has been used to determine distances in aqueous environment, but it is limited to the volatility and instability of the fluorophore emission, which limits the applicability to aqueous samples.

4.3 Antibunching Measurements inside the Cell Nucleus of Fixated and Living Cells

Towards the second goal of this work - accomplishing the quantification of single polymerase II units in transcription factories of a cell - experiments in fixated and living cells are undertaken. With the results from the fluorescence dye tests in chapter 4.1 and the knowledge of the behavior of fluorophores in dry and aqueous samples acquired in chapter 4.2, a method capable to separate fluorescent dyes from autofluorescent cell signal needs to be found. Furthermore, colocalization and antibunching behavior of labeled biological probes have to be checked and characterized for their applicability in cellular environment.

Discrimination of Cell Autofluorescence against Fluorescent Dye Signals in Fixated Cells

It has been shown that antibunching measurements and thus the determination of the number of independent colocalized emitters is possible on dry surfaces [Weston 2002]. Now it needs to be proved, if or to what extent these experiments are applicable to biological systems, such as fixated and living cells.

This proof would open a new prospective in biological research, as it would allow the localization and tracking, as well as the simultaneous quantification of fluorophores. Thus, the functionality and interaction between different cell components could be clarified and the absolute number of components within aggregates smaller than the optical resolution limit could be deduced.

In this work the focus of interest mainly lies in the revelation of transcription processes, which are *in vivo* dominantly taking place in the cell nucleus [Pombo 1999]. Since most biological material is strongly autofluorescent when excited with wavelengths shorter than 550 nm [Sauer 1997], a laser diode at 635 nm is used for most measurements. Still, all cell samples exhibit a certain level of background, which has to be reduced as far as possible by the optimization of cell culture reagents and fixation methods. The maximum autofluorescence level in cells commonly appears in the cytoplasm surrounding the nucleus, which as a positive side effect enables an easy localization of the cell nuclei.

In figure 4.16 a blank cell sample (A) with its corresponding fluorescence lifetime (B) and F_2 -value (C) images is shown. For comparison a fluorescent dye marked fibroblast (D-F) is presented. The label consists of an Atto 620 labeled 40-mer poly-thymine (polyT), which is hybridized to the poly-adenosine tail of the cell messenger RNA:

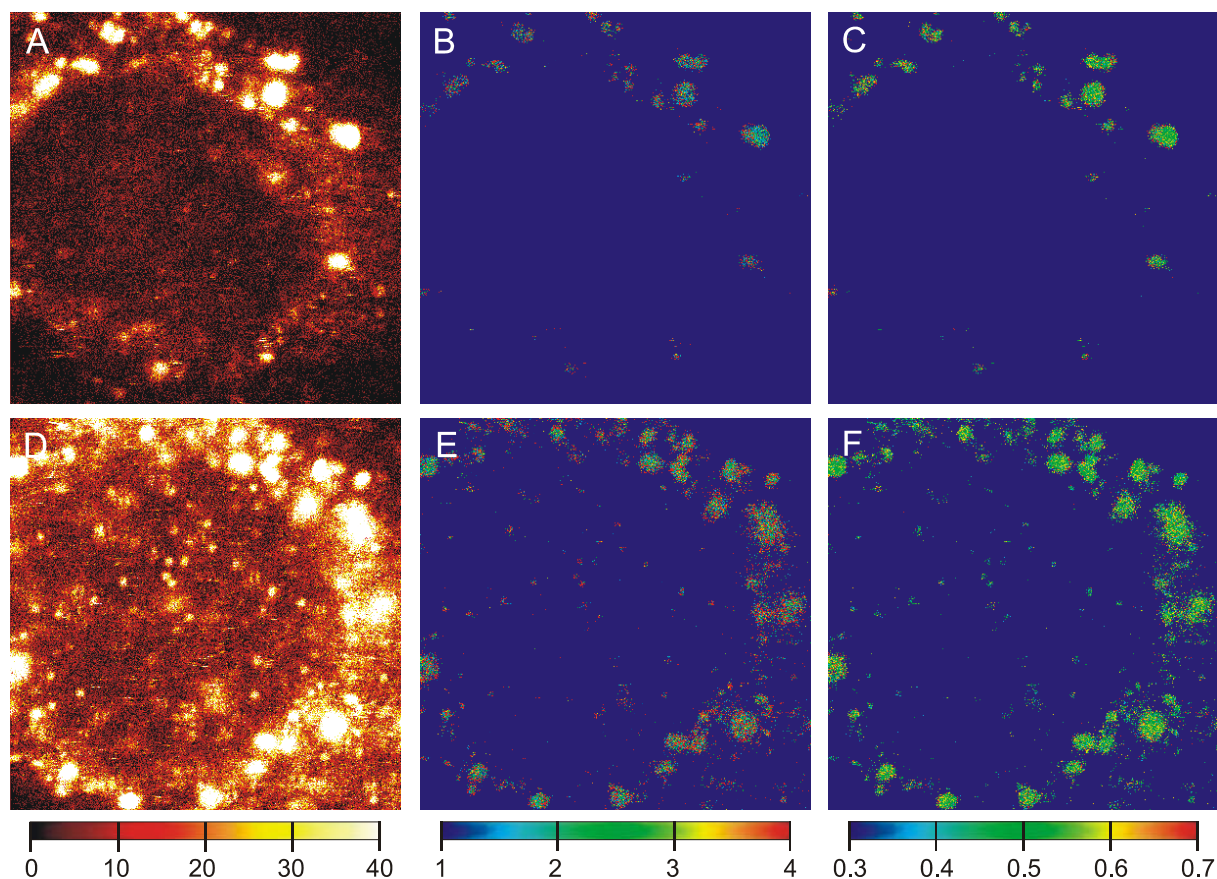


Figure 4.16: Comparison between blank (A) and labeled (D) fixated fibroblast cells with their corresponding fluorescence lifetime (B, E) and F_2 -value (C, F) images. The label polyT-Atto 620 consists of a 40-mer poly-thymine, which is hybridized to the poly-adenosine tails of the cell messenger RNA. Incorporation is accomplished by incubation of a $5 \cdot 10^{-11}$ M solution of the label for 30 minutes at 37°C . Image size $25 \times 25 \mu\text{m}$, resolution 50 nm/pixel , integration time 2 ms/pixel , excitation power 0.7 kW/cm^2 , repetition rate 10 MHz . Intensity threshold 40 photon counts. Lifetime and F_2 -image threshold 10 photon counts.

Due to the three-dimensional framework of the fibroblasts, all cell images are taken $3 \mu\text{m}$ above the glass reflex to measure the nucleus in the plane of its greatest diameter. Another point is that fluorophores tend to unselectively stick to the glass surface. By using an offset in the axial direction, surface signal is out of the focal plane and its influence can be neglected.

In the blank intensity image (A) of figure 4.16 the nucleus is visible as the dark circle with a diameter of 15 to 20 nm in the center of the picture. The nucleus is surrounded by the nuclear envelope, which separates the cell core from the cytoplasm. The bright signal around the nucleus mostly arises from autofluorescent mitochondria, which exhibit a broadly distributed lifetime (B). It is difficult to discriminate these centers against the fluorescent dye Atto 620 by just looking at the pictures, as both Atto 620 and the mitochondria have a fluorescent lifetime between 2 and 4 ns.

At a closer look the nucleus is not completely non-fluorescent, small weak spots, which are not always completely round, are apparent. In comparison to the blank sample (A) the labeled intensity sample (D) shows many, mostly circular spots with an intensity of about 15 counts per pixel, which exhibit a fluorescence lifetime of 4 ns in the lifetime image. These are due to the previously determined Atto 620 lifetime of 3 to 4 ns. Beside these, several often bigger diffuse areas are found above the almost non-existent background level (less than 5 photon counts per pixel).

To assure that the polyT-strands do properly bind to their mRNA targets, the complementary oligonucleotide polyA, a 40-mer poly-adenosine strand, was synthesized and incorporated into a cell. After washing, only few immobilized fluorophores remain inside the cell, as shown in figure 4.17.

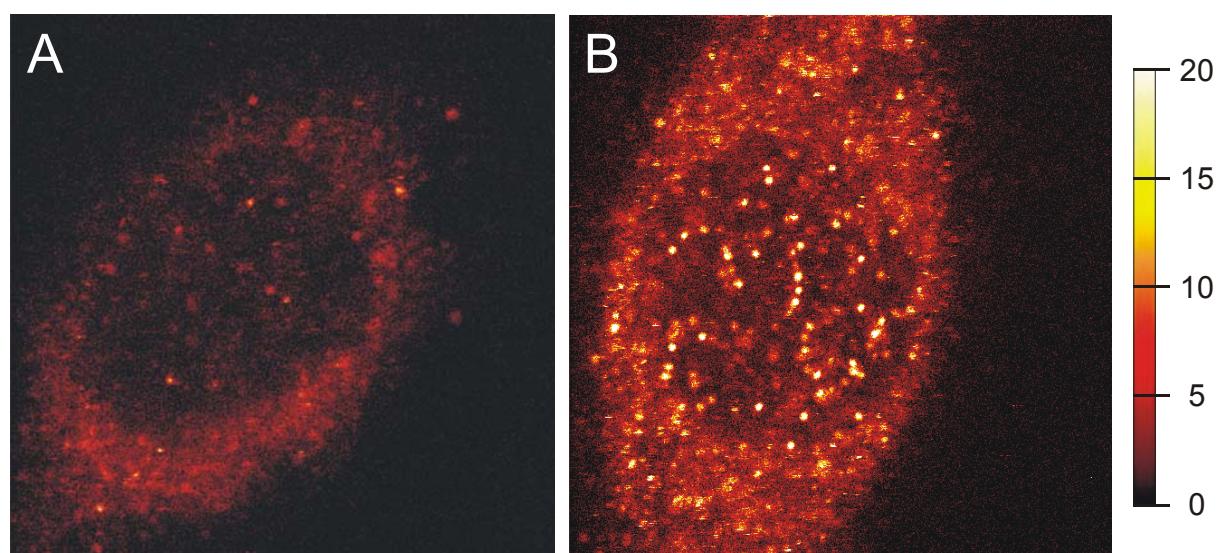


Figure 4.17: RGB intensity images of fixed fibroblast cells stained with polyA-Atto 620 (A) and polyT-Atto 620 (B). While polyT tags the poly-adenosine tails of the cell mRNA, polyA has no complementary strand and thus is not taken up. Image size $30 \times 30 \mu\text{m}$, resolution 50 nm/pixel , integration time 2 ms/pixel , excitation power 0.7 kW/cm^2 , repetition rate 10 MHz . Intensity threshold 20 photon counts.

For colocalization experiments it is essential to be able to distinguish between autofluorescence and the signal from the fluorescent dyes. Since within the nucleus the differences in fluorescence lifetime (B, E) and also F_2 -value (C, F) are not big enough for a save separation “by eye”, a lifetime- F_2 -value analysis of all spots inside, and in the close environment of the nucleus, has been carried out (figure 4.18):

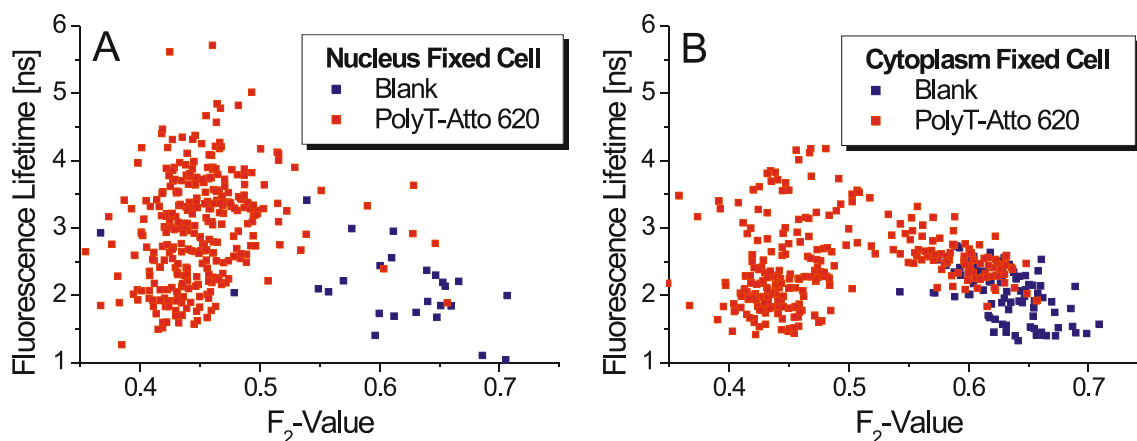


Figure 4.18: Comparison of fluorescence lifetime vs. F_2 -value plots of blank and polyT-Atto 620 labeled fixated cells. Histogram A shows the behavior of spots in the nucleus and B fluorophores in the cytoplasm close to the cell nucleus.

The statistic of the blank nucleus (blue spots, figure A) is relatively unpopulated, since only few autofluorescent spots are found inside the cell nucleus. Even by summation of the spots from several independent measurements, only an indication of a population is obtained. The maximum is situated at a fluorescence lifetime around 2 ns and an F_2 -value of 0.65, while with polyT-Atto 620 (red spots, figure A) a second, far more intense population between 3 and 4 ns and an F_2 -value around 0.45 appears. The same effect is visible outside the nucleus in the cytoplasm (figure B), where the autofluorescent signal is much stronger compared to the nucleus. Here both populations are definitely identifiable and a separation can be done by the fluorescence lifetime and the F_2 -value.

To achieve an optimum probability for separation, both criteria can be taken into account simultaneously. Therefore the histograms are split into their single distributions and fitted to Gaussian profiles (figure 4.19):

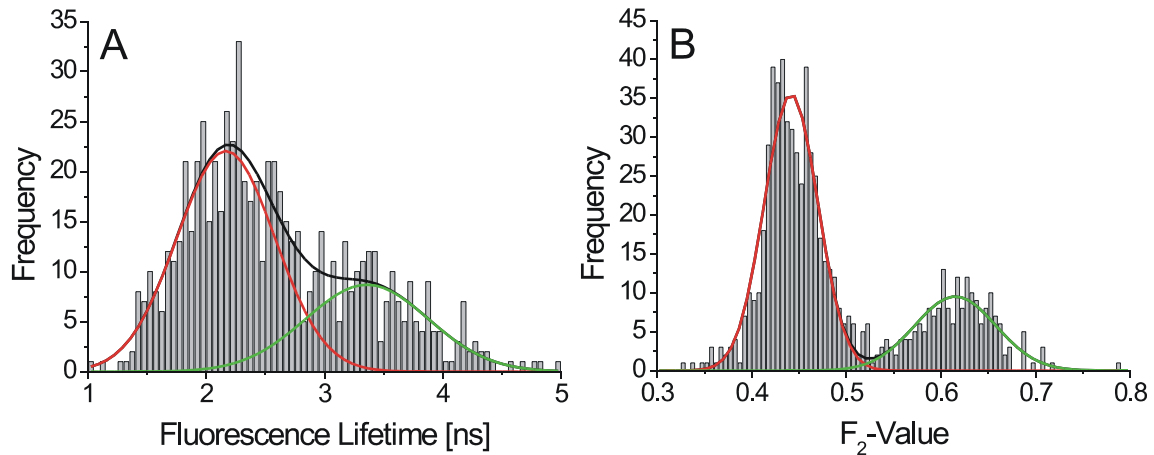


Figure 4.19: Fluorescence lifetime (A) and F_2 -value (B) histograms of fluorescent spots localized in the cell nucleus of fixated fibroblasts, as well as the Gaussian fits of the single dye populations (red) and the autofluorescent signal of the cell (green). The black line represents the sum of both fits (black).

The displayed colored graphs are based on a Gaussian curve fitting and subsequent standardization. The overlap $\Delta(P)$ between the populations is calculated using equation 4.3, where P_1 and P_2 characterize the two different Gaussian distributions:

$$\Delta(P_1, P_2) = \sqrt{\frac{2 \cdot P_1 \cdot P_2}{P_1^2 + P_2^2}} \quad 4.3$$

Application of the equation to the F_2 -distributions in figure 4.19 leads to a separation probability of 94 %. Using only the fluorescence lifetime, where the overlap of the populations is strong, a value of only 55 % is obtained. By taking into account both parameters simultaneously the discrimination possibility increases up to 98 %. For this calculation all spots – both those inside the nucleus and those in the surrounding cytoplasm – are used. As mentioned above, the sites of interest in this work are mainly localized inside the nucleus, where only low background fluorescence is found. Thus, discrimination might even be done with a probability above 98 %, or expressed differently, only rarely an analyzed fluorescent molecule cannot safely be assigned as autofluorescence or fluorescent dye. This leads to the conclusion that experiments with Atto 620 in fixated cells can be performed well under the above conditions.

Discrimination of Cell Autofluorescence against Fluorophores in Living Cells

Biology means the study of life and its underlying mechanisms. Thus *in vivo* complexes, such as RNA, replication foci, or transcription factories, are best researched in living material, where the single components can be monitored in real time during their assembly and interaction. To illustrate this effect, investigations with fixated cells only give a snapshot of a whole movie, which is displayed in living cells. Therefore it is a huge advantage if experiments can be carried out in live environment like in cells. On the other hand this does not implicate that fixated cells do not have a big relevancy as well, as they allow measuring the cell in a fix position without having to care about the persistency of the system.

To ascertain the applicability of the discrimination between autofluorescence and fluorescent dyes introduced for fixated cells in the previous chapter, living blank and labeled cells are imaged on the SFLIM-setup (figure 4.20):

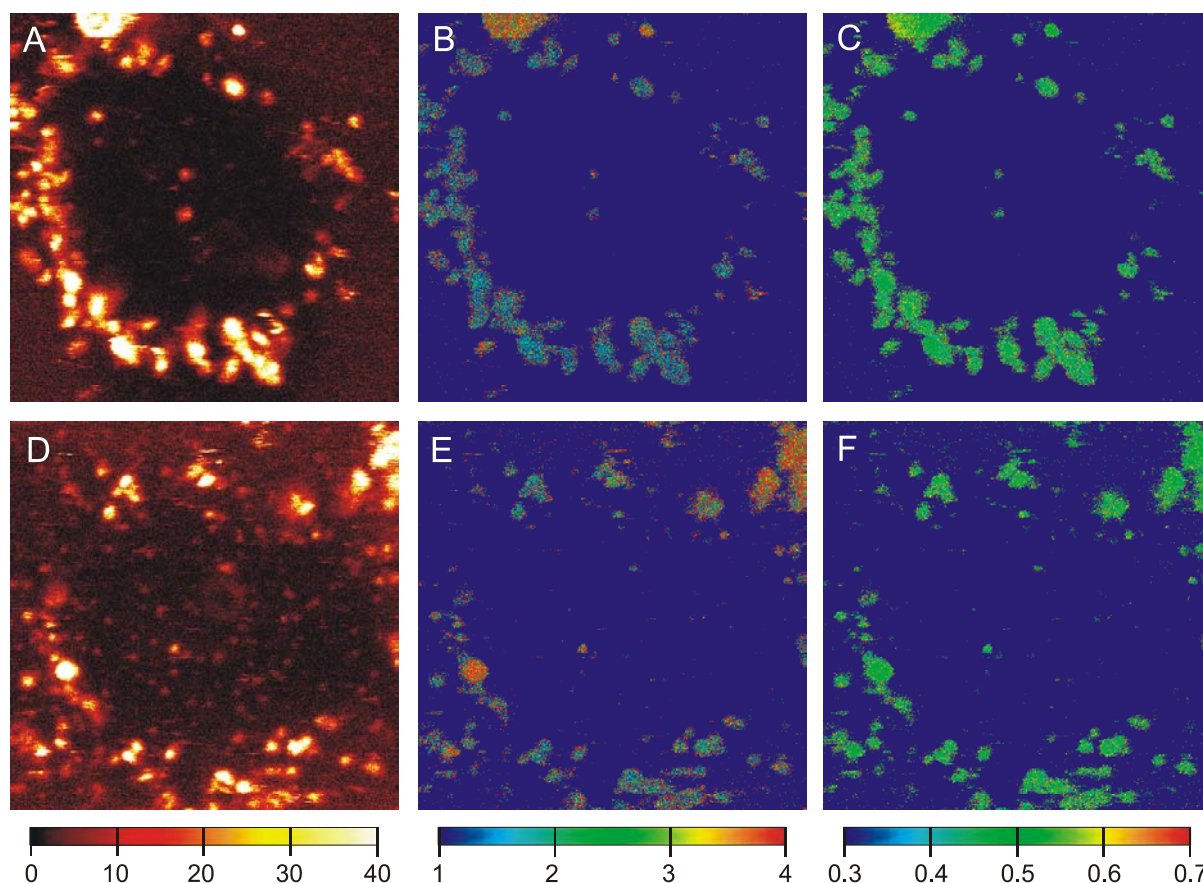


Figure 4.20: Comparison between blank (A) and labeled (D) living fibroblast cells with their corresponding fluorescence lifetime (B, E) and F₂-value (C, F) images. The label polyT-Atto 620 is incorporated by incubation of the cells with a $5 \cdot 10^{-8}$ M dye solution in medium for two hours at 37°C. Image size $25 \times 25 \mu\text{m}$, resolution 50 nm/pixel, integration time 2 ms/pixel, excitation power 0.7 kW/cm^2 , repetition rate 10 MHz. Threshold: intensity 40 photon counts, lifetime and F₂-image 10 counts.

Experiments with living cells are more difficult to accomplish than with fixated cells, since the cell constituents are continuously moving. The samples must be measured in nutrition medium containing fetal calf serum (FCS), which - due to its red color - strongly increases the background fluorescence. In the intensity images in figure 4.20 this is visible in the homogenous fluorescence around the cells, which is far brighter compared to the fixated samples in figure 4.16. Furthermore, due to the setup used in this work the cells have to be labeled and measured outside the incubator with its 10 % CO₂-atmosphere and 37 °C. Kept off their native conditions cells start to express autofluorescent proteins, which further increases the background signal. The autofluorescence is best visible in the bright signals of the mitochondria surrounding the nucleus. It has to be mentioned that blank fixated cells often show similar, but dimmer intensity maxima, too, which arise from stress factors induced by the fixation process. This is, by the way, the reason why fixation is done in the incubator under as native as possible conditions. A further point is that living cells contain lots of active enzymes, which quickly digest incorporated biological material. In this case the oligonucleotides are attacked by endo- and exonucleases, whose task normally is the regulation and transformation of RNA and DNA. In the samples this leads to freely floating fluorescent dye molecules, which are visible as single pixels or horizontal stripes in the images. Since in fixated samples most nucleases are denatured and/ or washed out, this effect only influences experiments in living environment.

Concerning the ease of measurements it is noteworthy that living cells only last for up to two hours at room temperature before visible decomposition occurs, observable in cells modifying their commonly round shape, crumbling, and finally detaching from the surface.

By comparison of labeled and blank samples in figure 4.20 the similar fluorescent spot in- and outside the nucleus are found as with fixated cells in figure 4.16. Thus to gain an insight into the populations a set of fluorescence lifetime vs. F₂-value plots has been rendered from the scan images (figure 4.21):

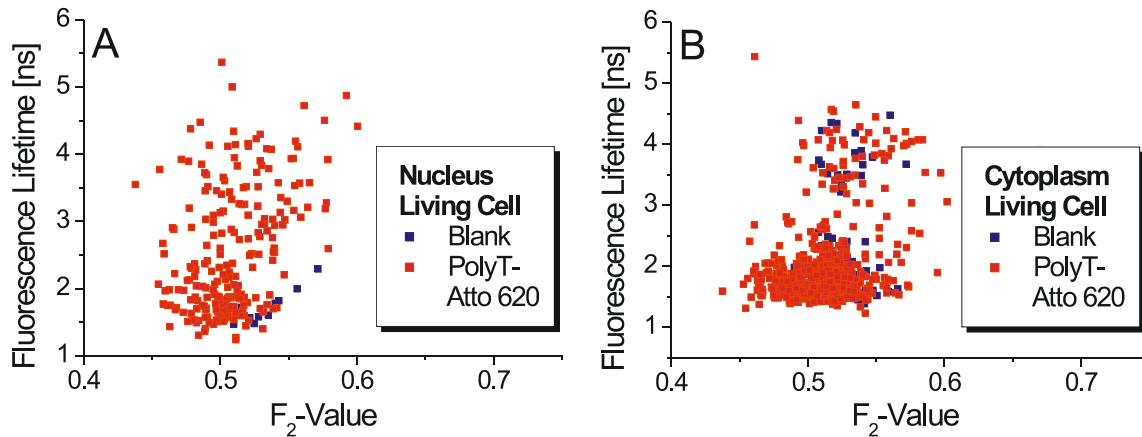


Figure 4.21: Comparison between fluorescence lifetime vs. F_2 -value plots of blank and polyT-Atto 620 labeled living cells separated into spot found in the nucleus (A) and in the cytoplasm (B).

As expected, the blank sample representing the nucleus autofluorescence (blue spots, figure A) shows similar behavior as its fixated counterpart. Only one autofluorescent population is visible, which is located at a fluorescence lifetime between 1 and 2.5 ns and an F_2 -value between 0.5 and 0.6. Surprisingly the values are not corresponding to the ones deduced from the fixated cells, but are shifted in both parameters. Upon addition of the fluorescence labeled oligonucleotide (red spots) a second distribution appears, which is also not exactly similar in its characteristics to the one in the fixated samples. Since all labeling procedures, for fixated and labeled cells, were optimized during the work to achieve a constant reproducible number of labels in a single nucleus, it is striking that the ratio of autofluorescent spots to Atto 620 signals is far higher in the living nuclei. This confirms the previous statement that autofluorescence is stronger in life material compared to dead. In the nucleus surrounding cytoplasm (figure B) the same effect occurs; a lot of autofluorescent signal fronts a small population of fluorescent dye. A further noticeable point is that the populations are more heterogeneous and mostly overlapping. The single characteristics are better visible when looking at the separate frequency histograms in figure 4.22. Since in the cytoplasm extremely strong autofluorescence is apparent, and subsequent measurements are to be done in the nucleus anyway, only the statistics from inside the nucleus are discussed in the following.

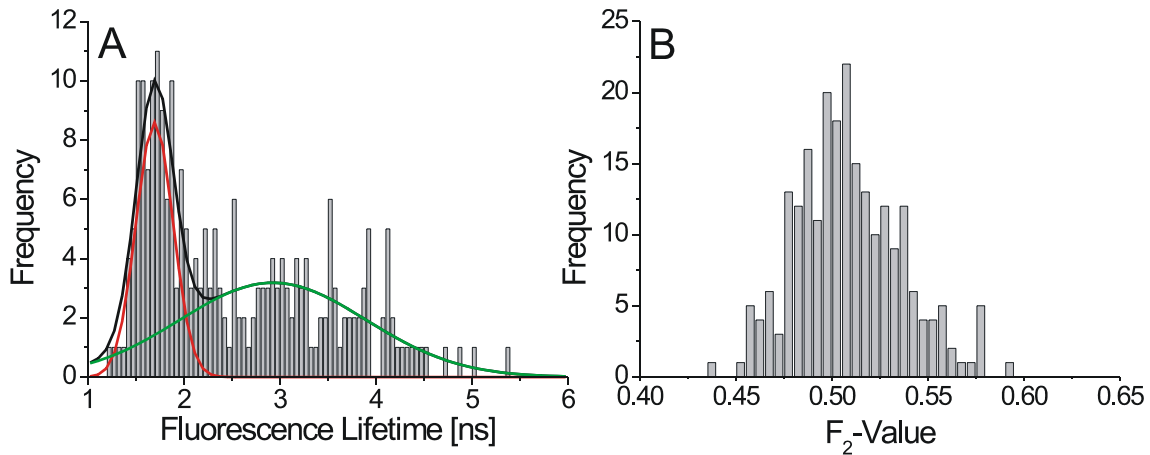


Figure 4.22: Fluorescence lifetime (A) and F_2 -value (B) histograms of fluorescent spots localized in the cell nucleus of living fibroblasts and the Gaussian fits corresponding to the single dyes (red) and the autofluorescent signal of the cell (green), as well as the sum of both graphs (black). In figure B the distributions are not resolvable due to a strong overlap of the two populations.

The fluorescence lifetime histogram verifies that the dye population is not completely separated from the autofluorescence, and the Gaussian fits approve a strong overlap of the two populations. In the F_2 -value histogram this effect is even more explicit; the populations completely overlap, so that no meaningful two-dimensional Gaussian fit can be applied. Consequently, for a higher background and only one parameter the error of separation is greater than in fixated cells.

Using equation 4.2 the overlap of the two Gaussian fits of the fluorescence lifetime histogram was determined to be of 44 %. Looking at the unlabeled cells, the density of autofluorescent spots inside the nucleus is very low. The probability for measuring background fluorescence within the nucleus averages 7 % and is obtained by counting the spots inside and in the area surrounding the nucleus. For the overall probability of the discrimination between fluorescent dyes and background the theorem of total probability (equation 4.4) is applied:

$$P(A) = \sum_{j=1}^n P(B_j) \cdot P(A | B_j) \quad 4.4$$

A is the error of discrimination for all measured cells, and B_j the condition that autofluorescence inside the nucleus either appears or not. In case of condition 1 – autofluorescence in the nucleus appears - the error for the discrimination is about $0.07 \cdot 0.44 = 3 \%$. The possibility for discrimination under condition 2 –

autofluorescence does not appear in the nucleus – is zero, because there is no need for discrimination, as there exists no background fluorescence to distinguish from. After taking into account all spots, the overall discrimination probability averages 97 % in the nucleus of living cells, which is unexpectedly good.

The emission characteristic of Atto 620 is similar to the autofluorescence, and still is very well separable from it. Other fluorescent dyes, which commonly differ more from the cell signal when looking at their emission wavelength and fluorescent lifetime, should yield an even higher probability. Thus, in the following no autofluorescence analysis will be applied in the single experiments anymore.

Recapitulating, these results show that the autofluorescence in fixated and living cells is not a problem when analyzing a whole picture, as the error of misassigning a dye is below 5 %. Only in spots, where an autofluorescent peak and fluorescent dye signal overlap, difficulties occur. Even if in these cases an assignment is possible, and the question for the information gained from the fluorophore arises. For example, in colocalization experiments already two fluorophores need to be recognized simultaneously, and the existence of a third emitter will strongly influence a classification. The same is valid for precision distance measurements, where the error in the determined length will rise significantly, or in quantifying antibunching analysis, where the height of the central peak is strongly influenced by background signal, which thus reduces the upper limit of countable molecules.

Anyway, in the following the main focus will be in measurements inside the cell nucleus, where only few autofluorescent areas are apparent, and spots containing too much autofluorescence will be taken out of the statistic manually. This is admissible, as long as no quantification or classification over a whole cell or cell area is done, and only single spots are considered exemplarily.

Antibunching Experiments and Quantifying Analysis in Cellular Environment

Beside the characterization of fluorophores and their discrimination against autofluorescence in cell samples, the quantification of colocalized molecules becomes increasingly important in the investigation of biomolecular machines. Quantifying experiments can, for example, give access to the number of colocalized genes or copies of a protein in such a complex. This information can be further used

to determine biological turnover rates, interactions and mechanisms, which are essential for the understanding of cell biology.

A simple possibility to realize quantitative estimations is the adoption of different distinguishable fluorescent tags to the biomolecule of interest. As differentiation characteristics the emission wavelengths, F_2 -values, absorption wavelengths, blinking behavior and other criteria are thinkable. The main drawback using different fluorophores is the non-zero probability to get several identical labels in one interacting complex, which are not resolveable and thus wrongly detected as a single label.

When the deployment of different fluorophores shall be avoided or if only one sort of fluorescent labels is at hand, rotation polarization experiments, which are limited to two emitters in the maximum, and antibunching measurements (chapter 3.3) are the only viable approaches for quantification. Antibunching has been shown to work on dry glass surfaces [Weston 2002], but in cellular environment, the feasibility of antibunching experiments still has to be proved.

The main interest in this chapter is the introduction of antibunching measurements to cells with a setup similar to the one used by Weston *et al.*, which allows to simultaneously access several characteristic parameters of the fluorescent emitters. Furthermore the advantages and limits of the method are discussed.

In figure 4.23 time trajectories of polyT-Atto 620 on a dry APS-surface (A), and incorporated into a cell as described in chapter 3 (B), are shown.

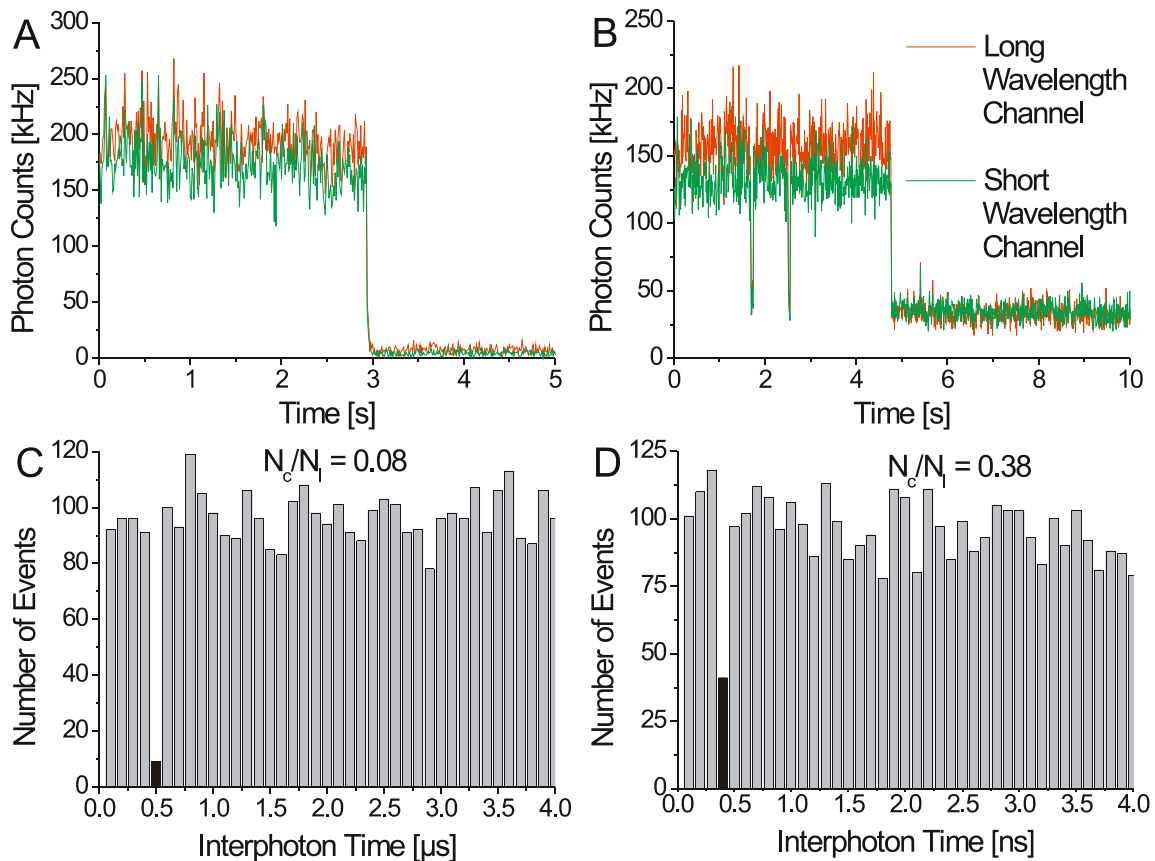


Figure 4.23: Typical time trajectories of single fluorescent polyT-Atto 620 molecules measured on an APS-surface (A) and in a fibroblast cell (B) with their corresponding coincidence histograms (C, D). The higher background level in graph B increases the height of the central peak (black), even though only one emitter is present in both time traces. Excitation power 1.9 kW/cm^2 , repetition rate 10 MHz, delay time $0.5 \mu\text{s}$.

As mentioned above, the background fluorescence intensity inside cells is far higher than on clean surfaces. In figure 4.23 B this becomes obvious in the high intensity level of $\sim 30 \text{ kHz}$ after photobleaching of the fluorophore. The photobleaching step is visible as the abrupt drop in the photon count intensity after 3 and 4.8 s, respectively. Compared to the dry sample (A), the intensity level is around ten times more intense. The corresponding coincidence histograms (C, D) represent one emitter each, even though the N_c/N_l -ratios are non-zero, as would be expected for one ideal emitter. By taking into account the signal to background levels, which are about 20:1 in trajectory A and 4:1 in B, and correcting them with the expected values deducible from figure 3.11 B, both center peaks are determined to be close to zero. Accordingly in both cases the fluorescence signal arises from only a single emitter.

This procedure can efficiently be done to distinguish one or two emitters, but with an increasing number of fluorophores, the measured N_c/N_l -ratios move closer towards a

continuum, which limits the number of determinable molecules. With increased background signal the maximum number of determinable emitters is further reduced and the error of the assignment is increased. This unavoidable problem represents the main limitation to the maximum number of quantifiable emitters. Thus, the reduction or suppression of autofluorescent signal is the most eminent goal when undertaking antibunching measurements in cellular environment.

To give a statement about a respectable upper number of molecules determinable in cells, not only ideal emitters, but also molecules with low photon statistics, mostly tantamount to a short time interval until photobleaching, or cells with strong background fluorescence, have to be discussed. In figure 4.24 a time trajectory exhibiting both criteria is displayed:

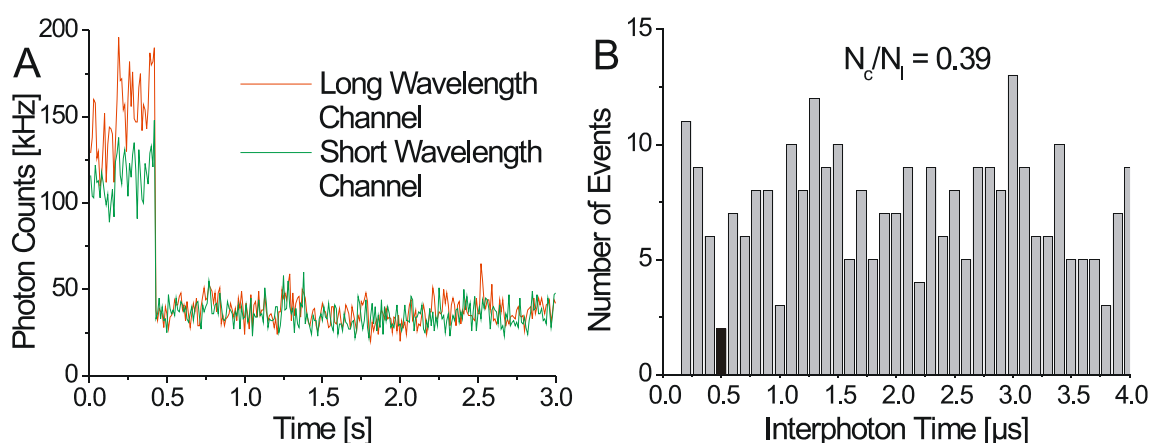


Figure 4.24: Time trajectory of a short lived single emitter measured in a fixated fibroblast cell (A) with its corresponding coincidence histogram (B). The central peak at 0.5 μ s is highlighted black. The intensity trace contains only about 10.000 photon counts between 0 and 0.4 s and shows a high background signal. Excitation power 1.9 kW/cm², repetition rate 10 MHz, delay time 0.5 μ s.

Even if the coincidence ratio of 0.39 (figure 4.24 B) is revised by the background ratio, which yields about 3:1, and the corrected ratio shows that it is around zero, the question for the reliance of such a value needs to be raised. When considering the time bins away from the central peak, it becomes obvious that they strongly vary in their height, even though they should be tendentially constant. If similar fluctuations affect the central bin, no proper assignment can be given. In this case, the central peak only holds two counts. If this bin is populated by one interphoton count more or less, the value is shifted to 0.51 or 0.26, respectively, and the information deduced from the N_c/N_l -ratio is not properly interpretable in the same way.

That means only trajectories with high photon counts grant meaningful values for the coincidence ratio. If several emitters are colocalized in the laser focus, rarely all fluorophores survive long enough to obtain sufficient photon counts in every photobleaching step. Therefore other arguments, like intensity steps due to photodestruction of an emitter, have to be taken into account as second criterion [Funatsu 1995]. Still, the following time trajectories and their corresponding coincidence histograms show, how difficult an assignment is, and how carefully an assertion has to be made:

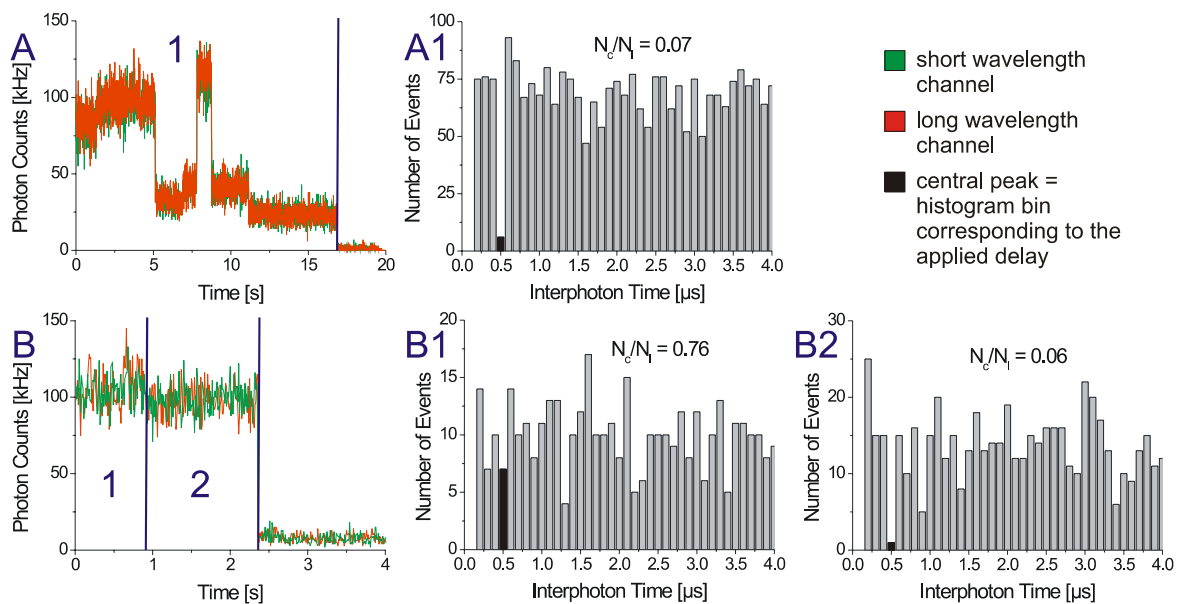


Figure 4.25: Time trajectories and corresponding coincidence histograms for selected time intervals taken from Atto 620 labeled polyT molecules in a fixated cell sample. The fluctuating intensity characteristics of figure A suggest the presence of several emitters, while the N_c/N_l -ratio proves a single emitter. Graph B shows the opposite behavior; two emitters are present, while only one would intuitively be anticipated from the intensity trajectory. Excitation power 1.9 kW/cm^2 , repetition rate 10 MHz , delay time $0.5 \mu\text{s}$.

Before the image analysis the properties of the polyT-Atto 620 label need to be introduced. In cells this tag hybridizes to the polyA-tail of the messenger RNA. Since this adenosine sequence is known to commonly consist of more than 200 identical nucleobases, the probability of double labeling when using a 40-mer polyT is given. This makes the mRNA a well suitable biomolecule for the purpose of molecule counting in cells. When using a 40-mer also the distances between the fluorophores are long enough to prevent effective energy transfer between the dyes.

In figure 4.25 A a fluctuating time trajectory is shown. It consists of three intensity drops and one rise, but no reliable conclusion about the number of emitters can be made from the steps alone. The corresponding coincidence histogram on the other hand definitely proves the presence of only a single emitter during the whole time period. Figure B shows a virtually constant intensity level until photodestruction at 2.4 s, which usually is taken as a property of one single emitter. By splitting the intensity trace into two parts and monitoring the interphoton time distributions on both sides of the trace, while simultaneously altering the split limit until the N_c/N_l -ratios differ most, the coincidence histograms 2 A and B are obtained. The underlying interphoton times are not numerous, but still tolerable, and the coincidence ratios of 0.76, and later 0.06, might account for the presence of two emitters, of which one photobleaches after ~ 1 s, followed by the next at 2.4 s. The procedure is not completely trustworthy for weak statistics as with low photon count numbers the coincidence ratios are subject to fluctuations.

This clearly points out the flaw of antibunching measurements. In the analysis of a big assembly of molecules, interphoton thresholds, minimum photon numbers and intensities, or a maximum background level, can be set to reduce cases like the ones described. If only a limited number of traces is available, or the interest is focused on a single fluorescent complex, the best possibility is to use both the intensity jumps and a possibly weak antibunching statistic to achieve a reliable result.

Anyway, apart from the problems, there is no other competitive method available, so if quantification with more than two molecules has to be accomplished, this is the only choice, and the focus needs to be laid on optimization of the fluorescent dyes and the reduction in background fluorescence.

Keeping this knowledge in mind, fixated cell samples have been prepared with the aim to suppress the background fluorescence as far as possible. A typical scan image with time trajectories of selected spots is presented in figure 4.26:

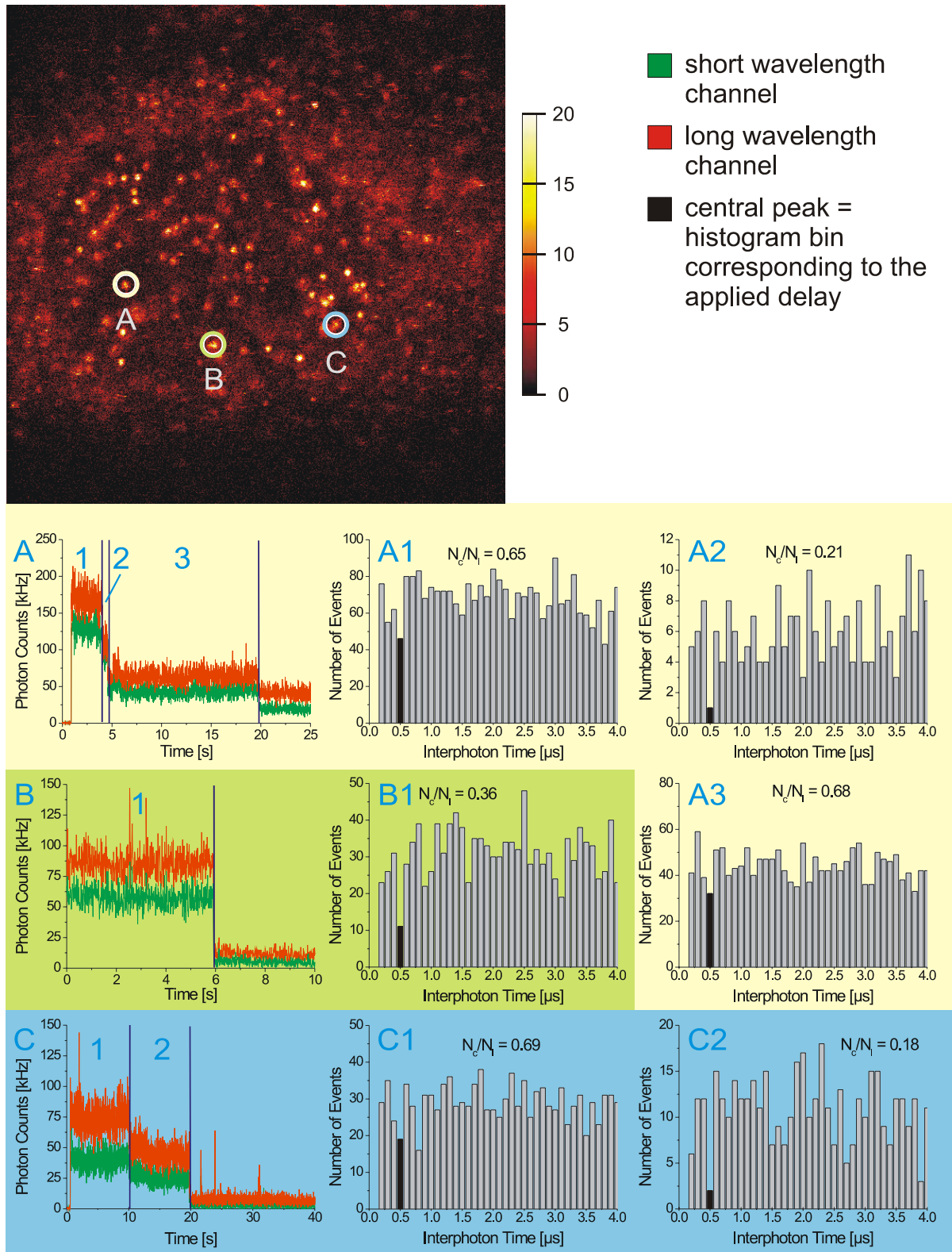


Figure 4.26: RGB intensity image of a fixated fibroblast cell with time trajectories collected at the location of three selected fluorescent spots (A-C). The histograms represent the interphoton time distributions found in the different time intervals separated by the blue vertical lines in the trajectories. Fluorescent tag polyT-Atto 620, image size $30 \times 30 \mu\text{m}$, resolution 50 nm/pixel , integration time 2 ms/pixel , excitation power for imaging 0.7 kW/cm^2 , for time trajectories 1.9 kW/cm^2 , repetition rate 10 MHz , delay time $0.5 \mu\text{s}$.

The spot selection algorithm developed in our workgroup makes possible the selection of discrete spots in a scan image, and subsequent collection of the photon emission until photodestruction at this location. This foremost facilitates the determination of the position of a tracked molecule within a cell. This means the areas of interest can be selectively investigated without having to worry about assignment towards a cell compartment, as would be the case when using a spot selection based on an intensity algorithm, which would randomly select the brightest spots independently of their position. Furthermore, the introduced method simultaneously extracts the maximum information from the emitters, namely fluorescence lifetimes, emission characteristics, the number of emitters, and their exact positions within nanometer range.

In the RGB image of figure 4.26 three exemplary spots are selected; their time trajectories (A-C), and the corresponding coincidence histograms are depicted beneath. In graph B constant fluorescence intensity is shown, which abruptly drops to the background level after 6 seconds due to photobleaching. The coincidence histogram with an N_o/N_i -ratio of 0.36 and a signal-to-background ratio of about 5:1, as well as the intensity trace, clearly indicate a single emitter. Figure C holds two intensity levels above the background. The small, but intense spikes in the intensity trace are not considered, because they are probably due to fluorescent markers freely diffusing through the laser focus. The coincidence ratios of 0.69 and 0.18 for the different steps propose the presence of initially two emitters, if the background signal is taken into account. Trace A shows three intensity jumps. The last intensity level is considered as background signal, because the intensity does not significantly change or drop within the next minutes (data not shown). Such long durability against the laser light is commonly an indication for autofluorescence, even if there is a low, but non-zero probability that a fluorescent dye keeps emitting for such a long time period. The three intensity levels are worth to be discussed in detail. The first level (1) shows an N_o/N_i -ratio of 0.65 and corresponds to two or three emitters. The next (2) only exhibits a ratio of 0.21, which should account for a single fluorophore, but the statistic is weak due to the short emission duration, and by adding only two more interphoton counts into the delayed time bin, the ratio would rise to 0.63, which presumes two or even three emitters. The last intensity step (3) is also not easy to interpret. The statistic is good, but the ratio of 0.68 and a signal-to-background ratio of about 1:1 is not well interpretable. Thus two sceneries can be assumed: Two

emitters, wherefrom the first photobleaches after step 1 and the second after step 3. The remaining intensity drop corresponds to a spectral jump, a movement or a rotation of the molecule. The other possibility is the presence of three emitters, which are decomposing after every single intensity drop.

This time trajectory points out the limits of coincidence analysis in cells, as subjective arguments like the sure instinct of the operator, which cannot be expressed within an error, need to be utilized.

To be able to give a reliable limit for the number of emitters resolvable, an automated selection algorithm using spot intensity and a roundness criterion, has been used to analyze fixated cell samples. All picked spots within the cell nucleus are evaluated and presented with their position and number of emitters in figure 4.27:

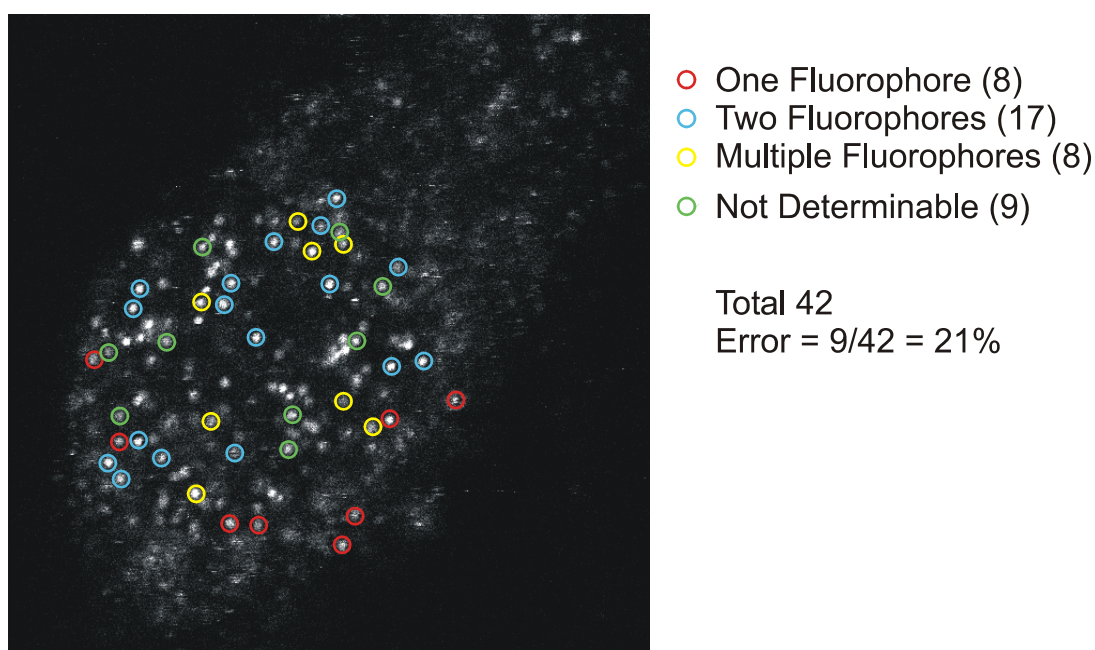


Figure 4.27: Black & white intensity image of a fixated fibroblast with polyT Atto 620 labels at the locations where a spot finding algorithm determined a fluorophore. The different colors represent the number of emitters deduced from the time traces collected at that place. Image size 30x30 μm , resolution 50 nm/pixel, integration time 2 ms/pixel, excitation power for imaging 0.7 kW/cm², for time trajectories 1.9 kW/cm², repetition rate 10 MHz, delay time 0.5 μs , image threshold 40 photon counts.

For evaluation the results from the time trajectories are separated in populations of one to three or more emitters, whereat three fluorophores are often not distinguishable from spots containing more than three molecules. Still, for one or two emitters mostly a reliable analysis is achieved. Also a differentiation into molecules of which no safe information is obtained was set up. To this population belong weak,

and thus non-significant (rare due to the threshold of the algorithm), or previously photobleached emitters, as well as purely autofluorescent spots (which often do not comply to the automated spot selection criteria). In comparison to the photobleaching rate prior to the start of the antibunching measurement, which was determined under similar conditions to be around 20 % for Atto 620 (figure 4.12), the number of selected spots consisting of autofluorescence approximates zero. That means the error of the picking is mostly due to photobleaching effects, which should be reduced as far as possible, for example by the adoption of stabilizing (anti-fading) reagents. These reagents may also stabilize the autofluorescent signal, so that test experiments need to be conducted beforehand.

Even with the low probability of selecting autofluorescent spots, which contain no fluorescent dye, the background signal of the cell still plays an important role. With the results from figure 4.27, and the investigation of different labeling conditions and cell lines, a save determination of the number of fluorescent dyes in the laser focus seems to be limited to 3 or 4 in the maximum when using cell samples. This number could possibly be increased by the use of more photostabile, and thus more photons emitting fluorophores, for example quantum dots. Anyway, under the current conditions the limit is at about 3 to 4 emitters.

Similar experiments were also accomplished in living cells. Generally living cells exhibit a higher background fluorescence signal compared to fixed cells, which complicates the detection and analysis of fluorescent spots. However, it was still possible to resolve complexes containing up to three fluorophores.

On the biological side of the experiment it is surprising that multi-labeling occurs. Since millions of mRNA molecules are present in a cell the probability of two comparatively rare fluorescent tags binding to the same target is theoretically not likely, if not impossible. Also, the argument that in fixated samples these are mostly washed out in the labeling steps, does not explain the experienced high label degree in living cells. A reason might be that most of the targets are inaccessible within proteins or disguised by enzymes. That way the few freely accessible RNA molecules are exposed to a bigger number of fluorophores and are thus labeled in a higher ratio.

4.4 Stoichiometric 1:1-Labeling of Biomolecules with Fluorescent Markers by the Usage of Affine Groups

Quantification experiments with identical colocalized molecules in biological systems, like the determination of the number of polymerases in a single transcription factory, require two conditions: first, all binding sites at the target molecule, here the transcription site, have to be occupied, which can be achieved using an excessive number of antibodies against polymerase II, followed by subsequent washing steps. The second point is, that all antibodies have to be equally detectable. Therefore they have to be stoichiometric labeled with a tag, for example a fluorescent dye. Stoichiometric labeling does not account for an average labeling degree like in ensemble spectroscopy or chemistry, but for an exact 1:1 labeling with the fluorophore, meaning that each marker carries only a single label, and no unlabeled product, neither marker or label, is present.

The problem of such labeling arises from the availability of several identical binding sites on larger biomolecules. Commonly amino-, thiol- or carboxylic functions are used for coupling, as they are easily accessible by standard reagents known from peptide chemistry. For the linking of carboxylic acids with amino functions mostly carbodiimides and active esters like DCC [Sheehan 1955] or EDCI [Sheehan 1961], as well as their successors, aminium, uranium and phosphonium salts based upon HOBt and HOAt are used. Examples are HBTU [Gross 1978], BOP [Castro 1975, Castro 1990], AOP [Carpino 1994], TNTU or TSTU [Knorr 1989]. Sulfohydate functions can be accessed by maleimides or iodoacetamides, as well in the presence of amino groups. Since in nature free SH-groups are inexistent in most biomolecules, an introduction can be achieved using heterobifunctional crosslinkers, or by oxidation of disulfide bonds of the biomolecule with TCEP [Singh 2002, Schnaible 2002] and DTT [Jocelyn 1987].

In most cases more than one specific labeling site is available, which inhibits stoichiometric products. For circumvention, advantage of biological binding reactions can be taken. Immunoenzymatic experiments, in which prelabeled complexes like horse radish peroxidase or alkaline phosphatase are bound to proteins, e.g. antibodies, can introduce tags in a fix coordination number [Ishikawa 1983, Cordell 1984]. In the same manner, antibody–antigen interactions can be used, but they block binding sites of the biomolecule, which often limits further reactions.

Gene expression is very popular for the selective labeling of biomolecules. Especially the expression of GFP became a standard tool in biotechnology [Poppenborg 1997, Chalfie 1998, Tsien 1998], even though GFP and its derivatives suffer from strong blinking and rapid photobleaching [Dickson 1997, Yang 1996]. Also the recombinant introduction of peptide sequences, for example cysteines with their reactive sulfhydryl groups into proteins, represents a versatile possibility for site-specific labeling [Baneyx 1999]. While on one hand these methods are work and cost intensive, as well as they are limited to proteins, whose DNA-sequences are known, they are on the other hand two of the most reliable methods for single-labeling today.

Labeling Strategy

To be able to perform quantifying experiments with polymerases as introduced in chapter 4.5, a simple and efficient pathway needs to be found to stoichiometrically label antibodies, and isolate pure products, free of fluorescent markers and unlabeled antibodies. By combining various coupling and purification steps known from biochemistry, a suitable procedure is developed, those single reaction steps are specified in chapter 3.7 and depicted in figure 4.28:

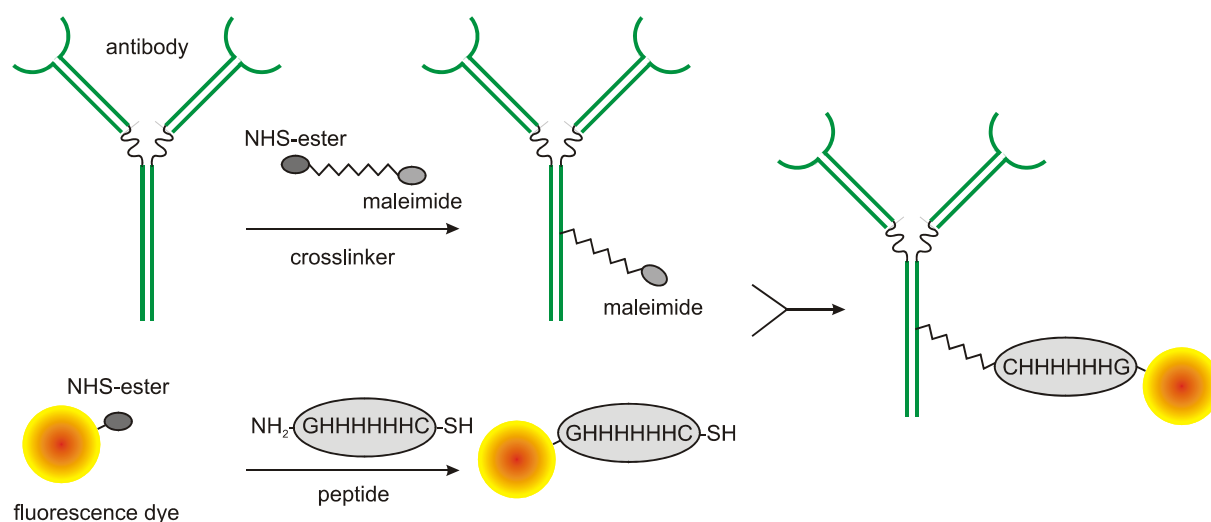


Figure 4.28: Reaction steps for the stoichiometric labeling of an antibody with a fluorescent dye. The basis is the introduction of an affine group, here a cysteine marked his-tag peptide, which subsequently enables the removal of fluorescent educts, and labeling with an excess of antibody to yield antibodies carrying only a single fluorophore.

The idea is to first label the fluorescent dye with a modified *his-tag* [Alberts 2002] peptide of the sequence GHHHHHC. The poly-histidine sequence is capable of binding reversibly to Ni-NTA agarose beads, and thus enables its separation from other reagents [O'Shann. 1995]. It furthermore contains a glycine, which solely holds the function of a spacer to gain better access of the histidines to the nickel complex. The SH-group on the cysteine activates the sequence for further reactions with maleimides, a selective reagent for thiols. Such a maleimide is coupled to the desired antibody utilizing heterobifunctional crosslinkers containing a N-hydroxy-succinimide (NHS) and the imide. Common crosslinkers are MBS, SMPB, GMBS, EMCS, and SMCC, as well as their water-soluble sulfo-analogues [Carlsson 1978, Peeters 1989]. The NHS-group, an activated carboxylic acid, reacts with free amino groups, usually the antibody lysines. In the following step the maleimide-activated antibody is reacted with the cysteine of the dye marked histidine. The important point is to do this step with an excess of antibody in a way, that the labeling degree is well below one, to avoid multi-labeling. The product is purified from the dye-histidine conjugate by a protein A column and from unlabeled antibody by Ni-NTA affinity chromatography. The approach with the SMCC crosslinker is favored over the direct coupling of NHS-activated peptides to free amino groups, because the surplus activation reagents interfere with the (subsequent) antibody coupling step and need to be removed, which is accompanied by extensive hydrolysis of the activated product or additional workup steps.

The goal of labeling a bigger biomolecule, such as an antibody, can easily be accomplished with the help of standard coupling reagents. In the product solution both educts need to be removed to achieve a definite labeling degree. Free fluorophores are rarely a problem, because the differences in the molecular mass can be used for separation. Separation can be done by affinity chromatography or filtering through mass specific pores. For isolation of the un-, mono-, bi- and higher marked fractions of the biomolecule, the differences in molecular mass and polarity are mostly too small for a proper performance. Also the verification of the products is not easy, because variations smaller than 1 % in weight have to be detected (antibody 150 kDa, fluorescent dye <1 kDa). Thus, an affine group has to be introduced to the fluorophore, which can be specifically bound and separated by chromatographic methods. This group may consist of a peptide containing a

specifically recognized sequence, for example his-, STAG- or FLAT-tags [Jungbauer 2004], or as an alternative a strong non-covalent bond such as biotin-streptavidin [Wilbur 1999].

The second trick is to perform the reaction with an excess of biomolecule. This way the labeling degree can be reduced, and set to be lower than one dye per antibody, thus limiting the poly-marked product. In a subsequent purification step the labeled biomolecules are separated with the help of the introduced affine group. The resulting product is underlying a narrow distribution, those broadness is determined only by the excess ratio of biomolecule used.

This system has been shown to work on two different antibodies [Heinlein 2004], a polyclonal mouse IgG, and the monoclonal anti-polymerase II mouse IgG ARNA-3. Since the single labeling steps are explained in detail in chapter 3.7, only the analysis and applications of the stoichiometric labeled product is given in the following.

Proof of the Stoichiometry

As previously discussed (chapter 3.4), the proof for single labeling can be given by polarization modulation and antibunching measurements. Both methods give information about the ratio of single to multiple marked antibodies, but the unlabeled fraction cannot be visualized that way. Therefore the results need to be compared with the absorption spectra, which hold information about the average labeling degree assuming the cognition of the extinction coefficients of the antibody and the fluorophore.

One way to distinguish the number of fluorophores attached to an antibody is by modulation of the excitation light polarization [Güttler 1993, Ha 1996]. Linear polarized laser light is rotated with an electro-optic modulator using a saw-tooth pattern (one full rotation per 5 scan pixels), and the emitted fluorescence is followed with time. The fluorescence signal of a single molecule drops to zero when its absorption dipole is perpendicular to the excitation dipole of the laser light and reaches its maximum for a parallel arrangement. With modulated polarization a single molecule appears as a striped spot in a scan image, but two molecules show up unmodulated, since they rarely have the same absorption dipole moment (figure 4.29):

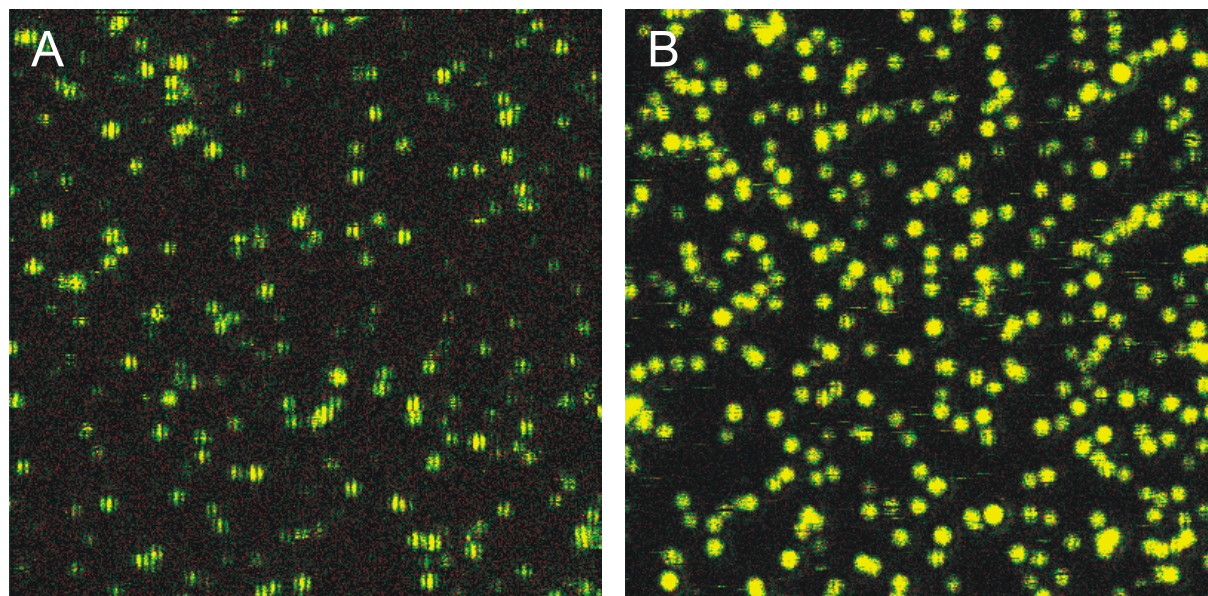


Figure 4.29: False color scan images of stoichiometric labeled ARNA-3 IgG (A) and commercially available 2-4 x labeled IgG antibodies (B) on dry APS-surfaces. Antibody A is labeled with Atto 620, whereas in B Alexa 633 is used (MoBiTec GmbH, Göttingen). The scans are performed with polarization modulated excitation light, whose plane rotates 36° per pixel continuously. Image size $20 \times 20 \mu\text{m}$, resolution 50 nm/pixel , integration time 3 ms/pixel , excitation power 0.7 kW/cm^2 , repetition rate 40 MHz , image thresholds 7 (A), and 15 (B) photon counts, respectively.

In figure A almost all molecules exhibit stripes, and thus contain only one emitter, as suggested by the labeling strategy. Figure B represents multi-fluorophore antibodies, whose labeling degree is underlying a broad distribution. Since from the manufacturer the excess of dye is stated to be between 2- and 4-fold, only few stripy spots are apparent. Analysis of about 500 spots of each of the stoichiometric labeled antibodies gives an average degree of 1.09 dyes on the poly- and 1.11 on the monoclonal product, assuming that every stripy spot carries one label and every homogenous spots two labels.

These values are compared with results from antibunching experiments, which allow giving the number of independent emitters attached to the molecule. Independency is important for higher labeled complexes, as the fluorophores may bind at positions close to each other and undergo electron transfer reactions, which leads to an unpredictable emission behavior, mostly accompanied by quenching (homo-FRET). With the low-labeled antibodies discussed here and thus with bigger distances between the fluorophores, this effect only rarely plays a role and is neglected in the following.

Since coincidence analysis – also for samples carrying only one emitter in average – does not give meaningful values in all cases, every single coincidence statistic independent of its quality is corrected with its specific signal-to-background ratio, and the resulting N_c/N_l -ratios are added to a histogram:

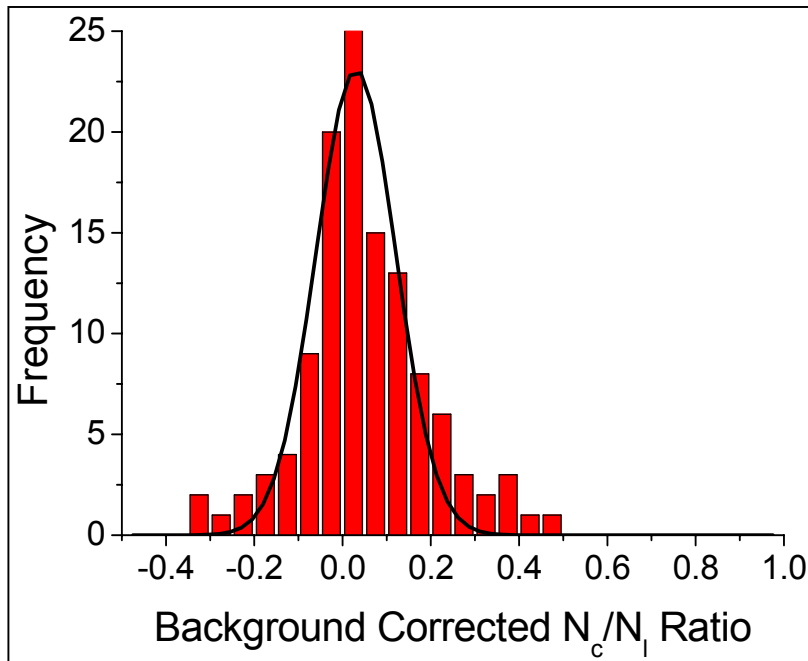


Figure 4.30: Histogram of background corrected coincidence ratios derived from about 230 ARNA 3-Atto 620 fluorophores attached to ARNA-3 antibodies. The measurement conditions are as quoted in figure 4.29 using circular polarized instead of linearly modulated excitation light.

The histogram clearly shows a strong population around zero, the expected value for a single emitter. Since the distribution has a high symmetry, no other significant population is assumed to be present. The maximum value little above zero indicates a low number of double labels, but not many. If alternatively the result is manually derived from the single traces labeling degrees of 1.06 and 1.10 are found, respectively.

A summary of the results from the polarization modulation and antibunching measurements is given in table 4.3:

| Antibody | Polarization Modulation | Coincidence Analysis |
|----------------------|-------------------------|----------------------|
| monoclonal ARNA-3 | 1.11 | 1.10 |
| polyclonal mouse IgG | 1.09 | 1.06 |

Table 4.2: Determination of the number of emitters per antibody by the analysis of polarization modulated image spots and coincidence analysis. In all cases around 450 to 550 events are evaluated.

The table clearly proves that the results are in good agreement with each other. That means a constant fraction of about 10 % of the antibodies carries two labels.

Antibunching and polarization modulation experiments hold information about the number of fluorescent emitters attached to the antibodies. What remains hidden is the quantity of unlabeled antibody in the product.

To bring the results in line absorption spectra from reactions started with different educt ratios are presented in figure 4.31:

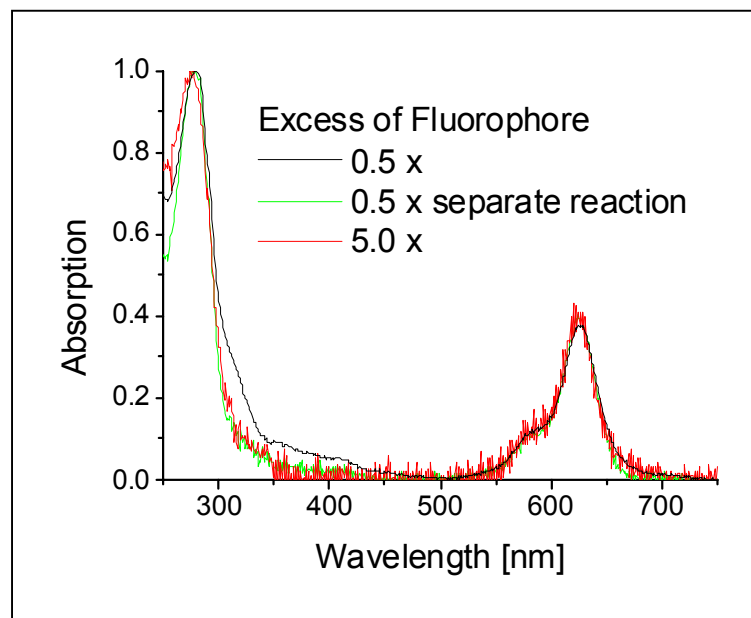


Figure 4.31: Absorption spectra of polyclonal IgG antibodies labeled with Atto 620 in different reactions. Even though the fluorophore educt has been deployed in different ratios and reactions the absorption spectra stay similar, which accounts for a stoichiometric labeled product.

All absorption spectra show similar curve progressions. This means the ratio of antibody to fluorophore is constant within the products, even though the starting materials were applied in different ratios. This indirectly proves that the implementation of the affine group in combination with the workup steps work as predicted, and that both, the unreacted dye and the unlabeled antibody, are removed from the solution. Consequently, the remaining product consists of a stoichiometric 1:1 labeled dye-antibody conjugate.

The intuitive idea to compare the extinction coefficients of both reactants to determine the exact labeling degree is not practicable, as the absorption coefficient of an antibody is never exactly known nor calculable, even though attempts have been made [Gill 1990]. Another point is that the extinction coefficient of the fluorescent dye is significantly changed in different environments [Lakowicz 1983]. In literature the most common value for IgG antibodies is 203.000 l/mol·cm, but the numbers vary with the information source. With this measure and the absorption spectra shown in figure 4.31, the extinction coefficient of Atto 620 is determined to be around 85.000 l/mol·cm instead of the literature value 120.000 l/mol·cm. This difference is credible as the antibody surely influences the chromophoric system of

the dye and likely reduces its absorption capability. However, a prediction cannot substitute the measurement, because the ratio of the values is assessable, but not exactly known, and only the comparison of absorption spectra leads to a safe characterization of the stoichiometric labeled product.

One more question, which arises from the results, needs to be discussed: Why do the absorption spectra indicate perfect single labeling, while polarization modulation and coincidence analysis both suggest around 10 % double labeled product? Furthermore it has been introduced in the previous chapters that on dry surfaces most fluorophores do not emit. This implies that the labeled antibody must in reality be even higher labeled than the measured 10 %. The only feasible solutions are protein aggregation or an overlap of the point-spread-functions of different antibodies, which cannot be visually resolved as multiple spots in the image. This possibility is not unlikely, as biomolecules tend to aggregate when exposed to unnatural conditions, as in the case of deposition on APS-surfaces.

Attempts to clarify the issue by comparison of the molecule density measured by SFLIM to results achieved from atomic force microscopy (AFM) have been conducted [Biebricher 2002]. Unfortunately the necessity for special surfaces limits the comparability of the results.

Since the introduced method has been implemented to detect antibodies and their targets in cellular environment, the activity of the labeled antibodies is proved in ensemble cell experiments. In figure 4.32 a comparison between the fluorescence light achieved from DAPI and from stoichiometric labeled Atto 620-ARNA-3 is shown:

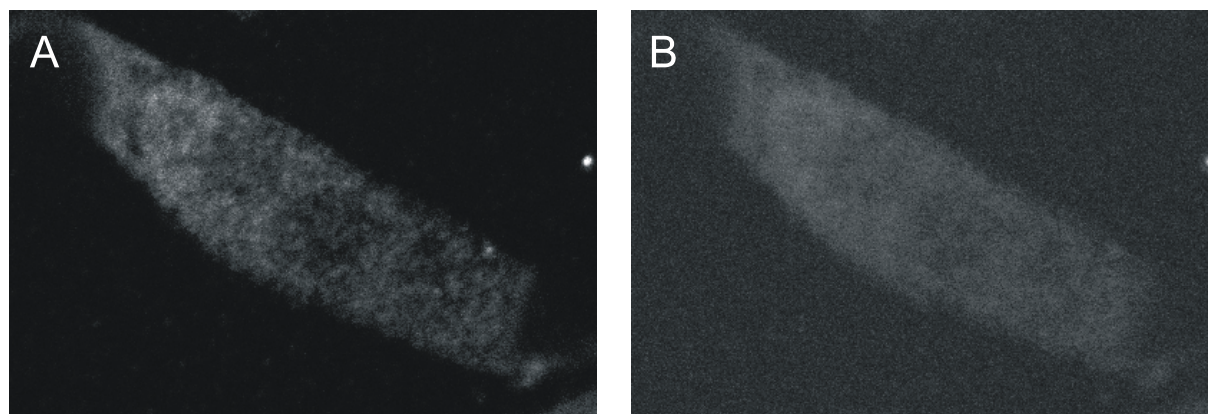


Figure 4.32: Fluorescence microscopy images of cells counterstained with DAPI (A) and ARNA-3-Atto 620 recorded with a CCD-camera. The images show the selective labeling of the tags and thus the biological activity of the antibody. Image size 60x40 μm .

As the amount of incorporated ARNA-3 is low (due to its expense) compared to DAPI, image B appears to be more diffuse, but still the selective labeling of the cell can be seen. The blank sample (not shown) does not give noteworthy signal under identical conditions.

The introduced labeling strategy has been shown to work well for labeling antibodies with fluorophores. The advantage of the reaction steps is that it can be easily generalized. As already mentioned, the his-tag can be replaced by STAG- or FLAG-tags, which are only more expensive to buy. Also the fluorescent marker is not necessary, as any other small molecule of interest, which contains one selective coupling group, can take its place. Bigger units can also be used, but with them other easier purification steps are possible, and the affine group is not needed. The probably most interesting alteration in the reaction sequence is the possibility to substitute the antibody. Here any molecule can be selected, which carries at least one functional group. Until now only the idea that other biomolecules could replace the antibody were introduced, but also coated inorganic substances like quantum or gold dots are thinkable.

Summarizing, the method developed is capable to stoichiometric attach small markers of any kind to a large molecule carrying multiple reaction sites, which by standard methods is difficult if not impossible to access in a distinct ratio.

4.5 Detection and Quantification of Polymerase II Molecules in Transcription Factories

In this final chapter the properties and characterization of polymerase II in transcription sites, so-called factories, is discussed, and experiments for the quantification of polymerases in such centers are introduced. All experiments reported were done in collaboration with the group of Ana Pombo (Medical Research Center, London).

Function and Localization of Transcription Sites

The role of transcription is - as introduced in chapter 2.2 - the generation of RNA from genes. In this work the main focus is to apply antibunching measurements to cell

samples, and achieve information about the number of polymerase II molecules in a single transcription site. Therefore a closer introduction about the hitherto employed detection methods and their results is given.

Sites of transcription by polymerase II have mostly been detected by labeling nascent RNA with tagged nucleotides. In 1993 Jackson *et al.* encapsulated HeLa cells in agarose beads, permeabilized and incubated them with bromo-uridine-triphosphate (Br-UTP). The sites of containing newly-made RNA were immunolabeled using an antibody that reacts with Br-RNA. Approximately 300 to 500 focal sites were confirmed in each nucleus by fluorescence microscopy. This value was independently determined by *in vivo* experiments using the same labeling method [Wansink 1993]. Here, nascent polymerase II transcripts were found in over 100 defined areas, scattered throughout the nucleoplasm. In 1996 Iborra *et al.* first published the term “transcription factory“. They also incorporated Br-UTP labels, or as an alternative biotin-14-CTP, and visualized the secondary labeled sites at higher resolution by light and electron microscopy. They found transcription to be active at approximately 2.100 discrete locations, but this was later corrected to ~6.000. The size of a typical site was given a diameter of 71 nm, enough to accommodate 4 to 20 polymerase II molecules plus associated transcripts. The most recent publication, in which Br-UTP was also used, further optimised the cellular preservation which allowed the detection of short transcripts made by polymerase III and lead to an increase in the number of transcription sites up to 10.000 [Pombo 1999]. As polymerase III is found in 2.000 dedicated sites, RNA polymerase II is found in ~8.000 sites with a diameter of 40 nm. As the same cells have ~65.000 active RNA polymerase II and ~10.000 active RNA polymerase III complexes, it was concluded, that each site contains on average eight and five active polymerases II and III, respectively.

Alongside with these experiments, more and more indirect pathways to resolve transcription factories were undertaken. Nowadays commonly the location and transport of transcription factors, proteins necessary to activate a polymerase, are investigated [Grande 1997, Zeng 1997, Pombo 1999], but mostly the same methods as already mentioned are used.

Recapitulating, in the nucleoplasm of a HeLa cell about 8.000 discrete sites of polymerase II transcription are distributed. These have diameters of 40 to 80 nm, and contain on average 8 polymerase II molecules.

To be able to resolve such a high number of transcription factories with a single cell nucleus, cell slices, so-called cryosections, are used (preparation see chapter 3.8). In this work the sections hold a diameter of 100 nm, and are counterstained with DAPI. The dye, a DNA intercalator, which selectively labels cell nuclei, is necessary to localize the samples, as cells this thick cannot be seen in light microscopy. In figure 4.33 a typical CCD-camera image of cryosections deposited on a glass slide are shown:

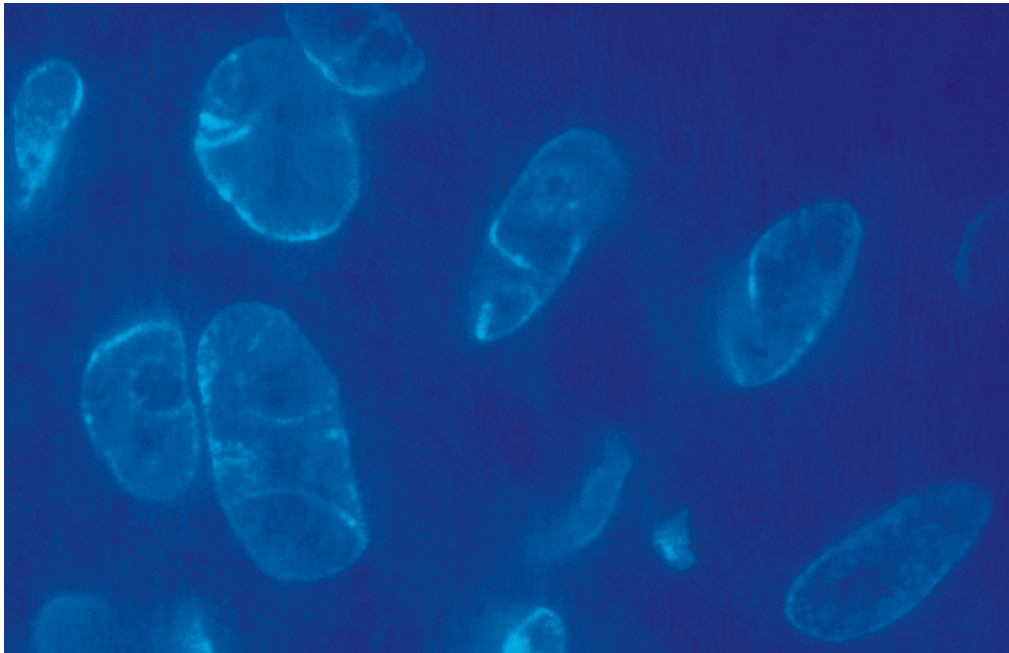


Figure 4.33: CCD-camera image of DAPI-labeled cryosections of HeLa-cells immobilized on a glass surface. As excitation source a mercury lamp is used, which homogenously illuminates a large visual field . The image size is about 180x120 μm .

In the image several differently shaped cell slices are mapped. For meaningful experiments it is important to select only flat and homogenous sections, and not the ones with the highest fluorescence signal. The bright edges of the slices indicate wavy, crumpled or collapsed cells. In this image the only suitable cell is in the lower right corner.

Investigation of Antibodies by Polarization Modulation

An important issue within cell labeling experiments is the prove of the specificity of the used tags.

Following the pathway for the immunolabeling of cells as described earlier in this chapter, Br-dUTP is integrated into the RNA sequences of live HeLa cells. After fixation the antibody MD5010 (CalTag Laboratories, USA), which specifically recognizes both bromodeoxyuridine and iododeoxyuridine in DNA, nucleotides and nucleosides, is incorporated into treated cells. To be able to visualize the result of this process, the antibody was previously labeled with the fluorescent dye Cy 5.5. A typical immunolabeled HeLa cell is shown in figure 4.34:

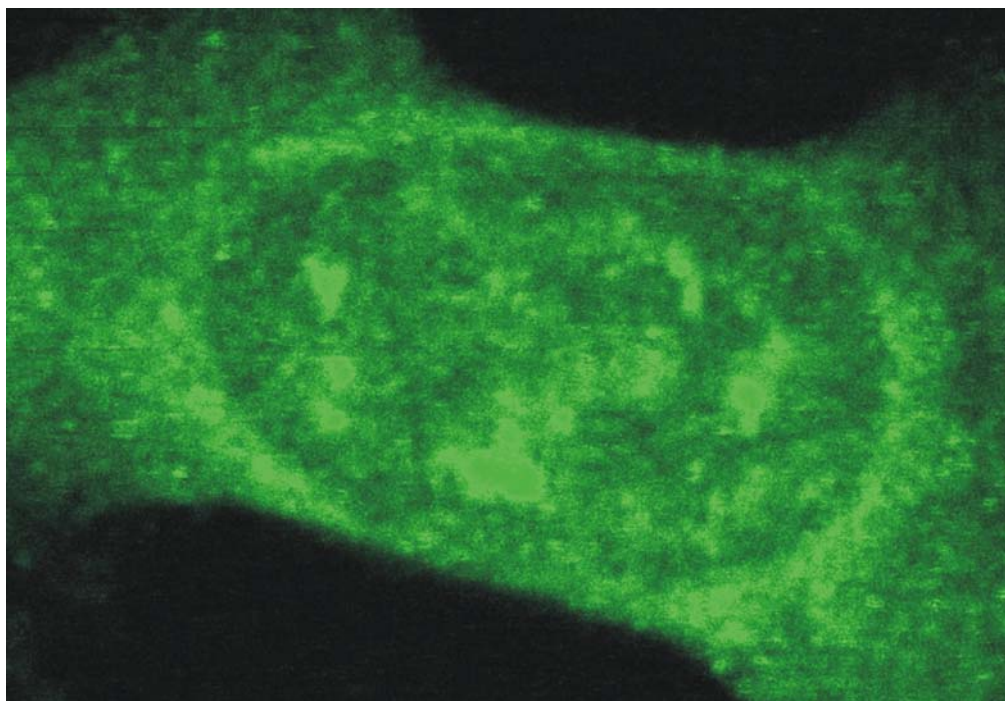


Figure 4.34: Image scan of an antibody labeled HeLa cell. For immunolabeling Br-dUTP is incorporated into live cells, and after fixation the Cy 5.5 labeled antibody MD5010 against Br-dUTP is added. The image is acquired using only one detector, those signal is encoded in green. Image size 45x30 μm , resolution 50 nm/pixel, integration time 4 ms/pixel, excitation power 0.2 kW/cm², repetition rate 40 MHz, image threshold 150 photon counts.

In the cell high fluorescence intensity is apparent, especially around the nuclear envelope and in certain regions inside the nucleus. The locations of these areas are in good agreement with the positions of nascent RNA, and thus also with the transcription sites [Cook 1999], which verifies the selectivity of the tag.

The MD5010 antibody binds to Br-marked RNA molecules, which are colocalized with polymerases in transcription sites. Thus, this antibody is not directly suitable for the quantification of polymerase II, but at least for the localization of their positions.

Since this compound is far cheaper than the antibodies available for selective marking of polymerase II, all early studies are accomplished with MD5010.

To check the labeling properties of antibodies in cells on single-molecule level, dry cell samples labeled with the antibody MD5010 as described above are prepared and imaged (figure 4.35):

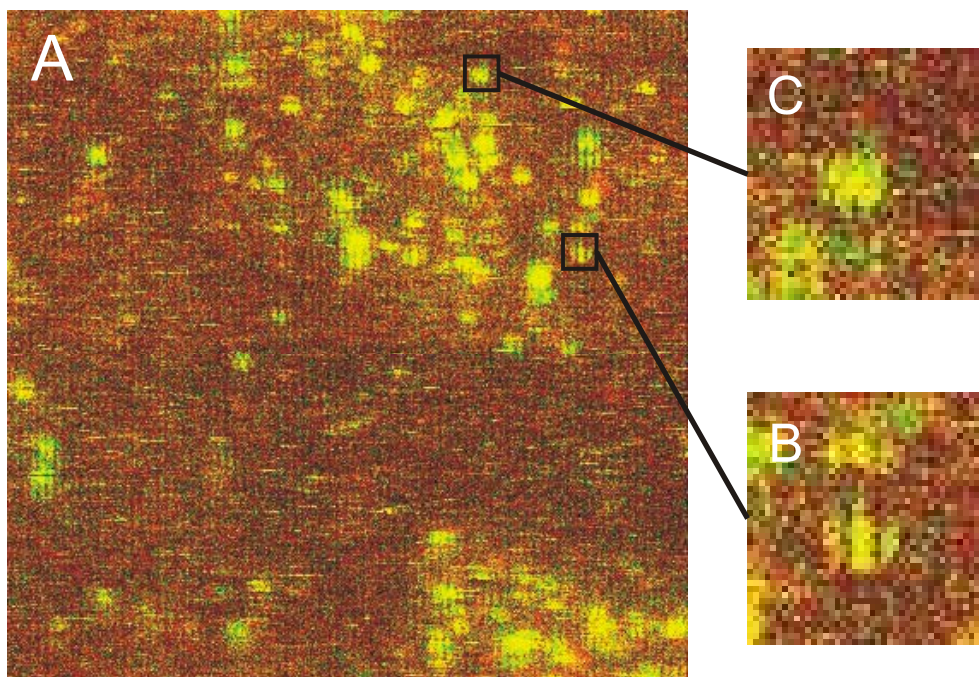


Figure 4.35: Polarization modulated scan image of dry HeLa cell cryosections (A) labeled with Cy 5.5 marked MD5010 antibodies via Br-dUTP. By polarization modulation of the excitation light a single spot (B) appears stripy, while several colocalized fluorophores give a homogeneous PSF in the image. The image was acquired using a 50/50-emission beamsplitter, which encodes as yellow signal independent of the emission wavelength. Modulation frequency $36^\circ/\text{pixel}$, image size $20 \times 20 \mu\text{m}$, resolution $50 \text{ nm}/\text{pixel}$, integration time $3 \text{ ms}/\text{pixel}$, excitation power $0.4 \text{ kW}/\text{cm}^2$, repetition rate 40 MHz , image threshold 10 photon counts.

In the scan image (A) several spots inside a cell cryosection are visible. Due to the polarization-modulated excitation light single molecules appear stripy (B), while accumulated, or highly labeled antibodies, give homogenous spots (C). This experiment shows that single-molecule measurements with labeled antibodies are well possible in cells, and that one or more molecules can be distinguished from each other. Since it is known, that on dry surfaces fluorescent dyes are not quantitatively emitting (chapter 4.2), no meaningful statistic over the labeled spots can be given directly. This does not imply, that the same effects, which appear on dry surfaces, are automatically valid for dry cell samples, as always spare water molecules are present

inside the cell complex. The extent of the effect needs to be inquired by calibration measurements between dry and aqueous samples.

Properties of Dry and Aqueous Mounted Samples

To compare the characteristics of antibodies in dry and aqueous cell environment, and determine in which medium measurements are done best, polarization modulated images of dry (A) and aqueous (B) samples are taken (figure 4.36):

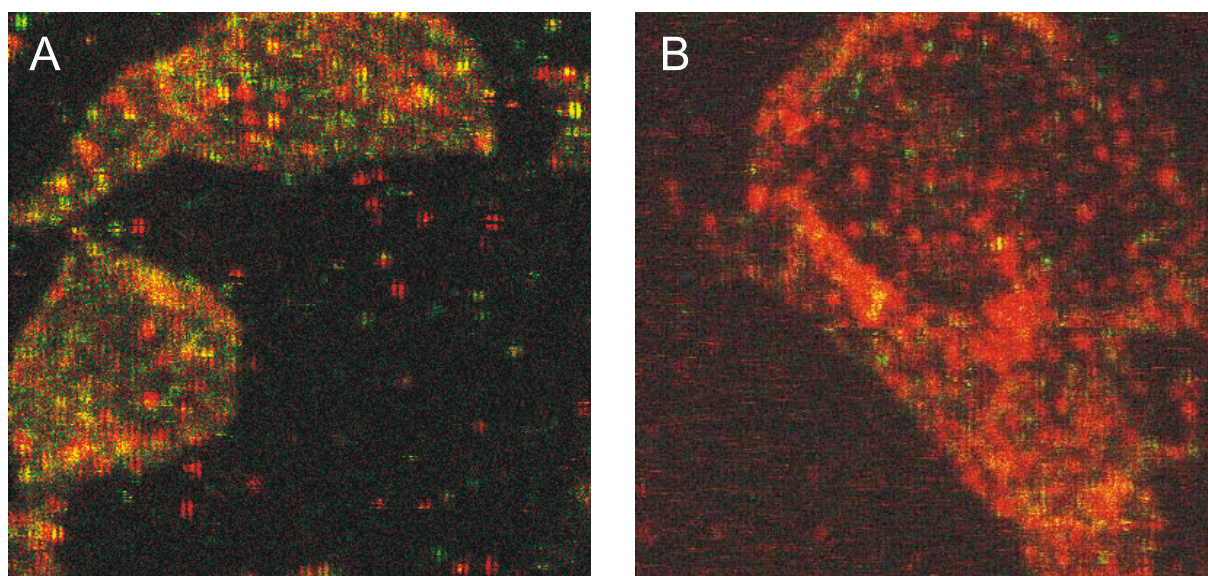


Figure 4.36: Comparison of polarization modulated scan images of HeLa cell cryosections recorded in dry (A) and aqueous environment (B). As label Cy 5.5-labeled MD5010 antibodies are used, which are depicted as red spots. By drying sample A yellow autofluorescent spots appear, which are not present in the similarly prepared aqueous sample. Modulation frequency $36^\circ/\text{pixel}$, image size $20 \times 20 \mu\text{m}$, resolution $50 \text{ nm}/\text{pixel}$, integration time $3 \text{ ms}/\text{pixel}$, excitation power 2.5 (A) , and $5.0 \text{ kW}/\text{cm}^2 \text{ (B)}$, repetition rate 40 MHz , image thresholds 20 (A) , and 40 (B) photon counts, respectively.

The most significant difference between the two images are the yellow spots visible in figure 4.36 A. Since for data acquisition a spectrally separating beamsplitter is used, and Cy 5.5 dominantly holds a long emission wavelength equivalent to a red color in the image, the yellow spots can only arise from a contaminant. The contaminant could be due to autofluorescence, or maybe floating particles, and thus in solution undetected fluorophores, which are immobilized by drying the sample. Effects from the fluorescent dye itself, like a hypsochromic shift in the emission

wavelength are excluded, as such an option has already been negated in chapter 3.2.

It is also interesting to compare the number of stripy spots in the images. While in A almost all molecules show this effect, in solution immobilized molecules (B) are only visible in the cytoplasm, but inside the nucleus only homogeneously round spots are apparent. Assuming that the antibody-RNA complex is neither mobile nor rotating, this means the fluorophores can freely rotate around their linker to the antibody. The presence of multi-labeled systems can be excluded, as the cytoplasm sometimes shows modulated spots. The only possibility could be that aggregate are formed, which underlie electron transfer reaction and thus wrongly indicate a single emitter. This implies that no proper information about the number of emitters can be given by polarization modulation experiments, when working with fluorescent dye attached antibodies, at least not in this case. Thus, the method of polarization modulation is not further applied in the following.

However, from the appearance of autofluorescent signal upon the drying of cell samples reduces meaningful experiments to the aqueous phase.

Quantification of Stoichiometric Labeled Antibodies in Transcription Sites

With this knowledge stoichiometric labeled antibodies against polymerase II are incorporated into HeLa cell cryosections (figure 4.37).

With DAPI as label the shape and exact position of the cryosections is determined (A-C). The cells found in the image are scanned on the SFLIM-setup (D-F) using a 50/50 non-polarizing beamsplitter and a repetition rate of 10 MHz to be able to access antibunching data simultaneously. A good demonstration that the identical cells are displayed in both in the DAPI and in the scan image is by comparison of the nucleoli positions. These are represented by the bigger dark blue spots in the DAPI, and by the brighter red areas in the scan picture. Their number ranges between 2 to 5 per cell, which is consistent with literature [Alberts 2002].

In figure G-I the corresponding fluorescence lifetime images are presented. At a first glance a significant difference between antibody labeled and blank samples is obvious. In the labeled sample several red spots, whose properties match with reference data for Atto 620, are visible, whereas rarely such areas are apparent in the blank sample, especially not inside the cell nucleus, where the transcription sites are located.

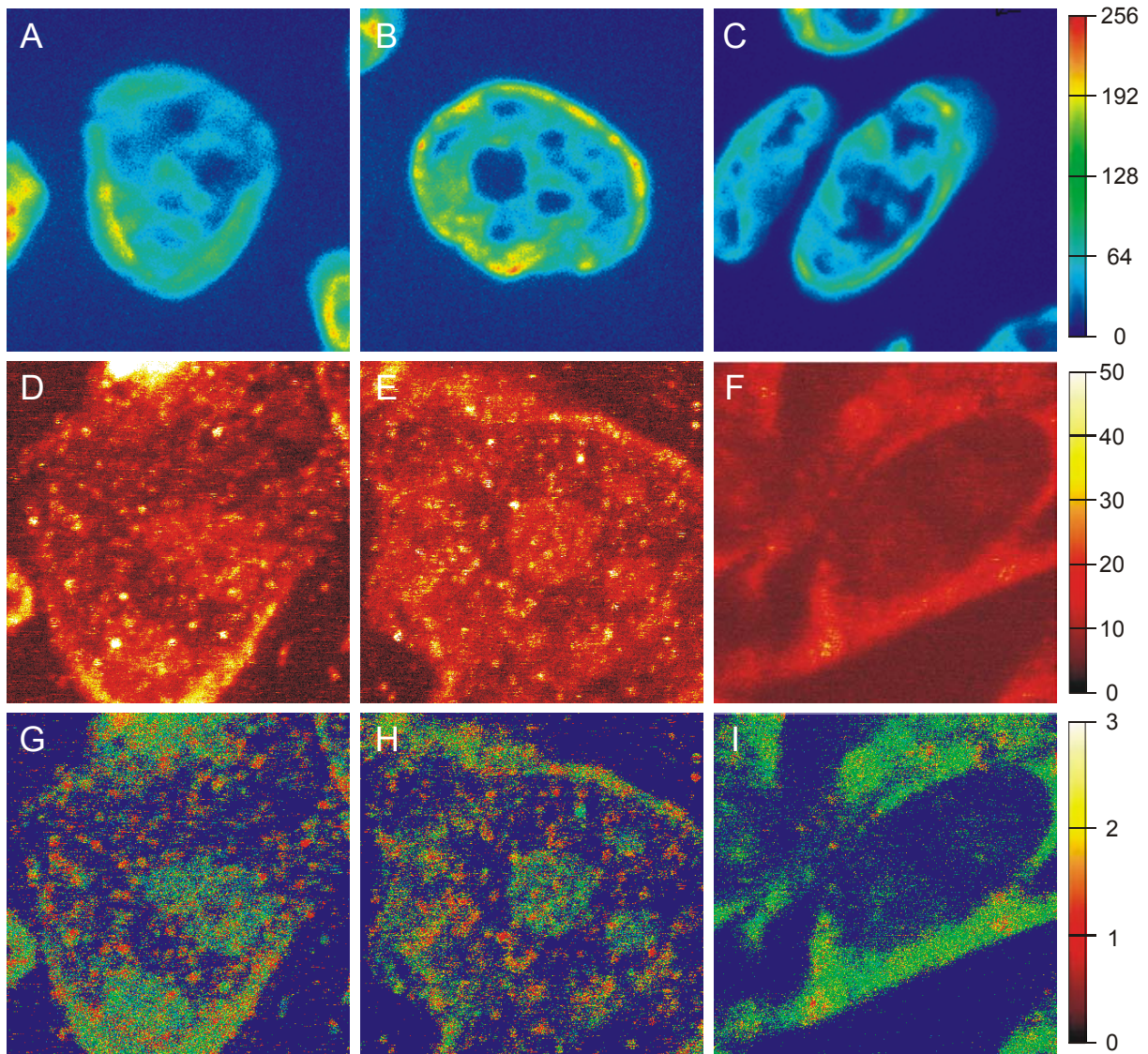


Figure 4.37: Pictures A-C are images of HeLa cell cryosections counterstained with DAPI, and measured with a CCD-camera. The next images (D-F) represent a detail of the same cell nuclei in RGB-color scanned with the SFLIM-setup. D and E are treated with a stoichiometric Atto 620 labeled antibody (ARNA-3) against polymerase II, while F shows a blank sample for comparison. To better visualize the single spots the corresponding color-coded fluorescence lifetime images are plotted in G-I. The DAPI pictures are collected using a mercury lamp as excitation source. Image size A-C $\sim 30 \times 30 \mu\text{m}$ (no calibrated), integration time 100 ms. Images D-I: size $20 \times 20 \mu\text{m}$, resolution 50 nm/pixel, integration time 3 ms/pixel, excitation power 1.2 kW/cm^2 , repetition rate 10 MHz, threshold 20 photon counts (G-I).

This implies that the labeling process has been successful, and ARNA-3 Atto 620 molecules are bound inside the cell. To further investigate about the number of colocalized antibodies, spots are selected using the previously introduced pick algorithm. Two exemplary time trajectories with their lifetime decays are presented in figure 4.38:

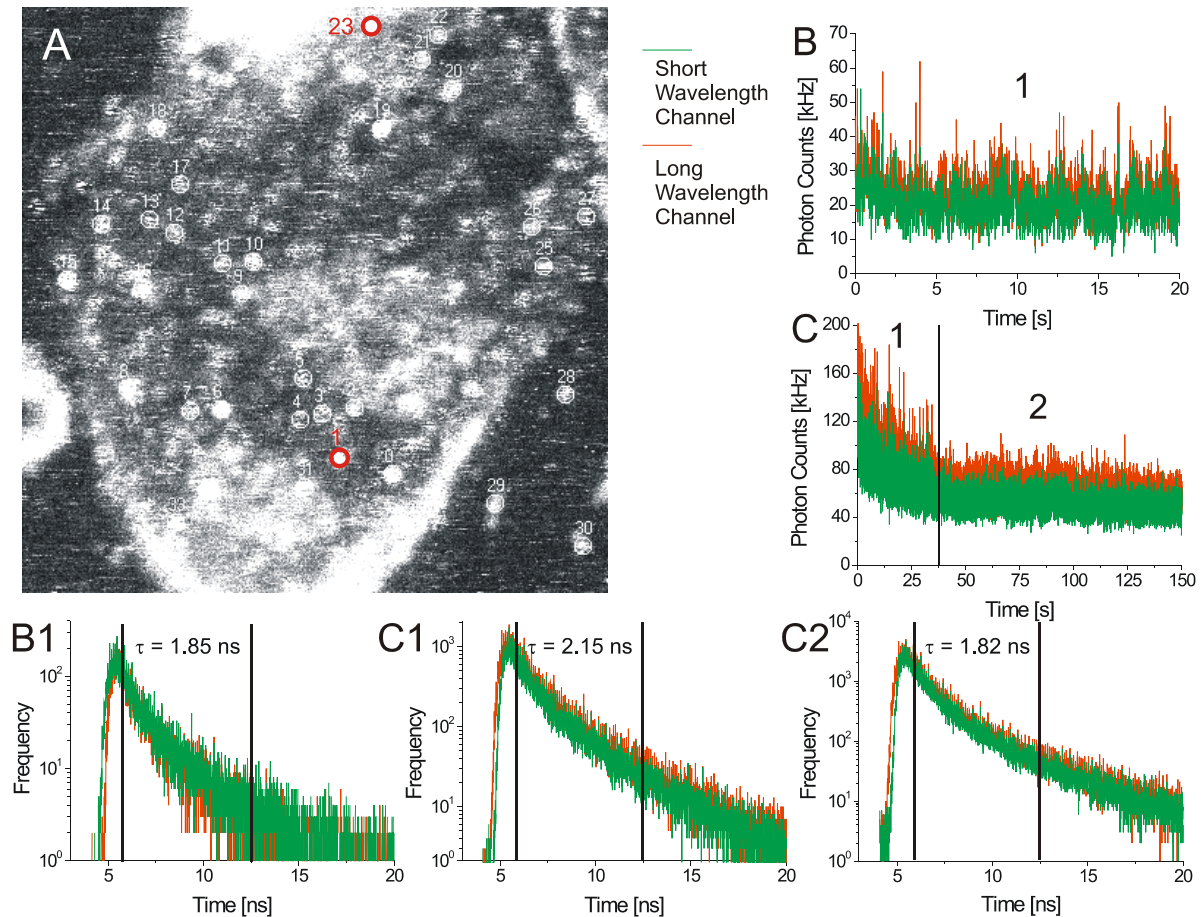


Figure 4.38: Black & white image (A) of an ARNA-3 labeled cryosection as presented in figure 4.37. The spots recognized by the pick algorithm are consecutively numbered. In figure B and C two typical time trajectories with their corresponding photon lifetime histograms (B1, C1, C2) are presented. The fluorescent lifetimes are determined by application of a MLE using the black vertical lines as limits. For the time traces an increased laser power of 1.5 kW/cm^2 is used.

Spot number 1 is a homogenous round spot, which obviously does not show blinking. Its time trajectory (B), which is typically for almost all spots in the sample, shows constant fluorescence intensity for minutes. To investigate, if the fluorescence is due to Atto 620, the corresponding lifetime histogram (B1) has to be taken into account. The decay is not linear, as would be expected for a fluorescence dye, but rather indicates a bi- or probably a polyexponential behavior, as commonly found for autofluorescent signals. It could well be that below the strong autofluorescence a weak fluorescence dye signal is present, but this is not supported as the fluorescence lifetime constantly stays around 1.85 ns (fitted with a MLE). A higher and decreasing lifetime at the beginning of the trace could account for photobleaching of Atto 620 fluorophores, which are compared to autofluorescence more photounstable and exhibit a longer fluorescence lifetime of ~ 3 to 3.5 ns. Also the constant intensity

signal rules out this option, as previous studies with Atto 620 never showed comparable dye stabilities, but rather photobleaching during the first seconds.

To check whether a fluorophore has been there at all, or if the red image spots are due to an autofluorescent signal, the same scan is repeated several times. Afterwards the red spots are often vanished, but others also remain, which accounts for the presence of fluorescent dyes and a so far unknown fluorescent species.

As an alternative way to confirm the presence of fluorescence dyes in the sample, a spot close to a strongly fluorescent area is selected (nr. 23 in figure A). In the time trajectory (C) the fluorescence intensity quickly decreases until after about 40 seconds a constant level is reached. By comparison of the fluorescence decays of both areas, before and after 40 seconds, a decreasing fluorescent lifetime with time is found. This shows the presence of at least one fluorescent dye at the beginning of the trace. When the constant intensity level is reached, all dyes are photobleached, and only autofluorescence remains. Attempts to quantify the number of emitters of this time trajectory is not expedient, as the spot is part of an ensemble of autofluorescent and dye molecules, and anyway it is not possible, as the background level is at least 1:1 to the dye fluorescence, which corresponds to a correction factor of the coincidence ratio of 0.8.

Another conspicuous thing is, that most red spots exhibit blinking, which is not, or rarely, seen with autofluorescence. This implies that the fluorescent dyes are strongly influenced by their environment, possibly the cell, the antibody, or the solvent. Since Atto 620 has been measured in cells and on antibodies without problems, the most probable source is the solvent, in which rests of fixation reagent or similar are present. Also with VectaShield™ as solvent, a commercially available anti-fading reagent does not give a significant improvement of the dye stability or a reduction in blinking.

Within the scope of this work, it is impossible to perform a proper quantification of the polymerases in a transcription factory of a cell, even though that all primary goals for quantification are reached. From the determination of a suitable dye, its discrimination against autofluorescence, the application of antibunching measurements to living and fixated cells, to the preparation of single labeled antibodies, everything has been implemented.

The way to the quantification of polymerases in transcription sites is now short. The main task is the optimization of the measurement conditions, including studies about the cohesiveness of the antibody on the polymerase to assure the saturation of all polymerase binding sites.

5 Conclusion and Outlook

In this work it is demonstrated that novel single-molecule techniques are well applicable to solve biological problems. Especially the deployed method of scanning fluorescence lifetime imaging microscopy (SFLIM) with its combination of high sensitivity and multi-parameter detection enables a deep insight into the photophysical properties of single molecules. Attachment of fluorescent dyes to biomolecules introduces the possibility to follow processes *in vivo* and *in vitro*, for example in single cells or even in cell assemblies. Not only information about the localization of these complexes can be achieved, but also knowledge about the close environment around the dyes can be deduced. This possibility to probe certain areas with minimal disturbance, and thus least invasive, opens excellent perspectives for diagnostic applications. The main objective nowadays is the detection and localization of pathogens and aggrieved tissues. Single-molecule spectroscopy proved its versatility in the detection of viral and bacterial infections [Eigen 1994, Knemeyer 2000] and early stage cancer [Sauer 1997, Neuweiler 2002]. The underlying techniques are usually performed in solution measurements, as the setup needed for such experiments is relatively cheap and easy to operate. Furthermore, molecules in solution are far more homogeneous in their photophysical behavior than immobilized molecules, because they are not unidirectional perturbed by their environment, for example by surfaces or cell compartments. Exactly this effect, the occurrence of small differences due to interactions of the fluorophore with its neighbored molecules, can be utilized. Molecular hairpins for example, can possibly give evidence of the location and frequency of various target sequences in a fixated cell position. Colocalization experiments with different fluorophores attached to interacting biomolecules allow proving the composition of molecular complexes, and are also able to visualize the accumulation and mechanisms of biomolecular machines.

5.1 Three-Dimensional Precision Distance Measurements

One of the most important issues in the investigation of molecule assemblies is the determination of distances between interacting units. On the biological level, for example in cells, such distances mostly range between 10 and 100 nm

[Alberts 2002]. As introduced in chapter 4.2, several methods to measure lengths below the diffraction limit of about 200 nm, given by the Rayleigh criterion, have been developed. The main drawback of fairly all these techniques is their limitation to two dimensions. Consequently, only the projection of three-dimensional distances onto a plane can be determined, which greatly reduces the information content. Thus, biological relevant questions like the relative positions of interacting molecules, the determination of their binding sites for example, or conformational changes, are not definitely resolvable anymore.

The method for time and spectrally resolved precision-distance microscopy on the single-molecule level presented in chapter 3.5 has been proved to successful work for two dimensions. Since in far-field microscopy, the resolvable limits are at about 200 nm in the lateral, and 500 nm in the axial directions [Pawley 1995]. Three dimensions are more delicate, but possible to monitor. Furthermore, the applicability of the method has been proved in the quasi-cellular medium agarose, but the final implementation to cells is still a goal important to reach.

In figure 5.1 a single fluorophore incorporated into a fixated 3T3-fibroblast cell is shown. The cell was imaged using a set of standard XY-scans, but additional offsets in steps of 50 nm in axial direction.

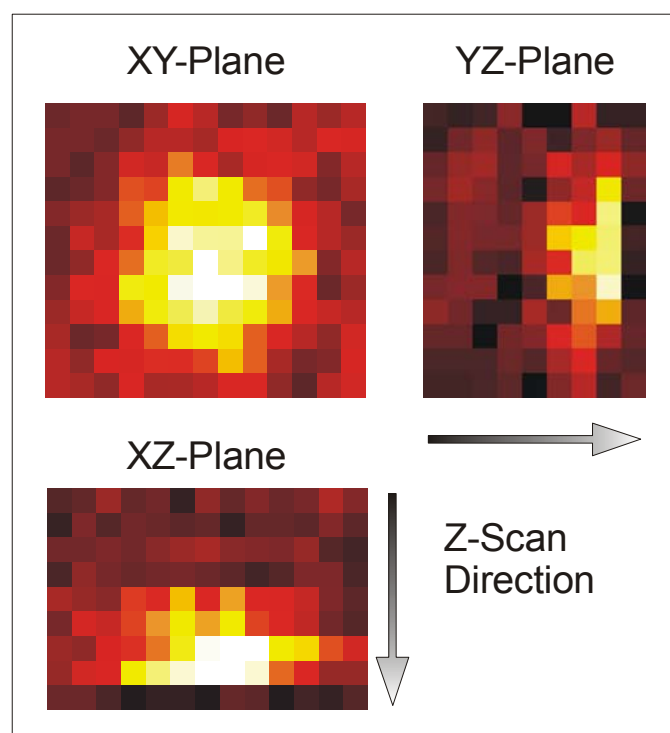


Figure 5.1: RGB-images of a Bodipy 630 fluorophore in a fixated 3T3-fibroblast cell viewed from different directions. While in the XY-picture the collected fluorescence pretends to be homogenous, the Z-stacks prove photobleaching after the 9th image plane. Resolution 50 nm/pixel, integration time 1 ms/pixel, excitation power 0.3 kW/cm², repetition rate 40 MHz.

The images in figure 5.1 indicate, that a major limitation to three-dimensional measurements is the photo-stability of the fluorophores. Measurements with an already very low excitation power of 0.3 kW/cm^2 dominantly show photobleaching of the emitters during the scan. With reduced laser power, the spots are getting increasingly dimmer, thus raising the error of the position determination. To prove that apart from the problem of photo-stability precision distance measurements are at least possible, a solution of a double-stranded 148-mer DNA terminally labeled with the fluorophores Cy 5.5 and Bodipy 630 was injected into a living 3T3-fibroblast cell. The images generated from the measurements data of such a dye pair are depicted in figure 5.2:

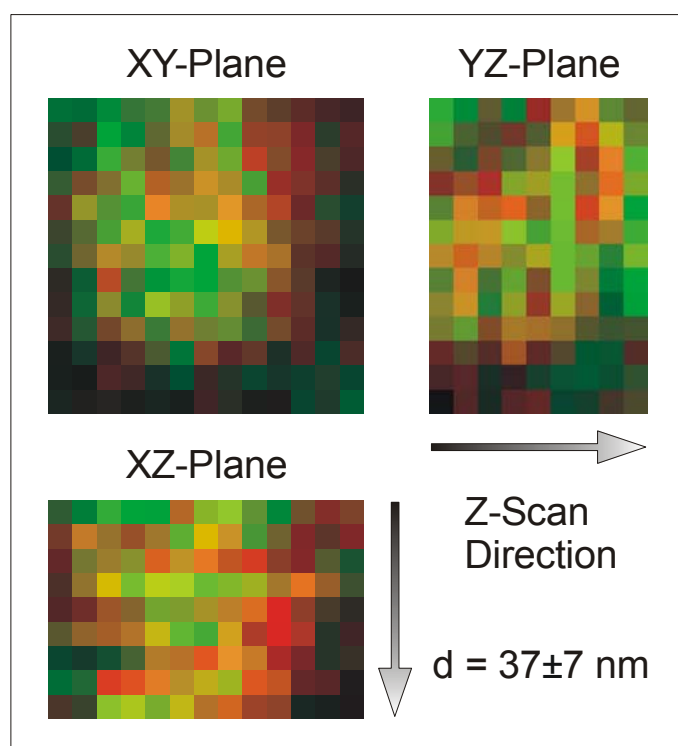


Figure 5.2: Views of two colocalized Cy 5.5 and Bodipy 630 fluorophores in a living 3T3-fibroblast cell in false colors. The fluorophores are separated by a double-stranded 148-mer DNA to obtain a defined distance. Resolution 50 nm per pixel, integration time 1 ms per pixel, excitation power 0.1 kW/cm^2 , repetition rate 40 MHz.

In comparison to the images in figure 5.1 the spot is much more diffuse due to the low excitation power. Anyway, the distance between the fluorophores has been calculated to be $37 \pm 7 \text{ nm}$. Since the maximum of the theoretical distribution (figure 4.14 C) is at about 45 nm, this value is in good agreement with the expected length.

The presented results show the feasibility of SFLIM for ultra-high resolution colocalization in three dimensions even under biological relevant conditions. In the future, this technique will help to reveal molecular interactions of biologically active macromolecules that take place in the range between 10 and 200 nm. Even with the

drawback, that until today only too instable fluorophores for this application are available, there are currently only few alternative techniques to perform such investigations in three dimensions with comparable precision [Failla 2002; Cremer 2002]. Moreover, it is in reach to apply this method for a Cellular Positioning System (CPS) in analogy to the Global Positioning System (GPS). Therefore, three fixated points within the cell are required as reference points, to which relative positions of the molecules of interest are determined. The vision behind this idea is to obtain a three dimensional map of the cell with its compartments and machinery.

5.2 Quantitative Revelation of Biomolecular Machines

The promising results obtained by the first experiments with single stoichiometric labeled antibodies in cell transcription sites open new perspectives for further quantitative investigations.

Beside transcription factories other biomolecular machines like ATP synthase [Diez 2004] or ribosomes [Benenson 2001] are excellent subjects for single-molecule studies. In these studies not only the revelation, but increasingly also the design and practical application of such complexes moves into the focus of scientists [Regev 2002].

An interesting research problem resolvable by single-molecule spectroscopy is the investigation of the exo- and endocytosis of the cell plasma membranes [Geldner 2001]. Exocytosis incorporates transport proteins (*i.e.* ion and water channels) into the membranes, which are later removed by endocytosis [Homann 2002; Nielsen 1995]. Despite the fact that these processes are of substantial interest, little is known about the partial stages, regulation or kinetics of the underlying molecular mechanisms.

Confocal microscopy in combination with antibunching experiments is an excellent tool to deduce information about intracellular transport and interactions. Especially the localization, movement, size determination and quantification of single molecular vesicles associated with endo- and exocytosis could be well studied with methods like fluorescence recovery after photobleaching (FRAP) or fluorescence resonance energy transfer (FRET).

5.3 Orientational Studies of Interacting Fluorophores by Polarization Modulation

Beside fluorescence lifetime or spectral characteristics, one of the most important physical parameters is the orientation of a molecule, or more specifically, the orientation of its transition dipole moment.

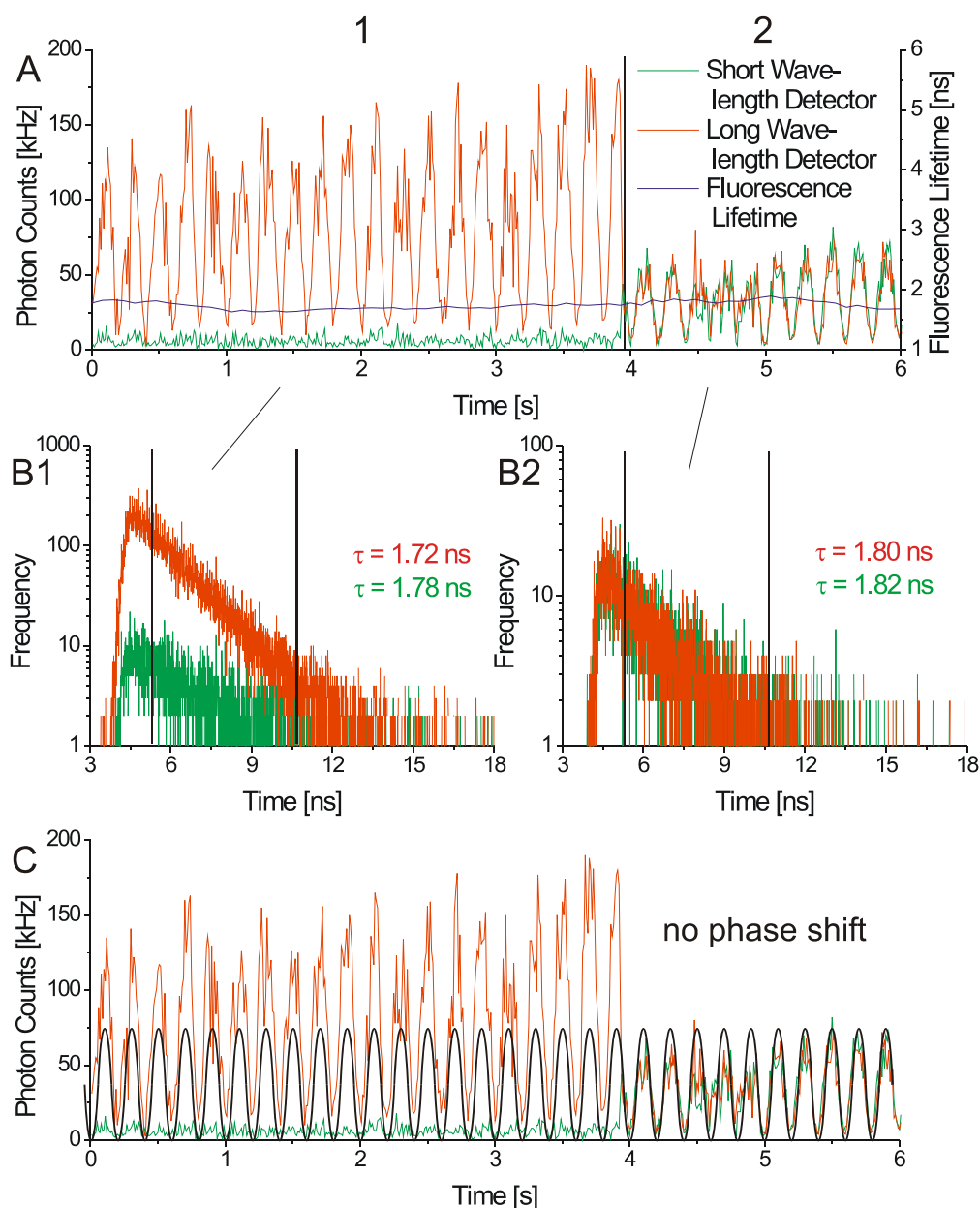


Figure 5.3: Fluorescence time trace of a single Cy 5.5 molecule with its corresponding fluorescence lifetime trajectory (A). The polarization angle of the excitation light is continuously rotated by 180 degrees with a repetition rate of 5 Hz. For the two time intervals denoted in A, separate photon arrival time histograms for the two detector channels are given (B). In C a sine function is fitted to the intensity signal to gain information to identify an phase shift in the emitted fluorescence light.

By polarization microscopy the projection of this orientation into the plane of the sample can be measured [Güttler 1993, Ha 1996]. In combination with SFLIM, which enables the acquisition of multiple characteristics of a fluorophore, a whole set of information can be collected in a single measurement, as shown in figure 5.3.

The time trace in figure A shows the fluorescence intensity of a single Cy 5.5 fluorophore excited with polarization modulated excitation light. In the first part of the trajectory the emitted fluorescence light predominantly falls on the long wavelength detector, which collects photons with a wavelength above 685 nm. At about 4 s the emission characteristics change due to a spectral jump, and both detector channels are equally met by shorter wavelength fluorescence light. To prove that this change is not due to an interaction between different molecules, the fluorescence lifetime trace (blue line) and separate photon arrival time histograms (B) are plotted for the different detection channels. All indexes approve an approximately constant behavior of the lifetime over the complete measurement time, which assures the presence of a single emitter. By separately fitting a sine function to the oscillating intensity signals of both time intervals, a complete positive overlap of the two functions is given, as would be expected for a spectral jump.

Experiments that measure bulk solution properties, and therefore the combined action of many molecules, cannot determine distribution functions, since the measured quantities will necessarily report on the average properties of the ensemble of molecules in the sample. In contrast, single-molecule studies can reveal information on the distributions of molecular properties and on time trajectories. Single-molecule polarization modulation has been extensively applied to measure both static distributions at low temperatures [Güttler 1996, Bloëß 2001] and rotational dynamics at room temperatures [Ha 1999].

However, single fluorophores can often display various kinds of fluorescence intensity and spectral fluctuations, which are not always clearly identifiable in the first place. To help reveal these issues, two properties of a single fluorescent probe attached to a macromolecule can be exploited in ways that are not possible in an ensemble study. The first is the distance dependent fluorescence energy transfer to or from a second fluorophore. The second is the unique absorption and emission transition dipole, which can be interrogated by polarized excitation light and/or by analyzing the emission polarization. Conformational changes can be detected by

measuring the distance changes between two sites on a macromolecule, or by detecting changes in the dipole orientation of a rigidly attached probe.

In figure 5.4 a part of the time trace of a double-stranded 44-mer oligonucleotide (DNA-44) terminally labeled with Cy 5.5 and Bodipy 630 is shown:

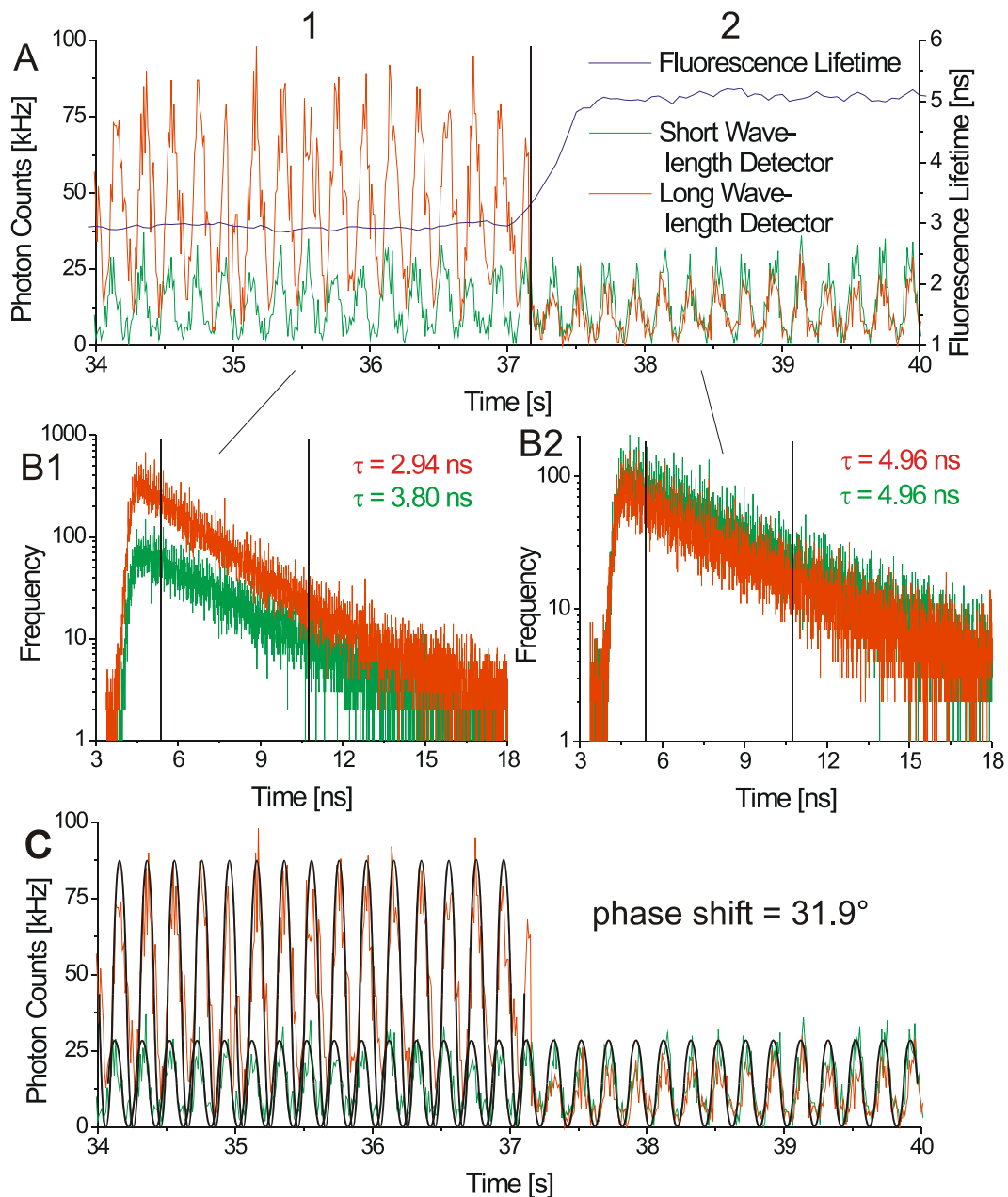


Figure 5.4: Part of a polarization modulated fluorescence time trace of a double-stranded 44-mer oligonucleotide with its corresponding fluorescence lifetime trajectory (A). For the time intervals selected in A, photon arrival time histograms for the two detector channels are shown (B). In C sine functions are fitted to the intensity signal to gain information about the relative emission dipole between the two emitters.

The advantage of using the oligonucleotide strand as spacer between the fluorophores is, that under the right conditions no resonant energy transfer occurs. At the beginning of time trace both fluorophores, Cy 5.5 and Bodipy 630, are emitting. The separate lifetime channels in B1 confirm this, as Cy 5.5 mostly emits only into the red channel (figure 5.3) thereby holding a short lifetime between 1.5 and 2.5 ns, whereas Bodipy 630 shows an equal channel distribution under these conditions and a lifetime between 3 and 5 ns. The lifetime trace, too, consists of a mixture of both fluorophores during this period. After 37 s the overall intensity drops due to photobleaching of the Cy 5.5 emitter. This is accompanied by an increased fluorescence lifetime as can be seen in the trajectory and in graph B2, which therefore contains similar decays in both detection channels. The interesting opportunity with this data is to separately fit the different intensity parts of the trace each with a sine. By comparison of the phase shift between the two functions a conclusion about the relative orientations of the dyes against each other can be given; in this case the shift is almost 32 degrees.

This method points out excellent pathways for further photophysical studies with coupled fluorophores. If, for example, the same dye pair is brought closer together, energy transfer is likely to happen. In standard FRET-studies only one fluorophore, the donor, is excited well, whereas in this case both fluorophores can absorb. The direct excitation of a FRET-acceptors can lead to a so-called exciton blockade [Hofkens 2003]. For high laser intensities the resonant energy transfer pathway to the acceptor is blocked, because the acceptor itself is directly excited by the incident light. As result both dyes occupy an emitting state, whereas with FRET the donor is usually dim and only the acceptor fluoresces.

With knowing the interplay mechanisms and relative positions of two – or even more – emitters, optimization of FRET-systems by the selective rotation of one fluorophore becomes possible on single-molecule basis. Furthermore this opens a possibility to control energy pathways, which is essential for future technologies, e.g. optical switches or quantum computing.

5.4 Preparation and Application of DNA-Spaced Quantum Dots

For the investigation of complex structures and dynamics in biological systems, it is desirable to monitor the interactions of proteins or cells within an organism [Finley 2001, Giuliano 1995]. With the increasing number of single-molecules

techniques developed in the recent years, also the demand towards sensitivity, resolution and accuracy is rising. Especially the development of new fluorescent markers represents an important challenge for scientists. Organic fluorophores are commonly used for tagging cells and biomolecules [Johnson 1998]. Unfortunately, these dyes hold several drawbacks, of which some can be circumvented by quantum dots (QDs), semiconductor nanoparticles, which are considered as promising alternatives to organic fluorophores [Bruchez 1998, Mattoussi 2000]. Whereas common dyes are restricted by their narrow excitation spectra, QDs can be excited by any wavelength from UV to red. This enables efficient excitation and collection of fluorescent emission [Michalet 2001, Chan 2002, Han 2001]. Another limitation of organic fluorophores is their broad emission spectra, which reduces the number of fluorescent probes that can be simultaneously resolved. In contrast, QDs have narrow, tunable emission spectra, and thus emissions from many QDs can be resolved over the same spectral range. Moreover, pure QDs are highly resistant to chemical and metabolic degradation and have a higher photobleaching threshold.

On the other hand there are also disadvantages on the QD side. Quantum dots are naturally not water-soluble, nor do they exhibit definite labeling groups. For circumvention, methods for the enclosure of QDs in hydrophilic coatings have been developed, which are especially needed for applications in aqueous or biological environment [Jaiswal 2003]. With the coating, reactive groups such as biotin, streptavidin, amino-, carboxylic-, and biomolecular tags, can be attached to the nanocrystals thereby introducing reactive groups.

Two of the biggest drawbacks of QDs are their huge size of several tens of nanometers, which reduces the applicability in biological material, and the nonexistence of specific single labeling site. The missing of the latter prevents quantitative applications, for example antibunching measurements.

With the labeling strategy for antibodies and proteins discussed in chapters 3.7 and 4.4, the feasibility to generate single labels with quantum dots is given. The main difference to the reaction pathway shown in figure 4.28 is that here the quantum dot occupies the position of the protein with its manifold coupling sites, and not the place of the mono-reactive fluorescent dye. This implicates that the affine group needs to be attached to molecule of interest instead of the protein or quantum dot.

Applications for this method are the labeling of a QD with a single fluorescent molecule, an oligonucleotide, a biotin, or any other small marker of interest. In

context of this work it would be desirable to prepare and measure two different quantum dots spatially separated at fixed distance. A possible reaction scheme to accomplish such QD-pairs is presented in figure 5.5:

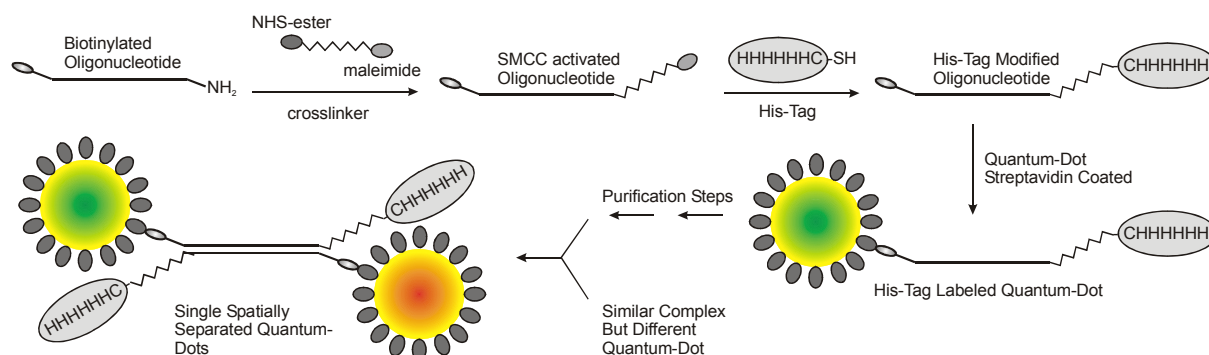


Figure 5.5: Possible reaction steps using a method similar as described in chapter 3.7, that allows to produce a pair of spatially separated quantum dots. By attachment of a SMCC crosslinker to a biotinylated oligonucleotide and subsequent addition of an affine group, here a modified his-tag, a reactant is obtained, which, if treated with an excess of a quantum dot, yields a mono-labeled single-strand. By hybridization of two complementary strands, a set of two quantum dots with a defined distance is achieved.

A terminal biotinylated and amino-functionalized oligonucleotide is modified with a heterobifunctional crosslinker for activation as maleimide. Subsequent reaction with a cysteine modified his-tag and a streptavidin-coated quantum dot gives a crude product mixture, off which the unbound QDs can be removed by Ni-NTA agarose beads, and the free his-tag oligonucleotide by mass dependent filtering. By hybridizing the product with a different quantum dot treated similarly, but with the complementary oligonucleotide sequence, a pair of fluorophores separated by the distance of the oligonucleotide is achieved.

In figure 5.6 two false color images of a single (A) and two colocalized (B) quantum dots are shown, which point out an interesting property of quantum dots in comparison to organic fluorescence dyes: QDs show excessive blinking on millisecond to second timescale. Also off-times of several minutes are known [Biebricher 2004]. Consequently, precision distance measurements with quantum dots have to be done with considerable longer integration times per pixel to prevent effects from non-fluorescent states. Furthermore, reagents for the suppression of blinking, like the addition of 2-mercapto-ethylamine or glucose oxidase, should be added. Another possibility would be to employ a different method for the

measurements, for example spatially modulated illumination microscopy (SMI) [Cremer 2002].

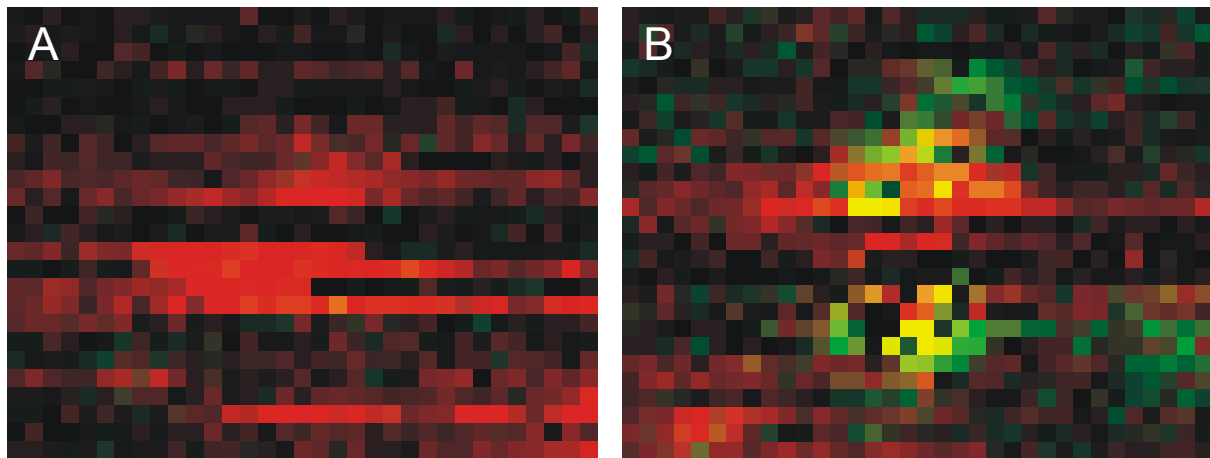


Figure 5.6: False color scan images of a single quantum dot emitting at 705 nm (A) and two colocalized dots with emission wavelengths of 655 and 705 nm, respectively (B). The patchy point spread functions are due to blinking, a typical characteristic of semiconductor nanocrystals. Resolution 50 nm/pixel, integration time 2 ms/pixel, excitation power 0.7 kW/cm², repetition rate 40 MHz, threshold 20 counts.

SMI microscopy uses the so-called point spread function engineering to modify an image taken on a microscope in order to either increase the optical resolution or to maximize the precision of distance measurements at punctual objects, *i.e.* small fluorescent objects in the comparison to the wavelength. This can be accomplished using the fact that the illumination intensity is not homogeneous in the object area, but rather spatially modulated. Two laser beams propagating in opposite directions and interfering in axial direction are used to set up a standing wave field with intensity modulation along the optical axis. From this an increase in the axial resolution is obtained, and distances down to 10 nm can be measured.

Another, simpler idea takes advantage of the blinking and extreme photostability of quantum dots. When monitoring the fluorescence signal of two colocalized QDs with a highly sensitive CCD-camera, the probability to find only one fluorophore emitting at a certain time is relatively high. This implicates that the QDs can be measured separately without photobleaching them beforehand, as it is necessary with other methods [Yildiz 2003, Gordon 2004]. By the determination of the centers of gravity, no interdependency between the two QDs disturbs the measurement, which keeps the error low, and enables a smooth distance determination.

This shows that quantum dots are versatile tools for physical and biological studies. Apart from their size, they can well compete with organic fluorophores, and offer interesting features for further research.

6 Appendix

6.1 Index of Abbreviations

| | |
|--------|--|
| ADC | analog-digital converter |
| AFM | atomic force microscopy |
| APD | avalanche photo diode |
| APS | 3-aminopropyltriethoxy silane |
| bp(s) | basepair(s) |
| Br-UTP | bromodeoxyuridine |
| BSA | bovine serum albumin |
| CCD | charge-coupled device |
| CDR | complementarity determining region |
| COT | cyclooctatetraene |
| DABCO | 1,4-diazabicyclooctane |
| DAPI | 4',6-diamidino-2-phenylindole |
| DMF | dimethyl formamide |
| DNA | deoxyribonucleic acid |
| dsDNA | double-stranded DNA |
| DTT | dithiothreitol (Cleland's reagent) |
| EOM | electro optic modulator |
| FBS | fetal bovine serum |
| FIFO | first-in first-out |
| FJC | freely jointed chain (model) |
| FRAP | fluorescence recovery after photobleaching |
| FRET | fluorescence resonance energy transfer |
| HPLC | high performance liquid chromatography |
| Ig(s) | immunoglobulin(s) |
| KHz | kilo Hertz |
| MEA | 2-mercaptoethyl-amine |
| MES | 2-morpholinoethanesulfonic acid |
| MLE | maximum likelihood estimation (estimator) |
| NHS | N-hydroxy-succinimide |
| NSOM | near-field optical scanning microscopy |
| NTA | nitrilotriacetic acid |
| PBS | phosphate buffered saline |
| PCR | polymerase chain reaction |
| PGA | programmable gain amplifier |
| PS | polystyrene |
| PSF | point spread function |
| QD(s) | quantum dot(s) |
| RNAP | RNA polymerase |
| SFLIM | spectrally resolved lifetime imaging microscopy |
| SMCC | 4-(N-Maleimidomethyl)cyclohexanecarboxylic acid N-hydroxysuccinimide ester |
| SMI | spatially modulated illumination |
| SPAD | single-photon avalanche photo diode |
| SSC | saline-sodium citrate |

| | |
|-------|---|
| ssDNA | single-stranded DNA |
| STED | stimulated transmission emission depletion |
| TAC | time to amplitude converter |
| TCEP | Tris(2-carboxyethyl)phosphine hydrochloride |
| TCSPC | time correlated single photon counting |
| TIR | total internal reflection |
| TNT | Tris-HCl, NaCl, Tween 20 |
| TRIS | Tris (hydroxymethyl) aminomthane |
| WLC | worm-like chain |

6.2 Fluorescence Dyes Structures

The structures of Atto 620 and Atto 647 are not published. Literature concerning the chemical structure of Rhodamin 700, also known as LD 700 perchlorate, is not available.

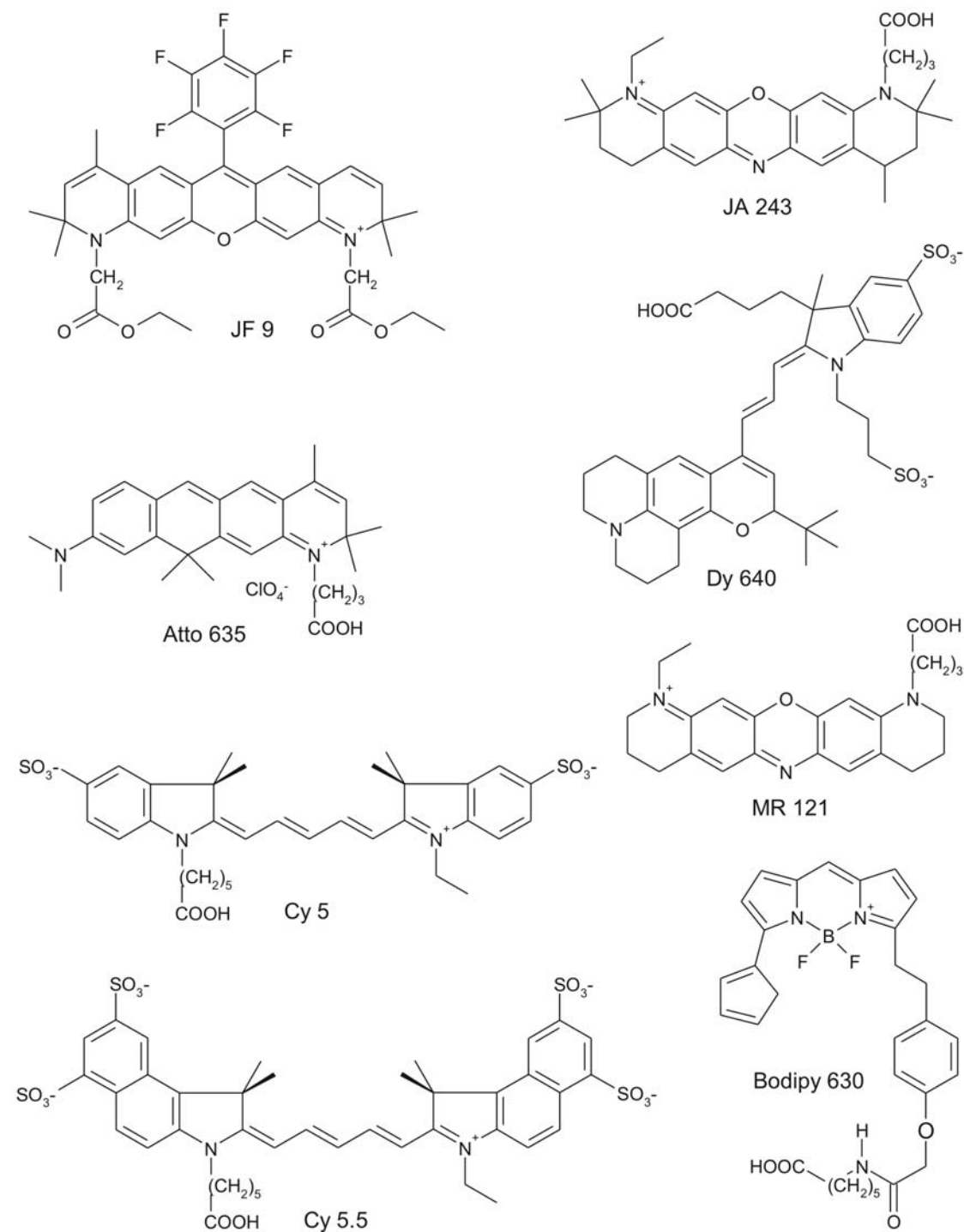


Figure 6.1: Chemical structures of the dyes used in this work.

7 References

- [Affleck 1996] R.L. Affleck, W.P. Ambrose, J.N. Demas, P.M. Goodwin, J.A. Schecker, M. Wu, and R.A. Keller; Reduction of luminescent background in ultrasensitive fluorescence detection by photobleaching. *Anal. Chem.* **1996**, *68*: 2270.
- [Alberts 2002] B. Alberts, D. Bray, J. Lewis, M. Raff, K. Roberts, and J.D. Watson; Molecular Biology of the Cell. 4th edition, *Darland Science Publishing, New York*, **2002**.
- [Ambrose 1994] W.P. Ambrose, P.M. Goodwin, J.C. Martin, and R.A. Keller; Alterations of Single-Molecule Fluorescence Lifetimes in Near-Field Optical Microscopy. *Science* **1994**, *265*: 364.
- [Ambrose 1997] W.P. Ambrose, P.M. Goodwin, J. Enderlein, D.J. Semin, J.C. Martin, and R.A. Keller. Fluorescence photon antibunching from single molecules on a surface. *Chem. Phys. Lett.* **1997**, *269*: 365.
- [Antonov 1983] V.S. Antonov, and K.L. Hohla; Dye stability under excimer-laser pumping I. Method and modeling for infrared dyes. *Appl. Phys. B* **1983**, *30*: 109. V.S. Antonov, and K.L. Hohla; Dye stability under excimer-laser pumping II. Visible and UV dyes. *Appl. Phys. B* **1983**, *32*: 9.
- [Arden 1997] J. Arden-Jacob, N.J. Marx, and K.H. Drexhage; New fluorescent probes for the red spectral region. *J. Fluoresc.* **1997**, *7*: 91.
- [Aubin 1979] J.E. Aubin; Autofluorescence of viable cultured mammalian cells. *J. Histochem. Cytochem.* **1979**, *27*: 35.
- [Austin 1997] R.H. Austin, J.P. Brody, E.C. Cox, T. Duke, and W. Volkmuth; Stretch Genes: Aligning Single Molecules of DNA. *Physics Today* **1997**, *2*: 32.
- [Axelrod 1992] D. Axelrod, D., E. Hellen, and R. Fulbright; Total internal reflection fluorescence in *Topics in Fluorescence Spectroscopy, Volume 3: Biochemical Applications*, J. Lakowicz (ed), *Plenum Press, New York*, **1992**, 289.
- [Badjic 2004] J.D. Badjic, V. Balzani, A. Credi, S. Silvi, and J.F. Stoddart; A molecular elevator. *Science* **2004**, *303*: 1845.
- [Baneyx 1999] F. Baneyx; Recombinant protein expression in *Escherichia coli*. *Curr. Opin. Biotechnol.* **1999**, *10*: 411.
- [Basche 1992] T. Basche, W.E. Moerner, M. Orrit, and H. Talon; Photon antibunching in the fluorescence of a single dye molecule trapped in a solid. *Phys. Rev. Lett.* **1992**, *69*: 1516.
- [Becker 1999] W. Becker, H. Hickl, C. Zander, K.H. Drexhage, M. Sauer, S. Siebert, and J. Wolfrum; Time-resolved detection and identification of single analyte molecules in microcapillaries by time-correlated single-photon counting (TCSPC). *Rev. Sci. Instrum.* **1999**, *70*: 1835.

- [Benenson 2001] K. Benenson, T. Paz-Elitzur, R. Adar, E. Keinan, Z. Livneh and E. Shapiro; Programmable computing machine made of biomolecules. *Nature* **2001**, *414*: 430.
- [Betzig 1993] E. Betzig, and R.J. Chichester; Single Molecules Observed By Near-Field Scanning Optical Microscopy. *Science* **1993**, *262*: 1422.
- [Betzig 1994] E. Betzig; Proposed method for molecular optical imaging. *Opt. Lett.* **1994**, *20*: 237.
- [Biebricher 2002] A. Biebricher; Hochaufgelöste Kolokalisation einzelner Moleküle durch spektral- und zeitaufgelöste Fluoreszenzmikroskopie. *Diploma Thesis, Heidelberg*, **2002**.
- [Biebricher 2004] A. Biebricher; unpublished results.
- [Bloeß 2001] A. Bloeß, Y. Durand, M. Matsushita, J. Schmidt, and E.J. Groenen; A single-molecule study of the relation between the resonance frequency and the orientation of a guest molecule in a Shpol'skii system. *Chem. Phys. Lett.* **2001**, *344*: 55.
- [Brand 1997] L. Brand, C. Eggeling, C Zander, K.H. Drexhage, and C.A.M. Seidel; Single-molecule identification of coumarin-120 by time-resolved fluorescence detection - comparison of one- and two-photon excitation in solution. *J. Phys. Chem. A* **1997**, *101*: 4313.
- [Bruchez 1998] M. Bruchez, M. Moronne, P. Gin, S. Weiss, and A.P. Alivisatos; Semiconductor nanocrystals as fluorescent biological labels. *Science* **1998**, *281*: 2013.
- [Buschmann 2003] V. Buschmann, K.D. Weston, and M. Sauer; Spectroscopic Study and Evaluation of Red-Absorbing Fluorescent Dyes. *Bioconjugate Chem.* **2003**, *14*: 195.
- [Bustamante 1994] C. Bustamante, J.F. Marko, E.D. Siggia, and S. Smith; Entropic elasticity of lambda-phage DNA. *Science* **1994**, *265*: 1599.
- [Carlsson 1978] J. Carlsson, H. Drevin, and R. Axen; Protein thiolation and reversible protein-protein conjugation. N-Succinimidyl 3-(2-pyridyldithio)propionate, a new heterobifunctional reagent. *J. Biochem.* **1978**, *173*: 723.
- [Carmichael 1986] I. Carmichael, and G.L. Hug; Triplet-triplet absorption spectra of organic molecules in condensed phases. *J. Phys. Chem. Ref. Data* **1986**, *15*: 1.
- [Carpino 1994] L. A. Carpino, and A. El-Faham; Effect of Tertiary Bases on O-Benzotriazolyluronium Salt-Induced Peptide Segment Coupling. *J. Org. Chem.* **1994**, *59*: 695.
- [Carrington 1995] W.A. Carrington, R.M. Lynch, E.D.W. Moore, G. Isenberg, K.E. Fogarty, and F.S. Fay; Superresolution Three-Dimensional Images of Fluorescence in Cells with Minimal Light Exposure. *Science* **1995**, *268*: 1483.
- [Castro 1975] B. Castro, J.R. Dormoy, G. Evin, and C. Selve; Peptide coupling reagents. *Tetrahedron Lett.* **1975**, *14*: 1219.

- [Castro 1990] B. Castro, J. Coste, and D. Le-Nguyen; PyBOP r : a new peptide coupling reagent devoid of toxic by-product. *Tetrahedron Lett.* **1990**, *31*: 205.
- [Chalfie 1998] M. Chalfie, and S. Kain; Green fluorescent protein: properties, applications, and protocols. **1998**, *New York, Wiley-Liss.*
- [Chan 2002] W.C. Chan, D.J. Maxwell, X. Gao, R.E. Bailey, M. Han, and S. Nie; Luminescent quantum dots for multiplexed biological detection and imaging. *Curr. Opin. Biotechnol.* **2002**, *13*: 40.
- [Chen 1999] Y. Chen, J.D. Müller, P.T.C. So, and E. Gratton; The Photon Counting Histogram in Fluorescence Fluctuation Spectroscopy. *Biophys. J.* **1999**, *77*: 553.
- [Cluzel 1996] P. Cluzel, A. Lebrun, C. Heller, R. Lavery, J.-L. Viovy, D. Chatenay, and F. Caron; DNA: an extensible molecule. *Science* **1996**, *271*: 792.
- [Connor 1984] D.V. O'Connor, and D. Phillips, Time Correlated Single Photon Counting. *Academic Press, London* **1984**.
- [Cook 1999] P.R. Cook; The Organization of Replication and Transcription. *Science* **1999**, *184*: 1790.
- [Cordell 1984] J.L. Cordell, B. Falini, W.N. Erber, A.K. Ghosh, Z. Abdulaziz, S. MacDonald, K.A. Pulford, H. Stein, and D.Y. Mason; Immunoenzymatic labeling of monoclonal antibodies using immune complexes of alkaline phosphatase and monoclonal anti-alkaline phosphatase (APAAP complexes). *J. Histochem. Cytochem.* **1984**, *32*: 219.
- [Cremer 2002] A.V. Failla, U. Spoeri, B. Albrecht, A. Kroll, C. Cremer; Nanosizing of fluorescent objects by spatially modulated illumination microscopy. *Appl. Optics* **2002**, *41*: 7275.
- [Dagenais 1983] M. Dagenais, and L. Mandel; Observation of Sub-Poissonian Photon Statistics. *Phys. Rev. Lett.* **1983**, *51*: 384.
- [Davison 1927] C.J. Davison, and L.H. Germer; The Scattering of Electrons by a Single Crystal of Nickel. *Nature* **1927**, *119*: 558.
- [Deniz 2001] A.A. Deniz, T.A. Laurence, M. Dahan, D.S. Chemla, P.G. Schultz, and S. Weiss; Ratiometric single-molecule studies of freely diffusing biomolecules. *Annu. Rev. Phys. Chem.* **2001**, *52*: 233.
- [Dickson 1996] R.M. Dickson, D.J. Norris, Y.-L. Tzeng, and W.E. Moerner; Three-Dimensional Imaging of Single Molecules Solvated in Pores of Poly(acrylamide) Gels. *Science* **1996**, *274*: 966.
- [Dickson 1997] R.M. Dickson, A.B. Cubitt, R.Y. Tsien, W.E. Moerner; On/off blinking and switching behaviour of single molecules of green fluorescent protein. *Nature* **1997**, *388*: 355.

- [Diez 2004] M. Diez, B. Zimmermann, M. Börsch, M. König, E. Schweinberger, S. Steigmiller, R. Reuter, S. Felekyan, V. Kudryavtsev, C.A.M. Seidel, P. Gräber; Proton-powered subunit rotation in single membrane-bound F_0F_1 -ATP synthase. *Nature Struct. Mol. Biol.* **2004**, *11*, 135.
- [Dunn 1999] R.C. Dunn; Near-Field Scanning Optical Microscopy. *Chemical Reviews* **1999**, *99*: 2891.
- [Dyba 2002] M. Dyba, and S.W. Hell; Focal spots of size $\lambda/23$ open up far-field fluorescence microscopy at 33 nm axial resolution. *Phys. Rev. Lett.* **2002**, *88*: 163901.
- [Eggeling 1999] C. Eggeling, J. Widengren, R. Rigler, C.A.M. Seidel; Photostability of Fluorescent Dyes for Single-Molecule Spectroscopy in *Applied Fluorescence in Chemistry, Biology and Medicine*, Springer Verlag, Berlin, Heidelberg, New York, **1999**.
- [Eggeling 2001] C. Eggeling, S. Berger, L. Brand, J.R. Fries, J. Schaffer, A. Volkmer, and C.A.M. Seidel; Data registration and selective single-molecule analysis using multiparameter fluorescence detection. *J. Biotechnol.* **2001**, *86*: 163.
- [Eigen 1994] M. Eigen, and R. Rigler. Sorting Single Molecules - Application to Diagnostics and Evolutionary Biotechnology. *Proc. Natl. Acad. Sci. USA* **1994**, *91*: 5740.
- [Enderle 1997] T. Enderle, T. Ha, D.F. Ogletree, D.S. Chemla, C. Magowan, and S. Weiss; Membrane specific mapping and colocalization of malarial and host skeletal proteins in the *Plasmodium falciparum* infected erythrocyte by dual-color near-field scanning optical microscopy. *Proc. Natl. Acad. Sci. USA* **1997**, *94*: 520.
- [Failla 2002] A.V. Failla, U. Spoeri, B. Albrecht, A. Kroll, C. Cremer; Nanosizing of fluorescent objects by spatially modulated illumination microscopy. *Appl. Optics* **2002**, *41*: 7275.
- [Fay 1997] F.S. Fay, K.L. Taneja, S. Shenoy, L. Lifshitz, and R.H. Singer; Quantitative digital analysis of diffuse and concentrated nuclear distributions of nascent transcripts, SC35 and poly(A). *Exp. Cell. Res* **1997**, *231*: 27.
- [Fazel 1997] S. Fazel, E.J. Wiersma, and M.J. Shulman; Interplay of J chain and disulfide bonding in assembly of polymeric IgM. *International Immunology* **1997**, *9*: 1149.
- [Finley 2001] K.R. Finley, A.E. Davidson, and S.C. Ekker; Three-color imaging using fluorescent proteins in living zebrafish embryos. *Biotechniques* **2001**, *31*, 66.
- [Flanagan 1997] J.H. Flanagan, S.H. Khan, S. Menchen, S.A. Soper, and R.P. Hammer; Functionalized tricyanocyanine dyes as near-infrared fluorescent probes for biomolecules. *Bioconj. Chem.* **1997**, *8*: 751.
- [Flory 1969] P.J. Flory; In Statistical Mechanics of Chain Molecules. *Interscience Publishers, New York* **1969**.

- [Förster 1946] T. Förster; Energiewanderung und Fluoreszenz. *Naturwissenschaften* **1946**, *6*: 166.
- [Fritz 2000] J. Fritz, M.K. Baller, H.P. Lang, H. Rothuizen, P. Vettiger, E. Meyer, H.-J. Güntherodt, C. Gerber, and J.K. Gimzewski; Translating Biomolecular Recognition into Nanomechanics. *Science* **2000**, *288*: 316.
- [Funatsu 1995] T. Funatsu, Y. Harada, M. Tokunaga, K. Saito, and T. Yanagida; Imaging of Single Fluorescent Molecules and Individual ATP Turnovers By Single Myosin Molecules in Aqueous-Solution. *Nature* **1995**, *374*: 555.
- [Garcia 1998] M.F. Garcia-Parajo, J.A. Veerman, S.J.T. van Noort, B.G. de Grooth, J. Greve, and N.F. van Hulst; Near-field optical microscopy for DNA studies at the single molecular level. *Bioimaging* **1998**, *6*: 43.
- [Gey 1952] G.O. Gey, W.D. Coffman, and M.T. Kubicek; Tissue culture studies of the proliferative capacity of cervical carcinoma and normal epithelium. *Cancer Res.* **1952**, *12*: 264.
- [Giesendorf 1998] B.A.J. Giesendorf, J.A.M. Vet, S. Tyagi, E.J.M.G. Mensink, F.J.M. Trijbels, and H.J. Blom. Molecular beacons: a new approach for semiautomated mutation analysis. *Clinical Chemistry* **1998**, *44*: 3.
- [Gill 1990] S.C. Gill, and P.H. von Hippel; Calculation of protein extinction coefficients from amino acid sequence data. *Anal. Biochem.* **1990**, *182*: 319; Erratum. *Anal. Biochem.* *189*: 283.
- [Göhde 1997] W. Göhde, J. Tittel, Th. Basché, C. Bräuchle, U.C. Fischer, and H. Fuchs. A low-temperature scanning confocal and near-field optical microscope. *Rev. Sci. Instrum.* **1997**, *68*: 2466.
- [Gordon 2004] M.P. Gordon, T. Ha, and P.R. Selvin; Single-molecule high-resolution imaging with photobleaching. *Proc. Natl. Acad. Sci. USA* **2004**, *101*: 6463.
- [Grande 1997] M.A. Grande, I. van der Kraan, L. de Jong, and R. van Driel; Nuclear distribution of transcription factors in relation to sites of transcription and RNA polymerase II. *J. Cell. Sci.* **1997**, *110*: 1781.
- [Green 1974] H. Green and O. Kehinde;. Sublines of mouse 3T3 cells that accumulate lipid. *Cell* **1974**, *1*: 113.
- [Griffiths 1986] G. Griffiths and H. Hoppeler; Quantitation in immuncytochemistry, correlation of immunogold labeling to absolute numbers of membrane antigens. *J. Histochem. Cytochem.* **1986**, *34*: 1389.
- [Griffiths 1993] G. Griffiths; Fine structure immunocytochemistry. *Springer Verlag, Heidelberg* **1993**.
- [Gross 1978] V. Dourtoglou, J.-C. Ziegler, and B. Gross; o-Benzotriazolyl-N,N-tetramethyluronium hexafluorophosphate: a new and effective reagent for peptide coupling. *Tetrahedron Lett.* **1978**, *15*: 1269.

- [Giuliano 1995] K.A. Giuliano, P.L. Post, K.M. Hahn, and D.L. Taylor; Fluorescent protein biosensors: measurement of molecular dynamics in living cells. *Annu. Rev. Biophys. Biomol. Struct.* **1995**, *24*: 405.
- [Güttler 1993] F. Güttler, J. Sepiol, T. Plakhotnik, A. Mitterdorfer, A. Renn, and U.P. Wild; Single molecule spectroscopy: fluorescence excitation spectra with polarized light. *J. Lumin.*, **1993**, *56*: 29.
- [Güttler 1996] F. Güttler, M. Croci, A. Renn, and U.P. Wild; Single molecule polarization spectroscopy: pentacene in p-terphenyl *Chem. Phys.* **1996**, *211*: 421.
- [Ha 1996] T. Ha, T. Enderle, and D.S. Chemla; Single Molecule Dynamics Studied by Polarization Modulation. *Phys. Rev. Lett.*, **1996**, *77*: 3979.
- [Ha 1999] T. Ha, A. Laurence, D. S. Chemla, and S. Weiss; Spectroscopy of Single Fluorescent Molecules. *J. Phys. Chem. B* **1999**, *103*: 6839.
- [Han 2001] M. Han, X. Gao, J.Z. Su, and S. Nie; Quantum-dot-tagged microbeads for multiplexed optical coding of biomolecules. *Nat. Biotechnol.* **2001**, *19*: 631.
- [Hanbury 1956] R. Hanbury-Brown, and R.Q. Twiss; Correlations between photons in two coherent beams of light. *Nature* **1956**, *177*: 27.
- [Harms 2001] G.S. Harms, L. Cognet, P.H.M. Lommerse, G.A. Blab, and T. Schmidt; Autofluorescent Proteins in Single-Molecule Research: Applications to Live Cell Imaging Microscopy. *Biophys. J.* **2001**, *80*: 2396.
- [Haugland 2004] R.P. Haugland; Handbook of fluorescent probes and research chemicals, *Web Edition*, **2004**, *Molecular Probes*, Eugene.
- [Heilemann 2002] M. Heilemann, D.-P. Herten, P. Tinnefeld, R. Heintzmann, C. Cremer, K.D. Weston, J. Wolfrum, and M. Sauer; High-resolution colocalization of single dye molecules by fluorescence lifetime imaging microscopy (FLIM). *Anal. Chem.* **2002**, *74*: 3511.
- [Hell 1995] S. Hell, and E.H.K. Stelzer; Properties of a 4Pi-confocal fluorescence microscope. *J. Opt. Soc. Am. A* **1992**, *9*: 2159.
- [Heinlein 2003] T. Heinlein, J.-P. Knemeyer, O. Piestert, and M. Sauer; Nucleobase-specific quenching of fluorescent dyes in DNA-hairpins. *J. Phys. Chem. B* **2003**, *107*: 7957.
- [Heinlein 2004] T. Heinlein, A. Pombo, M. Sauer, and D.P. Herten; Stoichiometric Fluorescence Labeling of Antibodies for Single-Molecule Spectroscopic Applications. *JACS submitted*.
- [Hernando 2004] J. Hernando, P.A.J. de Witte, E.M.H. van Dijk, J. Korterik, N.J.M. Roeland, A.E. Rowan, M.F. Garcia-Parajo, and N.F. van Hulst; Multichromophoric polymers: Investigation of perylene photonic wires by combined single-molecule fluorescence and atomic force microscopy. *Angew. Chem. Int. Ed.* **2004**, *43*: 4045.

- [Herten 2003] D.P. Herten, and M. Sauer; Einzelmolekül-Fluoreszenzspektroskopie – Analytik and der ultimativen Grenze der Empfindlichkeit. *Bunsenberichte* **2003**, 1: 5.
- [Hirschfeld 1979] T. Hirschfeld; Fluorescence background discrimination by prebleaching. *J. Histochem. Cytochem.* **1979**, 27: 96.
- [Hofkens 2003] J. Hofkens, T. Vosch, M. Cotlet, S. Habuchi, K. Van Der Biest, K. Müllen, G. Dirix, J. Michiels, J. Vanderleyden, M. Sauer, F.C. De Schryver; Excited state processes in individual multichromophoric systems. *Proceedings of SPIE* **2003**, 4962: 1.
- [Hogen 1987] M.E. Hogen, and R.H. Austin; Importance of DNA stiffness in protein–DNA binding specificity. *Nature* **1987**, 329: 263.
- [Hozák 1994] P. Hozák, P.R. Cook, C. Schöfer, W. Mosgöller, and F. Wachtler; Site of transcription of ribosomal RNA and intra-nucleolar structure in HeLa cells. *J. Cell Sci.* **1994**, 107: 639.
- [Iborra 1996] F.J. Iborra, A. Pombo, D.A. Jackson, and P.R. Cook; Active RNA polymerases are localized within discrete transcription ‘factories’ in human nuclei. *J. Cell. Sci.* **1996**, 109: 1427.
- [Iborra 1998] F.J. Iborra, A. Pombo, J. McManus, D.A. Jackson, and P.R. Cook; The topology of transcription by immobilized polymerases. *Exp. Cell. Res.* **1998**, 229: 167.
- [Ishii 2001] Y. Ishii, A. Ishijima, and T. Yanagida; Single molecule nanomanipulation of biomolecules. *Trends in Biotechnology* **2001**, 19: 211.
- [Ishikawa 1983] E. Ishikawa, M. Imagawa, S. Hashida, S. Yoshitake, Y. Hamaguchi, and T. Ueno; Enzyme-Labeling of Antibodies and Their Fragments for Enzyme Immunoassay and Immunohistochemical Staining. *J. Immunoassay*, **1983**, 4: 209.
- [Iyer 1996] V. Iyer, and K. Struhl; Absolute mRNA levels and transcriptional initiation rates in *Saccharomyces cerevisiae*. *Proc. Natl. Acad. Sci. USA.* **1996**, 93: 5208.
- [Jackson 1993] D.A. Jackson, A.B. Hassan, R.J. Errington, and P.R. Cook; Visualization of focal sites of transcription within human nuclei. *EMBO J.* **1993**, 12: 1059.
- [Jackson 1998] D.A. Jackson, F.J. Iborra, E.M.M. Manders, and P.R. Cook; Numbers and organization of RNA polymerases, nascent transcripts and transcription units in HeLa nuclei. *Mol. Biol. Cell.* **1998**, 9: 1523.
- [Jaiswal 2003] J.K. Jaiswal, H. Mattoussi, J.M. Mauro, and M.S. Simon; Long-term multiple color imaging of live cells using quantum dot bioconjugates. *Nature Biotech.* **2003**, 21: 47.
- [Jasny 1994] J. Jasny, J. Sepit, J. Karpiuk, and J. Gilewski; Nanosecond transient absorption spectrophotometer with dye laser probing and computer control. *J. Rev. Sci. Instrument.* **1994**, 65: 3646.

- [Jocelyn 1987] P.C. Jocelyn; Chemical reduction of disulfides. *Methods Enzymol.* **1987**, 143: 246.
- [Johnson 1998] I. Johnson; Fluorescent probes for living cells. *Histochem. J.* **1998**, 30: 123.
- [Jungbauer 2004] A. Jungbauer, and R. Hahn; Monoliths for fast bioseparation and bioconversion and their applications in biotechnology. *J. Separat. Sci.* **2004**, 27: 767.
- [Kaplan 1976] J. Kaplan, J. Tilton, and W.D. Peterson; Identification of T-cell lymphoma tumor antigens on human T-cell lines. *Am. J. Hematol.* **1976**, 1: 219.
- [Kemnitzer 2001] N.U. Kemnitzer; Amidopyrylium-Fluoreszenz-Farbstoffe, Der Andere Verlag: Osnabrück **2001**.
- [Kim 2004] J.M. Kim, T. Ohtani, and H. Muramatsu; 25 nm resolution single molecular fluorescence imaging by scanning near-field optical/atomic force microscopy. *Surface Science* **2004**, 549: 273.
- [Kimura 2002] H. Kimura, K. Sugaya, and P.R. Cook; The transcription cycle of RNA polymerase II in living cells. *J. Cell Biol.* **2002**, 159: 777.
- [Klar 1999] T.A. Klar, and S.W. Hell; Sub-diffraction resolution in far-field fluorescence microscopy. *Opt. Lett.* **1999**, 24: 954.
- [Klar 2000] T.A. Klar, S. Jakobs, M. Dyba, A. Enger, and S.W. Hell; Fluorescence microscopy with diffraction resolution barrier broken by stimulated emission. *Proc. Natl. Acad. Sci. USA* **2000**, 97: 8206.
- [Knemeyer 2000] J.P. Knemeyer, N. Marme, and M. Sauer. Probes for detection of specific DNA sequences at the single- molecule level. *Anal. Chem.* **2000**, 72: 3717.
- [Knorr 1989] R. Knorr, A. Trzeciak, W. Bannwarth, and D. Gillessen; New coupling reagents in peptide chemistry. *Tetrahedron Lett.* **1989**, 30: 1927.
- [Köppel 1974] D.E. Köppel; Statistical accuracy in fluorescence correlation spectroscopy. *Phys. Rev. A.* **1974**, 10: 1938.
- [Lacoste 2000] T.D. Lacoste, X. Michalet, F. Pinaud, D.S. Chemla, A.P. Alivisatos, and S. Weiss; Ultrahigh-resolution multicolor colocalization of single fluorescent probes. *Proc. Natl. Acad. Sci. USA* **2000**, 97: 9461.
- [Lakowicz 1983] J.R. Lakowicz; Principles of Fluorescence Spectroscopy; *Plenum Press, New York* **1983**.
- [Lee 2000] T. Lee, and R.A. Young; Transcription of Eukaryotic Protein-coding Genes. *Ann. Rev. Genet.* **2000**, 34: 77.
- [Lieberwirth 1998] U. Lieberwirth, J. Arden-Jacob, K.H. Drexhage, D.-P. Herten, R. Müller, M. Neumann, A. Schulz, S. Siebert, G. Sagner, S. Klingel, M. Sauer, and J. Wolfrum; Multiplex dye DNA sequencing in capillary gel electrophoresis by diode laser-based time-resolved fluorescence detection. *Anal. Chem.* **1998**, 70: 4771.

- [Louis 1988] T. Louis, G. H. Schatz, P. Klein-Bölting, A. R. Holzwarth, G. Ripamonti, and S. Cova; Performance comparison of a single-photon avalanche diode with a microchannel-plate photomultiplier in time-correlated single-photon counting. *Rev. Sci. Instrum.* **1988**, *59*: 1148.
- [Löscher 1998] F. Löscher, S. Böhme, J. Martin, and S. Seeger; Counting of Single Protein Molecules at Interfaces and Application of This Technique in Early-Stage Diagnosis. *Anal. Chem.* **1998**, *70*: 3202.
- [Mattoussi 2000] H. Mattoussi, J.M. Mauro, E.R. Goldman, G.P. Anderson, V.C. Sundar, F. Mikulec, and M.G. Bawendi; Self-assembly of CdSe-ZnS quantum dot bioconjugates using an engineered recombinant protein. *J. Am. Chem. Soc. USA* **2000**, *122*: 12142.
- [Maus 2001] M. Maus, M. Cotlet, J. Hofkens, T. Gensch, F.C. De Schryver, J. Schaffer, and C.A.M. Seidel; An experimental comparison of the maximum likelihood estimation and nonlinear least squares fluorescence lifetime analysis of single molecules. *Anal. Chem.* **2001**, *73*: 2078.
- [Michalet 2001] X. Michalet, F. Pinaud, T.D. Lacoste, M. Dahan, M.P. Bruchez, A.P. Alivisatos, S. Weiss; Properties of fluorescent semiconductor nanocrystals and their application to biological labeling. *Single Molec.* **2001**, *2*: 261.
- [Michler 2000] P. Michler, A.I. Lu, M.D. Mason, P.J. Carson, G.F. Strouse, and S.K. Buratto; Quantum correlation among photons from a single quantum dot at room temperature. *Nature* **2000**, *406*: 968.
- [Moerner 1989] W.E. Moerner, and L. Kador; Optical detection and spectroscopy of single molecules in a solid. *Phys. Rev. Lett.* **1989**, *62*: 2535.
- [Mujumdar 1993] R.B. Mujumdar, L.A. Ernst, S.R. Mujumdar, C.J. Lewis, and A.S. Waggoner; Cyanine dye labeling reagents: Sulfoindocyanine succinimidyl esters. *Bioconj. Chem.* **1993**, *4*: 105.
- [Müller 2003] C. Müller; Entwicklung einer Methode zur zeit- und spektralaufgelösten Präzisionsdistanzmikroskopie auf Einzelmolekülebene. *PhD Thesis, Universität Heidelberg*, **2003**.
- [Munteanu 1998] M.G. Munteanu, K. Vlahovicek, S. Parthasarathy, I. Simon, and S. Pongor; Rod models of DNA: sequence-dependent anisotropic elastic modelling of local bending phenomena. *Trends Biochem Sci.* **1998**, *23*: 341.
- [Neuweiler 2002] H. Neuweiler, A. Schulz, A.C. Vaiana, J.C. Smith, S. Kaul, J. Wolfrum, and M. Sauer; Detection of Individual p53-Autoantibodies by Using Quenched Peptide-Based Molecular Probes. *Ang. Chem. Int. Ed.* **2002**, *41*: 4769.
- [Nie 1997] S.M. Nie, and R.N. Zare; Optical detection of single molecules. *Annu. Rev. Biophys. Biomolec. Struct.* **1997**, *26*: 567.
- [Ober 2004] R.J. Ober, S. Ram, and E.S. Ward; Localization Accuracy in Single-Molecule Microscopy. *Biophys. J.* **2004**, *86*: 1185.

- [O'Shann. 1995] D.J. O'Shannessy, K.C. O'Donnell, J. Martin, M. Brigham-Burke; Detection and quantitation of hexa-histidine-tagged recombinant proteins on western blots and by a surface plasmon resonance biosensor technique. *Anal. Biochem.* **1995**, 229:119.
- [Patonay 1991] G. Patonay, and M.D. Antoine; Near-infrared fluorogenic labels: New approach to an old problem. *Anal. Chem.* **1991**, 63: 321A.
- [Pawley 1995] J.B. Pawley; Handbook of Biological Confocal Microscopy. New York, Plenum Press, **1995**.
- [Perkins 1995] T.T. Perkins, D.E. Smith, R.G. Larson, and S. Chu; Stretching of a single tethered polymer in a uniform flow. *Science* **1995**, 268: 83.
- [Peeters 1989] J.M. Peeters, T.G. Hazendonk, E.C. Beuvery, and G.I. Tesser; Comparison of four bifunctional reagents for coupling peptides to proteins and the effect of the three moieties on the immunogenicity of the conjugates. *J. Immunol. Meth* **1989**, 120: 133.
- [Peterman 2004] E.J.G. Peterman, H. Sosa, and W.E. Moerner; Single-molecule fluorescence spectroscopy and microscopy of biomolecular motors. *Annu. Rev. Phys. Chem.* **2004**, 55: 79.
- [Piestert 2003] O. Piestert, H. Barsch, V. Buschmann, T. Heinlein, J.P. Knemeyer, K.D. Weston, and M. Sauer; A Single-Molecule Sensitive DNA Hairpin System Based on Intramolecular Electron Transfer. *Nano Letters* **2003**, 3: 979.
- [Pombo 1999] A. Pombo, D.A. Jackson, M. Hollinshead, Z. Wang, R.G. Roeder, and P.R. Cook; Regional specialization in human nuclei: visualization of discrete sites of transcription by RNA polymerase III. *EMBO J.* **1999**, 18: 2241.
- [Poppenborg 1997] L. Poppenborg, K. Friehe, and E. Flaschel; The green fluorescent protein is a versatile reporter for bioprocess monitoring. *J. Biotechnol.* **1997**, 58: 79.
- [Qu 2004] X. Qu, D. Wu, L. Mets, and N.F. Scherer; Nanometer-localized multiple single-molecule fluorescence microscopy. *Proc. Natl. Acad. Sci. USA* **2004**, 101: 11298.
- [Regev 2002] A. Regev, and E. Shapiro; Cellular abstractions: Cells as computation. *Nature* **2002**, 419: 343.
- [Sako 2000] Y. Sako, S. Minoghchi, T. Yanagida. Single-molecule imaging of EGFR signalling on the surface of living cells. *Nat. Cell Biol.* **2000**, 2: 168.
- [Sase 1995] I. Sase, H. Miyata, J.E.T. Corrie, J.S. Craik, and K. Kinoshita Jr.; Real time imaging of single fluorophores on moving actin with an epifluorescence microscope. *Biophys. J.* **1995**, 69: 323.
- [Sauer 1995] M. Sauer, K.-T. Han, V. Ebert, R. Müller, A. Schulz, S. Seeger, J. Wolfrum, J. Arden-Jacob, G. Deltau, N.J. Marx, C. Zander, and K.H. Drexhage; New fluorescent dyes in the red region for biodiagnostics. *J. Fluoresc.* **1995**, 5: 247.

- [Sauer 1997] M. Sauer, C. Zander, R. Müller, B. Ullrich, K.H. Drexhage, S. Kaul, and J. Wolfrum; Detection and identification of individual antigen molecules in human serum with pulsed semiconductor lasers. *Appl. Phys. B* **1997**, *65*: 427.
- [Sauer 1998] M. Sauer, J. Arden-Jacob, K.H. Drexhage, F. Göbel, U. Lieberwirth, K. Mühlegger, R. Müller, J. Wolfrum, and C. Zander; Time-resolved identification of individual mononucleotide molecules in aqueous solution with pulsed semiconductor lasers. *Bioimaging* **1998**, *6*: 14.
- [Schaffer 1999] J. Schaffer, A. Volkmer, C. Eggeling, V. Subramaniam, G. Striker, C.A.M. Seidel. Identification of single molecules in aqueous solution by time- resolved fluorescence anisotropy. *J. Phys. Chem. A* **1999**, *103*: 331.
- [Schmidt 1995] T. Schmidt, G.J. Schutz, W. Baumgartner, H.J. Gruber, and H. Schindler; Characterization of photophysics and mobility of single molecules in a fluid membrane. *J. Phys. Chem.* **1995**, *99*: 17662.
- [Schmidt 1996] T. Schmidt, G.J. Schutz, W. Baumgartner, H.J. Gruber, and H. Schindler; Imaging of single molecule diffusion. *Proc. Natl. Acad. Sci. USA.* **1996**, *93*: 2926.
- [Schnaible 2002] V. Schnaible, S. Wefing, A. Bucker, S. Wolf-Kummeth, and D. Hoffmann; Partial Reduction and Two-Step Modification of Proteins for Identification of Disulfide Bonds. *Anal. Chem.* **2002**, *74*: 2386.
- [Schütz 1997] G.J. Schütz, H. Schindler, and T. Schmidt; Single-molecule microscopy on model membranes reveals anomalous diffusion *Biophys. J.* **1997**, *73*: 1073.
- [Schütz 2000] G.J. Schütz, V.P. Patuschenko, H.J. Gruber, H.G. Knaus, B. Pragl, H. Schindler. 3D imaging of individual ion channels in live cells at 40 nm resolution. *Single Mol.* **2000**, *1*: 25.
- [Selvin 2000] P.R. Selvin; The renaissance of fluorescence resonance energy transfer. *Nature Structural Biology* **2000**, *7*: 730.
- [Shames 1998] P.E. Shames, P.C. Sun, and Y. Fainman; Modeling of Scattering and Depolarizing EO Devices II: Device simulation. *Applied Optics* **1998**, *37*: 3726.
- [Sheehan 1955] J.C. Sheehan, and G.P. Hess; A New Method of Forming Peptide Bonds. *J. Am. Chem. Soc.* **1955**, *77*: 1067.
- [Sheehan 1961] J.C. Sheehan, P.A. Cruickshank, and G.L. Boshart; A convenient synthesis of water-soluble carbodiimides. *J. Org. Chem. Soc.* **1961**, *26*: 2525.
- [Shera 1990] E.B. Shera, N.K. Seitzinger, L.M. Davis, R.A. Keller, and S.A. Soper; Detection of single fluorescent molecules. *Chem. Phys. Lett.* **1990**, *174*: 553.
- [Singer 1986] K.T. Tokuyasu, and J.S. Singer; Improved procedures for immunoferritin labelling of ultrathin frozen sections. *J. Cell Biol.* **1976**, *71*: 894.

- [Singh 2002] R. Singh, and E.K. Maloney; Labeling of antibodies by *in situ* modification of thiol groups generated from selenol-catalyzed reduction of native disulfide bonds. *Anal. Biochem.* **2002**, *304*: 147.
- [Smith 1996] S.B. Smith, Y. Cui, and C. Bustamante; Overstretching B-DNA: the elastic response of individual double-stranded and single-stranded DNA molecules. *Science* **1996**, *271*: 795.
- [Smith 1992] S.B. Smith, L. Finzi, C. Bustamante; Direct mechanical measurement of the elasticity of single DNA molecules by using magnetic beads. *Science* **1992**, *258*: 1122.
- [Soper 1991] S.A. Soper, E.B. Shera, J.C. Martin, H.J. Jett, H. Hahn, L. Nutter, and R.A. Keller; Single-Molecule Detection of Rhodamine-6g in Ethanolic Solutions Using Continuous Wave Laser Excitation. *Anal. Chem.* **1991**, *63*: 432.
- [Soper 1994] S.A. Soper, B.L. Legendre. Error Analysis of Simple Algorithms For Determining Fluorescence Lifetimes in Ultradilute Dye Solutions. *Appl. Spectrosc.* **1994**, *48*: 400.
- [Stolz 2000] M. Stolz, D. Stoffler, U. Aebi, and C. Goldsbury; Monitoring Biomolecular Interactions by Time-Lapse Atomic Force Microscopy. *J. Struc. Biol.* **2000**, *131*: 171.
- [Strutt 1874] J.W. Strutt; On the manufacture and theory of diffraction gratings. *Philos. Mag.* **1874**, *47*: 193.
- [Stryer 1967] L. Stryer, and R.P. Haugland; Energy transfer: a spectroscopic ruler. *Proc. Natl. Acad. Sci. USA* **1967**, *58*: 719.
- [Szollosi 1998] J. Szollosi, S. Damjanovich, L. Matyus; Application of fluorescence resonance energy transfer in the clinical laboratory: routine and research. *Cytometry* **1998**; *34*:159.
- [Tellingh. 1993] J. Tellinghuisen, C.W. Wilkerson Jr. Bias and precision in the estimation of exponential decay parameters from sparse data. *Anal. Chem.* **1993**, *65*: 1240.
- [Tinnefeld 2000] P. Tinnefeld, V. Buschmann, D.-P. Herten, K.-T. Han, and M. Sauer; Confocal Fluorescence Lifetime Imaging Microscopy (FLIM) at the Single Molecule Level. *Single Mol.* **2000**, *1*: 215.
- [Tinnefeld 2002] P. Tinnefeld; Multiparameter Single Molecule Spectroscopy Based on Spectrally-Resolved Fluorescence Lifetime Imaging Microscopy [SFLIM]. PhD Thesis, Universität Heidelberg, **2002**.
- [Tokuysau 1973] K.T. Tokuysau; A technique for ultracryotomy of cell suspensions and tissues. *J. Cell. Biol.* **1973**, *57*: 551.
- [Tokuysau 1976] K.T. Tokuysau; Membranes as observed in frozen sections. *J. Ultrastruct. Res.* **1976**, *55*: 281.
- [Tokuysau 1986] K.T. Tokuysau; Application of cryoultramicrotomy to immunocytochemistry. *J. Microsc.* **1986**, *143*: 139.

- [Trautman 1994] J.K. Trautman, J.J. Macklin, L.E. Brus, and E. Betzig; Near-Field Spectroscopy of Single Molecules at Room-Temperature. *Nature* **1994**, *369*: 40.
- [Tsien 1998] R.Y. Tsien; Green fluorescent protein. *Ann. Rev. Biochem.* **1998**, *67*: 509.
- [Vácha 1999] Martin Vácha, Hiroshi Yokoyama, Takashi Tokizaki, Makoto Furuki, and Toshiro Tani; Laser scanning microscope for low temperature single molecule and microscale spectroscopy based on gradient index optics. *Rev. Sci. Instrum.* **1999**, *70*: 2041.
- [Vale 1996] R.D. Vale, T. Funatsu, D.W. Pierce, L. Romberg, Y. Harada, and T. Yanagida; Direct observation of single kinesin molecules moving along microtubules. *Nature* **1996**, *380*: 451.
- [van Oijen 1999] A.M. van Oijen, J. Köhler, J. Schmidt, M. Müller, and G.J. Brakenhoff; Far-field fluorescence microscopy beyond the diffraction limit. *J. Opt. Soc. Am. A*, **1999**, *16*: 909.
- [Wang 1997] M.D. Wang, H. Yin, R. Landick, J. Gelles, and S.M. Block; Stretching DNA with optical tweezers. *Biophys. J.* **1997**, *72*:1335.
- [Wang 1999] M.D. Wang; Manipulation of single molecules in biology. *Curr. Opin. Biotech.* **1999**, *10*: 81.
- [Wansink 1996] D.G. Wansink, O.C. Sibon, F.F. Cremers, R. van Driel, and L. de Jong; Ultrastructural localization of active genes in nuclei of A431 cells. *J Cell Biochem.* **1996**, *62* (1): 10.
- [Watson 1953] J.D. Watson, and F.H.C. Crick; A Structure for Deoxyribose Nucleic Acid. *Nature*, **1953**, *171*: 737.
- [Weiss 1999] S. Weiss; Fluorescence Spectroscopy of Single Biomolecules. *Science* **1999**, *283*: 1676.
- [Weiss 2001] A.M. Kelley, X. Michalet, and S. Weiss; Chemical physics - Single-molecule spectroscopy comes of age. *Science* **2001**, *292*: 1671.
- [Weston 2001] K.D. Weston, and L.S. Goldner; Orientation imaging and reorientation dynamics of single dye molecules. *J. Phys. Chem. B* **2001**, *105*: 3453.
- [Weston 2002] K.D. Weston, M. Dyck, P. Tinnefeld, C. Müller, D.-P. Herten, and M. Sauer; Measuring the Number of Independent Emitters in Single-Molecule Fluorescence Images and Trajectories Using Coincident Photons. *Anal. Chem.* **2002**, *74*: 5342.
- [Widengren 1996] J. Widengren, and R. Rigler; Mechanisms of photobleaching investigated by fluorescence correlation spectroscopy. *Bioimaging* **1996**, *4*: 149.
- [Wilbur 1999] D.S. Wilbur, P.M. Pathare, D.K. Hamlin, P.S. Stayton, R. To, L.A. Klumb, K.R. Buhler, and R.L. Vessella; Development of new biotin/streptavidin reagents for pretargeting. *Biomol. Eng.* **1999**, *16*:113.

- [William 1995] D.C. William, and S.A. Soper; Ultrasensitive near-IR fluorescence detection for capillary gel electrophoresis and DNA sequencing applications. *Anal. Chem.* **1995**, *67*: 3427.
- [Xie 1994] X.S. Xie, and R.C. Dunn; Probing Single-Molecule Dynamics. *Science* **1994**, *265*: 361.
- [Xu 1997] C. Xu, W. Zipfel, J.B. Shear, R.M. Williams, and W.W. Webb; Multiphoton fluorescence excitation: New spectral windows for biological nonlinear microscopy. *Proc. Natl. Acad. Sci. USA* **1996**, *93*: 10763.
- [Xu 1997] X.-H. Xu, and E.S. Yeung; Direct Measurement of Single-Molecule Diffusion and Photodecomposition in Free Solution *Science* **1997**, *275*: 1106.
- [Yang 1996] F. Yang, L.G. Moss, G.N. Phillips Jr.; The molecular structure of green fluorescent protein. *Nature Biotech.* **1996**, *14*: 1246.
- [Yildiz 2003] A. Yildiz, J.N. Forkey, S.A. McKinney, T. Ha, Y.E. Goldman, and P.R. Selvin; Myosin V Walks Hand-Over-Hand: Single Fluorophore Imaging with 1.5-nm Localization. *Science* **2003**, *300*: 2061.
- [Zeng 1997] C. Zeng, E. Kim, S.L. Warren, and S.M. Berget; Dynamic relocation of transcription and splicing factors dependent upon transcriptional activity. *EMBO J.* **1997**, *16*:1401.
- [Zou 1990] X.T. Zou, and L. Mandel; Photon-antibunching and sub-Poissonian photon statistics. *Phys. Rev. A* **1990**, *41*: 475.

8 Publication List

T. Heinlein, A. Pombo, P. Tinnefeld, M. Sauer, and D.P. Herten
Stoichiometric fluorescence labeling of antibodies for single-molecule spectroscopic applications
in preparation

P. Schlüter, T. Heinlein, D.P. Herten, and J. Wolfrum
Counting of single-molecules in living cells using coincidence analysis
in preparation

T. Heinlein, P. Schlüter, D.P. Herten, M. Sauer, and J. Wolfrum
Counting single molecules in living cells at high resolution by spectrally resolved fluorescence lifetime imaging microscopy (SFLIM) and coincidence analysis
SPIE proc., submitted

P. Tinnefeld, V. Buschmann, K.D. Weston, A. Biebricher, D.P. Herten, O. Piestert, T. Heinlein, M. Heilemann, and M. Sauer
How single molecule photophysical studies complement ensemble methods for a better understanding of chromophores and chromophore interactions
Recent Res. Devel. Physical. Chem. **2004**, 7: 95.

D.-P. Herten, A. Biebricher, M. Heilemann, T. Heinlein, C. Müller, P. Schlüter, P. Tinnefeld, K.D. Weston, M. Sauer, and J. Wolfrum
Optical single molecule techniques for analytical and biological applications.
Recent Res. Devel. Applied Phys. **2004**, 7: 345.

T. Heinlein, M. Heilemann, D.P. Herten, C. Müller, P. Tinnefeld, K.D. Weston, and M. Sauer
Spectrally-resolved fluorescence lifetime imaging microscopy (SFLIM) and coincidence analysis: New tools to study the organization of biomolecular machines.
SPIE Proc. Manipulation and Analysis of Biomolecules, Cells, and Tissues **2003**, 4962, 47-57.

O. Piestert, H. Barsch, V. Buschmann, T. Heinlein, J.-P. Knemeyer, K.D. Weston, and M. Sauer
A Single-Molecule Sensitive DNA Hairpin System Based on Intramolecular Electron Transfer.
Nano Lett. **2003**, 3 (7), 979.

T. Heinlein, J.-P. Knemeyer, O. Piestert, and M. Sauer
Photoinduced Electron Transfer between Fluorescent Dyes and Guanosine Residues in DNA-Hairpins.
J. Phys. Chem. B **2003**; 107 (31), 7957.

Acknowledgement

Here, at the end of this work, I thank everybody who helped or supported me during my thesis.

For the interesting research subject I am equally grateful to Prof. Dr. Jürgen Wolfrum, Prof. Dr. Markus Sauer, and Dr. Dirk-Peter Herten who always supported me and showed great interest in my work.

For the good collaboration in the cell biology part I thank Dr. Ana Pombo and Sheila Xie from the MRC in London. Without their commitment the cell experiments would not have been possible.

I gratefully acknowledge Andreas Biebricher for discussion and conducting the preparative DNA and dye measurements with me, as well as Dr. Christian Müller who set the mathematical basis for the DNA ruler.

Furthermore my thanks go to Dr. Kyung-Tae Han for stimulating discussion and information about fluorophores, coupling reactions and chromatographic work-ups.

To my colleges Hannes Barsch, Dr. Volker Buschmann, Mike Heilemann, Alexander Kiel, Dr. Hannes Neuweiler, Dr. Chong-Woo Park, Oliver Piestert, Christian Roth, Daniel Siegberg, Katharina Stöhr, and Dr. Philip Tinnefeld I want to give an extra thank for their team-spirit and help.

For proofreading of the manuscript I thank Dr. Haridas Pal.

Last but not least I greatly acknowledge the patience and optimism of Pia Schlüter who didn't always have an easy time with me, but never stopped supporting me.

Last but not least I greatly acknowledge the patience and optimism of Pia Schlüter who didn't always have an easy time with me, but never stopped supporting me.